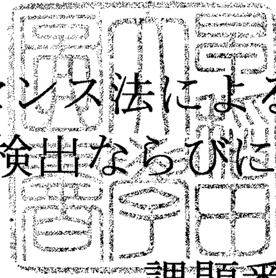

フォトルミネセンス法によるシリカ薄膜中の欠陥の検出ならびに構造解析

課題番号０９４５０１３２

平成９年度～１１年度科学研究費補助金
［基盤研究(B)(2)］研究成果報告書

平成１２年３月

研究代表者　大木義路
（早稲田大学理工学部教授）

はしがき

本報告書は下記の課題で助成を受けた平成９年度～平成１１年度科学研究費補助金[基盤研究(B)(2)]に関わる研究成果をまとめたものである。

研究課題

フォトルミネセンス法によるシリカ薄膜中の欠陥の検出ならびに構造解析
課題番号０９４５０１３２

研究組織

研究代表者：大木義路
（早稲田大学理工学部教授）
研究分担者：浜義昌
（早稲田大学理工学総合研究センター教授）
研究分担者：宗田孝之
（早稲田大学理工学部教授）

研究経費

平成　９年度３，９００千円
平成１０年度４，２００千円
平成１１年度１，５００千円
　　合計　　９，６００千円

研究発表

（ア）学会誌

1. Y. OHKI et al, Effects of internal post-oxidation on the oxygen deficiency and dielectric strength of buried oxide formed by the separation-by-implated-oxygen (SIMOX) process, Electrical Engineering in Japan, 130, No. 1, pp. 15-20 (2000).
2. Y. OHKI et al, Fabrication of long-period optical fiber gratings using ion implantations, Optics Letters, 25, No. 2, pp.　(2000).
3. Y. OHKI et al, Structures and Oprical Properties of Defects Correlated with Photo-induced Refractive Index Changes in Ge-doped SiO_2 Glass, Defect and Diffusion Forum, Vols. 177-178, 43-50 (1999).
4. Y. OHKI et al, Low Temperature Crystallization of $SrBi_2Ta_2O_9$ Film by Excimer Laser Irradiation, Mat. Res. Soc. Symp. Proc., 541, pp.293-298 (1999).
   Y. OHKI et al, Effect of ozone annealing on the charge trapping property of Ta_2O_5-Si_3N_4-p-Si capacitor grown by low-pressure chemical vapor deposition, Japanese Journal of Applied Physics, 38, Part 1, No. 12A, pp. 6791-6796 (1999).
   Y. OHKI et al, Effect of annealing on Ge-doped SiO_2 thin films, Journal of Applied Physics, 86, No. 9, pp. 5270-5273 (1999).
   Y. OHKI et al, Structural changes induced by KrF excimer laser photons in H_2-loaded Ge-doped SiO_2 glass, Phys. Rev. B **60**,p. 4682-4687 (1999).
   Y. OHKI et al, Characteristic red photoluminescence band in oxygen-deficient silica glass, J. Appl. Phys. 86, No. 1, p. 370-373, (1999).
   Y. OHKI et al, Direct deposition of a blanket tungsten layer on SiO_2 by preexposure of helium plasma, J. Appl. Phys., 85, No. 12, p. 8423-8426 (1999).
   大木義路他、プラズマＣＶＤ堆積 SiO_2 薄膜の絶縁破壊電界におよぼすフッ素添加の効果、電学論 119-A, No. 5, p. 658-664 (1999).

11. Y. OHKI et al, Effects of ion implantation and thermal annealing on the photoluminescence in amorphous silicon nitride, J. Appl. Phys. 85, No. 9, p. 6746-6750 (1999).
12. Y. OHKI et al, Paramagnetic centers induced in Ge-doped SiO_2 glass with UV irradiation, J. Phys. Condensed Matter, 11, No. 12, p. 2589-2594 (1999).
13. Y. OHKI et al, Temperature dependence of the lifetime of 4.3 eV photoluminescence in oxygen-deficient amorphous SiO_2, Phys. Rev. B, Vol. 59, No. 3, p. 1590-1593 (1999).
14. 大木義路他、プラズマCVD法による希土類添加シリカ薄膜――成膜法の開発と発光の物性研究への応用――、電学論 A, 119-A, No. 1, p. 113-117 (1999)
15. 大木義路他、内部酸化がSIMOX埋め込み酸化膜の酸素欠乏性と絶縁破壊電界におよぼす影響、電学論、118-A, No. 7/8, p. 826-831 (1998).
16. Y. OHKI et al, Concentration of neutral oxygen vacancies in buried oxide formed by implantation of oxygen, UVSOR Activity Report 25, April, p. 98-99 (1998).
17. Y. OHKI et al, Structures and generation mechanisms of paramagnetic centers and absorption bands responsible for Ge-doped SiO_2 optical fiber gratings, Physical Review B, Vol.57, No.7, p.3920-3926 (1998).
18. Y. OHKI et al, Concentration of neutral oxygen vacancies in buried oxide formed by implantation of oxygen, J. Appl. Phys., Vol. 83, No. 4, p. 2357-2359 (1998).
19. Y. OHKI et al, Photoluminescence of oxygen-deficient-type defects in a-SiO_2, J. Non-Cryst. Solids, Vol. 222, p. 221-227 (1997).
20. Y. OHKI et al, Rare-earth-doped SiO_2 films prepared by plasma-enhanced chemical vapour deposition, J. Phys. D: Appl. Phys. 30, p. 1908-1912 (1997).

（イ）国際会議報告

1. Low Temperature Crystallization of $SrBi_2Ta_2O_9$ Ferroelectric Films by Ultraviolet Laser Irradiation, 1999 Symposium on Dry Process, 1999/11.
2. Direct Deposition of Blanket Tungsten Layer on SiO_2 by Pre-exposure of Helium Plasma, 1998 Symposium on Dry Process, 1998/10
3. Structural Changes in Ge-Doped SiO_2 Planar Waveguides Induced by Ultraviolet Photons, 1998 IEEE International Symposium on Electrical Insulating Materials, in conjunction with 1998 Asian International Conference on Dielectrics and Electrical Insulation and the 30th Symposium on Electrical Insulating Materials, 1998/9
4. Photoluminescence and Electron-Spin-Resonance Studies of Defects in Amorphous SiO_2 Films, 1998 IEEE International Symposium on Electrical Insulating Materials, in conjunction with 1998 Asian International Conference on Dielectrics and Electrical Insulation and the 30th Symposium on Electrical Insulating Materials, 1998/9
5. Effects of Ion Implantation and Thermal Annealing on the Photoluminescence in Amorphous Silicon Nitride Films, 1998 IEEE International Symposium on Electrical Insulating Materials, in conjunction with 1998 Asian International Conference on Dielectrics and Electrical Insulation and the 30th Symposium on Electrical Insulating Materials, 1998/9
6. Effect of Ozone Annealing on the Charge Trapping Property of Ta_2O_5-Si_3N_4-p-Si Capacitor Grown by Low Pressure Chemical Vapor Deposition, IEEE International Symposium on Electrical Insulating Materials, in conjunction with 1998 Asian International Conference on Dielectrics and Electrical Insulation and the 30th Symposium on Electrical Insulating Materials, 1998/9
7. Dielectric Breakdown in F-Doped SiO_2 Films Formed by Plasma-Enhanced Chemical Vapor Deposition, 1998 IEEE International Conference on Conduction and Breakdown in Solid Dielectrics, 1998/6
8. Generation mechanism of germanium electron center in Ge-doped silica glass, International Workshop on Structure and Functional Optical Properties of Silica and Silica-related Glasses, 1997/7
9. Correlation between paramagnetic centers and absorption bands induced by KrF excimer laser photons in Ge-doped SiO_2 glass, The 14th University Conference on Glass Science, 1997/ 6

研究成果

1.　概要

半導体デバイスの絶縁膜や光ファイバなどとして使用され、現代のハイテク社会を担う基幹材料となっている非晶質シリカおよび酸化物無機絶縁性薄膜について、膜中の不純物や空格子点などの点欠陥が膜の電気的および光学的特性に及ぼす影響を系統的に明らかにすることを目的とした研究を行った。不純物や空格子点などの存在はフォトルミネッセンスやESR, FT-IR, 可視～真空紫外分光, EPMA, SIMS等で明らかにし、電気特性は高電界伝導、絶縁破壊、C-V測定などより明らかにしている。酸素空孔の存在と定量、不純物添加による構造の安定化、成膜法の差による欠陥の多寡などが明らかになった。

2.　主な成果

平成９年度の研究において、強力な紫外―真空紫外光であるエキシマレーザ光やシンクロトロン放射光を用いることにより、a-SiO_2薄膜からでも充分な強度を有したフォトルミネセンスが得られることが証明され、今まで、有力な評価手段のなかった a-SiO_2 薄膜の点欠陥に対する検出手法としてのフォトルミネセンス法が確立できた。さらに、この手法を用いて、シリコン熱酸化膜や SIMOX 埋め込み酸化膜を対象として、その膜の製法に起因して膜が本質的に含有する欠陥とイオン注入や高温熱処理等のデバイス製造プロセスにより生じる欠陥の検出と欠陥構造の同定を行うことができた。

イオン注入されたシリコン熱酸化膜に KrF エキシマレーザ光を照射することにより三つの発光帯（4.3 eV、2.7 eV、1.9 eV）を観測した。また、4.3 eV発光の励起帯が約5.0 eVと7.3 eVにあることをシンクロトロン放射光を用いた発光励起測定から観測した。さらに、シングルバンチ運転下のシンクロトロン放射光（光パルス幅約0.55 ns）を用いた時間相関単一光子計数法等の測定により 4.3 eV 発光の寿命は 5.0 eV 光励起では約 2.6 ns であり、7.3 eV光励起では約1.9 nsであること、2.7 eV発光の寿命は約6 msであることを明らかにし、これらの発光がイオン注入によりシリコン熱酸化膜に誘起された酸素空孔に起因していること、および、イオン注入により熱酸化膜に誘起された欠陥の消滅に対して、高温での熱酸化中に酸化膜に溶け込んでいた酸素が重要な役割を果たしていることを明らかにした。

つぎに、シリコン基板への酸素イオン注入後、高温の熱処理により形成された SIMOX 埋め込み酸化膜を試料として、埋め込み酸化膜上のSi層をKOH溶液でエッチング除去したのち、KrF エキシマレーザ光励起下で発光を観察すると、4.3 eV 発光の強度は SIMOX 埋め込み酸化膜の残存膜厚に対してほぼ直線的に比例することから、酸素空孔は酸化膜中にほぼ均等に分布しているとしていると推察できる。また、イオン注入のされていないシリコン熱酸化膜ではこれらの発光が観測されないことから、SIMOX埋め込み酸化膜はシリコン熱酸化膜より遥かに酸素欠乏性の程度が高いことを明らかにした。

平成１０年度は、引き続き、平成９年度と同様な手法を用いて SIMOX 埋め込み酸化膜、フッ素添加 SiO_2 薄膜やシリコン窒化膜を対象として欠陥の検出と欠陥構造の同定をさらに進めた。また、絶縁破壊測定により、欠陥構造が絶縁破壊強度に与える影響を調査した。

シリコン基板への酸素イオン注入後、高温熱処理により形成された SIMOX 埋め込み酸化膜を試料として、内部酸化効果をフォトルミネセンス法、絶縁破壊測定を用い調べた。フォトルミネセンス測定から、内部酸化によって埋め込み酸化膜の増加した部分の酸素欠乏性は元々あった埋め込み酸化膜とほぼ同じであり、熱酸化膜と比べればはるかに欠乏性が大きいことが分かった。また、自己修復破壊法による絶縁破壊測定によれば、初期の低電界での破壊を生じる回数は内部酸化により著しく減少する。これは内部酸化によりシリコン柱などの弱点部が著しく減少することを示唆しており、実用的見地から内部酸化法は有効であることが分かった。

次にフッ素を添加したSiO_2薄膜をプラズマCVD法により作製し、欠陥構造について調べ、

またフッ素添加が SiO_2 薄膜の絶縁破壊強度に及ぼす効果について調べた。その結果、フォトルミネセンス測定から、フッ素を添加することで微視的な構造の乱雑さによる歪みが減少し、より均一な構造になることが確かめられた。

平成１１年度においては、さらに各種 SiO_2 膜、SiN_x 膜、SiO_xN_y 膜、Ta_2O_5 膜などを研究の対象に加えた。主な成果を箇条書きに列記する。

(1) プラズマ CVD 堆積 SiO_2 薄膜にフッ素を添加することが、膜の絶縁破壊特性に及ぼす影響を調べた。無添加の SiO_2 膜に比べて、フッ素添加の試料では、破壊電界が 2MV/cm 以上も上昇することを見いだした。次に、フッ素添加による酸素欠乏性欠陥の増減やエネルギー構造の変化をエキシマレーザおよびシンクロトロン放射(SR)光によるフォトルミネッセンスおよび真空紫外吸収スペクトルの解析により調べた。フッ素添加により禁制帯幅が広がるが、その程度は破壊電界の上昇より予想できる値より小さい。破壊電界の厚さ依存性を詳細に調べ、フッ素による散乱によって電子のエネルギーが減少していることを推測した。

(2) 近年注目されている高誘電率膜である Ta_2O_5 薄膜の研究について、リーク電流減少の為に施されるオゾン熱酸化処理に注目した。リーク電流減少に伴う電荷捕獲メカニズムの変化を C-V 測定・TSC 測定により明らかにした。オゾン処理により電子トラップが減少し正孔トラップが生成されることと、電子トラップには 230,290K 付近に TSC ピークを持つことを明らかにした。一般的に酸化物は酸素過剰になると p 形挙動を示すことから、オゾン処理により Ta_2O_5 膜が酸素欠乏から酸素過剰へと変化したことが原因として考えられる。

(3) イオン注入や加熱処理により誘起される構造欠陥が、a-SiN_x 膜から観測される発光に与える影響について調べた。　未処理の試料を KrF エキシマレーザで励起したとき、2.4 eV 付近に幅広い発光が観測されるが、これは 2.66 eV および 2.15 eV の二つの発光帯から成ることがわかった。いずれの発光帯の強度もイオンドーズ量のべき乗に反比例する形で減少する。イオン注入を施した試料を 900℃の N_2 100%雰囲気中に 20 分間放置すると、発光強度が回復する。しかし、イオン注入を施していない試料を、真空中で熱処理すると、強度は、約 700℃から処理温度の増加にともない減少し、発光寿命は減少する。熱処理により、膜内の N－H 結合と Si－H 結合の量が、急激に減少すること、水素が膜外へ脱離することが、IR や TDS 測定により確認された。これらの実験結果から、結合切断や水素の脱離によって生成された構造欠陥が、PL 強度を減少させるような非発光中心として働いていると結論づけた。

(4) 光ファイバグレーティングの紫外光照射によるグレーティング作成機構を明らかにすることを目的として、KrCl エキシマランプや KrF エキシマレーザを照射したときに Ge 添加シリカガラス中に生じる光誘起構造変化を調べた。ESR によるラジカル性欠陥の増減を詳細に検討し、2 光子吸収過程と 1 光子吸収過程の両者を含む光化学反応式を明らかにした。

(5) 光ファイバグレーティングの作成においては Ge 添加シリカに水素を含まさせたのち紫外光を照射する。そこで水素含有 Ge 添加シリカガラスにおける紫外光誘起構造変化を、吸収スペクトル測定と ESR の両面から詳細に調べ、生じている光化学反応を明らかにした。

(6) イオン注入法を利用した高効率で安定な長周期グレーティングを光ファイバ内に形成する手法を開発した。

研究成果の詳細

which where then annealed at 1350 °C in an Ar + O_2 atmosphere for 6 h. Such SIMOX wafers were found to have a superficial Si layer ~350 to 360 nm thick and a BOX layer ~85 to 90 nm thick. To investigate the effect of postoxidation, samples postoxidized in O_2 of 1 atmosphere pressure mixed with a trace of Ar at 1350 °C were also prepared. The postoxidized samples have a thermal oxide ~650 nm thick on the top, with a Si layer ~60 to 70 nm thick and a BOX layer ~125 to 130 nm thick underneath. From the change in the BOX thickness by the postoxidation, it was found that ~40-nm-thick BOX was newly added to the original BOX. Here, the thickness of each layer in the sample was measured by cross-sectional transmission electron microscopy.

For PL measurement, the thermal oxide and the Si overlayer were, respectively, removed by HF solution and KOH solution to expose the BOX layer. The PL and PL excitation (PLE) spectra were measured at room temperature under excitation with KrF excimer laser (wavelength = 248 nm [photon energy = 5.0 eV], duration ~20 ns) and synchrotron radiation (BL1B Line, Institute for Molecular Science, Okazaki, Japan), respectively.

Since plasma exposure is known to activate effectively ESR-inactive point defects into ESR-active species [5, 6], the bared BOX layer was exposed to an Ar plasma excited by an rf power of 13.56 MHz (power: 60 W, gas pressure: 40 Pa). The induced paramagnetic defects were analyzed by ESR (JEOL RE-2XG) at room temperature. The observed derivative power absorption spectra were numerically double integrated and compared to a standard DPPH (1,1-diphenyl-2-picrylhydrazyl) sample to calculate the defect density.

The dielectric breakdown tests were carried out using samples with a MOS structure of Au/SiO_2(BOX)/p-Si. The breakdown strength was measured using a self-healing breakdown method by applying a negative rectangular voltage pulse with a duration of 1 μs to the Au electrode. The details are described elsewhere [7].

3. Results and Discussion

3.1 Effect of internal oxidation on the oxygen deficiency of BOX

Shown in Fig. 1(a) is the PL spectrum excited using 5.0-eV photons from the KrF excimer laser, measured for the BOX layer before the postoxidation. Two PL bands at 4.3 and 2.7 eV are seen. Figure 1(b) shows the PLE spectrum for the 4.3-eV PL band. Two PLE bands at 5.0 and ~7.5 eV are observed. Such PL and PLE bands are attributed to the neutral oxygen vacancies (NOV_S, $O_3{\equiv}Si{-}Si{\equiv}O_3$, "≡" denotes three separate bonds to oxygens) [8], and they strongly indicate that the sample is oxygen-deficient. Since

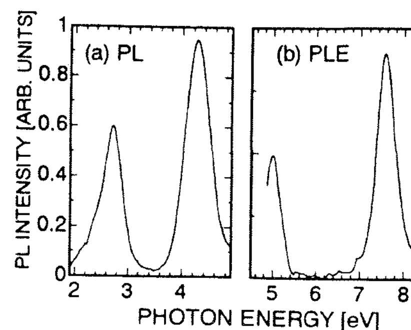

Fig. 1. PL spectrum induced by 5.0-eV photons (a) and PL excitation spectrum for the 4.3-eV PL (b) from the BOX before the internal postoxidation.

identical PLs were also observed in the BOX formed by a different dose (2×10^{18} cm^{-2}) [9], oxygen deficiency is an inherent feature of BOX.

In order to examine the spatial dependence of PL intensity, the BOX thickness was changed by etching with HF solution. Figure 2 shows the intensity of the 4.3-eV PL as a function of the remaining thickness of the BOX. The open squares connected with dashed lines and the solid circles connected with solid lines represent the BOXs before and after postoxidation, respectively. It is seen that the intensity of the 4.3-eV PL from the entire BOX thickness increases 1.6 times by postoxidation. Simultaneously, the

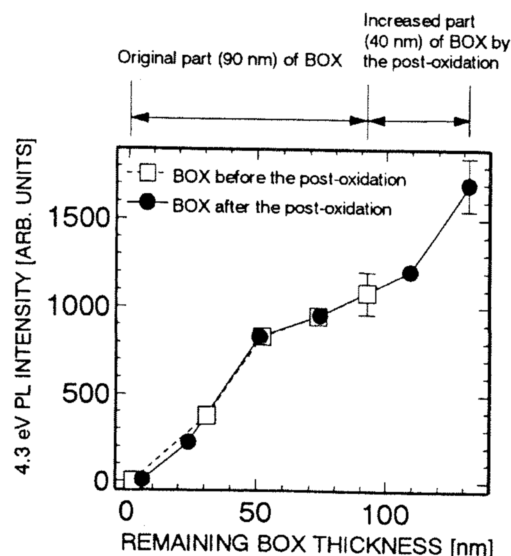

Fig. 2. Intensity of the 4.3-eV PL as a function of the remaining BOX thickness for BOXs with and without internal postoxidation.

BOX layer becomes about 1.5 times thicker. It is also clearly seen that as the BOX thickness is reduced by etching, the PL intensity decreases in a perfectly similar manner regardless of whether the sample was postoxidized or not. Thus, it is concluded that the increase in the PL intensity by postoxidation is merely due to the increase in the thickness of the oxide, and that the degree of oxygen deficiency of the increased part of BOX is about the same as that of the original BOX. Another important indication of the results obtained is that the present postoxidation does not reduce the oxygen deficiency of the original BOX, despite the report that a similar postoxidation process effectively eliminated Si pipes [3, 4]. As will be described in the next section, the present study has revealed that postoxidation can eliminate the occurrence of breakdowns at extremely low electric fields. This probably reflects the fact that Si pipes had been eliminated. Therefore, postoxidation is considered to be unable to diminish the oxygen deficiency completely, although it can oxidize the completely oxygen-deficient Si pipes and make them insulating.

Figure 3 shows the ESR spectrum of the BOX layer which was postoxidized and then exposed to the Ar plasma for 30 min. The spectrum is assigned to the E'_γ centers ($O_3\equiv Si^{\cdot}\,{}^{+}Si\equiv O_3$, "·" denotes an unpaired electron). Since no ESR signal was detected without the plasma exposure, it is considered that the plasma exposure activated NOVs to the E'_γ centers via the following reaction:

$$O_3\equiv Si\text{-}Si\equiv O_3 \rightarrow O_3\equiv Si^{\cdot}\,{}^{+}Si\equiv O_3 + e^{-} \quad (1)$$

Figure 4 shows the relation between the areal density of E'_γ centers and the plasma exposure time for the two BOX samples with and without postoxidation. For comparison, a similar relation for the thermal oxide, which was formed as the sample's superficial layer during postoxidation, is also shown in Fig. 4. The areal density observed in the sample whose increased part of the BOX had been etched off is also shown. Furthermore, the BOX thickness of the samples with and without postoxidation was reduced by etching, and the areal density of the plasma-induced E'_γ centers as a function of the remaining thickness is shown in Fig. 5. A good relationship is seen between the areal

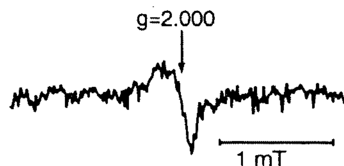

Fig. 3. ESR spectrum in the postoxidized BOX after being exposed to Ar plasma for 30 min.

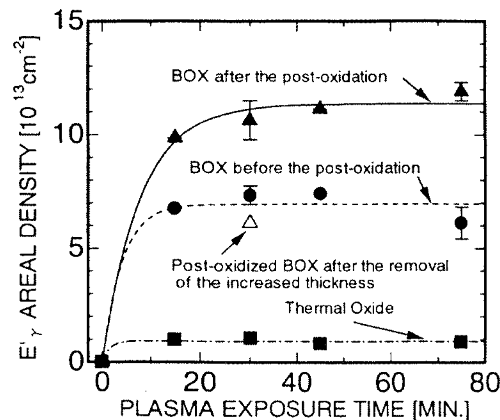

Fig. 4. Growth curves of E'_γ centers as a function of the plasma exposure time for BOXs with and without postoxidation and for thermal oxide.

density and the remaining thickness. In Fig. 5, the plasma-induced density of E'_γ centers observed after the increased part of the BOX thickness had been removed is also shown. This density agrees fairly well with the densities of the other two samples with the same thickness. These results indicate that the effect of plasma reached uniformly at least to a depth of 130 nm. As for the thermal oxide, a comparison such as shown in Fig. 5 was impossible since the number of induced E'_γ centers was small. Therefore, it is not clear whether the effect of plasma reached over the entire oxide thickness. However, the plasma seems to have some effect

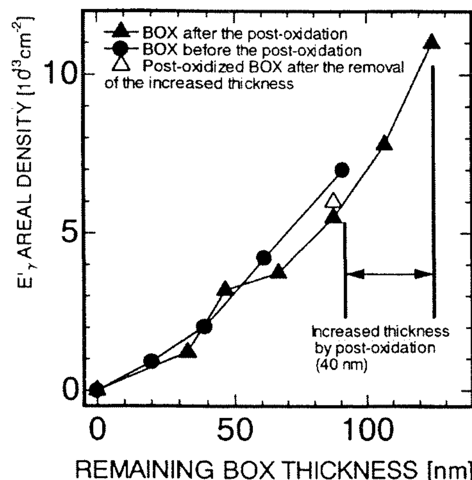

Fig. 5. Density of the plasma-induced E'_γ centers as a function of the remaining oxide thickness for BOXs with and without postoxidation.

at a depth of 650 nm, since it shows the uniform effect to the depth of 130 nm. From this viewpoint, the saturation levels of the areal density for all of the samples are calculated and summarized in Table 1, together with their oxide thicknesses and the apparent volume densities. The saturation level of about 1.1×10^{14} cm^{-2} of the postoxidized BOX is higher by a factor of about 1.6 than that of about 7×10^{13} cm^{-2} observed for the BOX before the postoxidation. This factor of 1.6 is again very close to the factor of the thickness increase. When the increased part of the BOX by the postoxidation was etched off, the saturation level became about 6×10^{13} cm^{-2}, which is very close to the density observed before the postoxidation. Furthermore, as shown in Fig. 5, the postoxidation seems not to have a significant effect on the relation between the areal density and the remaining thickness. These results suggest that the increase in the number of E_{γ}' centers by the postoxidation is simply explainable by the increase in the BOX thickness, similarly to the case of the PL results shown in Fig. 2. This is quite reasonable if we regard that a constant fraction (including 100% as an example) of NOVs were converted to E_{γ}' centers by the plasma exposure.

Another important indication of Fig. 4 is the difference in the E_{γ}' areal density between the BOXs and the thermal oxide. This difference is actually significant if we consider the apparent volume density shown in Table 1. This agrees with our previous report that BOX formed by the SIMOX process contains a far larger number of NOVs than thermal oxide [9]. Since it is known that plasma exposure activates NOVs to E_{γ}' centers very effectively compared with other activation sources such as x-rays and γ-rays [5, 10], the calculated apparent volume density shown in Table 1 might be very close to the real density of the precursors, namely, NOVs.

Table 1. Saturation level of E_{γ}' centers for various SiO_2 layers

Sample	Thickness [nm]	Areal density [10^{13} cm^{-2}]	Volume density [10^{17} cm^{-3}]
BOX before postoxidation	90	~7	~78
BOX after postoxidation	130	~11	~85
Postoxidized BOX after removal of the increased thickness	90	~6	~67
Thermal oxide	650	~1	~1.5

3.2 Effect of internal oxidation of the dielectric strength of BOX

Figure 6 shows the results of dielectric breakdown measurements of BOX. The two symbols in Fig. 6 are the data of the electric field strength at breakdowns for the BOX before the postoxidation with an oxide thickness of ~85 nm, and for the BOX after the postoxidation with an oxide thickness of ~125 nm. The breakdown strength increases and then saturates with an increase in the total number of breakdowns. It is clear that the number of breakdowns occurring at extremely low fields below ~8.9 MV/cm is decreased significantly by the postoxidation. This is very important from a practical or engineering viewpoint, showing that shorting defects such as Si pipes in the BOX can be eliminated by the postoxidation [4].

On the other hand, the maximum breakdown strength, which can be a measure of the intrinsic breakdown strength as a physical limit of the material, decreases in accordance with an increase in the BOX thickness induced by the postoxidation. That is to say, the breakdown voltage increased after the postoxidation, but the thickness increased much more and became about 50% thicker. Therefore, the breakdown field decreased. We have pointed out that NOV is the defect causing the breakdown in SiO_2 [7]. However, since the density of NOVs was unchanged as described in Section 3.1, the decrease in breakdown field is not due to the increase in the number of NOVs. Rather, for the following reasons, the fact that the breakdown field becomes lower with a thicker sample is considered to be quite natural for thin insulating samples such as the present one. First, in order to understand the cause of the decrease in the maximum breakdown field, its thickness dependence was examined. The result is shown in Fig. 7, where it is seen

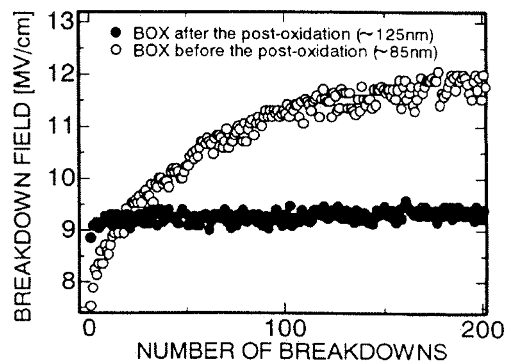

Fig. 6. Change in dielectric strength during repeated measurements of self-healing breakdowns for BOXs with and without postoxidation.

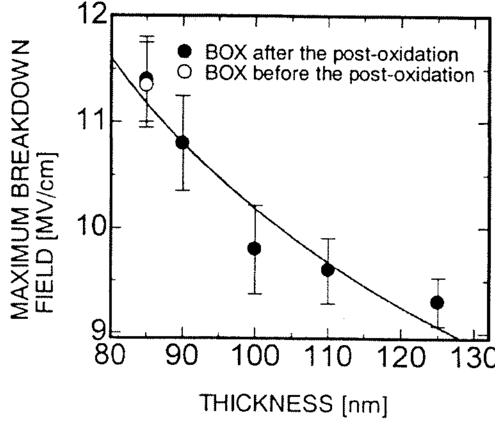

Fig. 7. The maximum dielectric strength as a function of the oxide thickness for BOXs with and without postoxidation. The solid curve shows calculated values based on the single avalanche theory.

that the maximum breakdown field increases if the BOX thickness is reduced by etching.

Assume that an electronic avalanche process [11] is responsible for breakdown. Equations (2) and (3) hold if a thermal breakdown process is negligible and if the breakdown is caused by a single avalanche triggered by electrons injected from the electrode. According to Shockley's equation [13], the ionization coefficient α is given as follows:

$$\alpha = c\ \exp(-\varepsilon_i / e F_b \lambda) \qquad (2)$$

where c is a constant, ε_i the ionization energy for collisional ionization, F_b the breakdown field, and λ the mean free path. The number of electrons necessary to cause breakdown N_c is given by

$$N_c = N_0\ \exp(\alpha d) \qquad (3)$$

where N_0 is the number of initial electrons and d is the thickness. From Eqs. (2) and (3), F_b is given by

$$F_b = \frac{1}{K_1 \log d + K_2} \qquad (4)$$

Here,

$$K_1 = \frac{e\lambda}{\varepsilon_i},\ K_2 = K_1 \log(\frac{c}{A}),\ A = \log(\frac{N_c}{N_0}) \qquad (5)$$

The solid curve in Fig. 7 was obtained by calculating the least-squares fit of the data points to Eq. (4). The values of K_1 and K_2 used were 5.42×10^{-10} and 9.72×10^{-9}, respectively. Since it is generally assumed that ε_i is about 1.5 times the optical gap energy [14, 15] and since the optical gap energy of SiO_2 is 8 eV, ε_i = 12 eV is substituted into the first equation of (5). The mean free path λ is then calculated to be about 6.5 nm. This value is close to the values of the mean free path of electrons, 5 to 6 nm for TEOS-SiO_2 synthesized by the plasma CVD method [16] and 3.2 nm for thermal oxide [17, 18].

In other words, this shows that the change in the maximum breakdown strength in BOX can be explained by the electronic avalanche model [11]. If the BOX thickness becomes thicker by the postoxidation, the number of avalanche multiplications that can be caused by the initial electron will become larger. This makes it possible for the avalanche to be multiplied to the number large enough to cause breakdown. That is, the decrease in the maximum breakdown field is a physically inevitable result that should be produced by the electronic avalanche, and never indicates that the degradation of film quality or the increase in the defect density was caused by the postoxidation. Furthermore, the fact that the breakdown field obtained for the remaining BOX of the postoxidized and etched BOX sample is the same as that obtained for the non-postoxidized BOX with the same thickness agrees with the fact that the PL intensity became almost the same if the increased BOX part had been removed as shown in Fig. 2. This indicates that the postoxidation does not have an influence on the physical quanta that determine the maximum breakdown strength.

4. Conclusions

The effects of internal postoxidation on the oxygen deficiency of the BOX layer of the SIMOX wafer are discussed. The important findings are as follows.

1. As a result of postoxidation, the BOX thickness increases. The PL and ESR measurements revealed that the oxygen deficiency of the increased part of BOX is almost the same as that of the original BOX, which is far more oxygen-deficient than thermal oxide. The postoxidation does not change the degree of oxygen deficiency of the original BOX.

2. By the self-healing breakdown measuring method, it has become clear that the number of low-field breakdowns at an early stage is significantly reduced by postoxidation. This suggests that weak spots such as silicon pipes are significantly diminished by the oxidation, indicating the effectiveness of the postoxidation process in engineering aspects. The maximum breakdown field decreases on postoxidation. This decrease is an inevitable result of the increase in oxide thickness, and is not related to the degradation of material. From the thickness dependence of

breakdown strength, the mean free path of electrons is estimated to be about 6.5 nm.

Acknowledgments

The authors thank Professor Yoshimasa Hama of Waseda University for his valuable comments on ESR measurements. This work was partly supported by a Grant-in-Aid for Scientific Research (09450132) and 1997 High-Tech Research Projects, both from the Ministry of Education, and by the Kawasaki Steel 21st Century Foundation. Measurements using synchrotron radiation were done as a Joint Research Project with the UVSOR Facility.

REFERENCES

1. Nakashima S, Izumi K. J Mater Res 1993;8:523.
2. Takahashi Y, Ishiyama T, Tabe M. Appl Phys Lett 1994;65:2987.
3. Mrstik BJ, McMarr PJ, Hughes HL, Anc MJ, Krull WA. Appl Phys Lett 1995;67:3283.
4. Kawamura K, Nakashima J, Hamaguchi I, Yano T, Nagake Y, Tachimori M. Proc 1995 IEEE International Conference on SOI:156.
5. Devine RAB, Leray J-L, Margail J. Appl Phys Lett 1991;59:2275.
6. Vanheusden K, Stesmans A. J Appl Phys 1993;74:275.
7. Ishii K, Isshiki D, Ohki Y, Nishikawa H, Takiyama M. Jpn J Appl Phys 1995;34:205.
8. Tohmon R, Mizuno H, Ohki Y, Sasagane K, Nagasawa K, Hama Y. Phys Rev B 1989;39:1337.
9. Seol KS, Ieki A, Ohki Y, Nishikawa H, Tachimori M. J Appl Phys 1996;79:412.
10. Devine RAB, Mathiot D, Warren WL, Fleetwood DM, Aspar B. Appl Phys Lett 1993;63:2926.
11. Ishii K, Ohki Y. Trans IEE Jpn 1992;112-A:118.
12. Arii K, Kitani I, Inuishi Y. Trans IEE Jpn 1973;93-A:313.
13. Shockley W. Solid-State Electron 1961;2:35.
14. Logan RA, White HG. J Appl Phys 1966;36:3945.
15. Shirafuji J, Inuishi Y. Oyobutsuri (Journal of the Japan Society of Applied Physics) 1971;39:508.
16. Takami A, Ishii K, Ohki Y. Extended Abstracts of the 44th Spring Meeting (1997) of the Japan Society of Applied Physics and Related Societies, 29a-A-6.
17. Tam S, Ko P-K, Hu C. IEEE Trans Electron Devices 1984;ED-31:1116.
18. Young DR. J Appl Phys 1976;47:2098.

AUTHORS (from left to right)

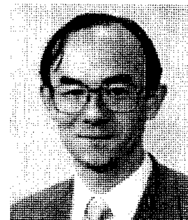

Kwang Soo Seol (student member) received his M.E. degree from Korea University in 1994 and his Ph.D. degree from Waseda University in 1998. He is now with the Institute of Physical and Chemical Research (RIKEN).

Hidemi Koike (nonmember) received his M.E. degree from Waseda University in 1998. He is now with Nippon Telegraph and Telephone Corporation.

Tsuyoshi Futami (nonmember) received his M.E. degree from Waseda University in 1999. He is now with Sony Corporation.

Yoshimichi Ohki (member) received his M.E. and Ph.D. degrees from Waseda University in 1975 and 1978. He is currently a professor and chairperson of the Department of Electrical, Electronics, and Computer Engineering of Waseda University. He is the recipient of several awards and a senior member of IEEE.

Fabrication of long-period optical fiber gratings by use of ion implantation

Makoto Fujimaki and Yoshimichi Ohki

Department of Electrical, Electronics, and Computer Engineering, Waseda University, 3-4-1 Ohkubo, Shinjuku-ku, Tokyo 169-8555, Japan

John L. Brebner and Sjoerd Roorda

Groupe de Recherche en Physique et Technologie des Couches Minces, Department of Physics, Université de Montréal, P.O. Box 6128, Station Centre-ville, Montreal, Quebec H3C 3J7, Canada

Received August 30, 1999

We report the fabrication of long-period optical fiber gratings by use of a refractive-index increase induced by ion implantation. Helium ions were implanted in an optical fiber core through a metal mask that had a 170-μm-pitch grating with spacing of 60 μm. We obtained a wavelength-dependent effective transmission loss by use of the grating. © 2000 Optical Society of America

OCIS codes: 060.0060, 220.4000, 230.1480, 160.6030, 230.0230, 350.2770.

Long-period optical fiber gratings formed by periodic refractive-index changes with periods of 100 μm to 1 cm in the core of an optical fiber work as narrow-band optical filters, mode converters, sensors, etc. by coupling two copropagating fiber modes.[1-5] Currently, these gratings are formed by refractive-index changes induced by ultraviolet photon irradiation.[1] To fabricate high-performance devices requires a high refractive-index change of ~0.001. However, standard optical fibers usually do not have enough photosensitivity for fabricating effective devices. Therefore, special fibers, e.g., high-Ge-concentration Ge-doped silica core fibers, are used to produce high-performance devices.[6] If fabricating the gratings in standard optical fibers is required, the fibers have to be sensitized by H_2 loading.[7,8] However, there still exist several kinds of optical fiber, such as pure silica-core fibers, that do not show sufficient photosensitivity even after sensitization.

It has been well known that relatively high refractive-index increases of as much as ~0.01 can be obtained by ion implantation in almost all silica-based glasses[9] and that the refractive-index increases are due mainly to compaction of the glasses.[9,10] Therefore, ion implantation makes it possible to fabricate optical fiber gratings in almost all kinds of silica-based optical fiber. In this Letter we report the successful fabrication of long-period cladding-mode-coupled gratings by implantation of He ions in an optical fiber.

The optical fiber used in the experiment was a Corning SMF-28 single-mode telecommunication fiber. The core of the fiber was Ge-doped silica glass of $97SiO_2{:}3GeO_2$ and had a diameter of 9 μm. The core was embedded in a cladding of pure silica glass with a diameter of 125 μm. The fiber was implanted with He^{2+} ions at room temperature in a vacuum of 10^{-6} Torr through a metal amplitude mask by use of the 1.7-MV tandem accelerator at the Université de Montréal. The acceleration energy of the He ions was 5.1 MeV, the maximum attainable. The mask was made of Ni:Co and had 29 periods of 170-μm-pitch grating with 60-μm spacing. Figure 1 shows a schematic of the alignment of the mask and the fiber. The transmission spectra of the fabricated gratings were observed with a spectrum analyzer (Hewlett-Packard 70951A).

Figure 2(a) shows a photograph of white light transmitted through the cross section of the He-ion-implanted optical fiber. The bright circle at the center is the light guided by the core of the fiber. The luminous arc across the fiber indicates the region in which the implanted He ions induced a significant refractive-index increase. As shown in Fig. 2(b), the depth of the arc from the optical fiber surface is ~24 μm, which corresponds to the projected range of the 5.1-MeV He ions in silica glass. Since ions must reach the core of the optical fiber to produce gratings in the core, we etched the cladding of the optical fiber with hydrofluoric acid (10% HF in H_2O) for 7 h and prepared an optical fiber with a cladding diameter of ~53 μm, as shown in Fig. 2(c). Figure 3 shows the transmission spectrum of the grating fabricated by the ion implantation with a dose of 20×10^{15} He^{2+}/cm^2. Very sharp and effective transmission loss owing to the coupling of the fundamental guided mode to a cladding mode was observed at 1410 nm.

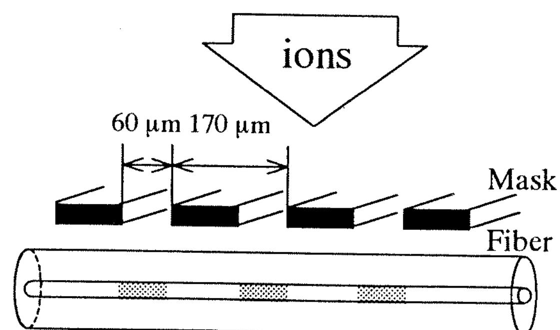

Fig. 1. Schematic of the alignment of the mask and the fiber.

0146-9592/00/020088-02$15.00/0 © 2000 Optical Society of America

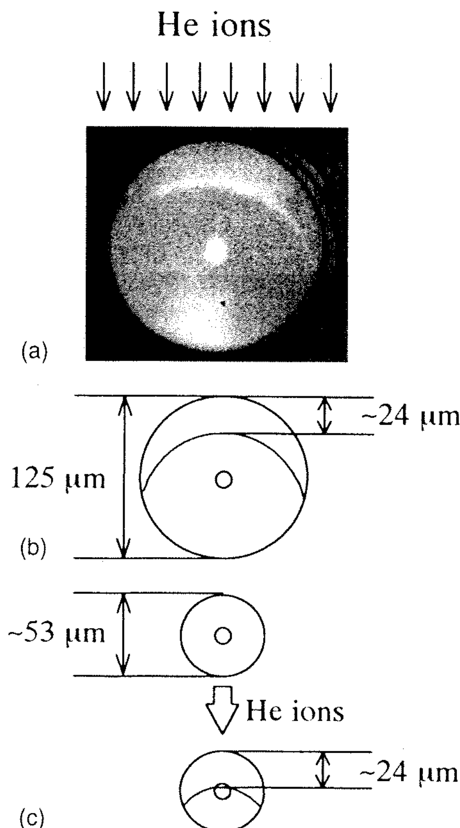

Fig. 2. (a) Photograph and (b) schematic of white light transmitted through the cross section of the He-ion-implanted optical fiber. (c) Schematic of the cross section of the optical fiber that was etched with hydrofluoric acid.

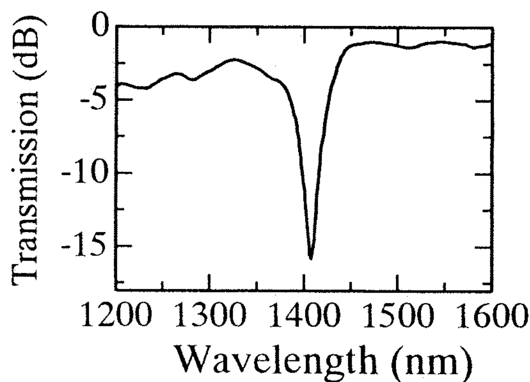

Fig. 3. Transmission spectrum of the grating fabricated by use of ion implantation.

As shown in Fig. 2, the induced refractive-index increase, indicated by the arc, was not only in the core but also in the cladding. This is so because the ion implantation induced a quite-high refractive-index increase even in pure silica glass. The refractive-index increase in the cladding causes a problem for the practical use of the gratings, because the fundamental guided mode can couple not only to the symmetric cladding modes but also to unsymmetrical ones, which results in high background loss, as can be seen in Fig. 3. However, this loss can be removed by use of a mask with narrow spacing, through which ions are implanted only in the core of the optical fiber. Furthermore, with a mask that has ~1-μm-pitch gratings, this method can be applied to the fabrication of Bragg gratings[11] in optical fibers.

In summary, we have shown that long-period optical fiber gratings can be fabricated by use of ion implantation. This method makes it possible to fabricate these gratings in almost all kinds of optical fiber.

The authors thank P. Berichon, R. Gosselin, and F. Schiettekatte for their assistance with the operation of the tandem accelerator. The authors also thank S. Lacroix of the École Polytechnique, Montreal, Quebec. This work was partly supported by a Grant-in-Aid to Japan Society for the Promotion of Science Fellows from the Ministry of Education, Science, Sports, and Culture of Japan and by the Natural Science and Engineering Research Council, Canada. Y. Ohki's e-mail address is yohki@mn.waseda.ac.jp.

M. Fujimaki is a research fellow of the Japan Society for the Promotion of Science.

References

1. A. M. Vengsarkar, P. J. Lemaire, J. B. Judkins, V. Bhatia, T. Erdogan, and J. E. Sipe, J. Lightwave Technol. **14**, 58 (1996).
2. E. M. Dianov, D. S. Stardubov, S. A. Vasiliev, A. A. Frolov, and O. I. Medvedkov, Opt. Lett. **22**, 221 (1997).
3. S. E. Kanellopoulos, V. A. Handerek, and A. J. Rogers, Proc. SPIE **2044**, 261 (1993).
4. K. O. Hill, B. Malo, K. Vineberg, F. Bilodeau, D. Johnson, and I. Skinner, Electron. Lett. **26**, 1270 (1990).
5. F. Bilodeau, K. O. Hill, B. Malo, D. Johnson, and I. Skinner, Electron. Lett. **27**, 682 (1991).
6. D. L. Williams, B. J. Ainslie, R. Kashyap, G. D. Maxwell, J. R. Armitage, R. J. Campbell, and R. Wyatt, Proc. SPIE **2044**, 55 (1993).
7. P. J. Lemaire, R. M. Atkins, V. Mizrahi, and W. A. Reed, Electron. Lett. **29**, 1191 (1993).
8. T. Erdogan, A. Partovi, V. Mizrahi, P. J. Lemaire, W. L. Wilson, T. A. Strasser, and A. M. Glass, Appl. Opt. **34**, 6738 (1995).
9. J. Albert, B. Malo, K. O. Hill, D. C. Johnson, J. L. Brebner, and R. Leonelli, Opt. Lett. **17**, 1652 (1992).
10. M. Verhaegen, L. B. Allard, J. L. Brebner, M. Essid, S. Roorda, and J. Albert, Nucl. Instrum. Methods Phys. Res. B **106**, 438 (1995).
11. K. O. Hill, Y. Fujii, D. C. Johnson, and B. S. Kawasaki, Appl. Phys. Lett. **32**, 647 (1978).

Defect and Diffusion Forum Vols. 177-178 (1999) pp. 43-50
© 1999 Scitec Publications, Switzerland

Structures and Optical Properties of Defects Correlated with Photo-induced Refractive Index Changes in Ge-doped SiO_2 Glass

Makoto Fujimaki[1] and Yoshimichi Ohki

Department of Electrical, Electronics, and Computer Engineering,
Waseda University, 3-4-1 Ohkubo, Shinjuku-ku, Tokyo 169-8555, Japan

[1]Research Fellow of the Japan Society for the Promotion of Science

Keywords: Ge Oxygen Deficient Centers, Optical Fiber Gratings, Paramagnetic Centers, Photosensitivity

Abstract. Photosensitivity of Ge-doped SiO_2 glass is closely related to defect formation with ultraviolet photon irradiation. In the present paper, optical properties of Ge oxygen deficient centers, which are involved in the defect formation, are reviewed. Furthermore, structures and generation mechanisms of the photo-induced defects are discussed.

1. Introduction

The Bragg grating [1] and long-period grating [2,3], which are formed with periodical refractive index changes in a core of an optical fiber, have been attracting much attention as optical devices. The simplest application of the Bragg grating in telecommunication is as a reflector [4-8]. Besides the reflector, the Bragg gratings are applied to semiconductor external fiber-cavity lasers [4], fiber lasers [4,5,7,9], sensors [10-12], dispersion cancellation [13,14], and so on. The long-period grating is used mainly as a band rejection filter [2]. To form the refractive index modulation, ultraviolet (uv) photon induced refractive index change in Ge-doped SiO_2 optical fiber core is utilized [1-3,15-17]. Therefore, it is very important to understand generation mechanisms of the refractive index changes in the glass to fabricate the gratings with high performance and high reliability. In the present paper, the photoinduced defect formations that contribute to the refractive index changes are reviewed. Since it has been reported that Ge oxygen-deficient centers (GODC's) existing in oxygen-deficient type glass are responsible for the defect formation that causes the refractive index change [18-21], the emphasis is placed on the review of researches about optical properties of the GODC's. Furthermore, mechanisms of uv-induced defects closely related to the GODC's are discussed.

2. Germanium Oxygen-deficient Centers

Oxygen-deficient type Ge-doped SiO_2 glass has intense absorption around 5.1 eV as shown in Fig. 1. It has been revealed that the 5-eV absorption is composed of two GODC's [18]. One is the neutral oxygen vacancy (NOV; ≡Ge–*T*≡, ≡ represents bonds with three separate oxygens and *T* is either Ge or Si) with a peak position at 5.06 eV [18], and the other is the Ge lone-pair center (GLPC; $-\ddot{\mathrm{G}}\mathrm{e}-$, '. .' denotes lone-pair electrons) with a peak position at 5.16 eV [22].

By absorbing 5 eV photons, the GLPC shows two photoluminescence (PL) bands at 4.3 and 3.1 eV. The PL spectrum observed with KrF excimer laser photon excitation (5.0 eV) is shown in Fig. 2. Skuja reported that the 4.3 and the 3.1 eV PLs are, respectively, due to the electronic transition from the lowest excited singlet state (S_1) to the ground state (S_0) and that from the lowest excited triplet state (T_1) to the S_0 state [23,24]. The lifetimes of the 3.1 and 4.3 eV PLs were

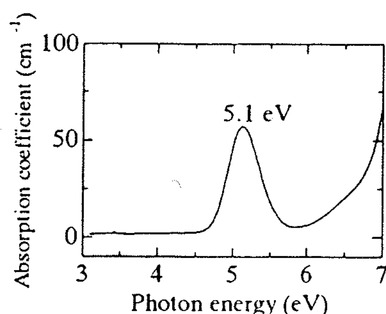

Fig. 1. Absorption spectrum of an oxygen-deficient type Ge-doped SiO_2 glass with Ge content of 1.0 mol %.

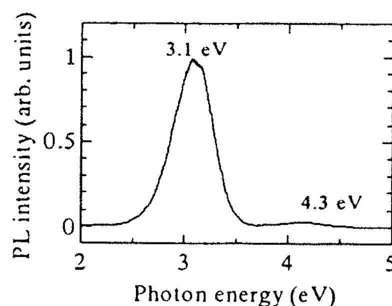

Fig. 2. PL spectrum of GLPC observed with KrF excimer laser photon excitation.

reported to be 113 μs [23] and 9 ns [25], respectively. As for the 3.1 eV PL, Gallagher and Osterberg [26] reported that there is a delay roughly 10 μs in duration between the 5-eV-photon excitation and the appearance of maximum PL intensity, and they concluded that there exists an energy transfer from an excited state in another defect to the T_1 state in the GLPC. The most probable candidate for the energy-absorbing defect was reported to be the NOV that has an absorption band at 5.06 eV. They also reported about the PL excitation (PLE) spectra in the vacuum-uv (vuv) region of the two PLs [27]. Based on the observed result that the PLE spectrum of the 3.1 eV PL extending below 215 nm was conspicuously absent in that of the 4.3 eV PL, they suggested that the PLE of the 3.1 eV PL in the vuv region is due to the electronic transition from the valence band to the S_1 state of the GLPC. However, in a recent research, we have observed a PLE band of the 4.3 eV PL in the vuv region [25]. The PLE spectra of the two PL bands observed at room temperature and 89 K are shown in Fig. 3. From this figure, it is observed that the 4.3 eV PL has PLE bands at 5.1 eV and above 6 eV. The peak seen around 4.3 eV is not a PLE band but a scattered excitation light. From this figure, it is understood that the 4.3 eV PL is stronger at 89 K than at room temperature for both PLE bands. The 3.1 eV PL has two similar PLE bands at 5.1 and above 6 eV and an additional small PLE band at 3.7 eV. When the PLE band at 5.1 eV is excited, the 3.1 eV PL is stronger at room temperature, but it becomes weaker at room temperature when it is excited by the PLE bands at 3.7 and above 6 eV.

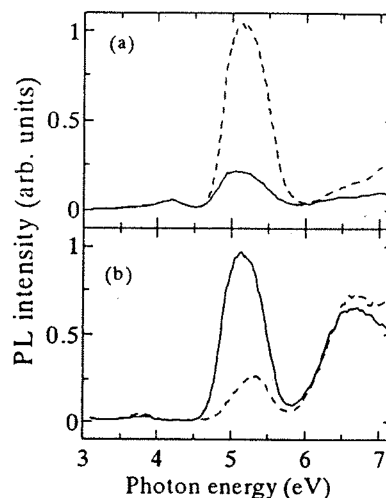

Fig. 3. PLE spectra of the 4.3 eV PL (a) and those of the 3.1 eV PL (b), at room temperature (solid curves) and at 89 K (broken curves).

Figure 4 shows the temperature dependence of the two PL intensities excited by 5.0 eV photons and 7.2 eV photons, respectively [25]. All signals are normalized by the maximum intensity of the 3.1 eV PL. Within an experimental error, the data were consistent with those shown in Fig. 3. When the PLs are induced by 5.0 eV photons, the 4.3 eV PL intensity decreases while the 3.1 eV PL intensity increases monotonically with an increase in the measurement temperature. In the case of 7.2 eV excitation, the 4.3 eV PL shows a similar temperature dependence to the one induced by 5 eV photons, while the 3.1 eV PL shows clearly different temperature dependence. The 3.1 eV PL induced by 7.2 eV photons does not show a significant

intensity change as seen in the PL induced by 5.0 eV photons, though it shows a blunt bottom around 200 K.

By using the energy diagram shown in Fig. 5 with the transition rate constants associated with the energy states, we explain the observed PL and PLE properties. In the figure, k_1 and k_2 are for radiative transitions and k_1' and k_2' are for nonradiative transitions. As mentioned above, the 4.3 eV and the 3.1 eV PLs are due to the electron transition from the S_1 state to the S_0 state and that from the T_1 state to the S_0 state at the GLPC, respectively. The small PLE band at 3.7 eV for the 3.1 eV PL is assigned to the direct electronic transition from the S_0 state to the T_1 state [23,28]. The temperature dependence of the 3.1 eV PL induced by the 5.0 eV photons showing a weaker intensity at a lower temperature is explainable by the suppression of k_3, i.e., the decrease in the number of electrons which move into the T_1 state thermally through the intersystem crossing [23]. This phenomenon and the suppression of the nonradiative relaxation from S_1 to S_0 (k_1') bring about a stronger intensity of the 4.3 eV PL at the lower temperature.

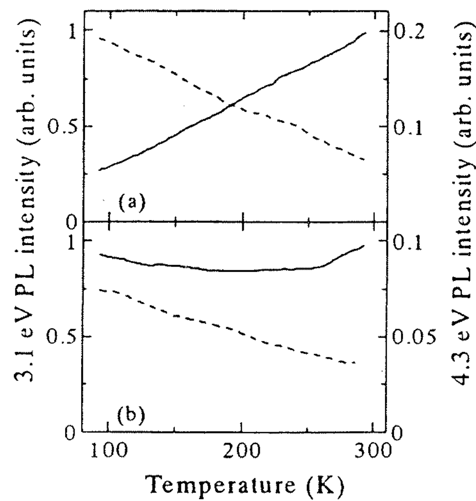

Fig. 4. Temperature dependence of the 4.3 eV PL (broken curves) and 3.1 eV PL (solid curves) excited by 5.0 eV photons (a) and 7.2 eV photons (b). All signals are normalized by the maximum intensities of the 3.1 eV PL.

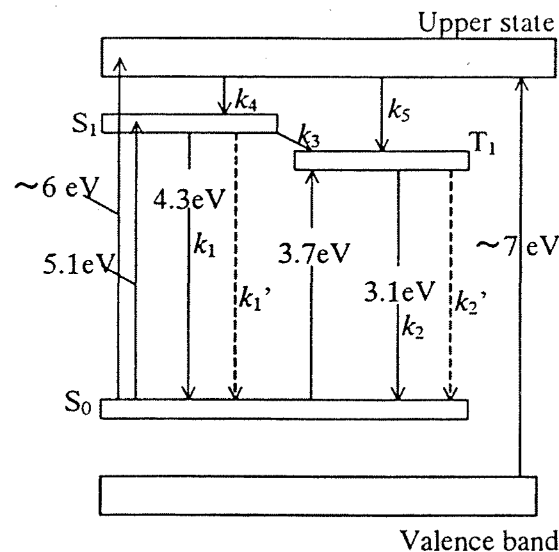

Fig. 5. Energy states of the GLPC. k_n (n =1 to 5), k_1' and k_2' denote the rate constants of the respective transitions.

As for the upper state that corresponds to the PLE band above 6 eV, through the calculations using the rate constants shown in Fig. 5 and the observed results shown in Fig. 4, we have figured out the strong contribution of the upper state to the 3.1 eV PL at low temperature [25]. From the obtained results, we deduced that the upper state is the conduction band of Ge-doped SiO_2 glass. Furthermore, by using a pump-probe method with a KrF excimer laser as a pumping photon source, we have succeeded in the observation of the absorption due to the electronic transition from the T_1 state to the conduction band [29].

The formation of the GODC's during the fabrication of the glass is mainly due to the thermodynamics of the gaseous Ge redox reaction at a high synthesis temperature [30]. With increasing temperature, reduction of GeO_2 is accelerated, which results in the promotion of GeO formation. This leads to the formation of GODC's in the glass. Treatment of Ge-doped SiO_2 glass in a hydrogen atmosphere at a high temperature also increases the GODC's concentration [28,31]. The following reaction (1) indicates the mechanism of the generation of the GLPC with H_2 treatment at a high temperature reported in [22].

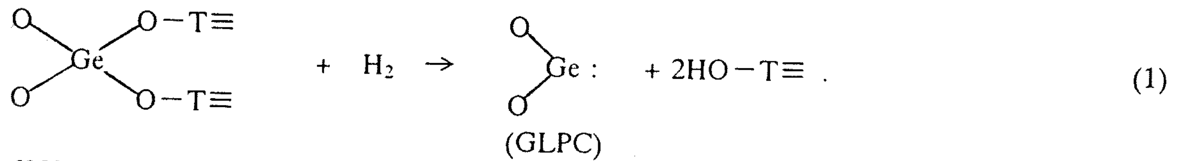

(GLPC)

In [32], it was also reported that the NOV is induced by thermal treatment at ~500 °C in a H_2 atmosphere. It is also reported that heat treatment of the glass in a H_2 atmosphere at > 800 °C induces Ge particles in the glass, resulting into brown coloring of the glass [32].

It has been reported that annealing in a N_2 atmosphere at 1000 °C increases the GODC concentration in a Ge-doped SiO_2 thin film with highly inhomogeneous Ge distribution, but not in a thin film with homogeneous Ge distribution [33]. This is because the deoxidization of ≡Ge-O-Ge≡ is easier than that of ≡Ge-O-Si≡ or ≡Si-O-Si≡ [18].

3. Germanium-related Paramagnetic Centers

Ionizing radiation induces Ge paramagnetic centers in Ge-doped SiO_2 glass. In 1974, four types of paramagnetic centers were distinguished, and it was supposed that the paramagnetic centers had a structure similar to the Si E' center (≡Si •, where "•" denotes an unpaired electron [34-36]) [37]. They were named Ge(n) centers (n=0,1,2,3), where n represents the number of Ge atoms in the next nearest neighbors. This interpretation was based on comparison of paramagnetic centers among crystal and glass samples of GeO_2 with a small content of Si and those of SiO_2 with a similar content of Ge.

In subsequent investigations on electron spin resonance (ESR) hyperfine structures in ^{73}Ge-doped SiO_2 glass, structures of two different paramagnetic centers were revealed: one is germanium electron center (GEC, where an electron is trapped at a fourfold-coordinated Ge) and the other is Ge E' center [38,39]. The latter is an analogue of the Si E' center. The ESR signal of GEC corresponds to Ge(1), and that of Ge E' center corresponds to Ge(3). In [40] and [41], the authors of [37] agreed with the GEC and Ge E' center models, and modified the models of Ge(1) and Ge(2) as the GEC that has 4 Si atoms at the next nearest neighbors and the GEC that has 3 Si atoms and 1 Ge atom at the next nearest, respectively. Figure 6 shows the ESR signals of the paramagnetic centers.

As the structure of Ge(2), another assignment has been reported in [42]. In the report, by using Ce^{3+} as a probe ion, the generation of the paramagnetic centers was investigated. Cerium enters into SiO_2 and Ge-doped SiO_2 glass mainly in the form of Ce^{3+} and is photoionized readily when excited in its absorption band of 320 nm, donating electrons in the process [43,44]. Through investigations about induced absorption and ESR spectra, it was found that selective photoionization of Ce^{3+} generates Ge(1) (=GEC), while Ge(2) is not induced by the ionization. From the results, the authors of [42] concluded that Ge(2) is a hole center at a GODC that acts as an electron donor to generate the GEC in the case that there are no electron donors such as Ce^{3+}. We have also investigated the defect structure of the Ge(2) and concluded that the Ge(2) is positively

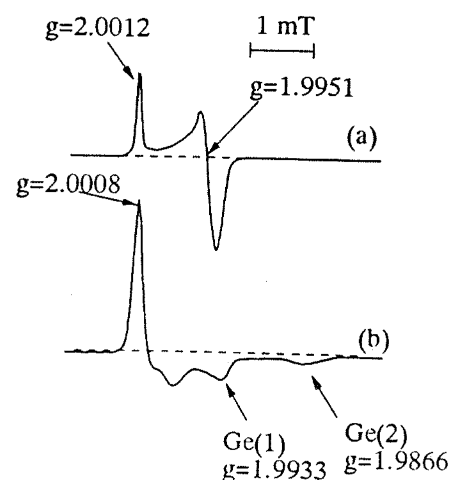

Fig. 6. ESR spectra of the paramagnetic centers. (a) Ge(3). (b) Ge(1) and Ge(2).

charged GLPC [=$(GLPC)^+$] [45]. The details are discussed in the next section.

These paramagnetic centers have absorption bands. The Ge E' center has an absorption band around 6.3 eV with the oscillator strength of 0.5 [46]. With the generation of GEC, two absorption bands around 4.4 and 5.8 eV are induced. These two absorption bands were, respectively, assigned to Ge(1) and Ge(2) in [40,47]. However, in a recent research, it was found that the 5.8 eV absorption band is induced by KrF excimer laser photon irradiation in H_2-loaded Ge-doped SiO_2 glass, while the Ge(2) is not. This result indicates that the 5.8 eV absorption band is not due to the Ge(2) [48]. Since the Ge(1) (=GEC) is induced in the H_2-loaded sample by the irradiation and it has been reported that both the intensities of the 4.5 and 5.8 eV absorption bands are proportional to the concentration of Ge(1) [45], it is concluded that both of the absorption bands are due to the Ge(1) [48].

4. Ultraviolet-induced Defect Formation

Photoinduced absorption changes accompanied with the induction of the paramagnetic centers cause the photorefractive index change through the Kramers-Kronig relation [21,49], which is utilized for the Bragg grating and long-period grating. Therefore, many studies have been done to elucidate the generation mechanisms of the paramagnetic centers.

In [18], a linear relation was found between the decrement in the intensity of the 5.06-eV absorption band and the concentration of the uv-induced Ge E' center. This relation was a basis for attributing the defect responsible for the 5.1 eV absorption component, NOV, to the precursor of the uv-induced Ge E' center. The photochemical reaction is expressed as follows:

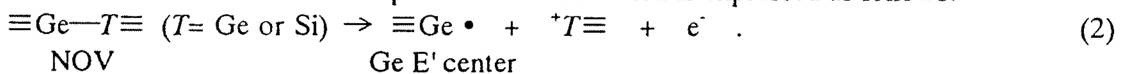

$$\equiv Ge—T\equiv \ (T = \text{Ge or Si}) \rightarrow \ \equiv Ge\bullet \ + \ {}^{+}T\equiv \ + \ e^- \ . \qquad (2)$$

NOV Ge E' center

In this report, the oscillator strength of the NOV at the 5.06 eV absorption band was evaluated to be approximately 0.4 from the decreased intensity of the absorption band and the induced density of the Ge E' center that corresponds to the decreased density of the NOV.

If the random distribution of Ge atoms in the glass is assumed, the most probable NOV is $\equiv$Ge–Si$\equiv$. Since the electronegativity (1.8 on the Pauling scale [50]) of Ge^{4+} is the same as that (1.8) of Si^{4+}, it is reasonable to expect that both the Si E' center and Ge E' center are created during uv-irradiation. However, only Ge E' center is observed experimentally in the glass after uv-irradiation [18,51]. In Ge-doped SiO_2 glass, there exists a Ge-rich phase, which was observed with a scanning electron microscope [52] and a transmission electron microscope [51]. The discrepancy between the prediction from the random distribution and the experimental observation can be explained by the existence of the Ge-rich phase in glasses, i.e., the NOV's exist in the Ge-rich phase and consequently they are coordinated by two Ge atoms.

Induction of the GEC is also very important for the refractive index change. It has been reported that the GEC's are induced by strong uv-photons from ArF (6.4 eV), KrF (5.0 eV), or XeCl (4.0 eV) excimer laser through a two-photon process [53-55]. The GEC's are converted to the Ge E' centers with prolonged uv-irradiation [55]. Since the precursor of the GEC is a fourfold coordinated Ge (a normal bonding Ge in GeO_2-SiO_2), the conversion means that a normal bonding in the glass becomes the Ge E' center via GEC. The Ge E' center that has a large absorption at 6.3 eV is the most stable paramagnetic center in Ge-doped SiO_2 glass. Therefore, the series of the photochemical reaction (normal bonding→GEC→Ge E' center) should cause a stable refractive index change. However, the generation mechanism of the GEC, especially the electron donor to generate GEC, is still debated. The electrons released from the NOV's (see Eq. (2)) do not generate the GEC, since the generation of the GEC is independent of the photo-chemical reaction indicated in Eq. (2).

As mentioned above, it was reported that the lowest energy required to induce the GEC was 8.0 eV, through the two-photon excitation of 4.0 eV photons from a XeCl excimer laser [53,55]. Since the energy, 8.0 eV, is bigger than the energy gap of Ge-doped SiO_2 glass (7.1 eV), the authors

of [55] concluded that electrons excited from the valence band to the conduction band form the GEC. Since the lone-pair electrons of the bridging oxygen in GeO_2-SiO_2 network form the upper level of the conduction band, the authors of [55] assigned that the electron donor is the bridging oxygen. However, in [45], we have shown that the threshold photon energy to generate the GEC is ~5.6 eV, which is much smaller than the band gap. Furthermore, through an investigation of the correlation between concentrations of photoinduced GEC and intensities of absorption changes in four different samples with different Ge contents, we found that the increase in the GEC concentration is always proportional to the decrease in the 5.1 eV absorption band irrespective of the samples [45]. This result clearly indicates that the electron donor is a GODC that has an absorption band at 5.1 eV. From the proportionality constant between the increase in the GEC concentration and the decrease in the 5.1 eV band intensity, the oscillator strength of the 5.1 eV band is calculated to be 0.1. Since the GODC that has 5.1 eV band with the oscillator strength of 0.1 is the GLPC [18], it is deduced that the electron donor is the GLPC. As reported in [55], the bridging oxygen can also be an electron donor. However, since the GEC is hardly induced in a glass without the 5.1 eV band, the contribution of the bridging oxygen is quite small.

The GLPC that released an electron becomes the $(GLPC)^+$. Since the $(GLPC)^+$ is a paramagnetic center, it should be detected in an ESR measurement. The observed signals in the experiment in [45] were only the Ge(1) and Ge(2), where the Ge(1) has been assigned to the GEC as mentioned above. Therefore, the Ge(2) should be the $(GLPC)^+$. It might be unreasonable to assign the Ge(2) signal, whose g value is smaller than 2.0023, to a hole center. However, it has been reported that the defect which shows the Ge(2) signal acts like a hole center [42]. Furthermore, a trapped hole on Sn^{2+} shows the ESR signal with g values smaller than 2.0023, $g_{\parallel}=1.972$ and $g_{\perp}=2.000$, where Sn^{2+} indicates the Sn lone-pair center in tin oxide [56]. Since Sn is a congener of Ge, this fact supports the assumption that the Ge(2) signal is due to the $(GLPC)^+$, even though the g value is smaller than 2.0023.

It has been reported that the intensity of the 3.1 eV PL band that is due to the GLPC decreases with photorefractive index changes [27,57-59]. The above-mentioned mechanism must contribute to the decrement of the PL intensity. Furthermore, it has been reported that thermally stimulated luminescence (TSL) is observed in KrF excimer laser photon irradiated samples [45]. The TSL spectrum is identical to the 3.1 eV PL of the GLPC. It was found that the GEC, which was induced by the KrF excimer laser photons, decreases during the TSL measurement and that this decrement is proportional to the TSL intensity [45]. As mentioned above, the electrons that are to be trapped to generate the GEC's are released from the GLPC's. Then, in the reverse reaction, these electrons are thermally detrapped from the GEC's to regenerate the GLPC's, and the TSL is caused by an electronic de-excitation in such formed GLPC's. The TSL phenomenon further validates the model that the GLPC is the electron donor to generate the GEC.

As mentioned in the previous section, the Ge(2), i.e., $(GLPC)^+$, is not observed in H_2-loaded Ge-doped SiO_2 glass even after the laser photon irradiation. This is because the $(GLPC)^+$ is terminated by hydrogen [48]. Therefore, the TSL is scarcely observed in H_2-loaded glass.

References

[1] K. O. Hill, Y. Fujii, D. C. Johnson, and B. S. Kawasaki, Appl. Phys. Lett. **32**, (1978), p.647.

[2] A. M. Vengsarkar, P. J. Lemaire, J. B. Judkins, V. Bhatia, T. Erdogan, and J. E. Sipe, J. Lightwave Technol. **14**, (1996), p. 58.

[3] E. M. Dianov, D. S. Stardubov. S. A. Vasiliev, A. A. Frolov, and O. I. Medvedkov, Opt. Lett. **22**, (1997), p. 221.

[4] D. M. Bird, J. R. Armitage, R. Kashyap, R. M. A. Fatah, and K. H. Cameron, Electron. Lett. **27**, (1991), p. 1115.

[5] G. A. Ball, W. W. Morey, and J. P. Waters, Electron. Lett. **26**, (1990), p. 1829.

[6] J. L. Zyskind, V. Mizrahi, D. J. DiGiovanni, and J. W. Sulhoff, Electron. Lett. **28**, (1992), p. 1385.

[7] R. P. Davey, K. Smith, R. Kashyap, and J. R. Armitaga, Electron. Lett. **27**, (1991), p. 2087.
[8] F. Bilodeau, B. Malo, D. C. Johnson, J. Albert, S. Theriault, and K. O. Hill, Tech. Dig. Ser.-Opt. Soc. Am. **8**, (1995), p. 130.
[9] A. Inoue, M. Shigematsu, M. Ito, M. Imai, M. Inai, Y. Hattori, and T. Mizunami, Optoelectron., Devices Technol. **10**, (1995), p. 119.
[10] W. W. Morey, G. Meltz, and W. H. Glenn, Proc. SPIE **1169**, (1990), p. 98.
[11] R. Kashyap, J. R. Armitage, R. J. Campbell, D. L. Williams, G. D. Maxwell, B. J. Ainsle, and C. A. Millar, BT Technol. J. **11**, (1993), p. 150.
[12] S. M. Melle, L. Kexing, and R. M. Measures, IEEE Photonics Technol. Lett. **4**, (1992) p. 516.
[13] F. Ouellette, Opt. Lett. **12**, (1987), p. 847.
[14] K. O. Hill, F. Bilodeau, B. Malo, T. Kitagawa, S. Theriault, D. C. Johnson, and J. Albert, Tech. Dig. Ser.-Opt. Soc. Am. **4**, (1994), p. 335.
[15] G. Meltz, W. W. Morey, and W. H. Glenn, Opt. Lett. **14**, (1989), p. 823.
[16] C. G. Askins, T. E. Tsai, G. M. Williams, M. A. Putnam, M. Bashkansky, and E. J. Friebele, Opt. Lett. **17**, (1992), p. 833.
[17] K. O. Hill, B. Malo, F. Bilodeau, D. C. Johnson, and J. Albert, Appl. Phys. Lett. **62**, (1993), p. 1035.
[18] H. Hosono, Y. Abe, D. L. Kinser, R. A. Weeks, K. Muta, and H. Kawazoe, Phys. Rev. B **46**, (1992), p. 11445.
[19] V. B. Neustruev, E. M. Dianov, V. M. Kim, V. M. Mashinsky, M. V. Romanov, A. N. Guryanov, V. F. Khopin, and V. A. Tikhomirov, Fiber Integrated Opt. **8**, (1989), p. 143.
[20] R. M. Atkins and V. Mizrahi, Electron. Lett. **28**, (1992), p. 1743.
[21] L. Dong, J. L. Archambault, L. Reekie, P. St. J. Russell, and D. N. Payne, Appl. Opt. **34**, (1995), p. 3436.
[22] K. Awazu, H. Kawazoe, and M. Yamane, J. Appl. Phys. **68**, (1990), p. 2713.
[23] L. Skuja, J. Non-Cryst. Solids **149**, (1992), p. 77.
[24] L. N. Skuja, A. N. Trukhin, and A. E. Plaudis, Phys. Stat. Sol. (a) **84**, (1984), p. K153.
[25] M. Fujimaki, Y. Ohki, and H. Nishikawa, J. Appl. Phys. **81**, (1997), p. 1042.
[26] M. Gallagher and U. Osterberg, Appl. Phys. Lett. **63**, (1993), p. 2987.
[27] M. Gallagher and U. Osterberg, J. Appl. Phys. **74**, (1993), p. 2771.
[28] M. Kohketsu, K. Awazu, H. Kawazoe, and M. Yamane, Jpn. J. Appl. Phys. **28**, (1989), p. 622.
[29] M. Fujimaki, K. S. Seol, and Y. Ohki, J. Appl. Phys. **81**, (1997), p. 2913.
[30] V. B. Neustruev, J. Phys.: Condens. Matter **6**, (1994), p. 6901.
[31] K. Muta, A. Kashiwazaki, and H. Kawazoe, Diffus. Defect Data **53-54**, (1987), p. 93.
[32] H. Hosono, H. Kawazoe, and K. Muta, Appl. Phys. Lett. **63**, (1993), p. 479.
[33] M. Fujimaki, S. Shimoto, N. Miyazaki, Y. Ohki, K. S. Seol, and K. Imamura, J. Appl. Phys. **86**, (1999), p. 5270.
[34] R. A. Weeks, J. Appl. Phys. **27**, (1951), p. 1376.
[35] D. L. Griscom, Phys. Rev. B **20**, (1979), p. 1823.
[36] D. L. Griscom, E. J. Friebele, and G. H. Sigel, Jr., Sol. State Commun. **15**, (1974), p. 479.
[37] E. J. Friebele, D. L. Griscom, and G. H. Sigel, Jr., J. Appl. Phys. **45**, (1974), p. 3424.
[38] Y. Watanabe, H. Kawazoe, K. Shibuya, and K. Muta, Jpn. J. Appl. Phys. **25**, (1986), p. 425.
[39] H. Kawazoe, J. Non-Cryst. Solids **71**, (1985), p. 231.
[40] E. J. Friebele and D. L. Griscom, in *Defects in Glasses*, edited by F. L. Galeener, D. L. Griscom, and M. J. Weber, MRS Symposia Proceedings No. 61 (Materials Research Society, Pittsburgh, 1986), p. 319.
[41] T. E. Tsai, D. L. Griscom, and E. J. Friebele, Diffus. Defect Data Pt. B **53-54**, (1987), p. 469.
[42] E. V. Anoikin, A. N. Guryanov, D. D. Gusovskii, V. M. Mashinskii, S. I. Miroshnichenko, V. B. Neustruev, V. A. Tikhomirov, and Yu. B. Zverev, Sov. Lightwave Commun. **1**, (1991), p. 123.
[43] J. S. Stroud, J. Chem. Phys. **35**, (1961), p. 844.
[44] V. I. Arbuzov, M. N. Tolstoi, M. A. Elerts, and Y. S. Trokshs, Fiz. Khim. Stekla **13**, (1987), p.

581.
[45] M. Fujimaki, T. Watanabe, T. Katoh, T. Kasahara, N. Miyazaki, Y. Ohki, and H. Nishikawa, Phys. Rev. B **57**, (1998), p. 3920.
[46] H. Hosono, M. Mizuguchi, H. Kawazoe, and J. Nishii, Jpn. J. Appl. Phys. **35**, (1996), p. L234.
[47] E. V. Anoikin, A. N. Guryanov, D. D. Gusovskii, V. M. Mashinskii, S. I. Miroshnichenko, V. B. Neustruev, and V. A. Tikhomirov, Sov. Lightwave Commun. **1**, (1991), p. 29.
[48] M. Fujimaki, T. Kasahara, S. Shimoto, N. Miyazaki, S. Tokuhiro, K. S. Seol, and Y. Ohki, Phys. Rev. B **60**, (1999), p. 4682.
[49] D. L. Williams, S. T. Davey, R. Kashyap, J. R. Armitage, and B. J. Ainslie, Electron. Lett. **28**, (1992), p. 369.
[50] L. Pauling, *The Nature of the Chemical Bond*, 3rd ed. (Cornell University Press, Ithaca, NY, 1960).
[51] H. Hosono, K. Kawamura, H. Kawazoe, and J. Nishii, J. Appl. Phys. **80**, (1996), p. 3115.
[52] K. Nagasawa and Y. Ohki, Jpn. J. Appl. Phys. **25**, (1986), p. L682.
[53] H. Hosono, H. Kawazoe, and J. Nishii, Phys. Rev. B **53**, (1996), p. R11 921.
[54] M. Fujimaki, K. Yagi, Y. Ohki, H. Nishikawa, and K. Awazu, Phys. Rev. B **53**, (1996), p. 9859.
[55] J. Nishii, K. Fukumi, H. Yamanaka, K. Kawamura, H. Hosono, and H. Kawazoe, Phys. Rev. B **52**, (1995), p. 1661.
[56] H. Kawazoe, J. Nishii, H. Hosono, T Kanazawa, and H. Imagawa, J. Physique Colloq. **43** (1982), p. C9-155.
[57] E. M. Dianov, D. S. Starodubov, and A. A. Frolov, Electron. Lett. **32**, (1996), p. 246.
[58] M. Poirier, S. Thibault, J. Lauzon, and F. Ouellette, Opt. Lett. **18**, (1993), p. 870.
[59] Y. Duval, R. Kashyap, S. Fleming, and F. Ouellette, Appl. Phys. Lett. **61**, (1992), p. 2955.

Jpn. J. Appl. Phys. Vol. 38 (1999) pp. 6791–6796
Part 1, No. 12A, December 1999
©1999 Publication Board, Japanese Journal of Applied Physics

Effect of Ozone Annealing on the Charge Trapping Property of Ta_2O_5–Si_3N_4–p-Si Capacitor Grown by Low-pressure Chemical Vapor Deposition

Hiromitsu KATO[1], Kwang Soo SEOL[2], Makoto FUJIMAKI[1,3], Takehiko TOYODA[1], Yoshimichi OHKI[1] and Makoto TAKIYAMA[4]

[1]*Department of Electrical, Electronics, and Computer Engineering, Waseda University, Shinjuku-ku, Tokyo 169-8555, Japan*
[2]*RIKEN (The Institute of Physical and Chemical Research), 2-1 Hirosawa, Wako, Saitama 351-0198, Japan*
[3]*Research Fellow of the Japan Society for the Promotion of Science*
[4]*NSC Electron Corporation, 3434 Shimada, Hikari, Yamaguchi 743-0063, Japan*

(Received April 19, 1999; accepted for publication September 16, 1999)

The effect of ozone annealing on the charge trapping property of Ta_2O_5/Si_3N_4/p-Si capacitors was examined by measuring high-frequency capacitance-voltage and thermally stimulated current characteristics. The results suggest that two types of electron traps exist in the Ta_2O_5 layer and that the ozone annealing efficiently eliminates them.

KEYWORDS: tantalum pentaoxide (Ta_2O_5), ozone annealing, charge trapping property, hysteresis loop, thermally stimulated current

1. Introduction

Recent integration of metal-oxide-semiconductor memories continuously requires the scaling down of capacitor dielectrics, and pushes the conventional SiO_2 or Si_3N_4 films close to the physical limit of dielectric strength in terms of reduction in thickness. This has led to the study of materials with a high permittivity used for capacitor dielectrics. Among the high permittivity materials, tantalum pentaoxide (Ta_2O_5) is considered to be an appropriate and technologically compatible material.[1–3]

Ta_2O_5 can be fabricated using several methods such as sputtering and chemical vapor deposition (CVD). For the CVD methods, organometallic precursors such as $Ta(OC_2H_5)_5$ and $Ta(OCH_3)_5$ are commonly used. The CVD-deposited film exhibits a good step-coverage, which is important in current ultra-large-scale integrated circuit structures. However, it does have a problem in its large leakage current.[4–8] Recently, it has been found that the leakage current can be decreased by a post-deposition treatment such as oxidation at high temperatures (650–800°C),[6–8] ozone annealing,[4] ultraviolet ozone annealing,[5] and oxygen plasma annealing.[9] The leakage current is considered to cause the deterioration of Ta_2O_5 films and to form carrier traps. In this paper, we report the effect of ozone annealing on the charge trapping property of Ta_2O_5 films grown on Si_3N_4 barrier layers by a low-pressure CVD (LPCVD) method.

2. Experimental Procedures

Figure 1 shows the structure of the capacitor investigated in this study. Silicon monocrystal wafers with a resistivity of 10 Ωcm were used as starting substrates. Boron implantation (1×10^{15} cm^{-2}, 15 keV) was performed on the back of wafers to provide a p$^+$ ohmic contact. Rapid thermal annealing at 900°C in a N_2 atmosphere for 30 min was used to activate the implanted boron. The Ta_2O_5 layer was deposited by LPCVD using $Ta(OC_2H_5)_5$ as a precursor on a Si_3N_4 barrier layer that had been grown by LPCVD on the silicon substrate. Some samples were annealed in a stream of oxygen gas containing ozone at 300°C for 5 min. Both the as-deposited and ozone-treated samples were then oxidized at 800°C for 30 s in oxygen using a rapid thermal reactor. The Ta_2O_5 and Si_3N_4 layers were divided into small cells by chlorine etching and the local

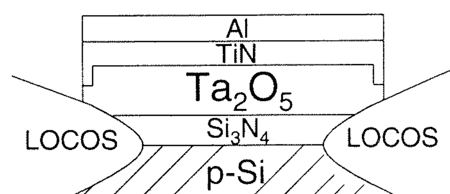

Fig. 1. Structure of capacitor examined. LOCOS: local oxidation of silicon.

oxidation of silicon (LOCOS). The thickness, the equivalent SiO_2 thickness, and the post-deposition treatment condition of each sample are listed in Table I. The thickness was measured using an ellipsometer and observed in sectional images taken using a scanning electron microscope. The equivalent SiO_2 thickness, which is the thickness of SiO_2 with the same capacitance as that of the actual Si_3N_4/Ta_2O_5 layer, was calculated from the capacitance value measured using a high-frequency capacitance–voltage (C–V) meter at 1 MHz. The relative permittivity values of SiO_2 and Si_3N_4 were assumed to be 3.9[10] and 7.9,[10] respectively. From these measurements, the relative permittivity of Ta_2O_5 was calculated to be 28 ± 3, which is quite a reasonable value.[10] As an upper electrode and its cover layer, TiN and Al, respectively, were sputtered on the Ta_2O_5 layer. Specimens S1 and S2 were used to measure the leakage current, and S3, S4, S5, and S6 were used for the measurement of charge trapping properties.

The charge trapping property was examined by C–V measurement. The voltage was applied to the gate metal electrode and was swept at a constant rate of 0.2 V/s.

The measurement condition of the thermally stimulated current (TSC) was as follows. The poling voltage, from +4 to +8 V, was applied to the gate metal electrode and the sample temperature was decreased from room temperature to −80°C. After 15 min at −80°C, the power supply was removed and an ammeter was connected. The current was measured while the sample temperature was raised from −80°C to +120°C at a constant rate of 2°C/min.

The leakage current was measured by applying a positive or negative dc voltage while changing its value from 0 to 10 V in a stepwise manner with a step of 0.05 V. The holding time at each step was 0.08 s. The voltage was always applied to the gate metal electrode and the p-Si side was grounded. The

Table I. Sample thickness, equivalent SiO_2 thickness, and treatment conditions.

Specimen	Thickness		Treatment conditions		Equivalent SiO_2 thickness
	Si_3N_4	Ta_2O_5	Ozone annealing	RTO	
S1	2 nm	31 nm	N	800°C, 30 s	5.3 nm
S2	2 nm	31 nm	300°C, 5 min	800°C, 30 s	5.7 nm
S3	3 nm	10 nm	N	800°C, 30 s	2.9 nm
S4	3 nm	20 nm	N	800°C, 30 s	4.7 nm
S5	3 nm	31 nm	N	800°C, 30 s	5.4 nm
S6	3 nm	31 nm	300°C, 5 min	800°C, 30 s	5.8 nm

N: not annealed.

electrode area was 0.1 mm^2 for the C–V and leakage current measurements, and 10 mm^2 for the TSC measurement.

3. Results and Discussion

Figure 2 depicts the leakage current characteristics for the samples with and without ozone annealing. It is shown that the ozone annealing is effective in reducing the leakage current.

Figure 3 shows typical C–V hysteresis curves measured at 1 MHz. Here, C_{in} is the capacitance of the insulation layer in which Ta_2O_5 and Si_3N_4 are in series. The thickness of the Ta_2O_5 layer was about 31 nm. The gate voltage (V_G) was swept from negative to positive at a constant rate of 0.2 V/s and then swept back. Samples both with and without the ozone annealing exhibit a counterclockwise hysteresis loop. However, there are two differences between the loops of the samples with and without ozone annealing: (i) a step appears in the hysteresis loop of the ozone-treated sample, (ii) the flat band voltage (V_{FB}) of the ozone-treated sample shifts more in the negative voltage direction than that of the sample without ozone annealing.

Regarding the reason for the hysteresis, two possibilities can be considered based on the direction of the hysteresis loop:

(1) The electrons appearing in the inversion layer built at the silicon surface are injected into the insulating Ta_2O_5/Si_3N_4 layer and are trapped there. The presence of electrons with negative charges is equivalent to the application of negative bias for p-Si. Therefore, the capacitance C increases. In the accumulation mode when $V_G < V_{FB}$, the trapped electrons are ejected and move back to silicon, and C ceases to increase.

(2) When $V_G < V_{FB}$ (accumulation), holes appear on the silicon surface and are injected into Ta_2O_5/Si_3N_4 and trapped, causing the decrease in C. They are then ejected and move back to silicon when $V_G > V_{FB}$ (depletion or inversion).

The possibility of electron trapping was examined by measuring C–V curves by changing V_G from inversion to accumulation with various starting voltages in order to obtain the right half of the hysteresis loop. If assumption (1) is true, more electrons should be injected into the insulation layer if V_G (>0) is higher. Figure 4 shows the results. Here, the starting voltages of V_G were set to be 4, 5, 6, 7, 8, 9 and 10 V. Note that seven curves converge into an apparently single line in Fig. 4(b). When the ozone annealing is not applied, the C–V curve clearly shifts to the right, i.e., the positive side, with an increase in the starting voltage. On the other hand, the

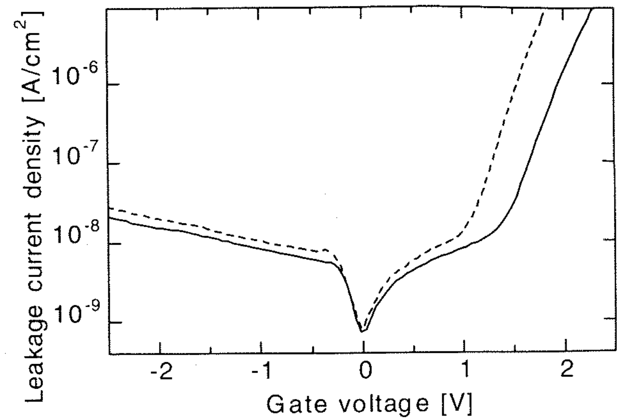

Fig. 2. Comparison of the leakage current density between samples with ozone annealing (solid curve) and without ozone annealing (broken curve).

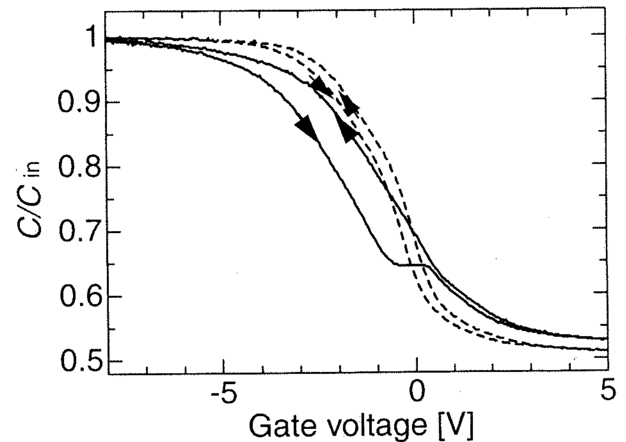

Fig. 3. Comparison of C–V curve measured at 1 MHz between the capacitor with ozone annealing (solid curve) and without ozone annealing (broken curve). Capacitance (C) was normalized by capacitance (C_{in}) of the Ta_2O_5/Si_3N_4 insulator layer.

ozone-treated sample does not exhibit any shift at all. The relationship between the starting voltage and the flat-band voltage V_{FB} estimated based on Fig. 4 for samples with and without ozone annealing is shown in Fig. 5. On the basis of these results, it is considered that electron trapping occurs only in the sample not subjected to ozone annealing.

In order to confirm the distribution of electron traps, the change in V_{FB} (ΔV_{FB}) in the hysteresis loop was measured as a function of the thickness of the Ta_2O_5 layer. The result is shown in Fig. 6. The effective trapped charge density (Q_{eff}) calculated from the relation, $Q_{eff} = -C_{in}\Delta V_{FB}$, is also shown. The value of Q_{eff} increases almost linearly with an increase in the Ta_2O_5 thickness. This fact indicates that the concentration of electron trap centers is high in the vicinity of the interface between the insulation layer and the silicon substrate.

Next, the possibility of hole trapping was examined. Figure 7 shows C–V curves measured for the samples with and without ozone annealing. The curves were obtained by sweeping V_G from various negative starting voltages in the accumulation region to the inversion region so as to obtain the left half of the hysteresis loop. From Fig. 7(a), it is clear that the curve of the sample without ozone annealing does not change at all, while the curve of the ozone-annealed sample

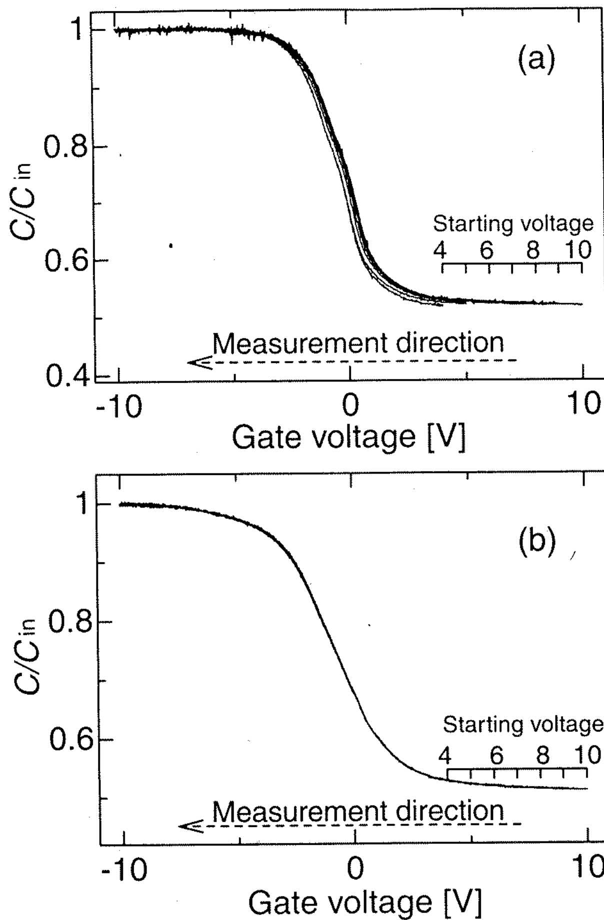

Fig. 4. C–V curves measured by sweeping V_G from inversion to accumulation. The voltage at which the sweep started was changed. (a) Without ozone annealing, (b) with ozone annealing.

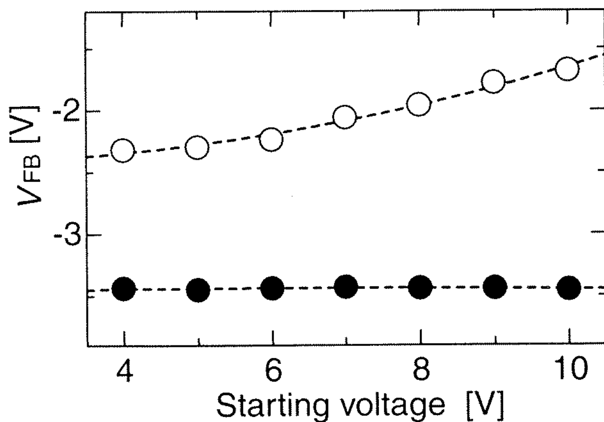

Fig. 5. Relationship between V_{FB} and the starting voltage of sweep, observed for samples with ozone annealing (solid circles) and without ozone annealing (open circles).

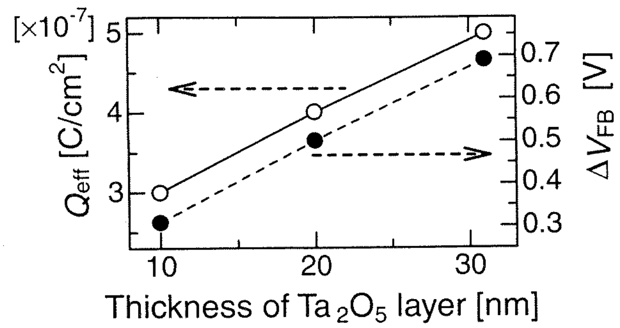

Fig. 6. Q_{eff} and ΔV_{FB} as a function of Ta_2O_5 layer thickness.

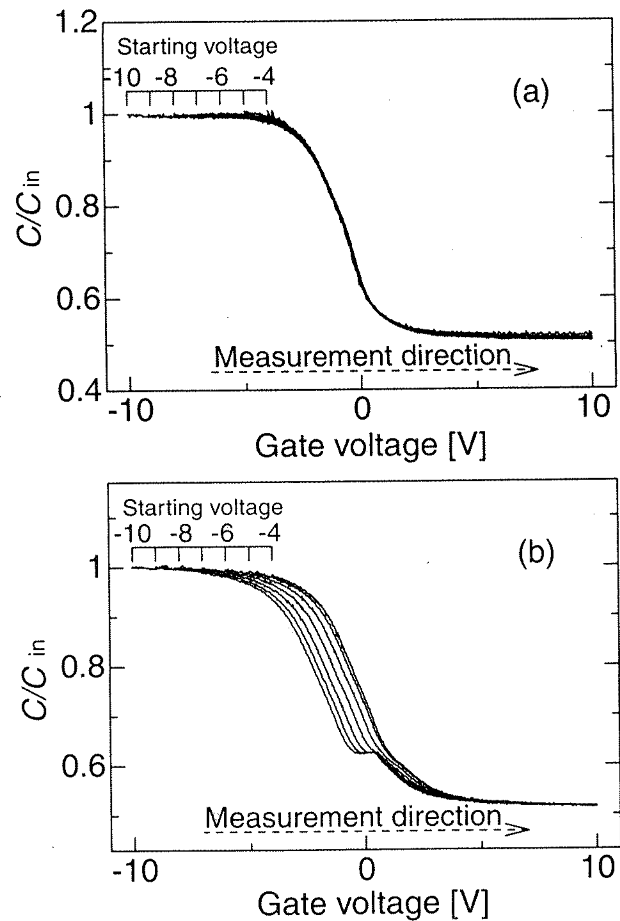

Fig. 7. C–V curves measured by sweeping V_G from accumulation to inversion. The voltage at which the sweep started was changed. (a) Without ozone annealing, (b) with ozone annealing.

shifts in the negative voltage direction as the starting voltage becomes more negative. The change in V_{FB} as a function of the starting voltage is shown in Fig. 8. This result indicates that hole trapping occurs only in the ozone-annealed sample.

The data shown in Fig. 7(b) also indicate another important factor, in that the step in the C–V curve appears when the starting voltage is below -7 V, and that the step width increases as the starting voltage becomes more negative. The step is considered to be due to the ejection of holes trapped in the depletion layer. The width of the depletion layer in the Si substrate grows with an increase in V_G, which decreases the total capacitance of the capacitor. However, if all the trapped holes in the Ta_2O_5/Si_3N_4 layer are ejected into the depletion layer, the growth of the depletion layer would cease and the capacitance would become constant with an increase in V_G. This is considered to be the mechanism of the step appearing in the C–V curve.

The hole traps that give rise to the step are thought to be induced by high electric fields, since the step appears when the starting voltage (which is negative) is below -7 V. Furthermore, on the basis of the finding that the shift of V_{FB} in the negative voltage direction occurs even above -7 V (at -4

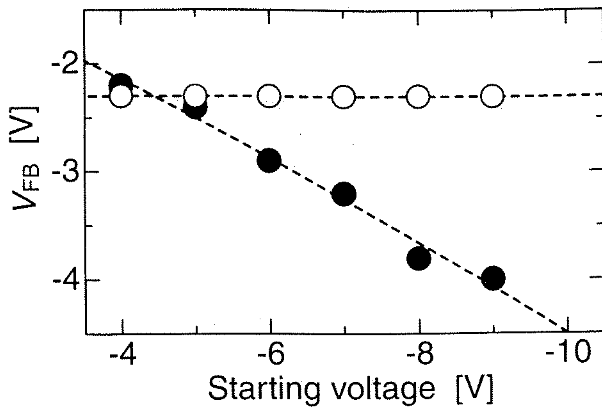

Fig. 8. Relationship between V_{FB} and the starting voltage of sweep, observed for the samples with ozone annealing (solid circles) and without ozone annealing (open circles).

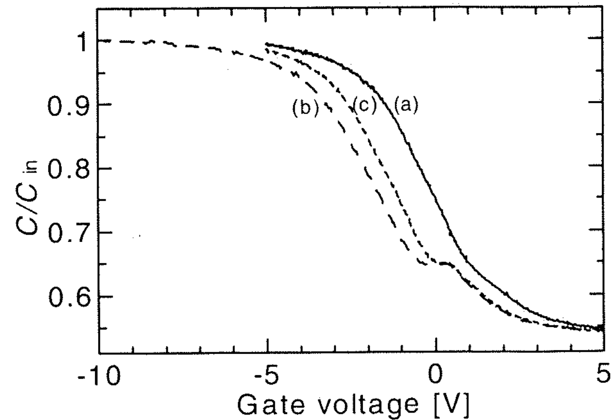

Fig. 9. Results of C–V measurement to confirm the trapping properties induced by negative high voltage. The first measurement from −5 to +10 V (curve a), second from −10 to +10 V (b), third from −5 to +10 V (c).

to −6 V) in the ozone-annealed sample, a different type of hole trap from the one responsible for the step is thought to be present in the ozone-annealed sample. In order to confirm this, the C–V curve was repeatedly measured for the ozone-annealed sample. First, the measurement was carried out from −5 V to +10 V, and second, from −10 V to +10 V. For the third and following measurements, the voltage was changed from −5 V to +10 V. The results are shown in Fig. 9. In the first measurement, a normal C–V curve without any step appeared. In the second measurement, the C–V curve shifted to the left and a step appeared in it. In the third measurement, a similar C–V curve with a similar step appeared, although the starting voltage and measurement range were the same as those of the first measurement. Exactly the same C–V curve as obtained for the third measurement was observed repeatedly in the subsequent measurements.

Figure 10 shows the C–V curves measured before and after a dc voltage of −8 V was applied to the gate metal electrode for 30 s. Since the voltage was changed from −5 V to +10 V, no step appeared in the C–V curve before the voltage application. However, if the dc voltage was applied, the step appeared. On the basis of these results, it is considered that the application of negative voltage induces irreversible hole traps in the ozone-annealed sample. In this respect, the nature of these traps is different from the nature of the traps that act as a simple reservoir of injected holes and that cause only a reversible shift in the C–V curve.

It was found by secondary ion mass spectroscopy (SIMS) that silicon, carbon, and hydrogen are present in the insulation layers of all the samples and that the ozone annealing does not affect their concentrations. However, aluminum pollution of the Ta_2O_5 layer was detected only in the ozone-annealed samples. Since the irreversible traps are also observed only in the ozone-annealed samples, there is a possibility that the pollution is responsible for the traps.

On the basis of the results shown in Figs. 4 and 10, it is concluded that the reason for the hysteresis shown in Fig. 3 differs for the ozone-annealed and non-annealed samples even though the direction of the hysteresis loop is the same. In the ozone-annealed sample, the hysteresis is due to hole trapping in the accumulation mode and ejection in the depletion or inversion mode, while that observed in the non-annealed sample is attributable to electron trapping in the inversion mode

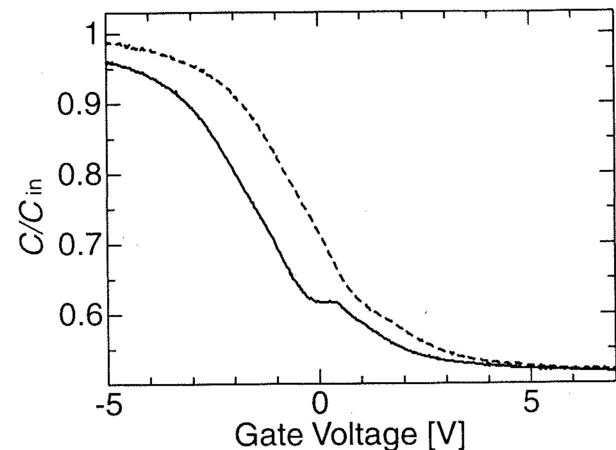

Fig. 10. C–V curves measured before (broken curve) and after (solid curve) application of DC voltage.

and ejection in the accumulation mode. This means that the ozone annealing on Ta_2O_5 reduces the number of electron traps and increases the number of hole traps present in the film.

Figure 11 shows TSC curves measured by changing the positive poling voltage applied to the gate metal electrode. The directions of TSC are opposite for the samples with and without ozone annealing, although both samples exhibit two TSC peaks at nearly the same temperatures around of 230 and 290 K. The charge quantity was estimated from the area surrounded by the TSC curve for the two component peaks, and their relationships to the poling voltage are shown in Fig. 12. The two peaks show different dependencies on poling voltage, which indicates that they have different origins.

As mentioned above, the gate electrode was positively biased during the poling. Therefore, the p-Si was in the inversion mode, and electrons are thought to have been injected into the insulating Ta_2O_5/Si_3N_4 layer during the poling. Furthermore, when the TSC was measured, the voltage was not applied. Under this condition, the potential difference across the insulating layer was caused by the difference in the work functions between aluminum and p-type silicon. Therefore, the energy band of the insulating layer bends as if the gate electrode were positively biased. This is demonstrated in the

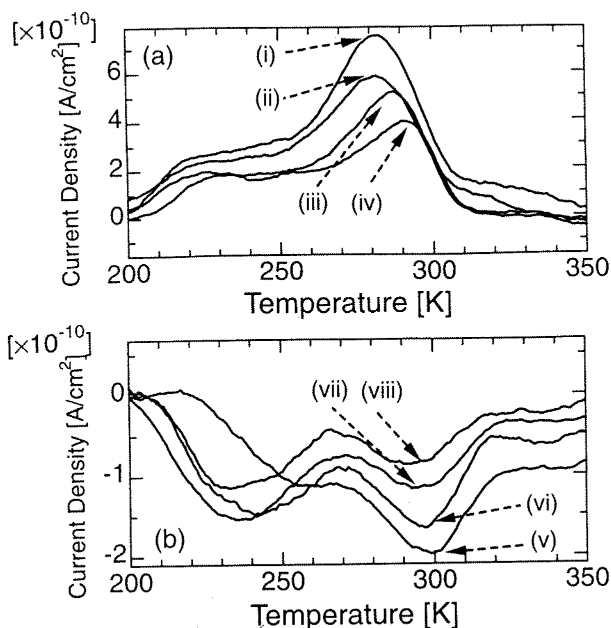

Fig. 11. (a) Thermally stimulated current spectra of the sample without ozone annealing after poling at voltages of +7 V (curve i), +6 V (ii), +5 V (iii), and +4 V (iv). (b) Those of the sample with ozone annealing after poling at voltages of +8 V (v), +7 V (vi), +6 V (vii), and +5 V (viii).

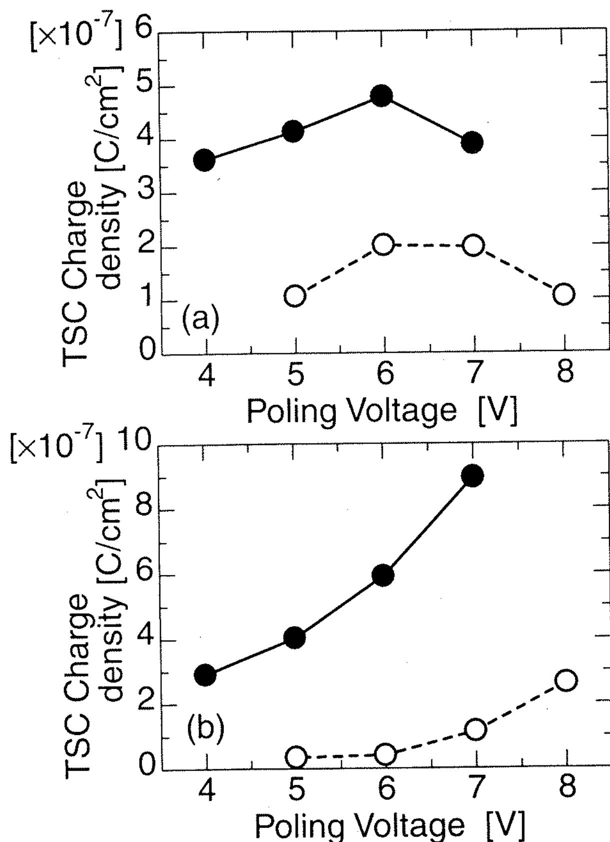

Fig. 12. Dependence of charge density estimated from the area surrounded by the two TSC component peaks at 230 K (a) and at 290 K (b). Open and solid circles indicate the samples with and without ozone annealing, respectively.

above-mentioned results of C–V measurement. Namely, in Fig. 3 or other figures showing C–V curves, C is always at a lower level when $V = 0$. This shows that the p-type silicon is in the depletion mode at $V = 0$, and has a negative potential against the gate electrode. Therefore, the direction of the TSC should be from the gate electrode to the p-Si. The measurement system used was connected in such a way that this direction was recorded as negative.

The TSC observed for the ozone-annealed sample is negative i.e., the predicted direction, while it is positive for the non-annealed sample. The following explanation is assumed to be the mechanism of this TSC inversion. The electrons injected into the insulating layer were trapped in the Ta_2O_5 layer, causing a significant distortion of the electric field. The direction of TSC must be reversed if $E_W < E_S$, where E_W denotes the field due to the difference in the work functions between the metal and p-Si, and E_S the field due to the trapped electrons. If this is the case, it is considered that a large number of electrons are trapped in the Ta_2O_5 layer of the non-annealed sample. The negative TSC in the ozone-annealed sample shows that the ozone annealing decreases the amount of electron traps. Here, the Si_3N_4 layer was deposited since the layer is known to be an effective barrier that prevents oxygen diffusion from the Ta_2O_5 layer.[11] Thus, it is thought to be the Ta_2O_5 layer and not the Si_3N_4 layer that was affected by the ozone annealing. This is in accordance with the above assumption that the electron traps of the non-annealed sample are present in the Ta_2O_5 layer.

Figures 6 and 12 indicate that the effective trapped charge density and the TSC charge density are of the same order of 10^{-7} C/cm^2. Figure 12 indicates that the ozone annealing decreases the number of trapped electrons, while a comparison of Figs. 4(a) and 4(b) also indicates a similar decrease. Therefore, it is concluded that the ozone annealing reduces the number of electron traps.

Previous studies[4,5,12] suggest that reactive oxidizing species such as ozone effectively reduce the density of oxygen vacancies in non-treated Ta_2O_5 films. It has been generally known that oxides such as ZnO, TiO_2, and SnO_2 behave as n-type or p-type semiconductors, depending on whether they are oxygen-deficient or oxygen-abundant.[13] It is therefore considered that the reduction of electron traps and the generation of hole traps by the ozone annealing is related to the change of the stoichiometry of Ta_2O_5 from oxygen-deficient to oxygen-abundant. However, ozone treatment is known to change a structural parameter such as the Ta–O bonding length of Ta_2O_5.[14] The possibility of such a structural change being responsible for the reduction of electron traps cannot be overlooked. With regard to the possibility that impurities are responsible, the above-mentioned SIMS observation did not reveal any species whose density is reduced by ozone annealing. Therefore, this situation does not seem plausible.

4. Conclusion

The effects of ozone annealing on the trapping property of Ta_2O_5/Si_3N_4/p-Si capacitors deposited by LPCVD have been examined. It is concluded that the ozone annealing efficiently eliminates electron traps present in the Ta_2O_5 layer but generates hole traps. A change in stoichiometry induced by the ozone annealing is suggested as the mechanism.

Acknowledgments

This work was partly supported by a Grant-in-Aid

(No. 09450132) from the Ministry of Education, Science, Sports and Culture, and by the Kawasaki Steel 21st Century Foundation.

1) T. Kaga, M. Ohkura, F. Murai, N. Yokoyama and E. Takeda: J. Vac. Sci. & Technol. B **13** (1995) 2329.
2) K. W. Kwon, C. S. Kang, S. O. Park, H. K. Kang and S. T. Ahn: IEEE Trans. Electron Devices **43** (1996) 919.
3) S. O. Kim and H. J. Kim: J. Vac. Sci. & Technol. B **12** (1994) 3006.
4) C. Isobe and M. Saitoh: Appl. Phys. Lett. **56** (1990) 907.
5) H. Shinriki and M. Nakata: IEEE Trans. Electron Devices **38** (1991) 455.
6) S. R. Jeon, S. W. Han and J. W. Park: J. Appl. Phys. **77** (1995) 5978.
7) P. A. Murawala, M. Sawai, T. Tatsuta and O. Tsuji: Jpn. J. Appl. Phys. **32** (1993) 368.
8) S. Ezhilvalavan and T. Y. Tseng: J. Appl. Phys. **83** (1998) 4797.
9) S. Kamiyama, H. Suzuki, H. Watanabe, A. Sakai, H. Kimura and J. Mizuki: J. Electrochem. Soc. **141** (1994) 1246.
10) *Oyo Buturi Deta Bukku* (Data Book of Applied Physics), ed. The Japan Society of Applied Physics (Maruzen, Tokyo, 1994) p. 497 [in Japanese].
11) S. P. Murarka, C. C. Chang and A. C. Adams: J. Electrochem. Soc. **126** (1979) 996.
12) Y. Ohji, Y. Matsui, T. Itoga, M. Hirayama, Y. Sugawara, K. Torii, H. Miki, M. Nakata, I. Asano, S. Iijima and Y. Kawamoto: Int. Electron Devices Meet. Tech. Dig. (1995) p. 111.
13) *Kotai no Denshi Kozo to Kagaku*, ed. K. Uozaki (Gihodo, Tokyo, 1990) p. 221 [in Japanese].
14) H. Shinriki, M. Hiratani, A. Nakano and S. Tachi: Ext. Abstr. 23rd Conf. Solid State Devices and Materials, Yokohama (1991) p. 198.

JOURNAL OF APPLIED PHYSICS VOLUME 86, NUMBER 9 1 NOVEMBER 1999

Effect of annealing on Ge-doped SiO_2 thin films

Makoto Fujimaki,[a] Shigeyuki Shimoto, Nahoko Miyazaki, and Yoshimichi Ohki
Department of Electrical, Electronics, and Computer Engineering, Waseda University, 3-4-1 Ohkubo, Shinjuku-ku, Tokyo 169-8555, Japan

Kwang Soo Seol
The Institute of Physical and Chemical Research (RIKEN), 2-1 Hirosawa, Wako-shi, Saitama 351-0198, Japan

Kazuo Imamura
Mitsubishi Cable Industries, Ltd., 4-3, Ikejiri, Itami-City, Hyogo 664-0027, Japan

(Received 3 May 1999; accepted for publication 24 July 1999)

Thermal annealing effects on optical and structural properties of Ge-doped SiO_2 thin films prepared by the chemical vapor deposition and flame hydrolysis deposition methods were investigated. The thin film prepared by the former method showed inhomogeneous Ge distribution, and Ge oxygen-deficient centers were observed. When it was thermally annealed at temperatures higher than 800 °C, the Ge distribution became uniform. The concentration of oxygen deficient centers was found to decrease with the thermal annealing in an O_2 atmosphere, while it increased with the thermal annealing at 1000 °C in N_2. This suggests that improvement of the film quality can be achieved by thermal annealing. On the other hand, neither inhomogeneity of Ge distribution nor the appearance of oxygen deficient centers was observed in the film prepared by the latter method, and its film quality was scarcely affected by the thermal annealing. © *1999 American Institute of Physics.* [S0021-8979(99)02621-3]

INTRODUCTION

The telecommunication system using optical fibers has been used all over the world and has performed the leading role in intelligent communication networks. For further development, fabrication of high grade, high performance, and reliable optical devices is indispensable.

Germanium-doped SiO_2 glass has been utilized mainly as a material for a core of an optical fiber. Ultraviolet (UV) photosensitivity of Ge-doped SiO_2 glass has been attracting much attention especially for the Bragg gratings[1] and the second harmonic generation.[2] It has been reported that the photosensitivity of Ge-doped SiO_2 glass is mainly due to photoinduced structural changes correlated with Ge oxygen-deficient centers (GODCs).[3–7] Quite a lot of research has been carried out on the fabrication of devices in optical fibers by UV photon irradiation.[8–12] Recently, to integrate the systems, fabrication of optical devices on planar waveguides with a Ge-doped SiO_2 core is being developed. To produce high quality optical devices, it is very important to fabricate planar waveguides with low optical loss. Therefore, improvement of the quality of the Ge-doped SiO_2 core is desired.

Germanium-doped SiO_2 core layers can be manufactured by conventional fabrication methods for large-scale-integrated circuits. In this article, we have investigated the quality of Ge-doped SiO_2 thin films prepared by the chemical vapor deposition (CVD) method and by the flame hydrolysis deposition (FHD) method on an amorphous SiO_2 substrate. Furthermore, we show that improvement of the film quality can be achieved by thermal annealing after the film deposition.

EXPERIMENTAL PROCEDURES

Germanium-doped SiO_2 thin films of 96.5 SiO_2:3.5 GeO_2, with a thickness of 7 μm, were prepared on amorphous SiO_2 substrates by the CVD and FHD methods, which are called samples A and B, respectively. Thermal annealing was applied to the samples in a N_2 or O_2 atmosphere at 1 atm.

Sample surfaces were observed using a Hitachi S-2500CX scanning electron microscope (SEM). For observation, a Pt–Pd film of 12 nm thick was sputtered on the surface and the sample was tilted at 45 degrees against the electron beam. Defects in the sample were detected through absorption spectroscopy from the visible-to-UV region with a Shimadzu UV-3100PC.

RESULTS

Figures 1(a) and 1(b) show the surfaces of as-deposited samples A and B, respectively. The surfaces are very smooth. Then, they were etched in hydrofluoric acid (10% HF in H_2O) for about 20 min at room temperature. The etched surfaces are shown in Fig. 2. The surface of sample A is very rough and has island structures with a diameter of ~300 nm, indicating that sample A was not etched uniformly. On the other hand, sample B seems to have been etched uniformly, since it keeps a smooth surface after the HF treatment.

Next, sample A was annealed in a N_2 atmosphere at 800 °C for 5 h and then it was etched in the HF solution. By

[a]Research Fellow of the Japan Society for the Promotion of Science.

 © 1999 American Institute of Physics

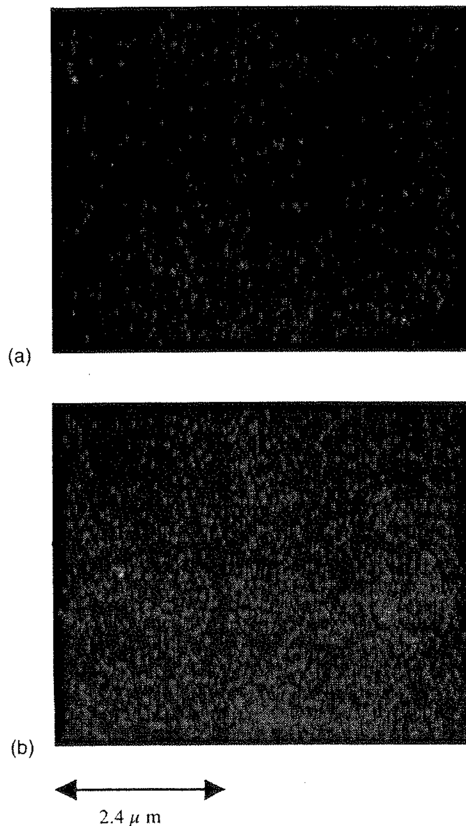

FIG. 1. SEM surface images of the as-deposited samples (a) A and (b) B.

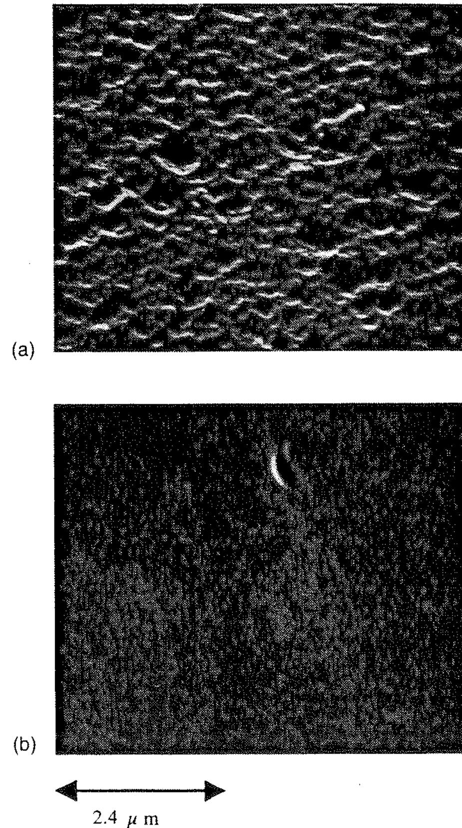

FIG. 2. SEM surface images of samples (a) A and (b) B after being etched by HF.

the thermal annealing, the surface, which was smooth before the thermal annealing as shown in Fig. 1(a), becomes rough. The islands observed in Fig. 3(a) are about 100–250 nm in diameter, and their number is larger than that observed in Fig. 2(a). The surface of sample A becomes slightly rough by the HF treatment done after the thermal annealing as shown in Fig. 3(b), where the islands of ~ 1 μm in diameter are observed. By comparing Figs. 2(a) and 3(b), it seems that the etching occurred more uniformly after the thermal annealing than before.

As a next step, sample A was thermally annealed either in an O_2 atmosphere at 800 °C or in a N_2 atmosphere at 1000 °C for 5 h. The surface observed was very similar to Fig. 3(a). Then, the HF treatment was applied after each thermal annealing. The surface observed this time was very similar to Fig. 3(b). The same procedures of thermal annealing and HF etching were also applied to sample B. However, no appreciable change was observed.

Figure 4(a) shows the absorption spectra of sample A before and after the thermal annealing, while Fig. 4(b) shows their thermally induced changes obtained by subtracting the spectrum before the annealing from the one after the annealing. The absorption at 5.1 eV, due to the GODCs,[3,13,14] is observed in the as-deposited sample. It decreases with the O_2 annealing at 800 °C, but does not change by the N_2 annealing at the same temperature. However, it increases drastically with the N_2 annealing at 1000 °C.

The absorption spectra of sample B before and after the thermal annealing are shown in Fig. 5. The 5.1 eV absorption is not observed in the as-deposited sample, and the absorption spectra are scarcely changed by the thermal annealing. Especially, the induction of the 5.1 eV absorption, which is observed in sample A with the thermal annealing in N_2 at 1000 °C, is not observed in sample B.

DISCUSSION

As shown in Fig. 1, the surfaces of as-deposited samples A and B are smooth. As shown in Fig. 2, the surface of sample A was inhomogeneously etched by the HF solution, while that of sample B was etched uniformly. It is well known that SiO_2 is soluble in HF but GeO_2 is not.[15] Therefore, the inhomogeneous etching of sample A means that the Ge distribution in this sample is inhomogeneous, while the uniform etching of sample B indicates that the Ge distribution is uniform.

As shown in Fig. 3(a), the surface of sample A becomes very rough by the thermal annealing. It is natural to assume that this is caused by the inhomogeneous distribution of Ge. The conceivable mechanisms are as follows. A strong stress may arise at the interface between the regions with different Ge contents because of the difference in atomic size of Ge and Si. The thermal annealing relieves the stress, which in turn causes protuberances on the surface. The difference in

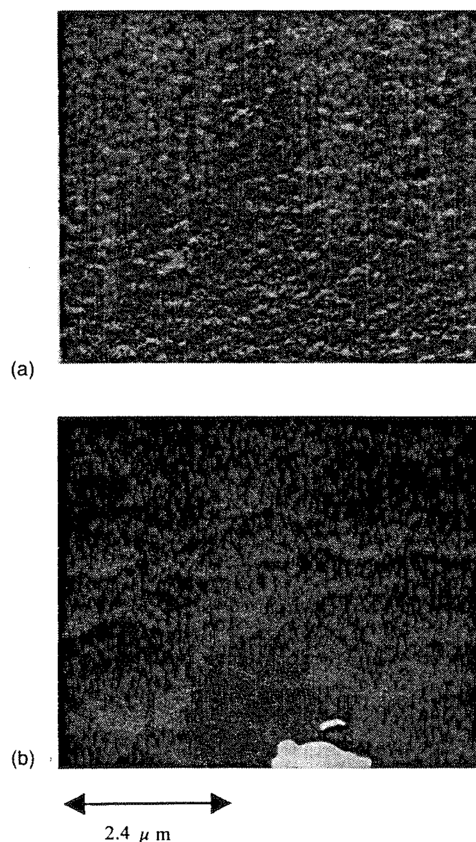

FIG. 3. (a) SEM surface image of sample A after the thermal annealing in a N_2 atmosphere at 800 °C for 5 h and (b) that of HF etched sample A after the thermal annealing.

thermal expansion between SiO_2 and GeO_2 may also cause the rough surface during the thermal annealing. The surface condition of sample B does not change with the thermal annealing. This is because the Ge distribution in sample B is originally uniform.

The islands shown in Fig. 3(a) are smaller in size and more in number than those shown in Fig. 2(a). This is probably because the HF treatment also solved the area of high Ge content to some extent since there still existed SiO_2 in that area. Therefore, it is considered that the size of the Ge-rich area in sample A seems to be equal to the size observed in Fig. 3(a), i.e., about 100–250 nm in diameter. It has been reported that the size of Ge-rich area in bulk Ge-doped SiO_2 glass is about 20 nm in diameter,[16,17] much smaller than the above values. It has been reported that the GODCs exist mainly in Ge-rich areas.[17] As shown in Fig. 4, the intensity of the 5.1 eV absorption due to the GODCs is about 150 cm^{-1} in as-deposited sample A, which is relatively large, compared with the intensities of absorption observed in oxygen-deficient Ge-doped SiO_2 bulk glasses.[3–5,13,18,19] In this sense, both the absorption intensity and the size of the inhomogeneous area indicate that the inhomogeneity of Ge distribution in sample A is large.

As shown in Fig. 3(b), the surface of sample A after the thermal annealing was etched more uniformly than the sur-

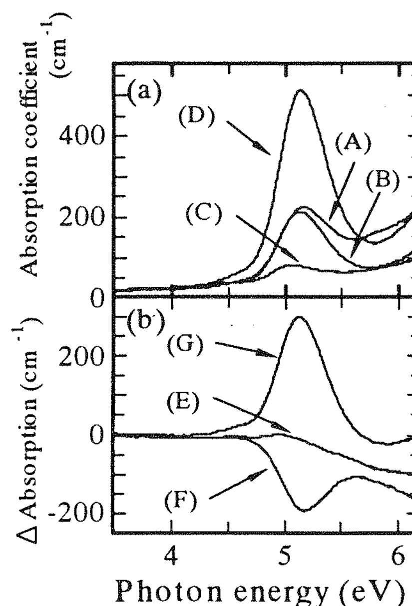

FIG. 4. (a) Absorption spectra of sample A: as-deposited (curve A), annealed in N_2 at 800 °C for 5 h (B), annealed in O_2 at 800 °C for 5 h (C), annealed in N_2 at 1000 °C for 5 h (D). (b) Absorption change induced by the thermal annealing: in N_2 at 800 °C for 5 h (E), in O_2 at 800 °C for 5 h (F), in N_2 at 1000 °C for 5 h (G).

face before the annealing. This is always the case regardless of the annealing temperature and atmosphere. This result indicates that Ge was thermally diffused and that the Ge distribution became homogeneous.

As seen in Fig. 4, the 5.1 eV absorption in sample A decreases with the thermal annealing in O_2. This is due to the reaction of thermally diffused oxygen molecules with the GODCs, which has been reported in bulk Ge-doped SiO_2 glass.[13,19] The thermal annealing in N_2 at 1000 °C increases the 5.1 eV absorption drastically in sample A, while no significant change is observed at 800 °C. In sample B, the N_2 annealing does not induce the 5.1 eV absorption even at

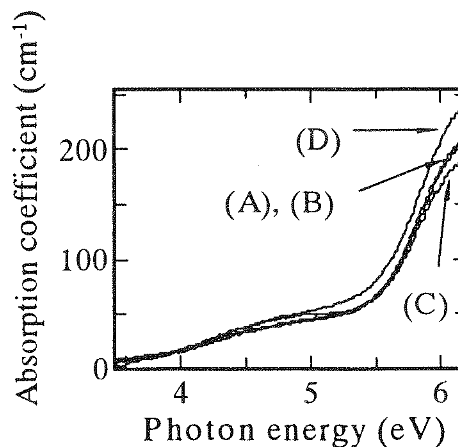

FIG. 5. Absorption spectra of sample B: as-deposited (curve A), annealed in N_2 at 800 °C for 5 h (B), annealed in O_2 at 800 °C for 5 h (C), annealed in N_2 at 1000 °C for 5 h (D).

1000 °C. This difference is explained by the fact that deoxidization of GeO_2 is easier than that of SiO_2.[3] Since sample A has inhomogeneous Ge distribution, the structure described as "≡Ge–O–Ge≡" (where "≡" denotes bonds with three separate oxygens) is dominant in the Ge-rich areas.[17] On the other hand, Ge takes the form of "≡Ge–O–Si≡" in sample B. Therefore, sample A is more easily deoxidized into the GODCs, causing larger absorption at 5.1 eV.

Photosensitivity of Ge-doped SiO_2 thin films is attributed to photoinduced defect formation and volume changes.[20,21] The GODC strongly contributes to the defect formation, and several methods to increase the GODC concentration have been reported.[22,23] Since inhomogeneity of glass structure increases light scattering and optical loss, fabrication of waveguides with uniform Ge distribution is preferable. However, high photosensitivity to the defect formation cannot be obtained in a sample that has originally uniform Ge distribution, since GODCs exist mainly in the Ge-rich areas.[17] In the present research, it is clearly shown that the GODC concentration in a film with inhomogeneous Ge distribution is controllable by choosing the thermal annealing condition. Furthermore, it is also shown that the annealing relaxes the inhomogeneity of Ge distribution. This is good in point of optical loss. Therefore, the present findings are valuable for the fabrication of high-performance waveguides.

CONCLUSION

Thermal annealing effects on Ge-doped SiO_2 thin films with homogeneous/inhomogeneous Ge distribution were investigated through absorption measurements and surface observation with SEM. In the sample with homogeneous Ge distribution, no significant change was observed. However, in the sample with inhomogeneous Ge distribution, the annealing at temperatures higher than 800 °C makes the Ge distribution uniform. The concentration of GODCs, which originally existed in this film, decreases with the annealing in O_2 at 800 °C, while it increases significantly by the annealing in N_2 at 1000 °C. This means that the quality and UV photosensitivity of Ge-doped SiO_2 thin films are controllable by thermal annealing.

ACKNOWLEDGMENTS

This work was supported in part by a Grant-in-Aid for JSPS Fellows and a Grant-in-Aid for Scientific Research (09450132), both from the Ministry of Education, Science, Sports, and Culture of Japan. This work was also supported by the Foundation of Ando Laboratory.

[1] K. O. Hill, Y. Fujii, D. C. Johnson, and B. S. Kawasaki, Appl. Phys. Lett. **32**, 647 (1978).
[2] U. Osterberg and W. Margulis, Opt. Lett. **11**, 516 (1986).
[3] H. Hosono, Y. Abe, D. L. Kinser, R. A. Weeks, K. Muta, and H. Kawazoe, Phys. Rev. B **46**, 11445 (1992).
[4] M. Fujimaki, T. Watanabe, T. Katoh, T. Kasahara, N. Miyazaki, Y. Ohki, and H. Nishikawa, Phys. Rev. B **57**, 3920 (1998).
[5] M. Takahashi, T. Fujiwara, T. Kawachi, and A. J. Ikushima, Appl. Phys. Lett. **71**, 993 (1997).
[6] D. L. Williams, S. T. Davey, R. Kashyap, J. R. Armitage, and B. J. Ainslie, Electron. Lett. **28**, 369 (1992).
[7] L. Dong, J. L. Archambault, L. Reekie, P. St. J. Russell, and D. N. Payne, Appl. Opt. **34**, 3436 (1995).
[8] D. M. Bird, J. R. Armitage, R. Kashyap, R. M. A. Fatah, and K. H. Cameron, Electron. Lett. **27**, 1115 (1991).
[9] G. A. Ball, W. W. Morey, and J. P. Waters, Electron. Lett. **26**, 1829 (1990).
[10] J. L. Zyskind, V. Mizrahi, D. J. DiGiovanni, and J. W. Sulhoff, Electron. Lett. **28**, 1385 (1992).
[11] L. Blair and S. A. Cassidy, Electron. Lett. **28**, 1734 (1992).
[12] F. Ouellette, Opt. Lett. **12**, 847 (1987).
[13] M. Kohketsu, K. Awazu, H. Kawazoe, and M. Yamane, Jpn. J. Appl. Phys., Part 1 **28**, 622 (1989).
[14] L. Skuja, J. Non-Cryst. Solids **149**, 77 (1992).
[15] *CRC Handbook of Chemistry and Physics*, 71st ed. (CRC, Boca Raton, FL, 1990), pp. 4–66; *ibid.* (1991), pp. 4–100.
[16] K. Nagasawa and Y. Ohki, Jpn. J. Appl. Phys., Part 2 **25**, L682 (1986).
[17] H. Hosono, K. Kawamura, H. Kawazoe, and J. Nishii, J. Appl. Phys. **80**, 3115 (1996).
[18] M. Martini, F. Meinardi, A. Paleari, L. Portinari, and G. Spinolo, J. Non-Cryst. Solids **216**, 26 (1997).
[19] K. Awazu, H. Kawazoe, and M. Yamane, J. Appl. Phys. **68**, 2713 (1990).
[20] M. V. Bazylenko, M. Gross, and D. Moss, J. Appl. Phys. **81**, 7497 (1997).
[21] M. Douay, W. X. Xie, T. Taunay, P. Bernage, P. Niay, P. Cordier, B. Poumellec, L. Dong, J. F. Bayon, H. Poignant, and E. Delevaque, J. Lightwave Technol. **15**, 1329 (1997).
[22] J. Nishii, H. Yamanaka, H. Hosono, and H. Kawazoe, Appl. Phys. Lett. **64**, 282 (1994).
[23] P. J. Hughes, A. P. Knights, B. L. Weiss, S. Kuna, P. G. Coleman, and S. Ojha, Appl. Phys. Lett. **74**, 3311 (1999).

Structural changes induced by KrF excimer laser photons in H_2-loaded Ge-doped SiO_2 glass

Makoto Fujimaki, Toshiaki Kasahara, Shigeyuki Shimoto, Nahoko Miyazaki, Shin-ichiro Tokuhiro, Kwang Soo Seol, and Yoshimichi Ohki

Department of Electrical, Electronics, and Computer Engineering, Waseda University, 3-4-1 Ohkubo, Shinjuku-ku, Tokyo 169-8555, Japan

(Received 9 November 1998; revised manuscript received 18 March 1999)

Photochemical reactions related to the Ge lone-pair center (GLPC) that are induced by KrF excimer laser photons in H_2-loaded Ge-doped SiO_2 glass have been investigated. Without the H_2 loading, the Ge electron center (GEC) and the positively charged GLPC were induced by the laser irradiation. In the H_2-loaded sample, the GEC, the Ge E' center, and the germyl radical (GR) were induced by the irradiation, while the positively charged GLPC was not observed after the irradiation. If the H_2-loaded sample was thermally annealed after the photon irradiation, the concentration of the photo-induced GEC decreased monotonically with an increase in the annealing temperature. On the other hand, the concentration of the GR increased up to the annealing temperature of 160 °C, and it decreased at higher temperatures. Without the pre-irradiation, the induction of the GR was not observed even in the H_2-loaded sample. From these results, it is concluded that the positively charged GLPC is terminated with a hydrogen atom in the H_2-loaded sample and then becomes the GR by trapping an electron thermally released from the GEC. [S0163-1829(99)05631-3]

I. INTRODUCTION

Recently, optical fiber gratings, where periodical refractive-index change is fabricated by ultraviolet (uv) photon irradiation in the core of an optical fiber made of Ge-doped SiO_2 glass,[1] have been expanding their applications to various devices, such as optical filters,[2–6] sensors,[7–10] fiber lasers,[2–4,11] dispersion eliminators,[12,13] and so on. Many trials, e.g., development of special fibers with increased Ge concentration and/or codopants, have been made to increase the refractive index change.[14] However, it is often more desirable to fabricate fiber gratings in standard optical fibers for compatibility with existing systems. Low-temperature H_2 loading is one of the most effective sensitization techniques to increase photo-induced refractive index changes in standard optical fibers. Molecular-hydrogen-loaded Ge-doped SiO_2 optical fibers exhibit markedly increased photo-induced refractive index changes.[15–17] Therefore, it is very important to understand the photo-induced structural changes in H_2-loaded Ge-doped SiO_2 glass for the fabrication of high performance optical fiber gratings.

It has been known that there are two types of Ge oxygen-deficient centers in Ge-doped SiO_2 glass.[18] One is the neutral oxygen vacancy (NOV; $\equiv$Ge$-T\equiv$, $\equiv$ represents bonds with three separate oxygens and T is either Ge or Si) and the other is the Ge lone-pair center (GLPC; —$\ddot{\text{Ge}}$—, "••" denotes lone-pair electrons).[18] With uv photon irradiation, the NOV becomes the Ge E' center ($\equiv$Ge•$+{}^{+}T\equiv$, • denotes an unpaired electron):[18]

$$\text{NOV}\rightarrow\text{Ge } E' \text{ center}+e^{-}. \tag{1}$$

By irradiation with uv photons of high-energy density, such as KrF excimer laser photons, the GLPC is ionized and becomes the positively charged GLPC $[(\text{GLPC})^{+}]$.[19] The electron released from the GLPC by the irradiation is trapped at fourfold coordinated Ge (abbreviated as GeO_4) and forms the Ge electron center (GEC, $GeO_4{}^{-}$):[19]

$$\text{GLPC}+\text{GeO}_4\rightarrow(\text{GLPC})^{+}+\text{GEC}. \tag{2}$$

These uv-induced structural changes are accompanied by the induction of absorption changes in the visible-to-uv region, which in turn causes the refractive index changes through the Kramers-Kronig relation.[20,21]

It has been reported that the Ge E' center and the GEC are also induced by photon irradiation in H_2-loaded Ge-doped SiO_2 glass.[19,22] Not only the NOV but also the GLPC becomes the Ge E' center with a high dose irradiation of uv photons in H_2-loaded Ge-doped SiO_2 glass.[22] In addition to these paramagnetic centers, the germyl radical (GR), which has the structure that H is bonded to the GLPC ($=\dot{\text{Ge}}$H),[23,24] is induced by uv photon irradiation. These phenomena strongly indicate that the GLPC plays an important role in the photo-induced structural changes. In the present paper, in order to understand structural changes related to the GLPC in H_2-loaded Ge-doped SiO_2 glass, we have investigated paramagnetic centers and absorption bands induced by KrF excimer laser photons and the changes in their behavior by thermal annealing.

II. EXPERIMENTAL DETAILS

A $99SiO_2$:$1GeO_2$ glass rod, prepared by the vapor-phase axial deposition method, was cut into disks having 0.3-mm thickness and polished for optical measurements. Molecular hydrogen loading was performed under a H_2 pressure of 170 atm for two weeks at room temperature. Hereafter, the H_2-loaded and non-H_2-loaded samples are called samples *H* and *N*, respectively. A KrF excimer laser (Lambda Physik, LPX 105i, 248 nm=5.0 eV), with an energy density of 70 mJ/cm^2 per pulse, was used as a photon source. The absorption spectra from the visible-to-uv region were measured by

 ©1999 The American Physical Society

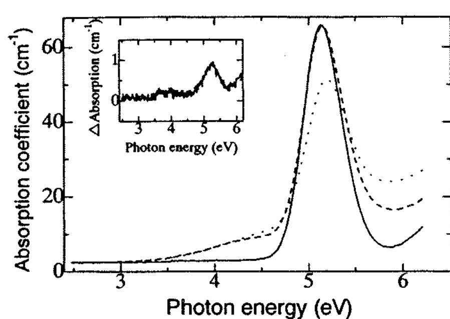

FIG. 1. Absorption spectra before and after the KrF excimer laser photon irradiation. The solid curve denotes the absorption spectrum of the as-received sample N before the laser photon irradiation, which overlaps with the spectrum of sample H before the irradiation in this scale. The inset shows the difference obtained by subtracting the absorption spectrum of sample N from that of sample H. The broken and the dotted curves denote the spectra of samples N and H after the 30-pulse irradiation of the laser photons, respectively.

a Shimadzu UV-3100PC spectrophotometer with wavelength resolution of ~2 nm. The induced paramagnetic centers were detected by electron spin resonance (ESR) with a JEOL JES-PX 1060 spectrometer at the X-band frequency, and their concentration was evaluated by comparing the double-integrated intensity of the first-derivative spectrum with that of the signal from a standard diphenylpicrylhydrazyl sample of a known weight (the accuracy of the standard is believed to be ±20%). All the photon irradiation and the measurements were done at room temperature.

III. RESULTS

A. Photo-induced structural changes

The solid curve in Fig. 1 indicates the absorption spectrum of the as-received sample, i.e., sample N before photon irradiation. Absorption is observed at 5.1 eV, which is known to be composed of the two absorption bands due to the NOV (5.06 eV) and the GLPC (5.16 eV).[18] The inset shows the difference obtained by subtracting the absorption spectrum of sample N from that of sample H. A slight increase in the 5.1 eV absorption is observed with the H_2 loading. The broken and the dotted curves in Fig. 1, respectively, show the absorption spectra of samples N and H after 30 laser pulses were irradiated. By subtracting the solid curve from the broken and dotted curves in Fig. 1, the photo-induced absorption changes in samples N and H were obtained as shown by the solid curves in Figs. 2(a) and 2(b), respectively. It has been reported that photo-induced absorption bands in a Ge-doped SiO_2 glass in the visible-to-uv region are well fitted with Gaussian shapes, and the parameters of the Gaussian components have been well identified.[19,25–29] Therefore, we applied Gaussian decomposition to the obtained spectra. The broken curves in Fig. 2 denote the spectral components obtained by the least-squares fitting with Gaussian shapes. The synthesized line shapes, indicated by the dotted curves, reproduce well the observed absorption spectra. The intensities and the values of the full width at half maximum (FWHM) of these absorption components are shown in Table I. The instrumental errors for the values of

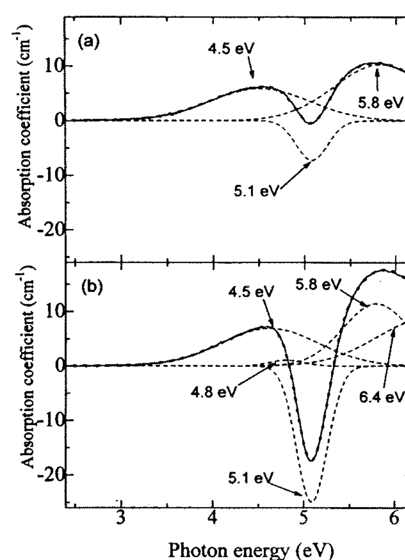

FIG. 2. Solid curves indicate the absorption changes in samples N (a) and H (b) induced after 30 laser pulses were irradiated. The broken and the dotted curves denote the spectral components obtained by the least-squares fitting with Gaussian shapes and the synthesized line shapes, respectively. Note that the solid and the dotted curves agree quite well with each other.

the peak positions and the FWHM's are within 0.05 eV, and those of the intensities are within 0.2 cm^{-1}. The errors shown in the table are due to the ambiguity of the calculation. As shown in Fig. 2, a decrease in the 5.1-eV absorption and the induction of two absorption bands at 4.5 and 5.8 eV are observed in samples N and H. In addition to these absorption changes, an absorption band at 6.4 eV, which is considered to be due to the Ge E' center,[25] is observed in sample H. A weak absorption band at 4.8 eV, which has not been assigned yet, is also induced in sample H.

Figures 3(a) and 3(b) show the ESR spectra induced by the photon irradiation of 30 laser pulses in samples N and H, respectively. Two signals, named Ge(1) and Ge(2) that are, respectively, assigned to the GEC and the $(GLPC)^+$,[19] are observed in sample N. The sum of the concentrations of the GEC and the $(GLPC)^+$ is calculated to be $4.8\times10^{17}\,cm^{-3}$. The authors have confirmed that the concentration of GEC and that of $(GLPC)^+$ induced in Ge-doped SiO_2 glass are

TABLE I. Peak positions, intensities, and values of FWHM of the absorption components induced in samples N and H.

Sample	Peak position (eV)	Intensity (cm^{-1})	FWHM (eV)
	4.5	5.9	1.3
N	5.1	−7.2	0.4
	5.8	10.2	1.2
	4.5	6.9±0.5	1.3±0.1
	4.8±0.1	1.1±0.5	0.4±0.1
H	5.1	−24.8±1.0	0.4
	5.8	11.5±2.0	0.9±0.2 (1.2±0.1)[a]
	6.4±0.15	9.0±3.0	1.2±0.2

[a]The calculated value based on the Gaussian fitting to the result shown in Fig. 5.

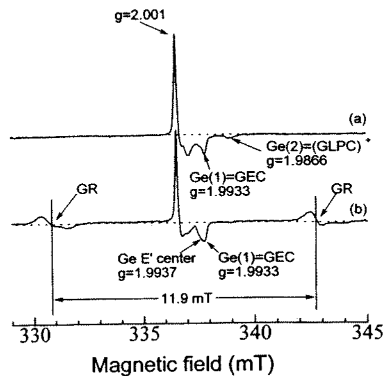

FIG. 3. ESR spectra of samples N (a) and H (b) induced by the irradiation of 30 pulses of laser photons.

equal when it is irradiated up to a few tens of pulses with the present KrF excimer laser.[19] Therefore, the induced concentration is $2.4\times10^{17}\,\mathrm{cm}^{-3}$ for both GEC, and $(\mathrm{GLPC})^+$. In sample H, the ESR signals due to the GEC, Ge E' center, and GR are seen. The concentration of the GEC induced in sample H is $2.6\times10^{17}\,\mathrm{cm}^{-3}$, which is quite similar to that induced in sample N. The concentrations of the Ge E' center and the GR are 0.6×10^{17} and $2.6\times10^{17}\,\mathrm{cm}^{-3}$, respectively. The fact that the Ge(2) signal is not seen in Fig. 3(b) means that the $(\mathrm{GLPC})^+$ does not exist in sample H even after the photon irradiation.

B. Thermal effects on the photo-induced structural changes

The following thermal annealing procedure was applied to sample H after 30 pulses of laser photons had been irradiated at room temperature. First, the sample was annealed at 160 °C for 5 min, and the absorption and ESR measurements were done at room temperature. This sequence of annealing and measurements was repeated with a step of 20 °C until the annealing temperature reached 300 °C. Figure 4 shows the ESR results. The circle and square show the concentrations of GEC and GR, respectively. The photo-induced Ge E' center in sample H scarcely changed its concentration with the thermal annealing. As seen in this figure, the concentration of GEC decreases monotonically with an increase in the annealing temperature. On the other hand, the concentration of GR increases with the thermal annealing at 160 °C, and then it decreases monotonically. The thermal annealing was also

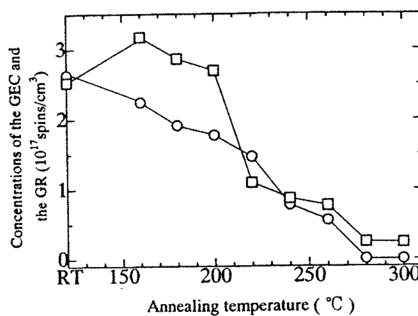

FIG. 4. Changes in the concentrations of the GEC (circles) and the GR (squares) in sample H with the thermal annealing following the 30-pulse irradiation of laser photons.

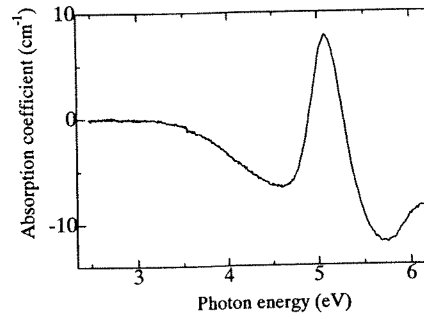

FIG. 5. Differential absorption spectrum of the photon-irradiated sample H obtained by subtracting the spectrum before the thermal annealing from the one after the total sequences of thermal annealing.

applied to sample H which had not been irradiated with the laser photons. In this case, induction of the GR was not observed. This result indicates that the precursor of thermally induced GR is a defect induced by the irradiation.

Figure 5 shows the differential absorption spectrum of the photon-irradiated sample H before and after the total sequences of thermal annealing. The 5.1-eV absorption, which was bleached by the photon irradiation, shows a recovery by the thermal annealing. Decrease in the 4.5 and 5.8 eV bands, which were induced by the photon irradiation, is also observed.

Figure 6 shows the correlation between the decrease in the concentration of GEC ($-\Delta N_{\mathrm{GEC}}$) and the increase in the intensity of 5.1-eV absorption ($\Delta\alpha_{5.1}$), measured after each sequence of thermal annealing. The open and closed circles are for samples N and H, respectively, and the numbers next to them denote the annealing temperature. For sample N, $\Delta\alpha_{5.1}$ is linearly proportional to $-\Delta N_{\mathrm{GEC}}$, while such a proportionality is not observed for sample H.

IV. DISCUSSION

A. Photo-induced structural changes

The absorption changes shown in Fig. 2(a), which occurred in sample N by the photon irradiation, can be explained by Eq. (2). Ionization of the GLPC into $(\mathrm{GLPC})^+$

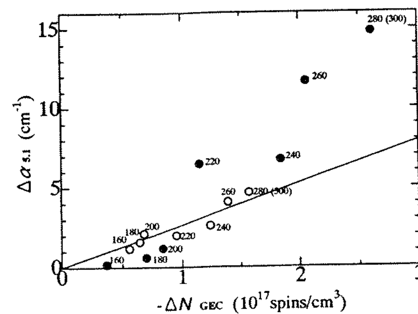

FIG. 6. Correlation between the decrease in the concentration of the GEC ($-\Delta N_{\mathrm{GEC}}$) and the increase in the intensity of the 5.1-eV absorption ($\Delta\alpha_{5.1}$) measured after each sequence of the thermal annealing. The open and the closed circles are for samples N and H, respectively, and the numbers next to them denote the annealing temperature.

decreases the 5.1-eV band and the generation of GEC induces the 4.5- and 5.8-eV bands.[19,26,27] This view is consistent with the result shown in Fig. 3(a). Since the Ge E' center is not observed in sample N after the photon irradiation, the photochemical reaction indicated by Eq. (1) does not occur in sample N under the irradiation condition. The decrease of GLPC ($-\Delta N_{\mathrm{GLPC}}$), i.e., the induction of $(\mathrm{GLPC})^+$, by $2.4\times 10^{17}\,\mathrm{cm}^{-3}$ brings about the decrease in 5.1-eV absorption ($-\Delta\alpha_{5.1}$) by $7.2\,\mathrm{cm}^{-1}$ shown in Fig. 2(a). From these values, the oscillator strength of the GLPC for the 5.1-eV absorption f_{GLPC} is calculated using the following Smakula's formula:[30]

$$Nf=0.87\times 10^{17} n\alpha\omega/(n^2+2)^2, \qquad (3)$$

where N is the defect concentration (cm^{-3}), n the refractive index of glass, α (cm^{-1}) the absorption intensity at the peak of the absorption band, and ω (eV) the FWHM. By substituting $-\Delta N_{\mathrm{GLPC}}$ of $2.4\times 10^{17}\,\mathrm{cm}^{-3}$, $-\Delta\alpha_{5.1}$ of $7.2\,\mathrm{cm}^{-1}$, n of 1.46, and ω of 0.4 eV, f_{GLPC} is calculated to be 0.09, which is the same value as the one reported in Ref. 19. From the result, the relation between ΔN_{GLPC} and $\Delta\alpha_{5.1}$ is expressed as follows:

$$\Delta\alpha_{5.1}=3.0\times 10^{-17}\times\Delta N_{\mathrm{GLPC}}. \qquad (4)$$

The concentration of GEC induced in sample H by photon irradiation is $2.6\times 10^{17}\,\mathrm{cm}^{-3}$. This indicates that this concentration of GLPC disappears in sample H, which brings about the decrease in 5.1-eV absorption. From Eq. (4), this decrease is calculated to be $7.8\,\mathrm{cm}^{-1}$.

The signal due to GR is also seen in Fig. 3(b) with a concentration of $2.6\times 10^{17}\,\mathrm{cm}^{-3}$. The precursor of the photo-induced GR is the GLPC:[23]

$$\mathrm{GLPC+H\rightarrow GR}. \qquad (5)$$

Therefore, the decrease in the 5.1-eV band associated with the generation of GR is calculated to be $7.8\,\mathrm{cm}^{-1}$ by substituting ΔN_{GLPC} of $-2.6\times 10^{17}\,\mathrm{cm}^{-3}$ into Eq. (4). Therefore, the total decrease in the 5.1-eV band due to the loss of GLPC becomes $15.6\,\mathrm{cm}^{-1}$.

As shown in Figs. 2(b) and 3(b), the Ge E' center is induced in sample H. The NOV and the GLPC are the precursors of the Ge E' center in a H_2-loaded Ge-doped SiO_2 glass.[22] However, in the present case, only 30 pulses of the laser photons, which correspond to $2.1\,\mathrm{J/cm}^2$, were irradiated to the samples. It is known that the GLPC does not change into the Ge E' center with such a low dose.[22] Therefore, the observed Ge E' center was totally generated from the NOV. The induced concentration of Ge E' center is $0.6\times 10^{17}\,\mathrm{cm}^{-3}$, which should be equal to the decreased concentration of NOV. Since the NOV shows the absorption at 5.1 eV with ω of 0.4 eV and f of 0.4, by using Eq. (3) the decrease in the 5.1-eV absorption is calculated to be 7.8 cm^{-1}. As a result, the decrease in the 5.1-eV absorption accompanied with the three paramagnetic centers, GR, GEC, and Ge E' center is calculated to be $23.4\,\mathrm{cm}^{-1}$. This is quite similar to the observed value.

From the above-mentioned discussion, it is concluded that the electron donor to generate the GEC in sample H is also the GLPC. However, the Ge(2) signal, which is assigned to the $(\mathrm{GLPC})^+$, is not observed by the ESR measurement for sample H even after the laser photon irradiation. The $(\mathrm{GLPC})^+$ is considered to be terminated with a hydrogen atom in sample H, since only the existence of H_2 molecules is the difference between samples H and N. The $(\mathrm{GLPC})^+$ terminated with a hydrogen atom, written as $(\mathrm{GLPC})^+$-H hereafter, is a diamagnetic center, and is not detectable in the ESR measurement.

B. Thermal effects on the photo-induced structural changes

As shown in Fig. 6, $\Delta\alpha_{5.1}$ is linearly proportional to $-\Delta N_{\mathrm{GEC}}$ when the sample N is thermally annealed. Here, we assume that the reverse reaction of Eq. (2) occurs with the thermal annealing. This means $-\Delta N_{\mathrm{GEC}}$ is equal to the recovered concentration of the GLPC. Therefore, $-\Delta N_{\mathrm{GEC}}$ should be equal to ΔN_{GLPC}. From this relationship between $\Delta\alpha_{5.1}$ and ΔN_{GLPC} or the slope of the linear line in Fig. 6, f'_{GLPC} is calculated to be 0.081, which is 9% less than f_{GLPC}. This difference is negligible if we take account of the error of ESR measurements. This strongly confirms the above-mentioned assumption that the reverse reaction of Eq. (2) occurred during the thermal annealing of sample N that had been irradiated by laser photons.

As shown in Fig. 4, the concentration of GR increases in sample H with thermal annealing at 160 °C following the photon irradiation. Since the GR is not induced by the thermal annealing in sample H without the preirradiation of the laser photons, the precursor of thermally induced GR is a defect induced by the photon irradiation. The precursor is the $(\mathrm{GLPC})^+$-H induced in sample H by the irradiation. As mentioned above, electrons are released from GEC's by the thermal annealing, and $(\mathrm{GLPC})^+$'s trap the electrons in sample N. However, the $(\mathrm{GLPC})^+$ is terminated with a hydrogen atom and becomes the $(\mathrm{GLPC})^+$-H in sample H. Therefore, if an electron is trapped by the $(\mathrm{GLPC})^+$-H, the GR is induced. This reaction is expressed as

$$\mathrm{GEC+(GLPC)^+\text{-}H\rightarrow GeO_4+GR}. \qquad (6)$$

This reaction explains the increase in the GR concentration caused in sample H by the thermal annealing at 160 °C shown in Fig. 4. When the annealing temperature is beyond 160 °C, the GR is bleached.

In sample N, $\Delta\alpha_{5.1}$ is linearly proportional to $-\Delta N_{\mathrm{GEC}}$, as mentioned above. Such proportionality is not observed for sample H. As shown in Fig. 6, the ratio of $\Delta\alpha_{5.1}$ to $-\Delta N_{\mathrm{GEC}}$ is lower in sample H than in sample N during the thermal annealing from 160 to 200 °C, while it becomes higher at higher annealing temperatures. As shown in Fig. 4, the GEC is bleached monotonically by the thermal annealing. The electron thermally released from the GEC is trapped at the $(\mathrm{GLPC})^+$-H and the $(\mathrm{GLPC})^+$-H becomes the GR as shown in Eq. (6). However, the GR is scarcely bleached by the thermal annealing from 160 to 200 °C. As a result, the intensity of the absorption band at 5.1 eV due to the GLPC scarcely increases at this temperature region. With the thermal annealing at higher temperatures, the GR is bleached and becomes the GLPC, which in turn increases the absorption intensity at 5.1 eV.

As mentioned in the previous section, the total decrease in the 5.1-eV band due to the loss of GLPC accompanied with the induction of GR and $(\mathrm{GLPC})^+$-H is $15.6\,\mathrm{cm}^{-1}$. There-

fore, the 5.1-eV band of 15.6 cm^{-1} should be induced with complete thermal bleaching of the GR and $(GLPC)^+$-H. This is quite similar to $\Delta\alpha_{5.1}$ of sample H that was annealed thermally at 300 °C (see Fig. 6). The 5.1-eV absorption band due to the NOV does not increase with the thermal annealing, since the concentration of the Ge E' center scarcely changes with the thermal annealing.

C. Assignment of the 5.8-eV absorption

As shown in Fig. 2, absorption bands are induced at 4.5 and 5.8 eV by the photon irradiation in sample N. In addition to these two bands, the 6.4-eV absorption is also induced in sample H. The bands at 4.5 and 6.4 eV are already known to be, respectively, due to the GEC (Refs. 19, 26 and 27) with the Ge(1) ESR signal and the Ge E' center.[25] However, the assignment of the 5.8-eV band is still a matter of discussion.

There have been papers[26,27] that assigned the 4.5- and 5.8-eV bands to two different defects that have the Ge(1) and Ge(2) ESR signals, respectively. On the other hand, the authors have indicated the possibility of both the 4.5- and 5.8-eV bands being due to the Ge(1) defect from the fact that the intensity of the 5.8-eV band is always linearly proportional to that of the 4.5-eV band with the identical proportionality coefficient regardless of the Ge content of the samples.[19] The present study gives a clear answer to this puzzle. By comparing Figs. 2 and 3, one can easily find that the photon-irradiated sample H shows the 5.8-eV band without showing the Ge(2) signals. This fact clearly contradicts the assumption that the 5.8-eV band and the Ge(2) signal are due to the same defect. By comparing the results shown in Fig. 2 (or Table I) and those in Fig. 3, it is found that the intensity of the 5.8-eV band is similar between samples N and H and that the Ge(1) signal intensity is also similar between the two samples. This similarity between the 5.8-eV band and the Ge(1) signal supports the model that the 5.8-eV band as well as the 4.5-eV band is due to the defect with the Ge(1) ESR signal, namely, GEC.

One might notice a difference of the FWHM value of the 5.8-eV band between the samples N and H shown in Table I. As for the absorption spectrum of sample H shown in Fig. 2(b), the calculated FWHM for the 5.8-eV band is not accurate due to the presence of the peak at 6.4 eV and the one located higher than 6.5 eV.[31] Because of the limitation of the measurement system, it was impossible to distinguish the three absorption bands clearly in the present calculation. Therefore, re-estimation of the FWHM was done based on the thermally decreased 5.8-eV absorption shown in Fig. 5, and the result came out to 1.2 ± 0.1 eV, the same FWHM as in the case of sample N. Since the thermal annealing does not change the concentration of the Ge E' center, the existence of the 6.4-eV band is negligible in the spectrum shown in Fig. 5. Therefore, the FWHM of 1.2 eV is more reliable for the 5.8-eV band. Although the Si E' center is known to have absorption at 5.8-eV,[32,33] there is no possibility of the present 5.8-eV band being due to the Si E' center since the ESR signal of the Si E' center never appeared. Therefore, the present 5.8-eV band is due to the same origin in both samples N and H, and the origin is the GEC with the Ge(1) ESR signal.

V. CONCLUSIONS

Structural changes induced in H_2-loaded Ge-doped SiO_2 glass have been investigated through absorption and ESR measurements using a KrF excimer laser as a photon source. Thermal annealing was also applied to the glass following the laser photon irradiation, and the behavior of absorption bands and that of paramagnetic centers were investigated. From the obtained results, the following conclusions are derived. (1) The paramagnetic centers, GEC, GR, and Ge E' center, are induced by the irradiation. (2) The GLPC, which donated an electron to generate the GEC, is terminated with a hydrogen atom and becomes the $(GLPC)^+$-H, an ESR-insensitive diamagnetic center. (3) The $(GLPC)^+$-H traps an electron thermally released from the GEC and becomes the GR at temperatures around 160 °C. (4) The GR becomes the GLPC with the thermal annealing. (5) The 5.8-eV absorption band induced by the KrF excimer laser photon irradiation is assigned to the GEC, which shows the Ge(1) signal in ESR measurements.

ACKNOWLEDGMENTS

The authors express their thanks to Dr. K. Muta and M. Kato of Showa Electric Wire and Cable, for providing the samples. This work was partly supported by a Grant-in-Aid from JSPS and a Grant-in-Aid for Scientific Research (Grant No. 09450132), both from the Ministry of Education, Science, Sports, and Culture of Japan. This work was also supported by the Foundation of Ando Laboratory. One of the authors (M.F.) would like to thank the Japan Society for the Promotion of Science for financial support.

[1] K. O. Hill, Y. Fujii, D. C. Johnson, and B. S. Kawasaki, Appl. Phys. Lett. **32**, 647 (1978).
[2] D. M. Bird, J. R. Armitage, R. Kashyap, R. M. A. Fatah, and K. H. Cameron, Electron. Lett. **27**, 1115 (1991).
[3] G. A. Ball, W. W. Morey, and J. P. Waters, Electron. Lett. **26**, 1829 (1990).
[4] R. P. Davey, K. Smith, R. Kashyap, and J. R. Armitage, Electron. Lett. **27**, 2087 (1991).
[5] J. L. Zyskind, V. Mizrahi, D. J. DiGiovanni, and J. W. Sulhoff, Electron. Lett. **28**, 1385 (1992).
[6] F. Bilodeau, B. Malo, D. C. Johnson, J. Albert, S. Theriault, and K. O. Hill, Tech. Dig. Ser.-Opt. Soc. Am. **8**, 130 (1995).
[7] W. W. Morey, G. Meltz, and W. H. Glenn, Proc. SPIE **1169**, 98 (1990).
[8] R. Kashyap, J. R. Armitage, R. J. Campbell, D. L. Williams, G. D. Maxwell, B. J. Ainsle, and C. A. Millar, BT Technol. J. **11**, 150 (1993).
[9] S. M. Melle, L. Kexing, and R. M. Measures, IEEE Photonics Technol. Lett. **4**, 516 (1992).
[10] L. Blair and S. A. Cassidy, Electron. Lett. **28**, 1734 (1992).

[11] A. Inoue, M. Shigematsu, M. Ito, M. Imai, M. Inai, Y. Hattori, and T. Mizunami, Optoelectron., Devices Technol. **10**, 119 (1995).
[12] F. Ouellette, Opt. Lett. **12**, 847 (1987).
[13] K. O. Hill, F. Bilodeau, B. Malo, T. Kitagawa, S. Theriault, D. C. Johnson, and J. Albert, Tech. Dig. Ser.-Opt. Soc. Am. **4**, 335 (1994).
[14] D. L. Williams, B. J. Ainslie, R. Kashyap, G. D. Maxwell, J. R. Armitage, R. J. Campbell, and R. Wyatt, Proc. SPIE **2044**, 55 (1993).
[15] P. J. Lemaire, R. M. Atkins, V. Mizrahi, and W. A. Reed, Electron. Lett. **29**, 1191 (1993).
[16] A. M. Vengsarkar, P. J. Lemaire, W. A. Reed, and K. W. Quoi, Tech. Dig. Ser.-Opt. Soc. Am. **4**, 48 (1994).
[17] T. Erdogan, A. Partovi, V. Mizrahi, P. J. Lemaire, W. L. Wilson, T. A. Strasser, and A. M. Glass, Appl. Opt. **34**, 6738 (1995).
[18] H. Hosono, Y. Abe, D. L. Kinser, R. A. Weeks, K. Muta, and H. Kawazoe, Phys. Rev. B **46**, 11 445 (1992).
[19] M. Fujimaki, T. Watanabe, T. Katoh, T. Kasahara, N. Miyazaki, Y. Ohki, and H. Nishikawa, Phys. Rev. B **57**, 3920 (1998).
[20] L. Dong, J. L. Archambault, L. Reekie, P. St. J. Russell, and D. N. Payne, Appl. Opt. **34**, 3436 (1995).
[21] D. L. Williams, S. T. Davey, R. Kashyap, J. R. Armitage, and B. J. Ainslie, Electron. Lett. **28**, 369 (1992).
[22] K. Awazu, H. Onuki, and K. Muta, J. Non-Cryst. Solids **211**, 158 (1997).
[23] K. Awazu, K. Muta, and H. Kawazoe, J. Appl. Phys. **74**, 2237 (1993).
[24] M. Kohketsu, K. Awazu, H. Kawazoe, and M. Yamane, Jpn. J. Appl. Phys., Part 1 **28**, 622 (1989).
[25] H. Hosono, M. Mizuguchi, H. Kawazoe, and J. Nishii, Jpn. J. Appl. Phys., Part 2 **35**, L234 (1996).
[26] E. J. Friebele and D. L. Griscom, in *Defects in Glasses*, edited by F. L. Galeener, D. L. Griscom, and M. J. Weber, MRS Symposia Proc. No. 61 (Materials Research Society, Pittsburgh, 1986), p. 319.
[27] E. V. Anoikin, A. N. Guryanov, D. D. Gusovskii, V. M. Mashinskii, S. I. Miroshnichenko, V. B. Neustruev, and V. A. Tikhomirov, Sov. Lightwave Commun. **1**, 29 (1991).
[28] V. B. Neustruev, J. Phys.: Condens. Matter **6**, 6901 (1994).
[29] J. Nishii, K. Fukumi, H. Yamanaka, K. Kawamura, H. Hosono, and H. Kawazoe, Phys. Rev. B **52**, 1661 (1995).
[30] A. Smakula, Z. Phys. **59**, 603 (1930).
[31] R. M. Atkins, P. J. Lemaire, T. Erdogan, and V. Mizrahi, Electron. Lett. **29**, 1234 (1993).
[32] C. M. Nelson and R. A. Weeks, J. Am. Ceram. Soc. **43**, 396 (1960).
[33] R. A. Weeks and C. M. Nelson, J. Am. Ceram. Soc. **43**, 399 (1960).

Direct deposition of a blanket tungsten layer on SiO_2 by preexposure of helium plasma

Takashi Noma[a)]
Engineering Department, MOS-LSI Division, Sanyo Electric Company, Ltd., Oizumi-Machi, Gumma 370-0596, Japan and Advanced Research Center for Science and Engineering, Waseda University, Shinjuku-ku, Tokyo 169-8555, Japan

Kwang Soo Seol,[b)] Makoto Fujimaki, and Yoshimichi Ohki
Department of Electrical, Electronics, and Computer Engineering, Waseda University, Shinjuku-ku, Tokyo 169-8555, Japan

(Received 30 October 1998; accepted for publication 12 March 1999)

By utilizing preexposure of helium plasma, a method of depositing a blanket tungsten layer directly on SiO_2 has been developed. When SiO_2 films are exposed to a helium plasma, oxygen atoms are knocked on by active species in the plasma and the surface becomes covered with reduced silicon. It is assumed that this silicon reacts with WF_6 to form tungsten nuclei, and that tungsten layers grow through the reaction of H_2 and WF_6 at these nuclei. The deposited tungsten layer is stable with a low resistivity in the form of the α-W crystal and shows strong adhesion to the SiO_2 film due to the anchoring effect of tungsten. © *1999 American Institute of Physics.* [S0021-8979(99)03912-2]

I. INTRODUCTION

Recently, scale reduction of very-large-scale-integrated (VLSI) circuits becomes even more important for semiconductor industries. In the present advanced wiring system, tungsten plugs filled in the blanket tungsten process are widely used in a contact or via contact. In this process, Ti and TiN (Ti/TiN) films are generally deposited between the W layer and SiO_2 underlayer by sputtering in order to secure a good adhesion with the underlayer, to protect the contact against encroachment of W to Si, and to keep acceptable contact resistance.[1] This makes the process complex and expensive. Moreover, the present sputtering technique is approaching the limit of the aspect ratio, and may result in the shortage of coverage. To overcome this point, a special sputtering apparatus such as the one using long-throw sputtering (LTS) (Ref. 2) or the one using ion metal plasma (IMP) (Ref. 3) has been developed. However, they are not necessarily satisfactory on many points such, as their high cost. As a result, it has become very important to deposit tungsten directly without using any adhesive layer. The main reason that the adhesive layer is requisite at present is because adhesion is very poor between the tungsten layer and the insulator SiO_2 or Si_3N_4.[1,4] As a method of direct deposition of tungsten, several methods have been proposed. One is the high-dose implantation of W or Si onto the oxide surface to serve as a nucleus for deposition.[5,6] Another trial is the implantation of Ti ions and the following irradiation of ArF excimer laser photons in a WF_6/H_2 atmosphere.[7] In the former method, it is reported that the deposition of tungsten occurs if the implanted dose of Si exceeds $5\times10^{16}\,cm^{-2}$, and that good adhesion is secured between doses of 5×10^{16} and $1\times10^{17}\,cm^{-2}$. This process seems attractive, but a high dose of implantation is required. This article reports a process of direct deposition of tungsten on the oxide that utilizes preexposure of helium plasma.

II. EXPERIMENTAL PROCEDURE

A thin layer of SiO_2, about 200 nm thick, was deposited on a *p*-type silicon monocrystal substrate with a conductivity of 9–12 Ω cm by plasma-enhanced chemical vapor deposition (PECVD) using tetraethoxysilane [TEOS, $Si(OC_2H_5)_4$] as a monomer at 400 °C. A helium plasma excited with a rf power of 60 W at 13.56 MHz in the apparatus shown in Fig. 1 was used to activate the surface of SiO_2. The flow rate of helium was 10 sccm and the pressure was about 30 Pa during the plasma exposure. After that, tungsten was deposited by a CVD reactor using WF_6 and H_2 gases at 450 °C. The specimens had been etched for 10 s in 1% HF solution prior to W

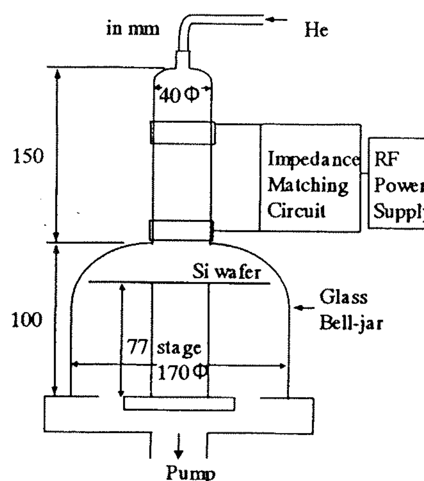

FIG. 1. Apparatus for plasma exposure.

a)Electronic mail: NOMA079814@swan.sanyo.co.jp
b)Present Address: Applied Laser Chemistry Laboratory, The Institute of Physical and Chemical Research (RIKEN), Hirosawa, Wako-shi, Saitama 351-0198, Japan.

 © 1999 American Institute of Physics

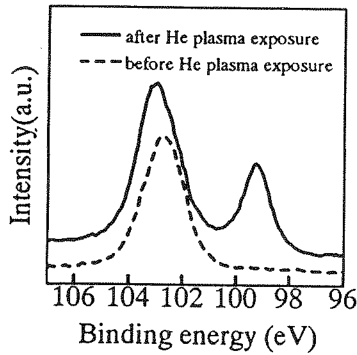

FIG. 2. XPS spectra of the surface of SiO_2 before and after the He plasma exposure.

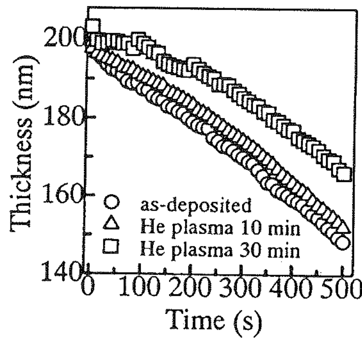

FIG. 3. Effect of exposure time to the He plasma on the etching speed.

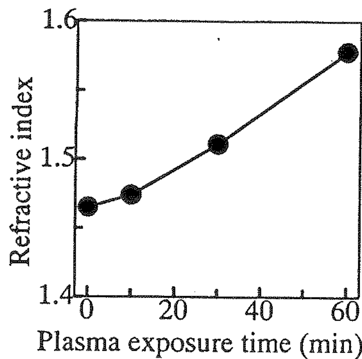

FIG. 4. Change in the refractive index with the plasma exposure time.

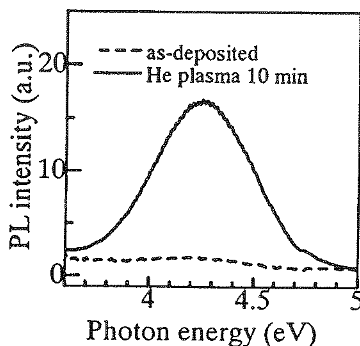

FIG. 5. PL spectra around 4.25 eV before and after the plasma exposure.

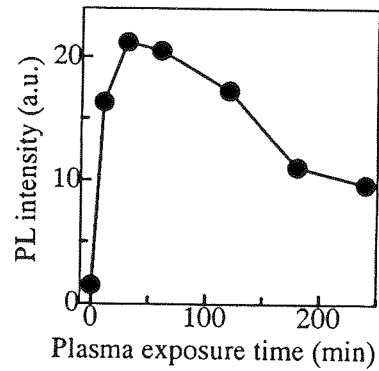

FIG. 6. Change in the 4.25 eV PL intensity with the plasma exposure time.

deposition to remove the native oxide. The x-ray photoelectron-spectroscopy (XPS) was obtained for the oxide surface after the plasma exposure with a JEOL JPS-90MX. The sample thickness and refractive index were measured at a wavelength of 632.8 nm with a microcomputer-aided Ulvac ESM-1 ellipsometer. The photoluminescence (PL) spectrum under excitation by a KrF excimer laser (wavelength: 248 nm=5 eV, pulse width: ~20 ns, Lambda Physik LPX105i) was obtained at room temperature by a multichannel detector (Princeton Instruments, SMA) equipped with a water-cooling system. The quality of deposited tungsten was examined by a four-probe resistance meter (Prometrix Omnimap RS20), a scanning electron microscope [(SEM), Hitachi S-900], and an x-ray diffractometer [(XRD), Rigaku Rint 2000].

III. RESULTS AND DISCUSSION

Figure 2 shows XPS spectra of the surface of SiO_2 before and after the helium plasma exposure for 1 h. Before the plasma exposure, only a single peak associated with Si $2p$ was observed at the binding energy of 103 eV. This peak corresponds to Si in the SiO_2 matrix. After the plasma exposure, two distinct peaks were observed at 103 and 99 eV. The 99 eV peak corresponds to elemental Si. This result shows that Si–Si bonds were formed on the surface of SiO_2 after the 1 h exposure of helium plasma. From the spectra, the ratio of O to Si was calculated to be 1.9 before the plasma

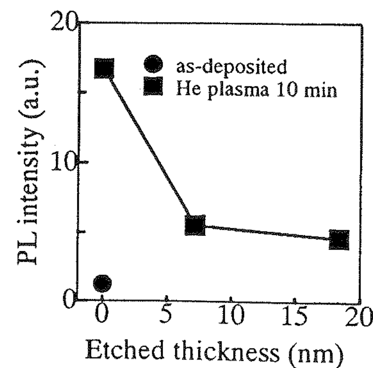

FIG. 7. Dependence of the 4.25 eV PL intensity on the remaining sample thickness for the sample that had been exposed to plasma exposure for 10 min.

TABLE I. Base sample of each specimen.

Specimen	Condition of base samples
A	as-deposited SiO_2
B	SiO_2 exposed to plasma for 30 min
C	SiO_2 exposed to plasma for 1 h
D	Si substrate

exposure, while the ratio became 1.0 after the exposure. However, due to experimental limitation, the sample had been exposed to air before the XPS measurement. This means that a native oxide layer must have existed on the surface. Therefore, it is assumed that the actual surface has to be more Si surplus than the above ratio.

Figure 3 shows the relation between the SiO_2 thickness and the etching time in a HF solution of 0.063%. It is clear that the surface becomes more resistive to etching after the plasma exposure. Since the change in etching speed is limited in the vicinity of the surface, the structure of SiO_2 in the surface layer was changed by the plasma exposure that would bring about the change in the XPS spectrum shown in Fig. 2. Since the elemental silicon is insoluble in HF, the present result agrees with the result of Thomas and coworkers who observed the delay in etching rate after implantation of Si in SiO_2 films.[6]

Figure 4 shows the change in refractive index with the plasma exposure time. The index increases. Since the refractive index at a wavelength of 632.8 nm is 1.46 for SiO_2 and 3.91 for Si,[8] this result also shows that a Si and/or Si-rich layer was formed on SiO_2 by the plasma exposure.

Figure 5 shows the PL spectra obtained before and after the plasma exposure. A PL band is seen at 4.25 eV. This PL band is considered to be due to the oxygen-vacancy defect ≡Si—Si≡, where "≡" denotes three separate oxygens.[9,10] It is considered that oxygen-deficient defects are formed since O atoms are scissored out of the bonds between Si and O by the reaction of the plasma. Figure 6 shows the 4.25 eV PL intensity as a function of the plasma exposure time, which indicates that the number of oxygen-vacancy defects decreases gradually after it shows an abrupt increase. If the oxygen atoms around one oxygen vacancy are expelled by the continued action of the plasma, the number of oxygen-vacancy defects decreases and a Si cluster or elemental Si appears.

Next, the spatial distribution of the oxygen-vacancy defects is examined. The sample was first exposed to the helium plasma for 10 min, and then etched in HF solution. The SiO_2 thickness before the plasma exposure was 0.2 μm. Figure 7 shows the change in the 4.25 eV PL intensity with the etched-off thickness. Here, the PL measurements were done immediately after the plasma exposure to avoid the formation of native oxide. Most of the oxygen-vacancy defects exist in the vicinity of the surface within the depth of 10 nm.

Tungsten was then deposited on the surface of various base specimens as listed in Table I, and the adhesive and other properties were examined. In the case of sample A, the deposition itself could not be done well; the tungsten was hardly deposited. The resistivity of the tungsten layer was

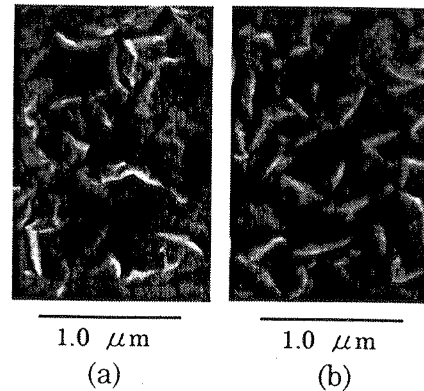

FIG. 9. SEM images of the W surface deposited on specimens B (a) and D (b).

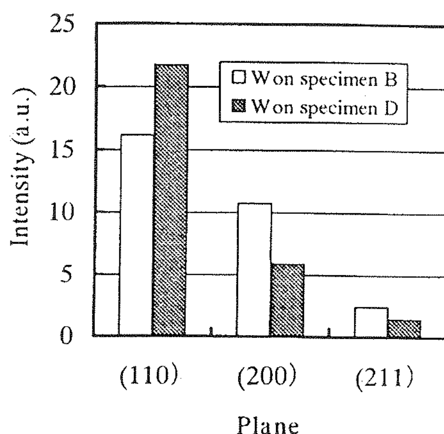

FIG. 8. Comparison of XRD spectral intensity between the tungsten layers deposited on specimens B and D.

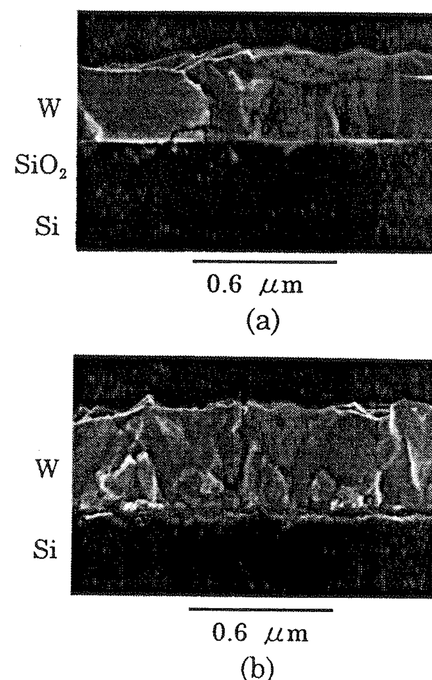

FIG. 10. Sectional structure of the tungsten layer on specimen B (a) and specimen C (b) observed by SEM.

measured to be $8.7\times10^{-8}\ \Omega$ m and the deposition rate was 4.0×10^{-7} m/min for sample D, while they were $8.9\times10^{-8}\ \Omega$ m and 2.4×10^{-7} m/min for sample B, respectively. These results can be understood by assuming the following reaction:[11]

$$WF_6+3Si\rightarrow W+3SiF_2. \quad (1)$$

Since specimen D is pure Si, tungsten can be deposited easily with a high deposition rate, while it cannot be deposited on the surface of specimen A, which is covered with SiO_2. The easiness of deposition on the surface of specimen B, which is covered with Si-rich SiO_2, should be in between specimens A and D.

Figure 8 shows the result of XRD measurements on the crystal structure of the tungsten layer. The tungsten structure is considered to be stable with a low resistivity in the form of α-W crystal in both cases of specimens B and D. The intensity of the (110) plane is stronger in W deposited on specimen D than W on specimen B. On the other hand, the intensities of the (200) and (211) planes are weaker for specimen D than for specimen B. It is considered that the orientation of the W layer depends on the base material.

Figures 9(a) and 9(b) show SEM images of the tungsten surface deposited on specimens B and D, respectively. It is clear that the tungsten grain size is larger in the case of the layer deposited on specimen B than the case of the deposition on specimen D.

The adhesion strength between the deposited tungsten layer and the surface of the underlying SiO_2 was examined using a pull test with adhesive tapes. The tungsten layer was peeled off from substrate C, but not from specimen B. A similar test repeated after exposing the tungsten layer on specimen B to air for a month again showed that the layer was not peeled off. This means that the tungsten layer adheres well to the Si-rich surface. Figure 10 shows the sectional structure observed by SEM. In the case of specimen B, some pins growing from the tungsten layer are observed. These pins are considered to be nucleated tungsten grown via Eq. (1) by choosing the Si-rich region in the SiO_2 film. Therefore, the contact area between the SiO_2 film and the tungsten layer is large, and this results in good adhesion. On the other hand, in the case of specimen C, it seems that the whole SiO_2 disappeared and that the tungsten reached the underlying Si substrate. It was observed by SEM that the tungsten layer was peeled off at its interface with the Si substrate. This reason is not clear, but probably due to some mismatching between the grown tungsten layer and the Si substrate. This suggests that a proper plasma-exposure time should be selected to secure good adhesion to SiO_2.

IV. CONCLUSION

By using preexposure of helium plasma, direct deposition of a blanket tungsten layer on SiO_2 has been successful. It was found that a Si-rich structure was formed on the SiO_2 surface by the plasma exposure. Since W is formed through a reaction of WF_6 with Si, the deposited tungsten shows strong adhesion to SiO_2.

ACKNOWLEDGMENTS

The authors express their thanks to T. Tabata, T. Kubota, M. Hara, and Y. Kanuma of Sanyo Electric Co., Ltd., and T. Koizumi of the Research Support Section, School of Science and Engineering, Waseda University for their cooperation.

[1] J. E. J. Schmitz, in *Chemical Vapor Deposition of Tungsten and Tungsten Silicides for VLSI/ULSI Applications* (Noyes, Park Ridge, NJ, 1992), p. 12.

[2] T. Smy, L. Tan, K. Chan, J. N. Broughton, R. N. Tait, S. K. Dew, and M. J. Brett, 14th International VLSI Multilevel Interconnection Conference Proceedings (1997), p. 204.

[3] H. J. Barth, H. Helneder, D. Piscevic, M. Schneegans, G. Birkmaier, G. Crowley, H. Kieu, S. Ramaswami, and U. Richter, 14th International VLSI Multilevel Interconnection Conference Proceedings (1997), p. 225.

[4] K. C. Ray Chiu and N. E. Zetterquist, in *Proceedings of the Workshop on Tungsten and Other Refractory Metals for VLSI Applications II*, edited by E. K. Broadbent (MRS, Pittsburgh, PA, 1987), p. 177.

[5] W. A. Hennessy, M. Ghezzo, R. H. Wilson, and H. Bakhru, J. Electrochem. Soc. **135**, 1730 (1988).

[6] D. C. Thomas, N. W. Cheung, I. G. Brown, and S. S. Wong, in *Proceedings of the Workshop on Tungsten and Other Advanced Metals for VLSI/ULSI Applications V*, edited by S. S. Wong and S. Furukawa (MRS, Pittsburgh, PA, 1990), p. 233.

[7] H. Okuhira, S. Nishimatsu, and K. Ninomiya, in *Extended Abstracts of the 22nd (1990 International) Conference on Solid State Devices and Materials, Sendai, 1990* (Business Center for Academic Societies Japan, Tokyo, Japan, 1990), p. 231.

[8] D. R. Lide, in *Handbook of Chemistry and Physics*, 74th ed. (CRC Press, Boca Raton, 1993).

[9] K. S. Seol, A. Ieki, Y. Ohki, H. Nishikawa, and M. Tachimori, J. Appl. Phys. **79**, 412 (1996).

[10] K. S. Seol, T. Karasawa, Y. Ohki, H. Nishikawa, and M. Takiyama, Microelectron. Eng. **36**, 193 (1997).

[11] J. E. J. Schmitz, in *Chemical Vapor Deposition of Tungsten and Tungsten Silicides for VLSI/ULSI Applications* (Noyes, Park Ridge, NJ, 1992), p. 57.

論　文

プラズマ CVD 堆積 SiO_2 薄膜の絶縁破壊電界におよぼすフッ素添加の効果

学生員　加藤宙光　（早稲田大学）
非会員　高見明宏　（早稲田大学）
非会員　酒井真吾　（早稲田大学）
正　員　石井啓介　（早稲田大学）
正　員　大木義路　（早稲田大学）

Effects of Fluorine Doping on the Dielectric Strength in SiO_2 Films Formed by Plasma-enhanced Chemical Vapor Deposition

Hiromitsu Kato, Student member, Akihiro Takami, Non-member, Shingo Sakai, Non-member, Keisuke Ishii, Member, Yoshimichi Ohki, Member (Waseda University)

Fluorine-doped thin silicon dioxide films were synthesized by plasma-enhanced chemical vapor deposition of tetraethoxysilane and CF_4, and the dielectric strength was measured with a self-healing breakdown technique by applying short duration voltage pulses. As a result, the film containing a higher amount of fluorine has a higher dielectric strength. The reason for this increase is discussed, and two persuasive mechanisms are presented.

キーワード：SiO_2, プラズマ CVD, 絶縁破壊, シリコン酸化膜

1.　まえがき

非晶質 SiO_2 薄膜は、MOS デバイスのゲート酸化膜や LSI における層間絶縁膜として、また、近年、需要が高まっているフラッシュメモリーなどの不揮発性メモリーにおいて、トンネル酸化膜として使われている。このため、これらのデバイスの信頼性の向上をはかるべく、SiO_2 膜の品質改良を目指した研究が重要性を増している。また、例えば、フラッシュメモリーにおいては、(Fowler-Nordheim)FN 電流による情報書き換えの際の動作電界は 10～12MV/cm を越えることが必要であるため、SiO_2 膜の絶縁耐圧をいっそう向上させる必要性が高まっている。従来の研究では、SiO_2 の破壊電界を測定する際、直流ランプ電圧を使用するなど、比較的長い時間の電圧印加が行われてきた。ところが、フラッシュメモリーにおける FN 電流での情報書き換えの際の、トンネル酸化膜に高電界が連続で印加されている時間は数 ms～数 100ms 程度に過ぎない。印加時間が長くなれば、絶縁破壊現象に与える熱等の影響がより大きくなるはずである。よって、従来のランプ電圧を用いた測定では、実際の動作環境に即した特性評価となっていない可能性がある。また、一般に絶縁体の物性的限界としての絶縁破壊電界は出来るだけ時間の短いパルス電圧の印加により測定されるべきであるので、たとえ実際に動作環境と異なっている場合にも、短いパルス電圧印加による絶縁破壊の研究は重要である。

我々はこれまでの研究より、プラズマ CVD 法により堆積された SiO_2 膜へフッ素を添加することにより、微視的な構造がより均一になることを明らかにしてきた[1]。そこで本研究では、パルス幅 1μs 以下の方形波パルス電圧を用い、全ての電圧印加時間が数 ms 以下になる条件で測定を行ない、フッ素添加が SiO_2 膜の絶縁破壊強度におよぼす効果を調べた。その結果、無添加の SiO_2 膜に比べ、フッ素を最大 3.2atomic%含有した試料では、絶縁破壊強度が 2MV/cm 以上上昇することが見いだされた。本報告では、この実験結果を報告するとともに、フッ素が破壊電界の上昇を引き起こす機構について議論する。

2.　実験方法

試料は、図 1 に示した装置において、容量結合を介した 13.56MHz の高周波電源によりプラズマ化された酸素・四フッ化メタン(O_2/CF_4)混合気体中にテトラエトキシシラン（ $Si(OCH_2CH_3)_4$,TEOS ）を導入し作成された SiO_2 薄膜である。薄膜中のフッ素含有率は、CF_4 の流量を O_2 に対して変化させることにより制御した。堆積条件と電子プローブマイクロアナリシス（JEOL,JXA-8600）で測定した薄膜中のフッ素含有率を表 1 に示す。 SiO_2

の堆積は抵抗率 1～3Ωcm の n 形単結晶 Si 基板上に行われた。堆積時の基板温度は 600℃であり、膜厚は約 100nm 一定になるようにエリプソメーターで実測した。絶縁破壊電界の測定には、上記の試料に図2のように金を $0.8mm^2$ の電極となるように蒸着し、この金電極を陽極として、パルス幅 1μs の方形波パルス電圧を印加し、自己修復性破壊を生じさせた。絶縁破壊電界の測定に用いたのと同一の試料・電極形状を用いて電極間にパルス幅 20～200μs の方形パルス電圧を印加し、流れるリーク電流をオシロスコープ（Tektronix TDS320）により測定した。また、容量-電圧曲線は Sanwa MegaBytek MI-494 により測定した。

可視～真空紫外域における吸収・発光スペクトルはシンクロトロン放射光（分子科学研究所,UV-SOR）を光源として測定した。詳しい測定方法は既報[1]に譲るが、発光スペクトルは他の測定と同じく Si 単結晶基板上の堆積膜について測定した。吸収スペクトルについては、11.8eV の光まで透明な LiF 結晶を基板として、厚さ約 10nm の SiO_2 膜を作成した。他の実験方法については後述する。

3．結果と考察

図3に1例としてフッ素含有率 0%の F0 試料において観察された破壊回数に対する破壊電界の変化を示す。各試料でこのような特性が得られたので、破壊回数約 50 回以降のほぼ一定値となったデータの上部を結ぶ値（図 3 中に破線で示す）を有効な破壊電界値として採用した。図 4 に絶縁破壊電界と薄膜中のフッ素含有率の関係を示す。縦軸は、供試した 10 枚～15 枚の試料において得られたデータの標準偏差である。破壊電界はフッ素含有率の増加とともに単調に増加しており、F4 では F0 に比べて 2.5MV/cm もの増加が観測された。図 4 に示されるように、フッ素は破壊電界を上昇させることがわかったが、この原因として次の 5 つの機構の可能性について検討してゆく。

（ⅰ） SiO_2 中に形成される正の空間電荷密度が減少し Si/SiO_2 界面よりの、Fowler-Nordheim 注入電子電流が減少する。

（ⅱ） Si/SiO_2 界面の障壁の高さが増加し、注入を抑制する。

（ⅲ） 絶縁破壊電界を低下させる原因として知られている酸素空孔の数が減少する。

（ⅳ） SiO_2 の構造が変化し、禁制帯幅が増大する。

（ⅴ） フッ素の散乱によって電子の平均自由行程が減少する。

機構(ⅰ),(ⅱ)は Si/SiO_2 界面へのフッ素添加の作用に注目したもので、機構(ⅲ)～(ⅴ)は試料全体へのフッ素添加の効果に注目したものである。本実験においては、常に n 形 Si 基板が陰極となるように電圧を印加した。SiO_2 においては電子の移動度は正孔の移動度より桁違いに大きい

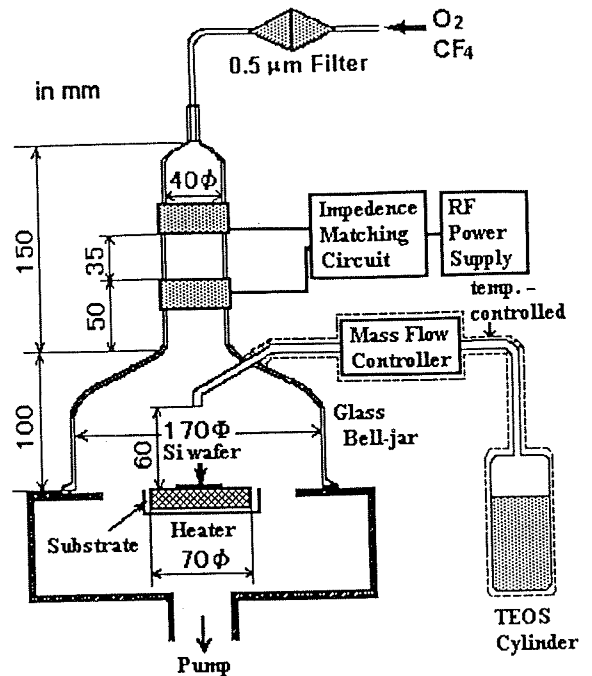

図1　プラズマ CVD 装置図
Fig.1. Plasma CVD apparatus for deposition of specimens.

表1　実験試料とフッ素含有率
Table Ⅰ. Specimens and their fluorine contents.

Specimen	Flow rate (sccm)			F content
	TEOS	O_2	CF_4	(atomic %)
F0	1	10	0	0
F1	1	10	5	1.3
F2	1	10	10	1.6
F3	1	10	20	2.3
F4	1	10	30	3.2

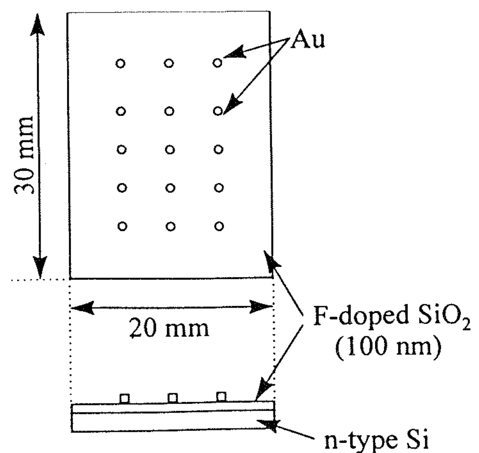

図2　破壊電界測定用試料構造
（試料名：F0, F1, F2, F3, F4）
Fig.2. Structure for the measurement of dielectric strength. (Specimens F0, F1, F2, F3, and F4)

ので、伝導や破壊を引き起こす電荷は n 形 Si より注入された電子である。よく知られているように、Si/SiO_2界面近傍の構造遷移層には、過剰な Si や、歪んだ Si-O 結合に代表される不完全構造が多量に存在する[2,3]。これらは、主に正孔トラップとして働き、正の空間電荷を形成するため、界面近傍の電界を強調し、電子の注入を促進させ、絶縁特性を劣化させる原因となる。一方、フッ素が添加された場合、それらの構造欠陥がフッ素により終端され、きわめて安定な≡Si-F 結合が形成されること、そのために正の空間電荷の形成が抑制されることが報告されている[4]。機構(ⅰ)は、フッ素添加により、界面での正の空間電荷の形成が抑制された結果、電子の注入が抑制され、SiO_2薄膜の破壊電界が上昇するというモデルである。

図 5 にリーク電流と印加電界との関係を示す。リーク電流はフッ素含有率にほとんど依存していない。この結果は、フッ素の導入により空間電荷の状態が変化している可能性は少ないことを示している。さらに、機構(ⅰ)では電圧が印加されるごとに空間電荷が蓄積されることを仮定しているわけであるが、機構(ⅰ)では最も空間電荷が蓄積されやすいと考えたはずのフッ素無添加試料 F0 においても破壊電界は電圧印加回数に対して図 3 の変化を示している。すなわち、初期の局所的な欠陥などが除去されたのちは電圧印加回数が増加しても、破壊電界は一定であり下ってはいない。したがって、少なくとも秒オーダーで安定に存在する空間電荷は蓄積されていなかったのではないかと考えられる。この事を検証するために、電圧を印加していない試料と、図 3 に示したような 50 回程度の破壊値の測定を終えた後の試料において、容量—電圧曲線を測定し、そのフラットバンド電圧シフトを求めた。なお、印加電圧は約 1V ステップで昇圧し、約 4V ステップで降圧したので、50 回の破壊は約 200 回の電圧印加に相当し、通過電荷量は約 2×10^{-8}C であった。図 6 に結果を示す。試料のフッ素含有率に依存せず、電圧を印加していない試料と、破壊測定を行った後の試料との間にフラットバンド電圧のシフト量に有意差は観測されない。すなわち、フラットバンドをシフトさせるような多くの量の空間電荷は蓄積されていないことが確かめられた。本研究で用いた方形波パルス電圧の時間幅は 1μs にすぎない。そのため、フッ素添加の有無に関わらず、測定の際、電圧印加を繰り返しても、高電界伝導特性や、容量—電圧特性、絶縁破壊特性に目立った変化を生じさせるほどの少なくとも秒オーダーで安定に存在可能な多量の空間電荷は形成されなかったのであると考えられる。以上の理由により、フッ素添加により正の空間電荷の形成が抑制され、n 形 Si 陰極よりの電子注入が減少することが、絶縁破壊電界を上昇させるという機構(ⅰ)は不適当であると思われる。

次に、フッ素の存在により、界面近傍のエネルギーバンド構造が変化し、Si/SiO_2間の障壁が変化した可能性、すなわち機構(ⅱ)を検討するために図 5 に示した高電界

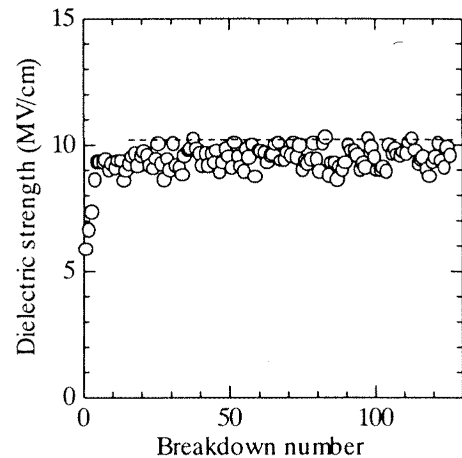

図 3 試料 F0 における破壊電界強度と破壊回数
(------: 有効破壊電界値)

Fig.3. Relation between the breakdown number and the dielectric strength in specimen F0. (----: The dielectric strength taken as an effective datum.)

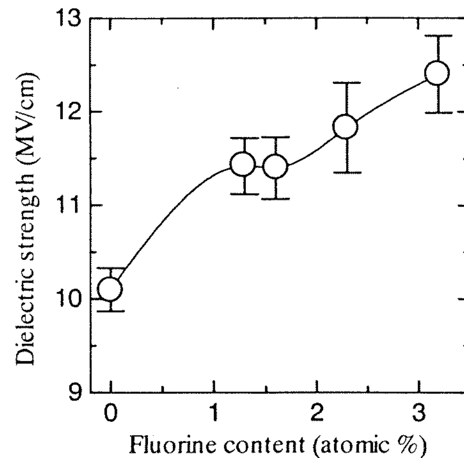

図 4 フッ素含有率と破壊電界

Fig.4. Relation between the dielectric strength and fluorine content.

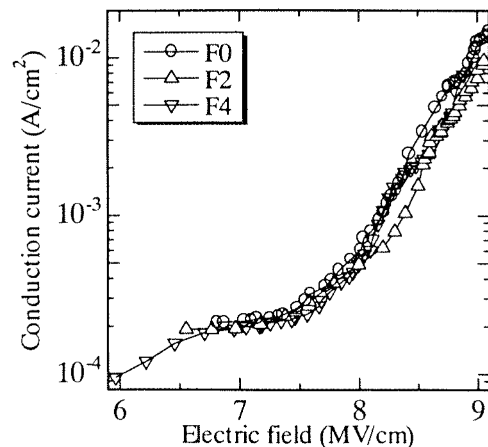

図 5 伝導電流特性 (J-E 曲線)

Fig.5. Relation between the conduction current and electric field.

域でのリーク電流を Fowler-Nordheim の関係によりプロットし直し、Si/SiO_2 界面における障壁高さを計算した結果を図 7 に示す。フッ素含有率が増加しても、障壁高さに顕著な変化は観測されない。これらは、機構(ii)に否定的な結果である。

次に機構(iii)であるが、SiO_2 中において、フッ素で終端された結合≡Si-F （≡は Si と 3 つの O 原子との結合を表わす）から酸素空孔≡Si-Si≡が生じる反応式として以下の式(1)が知られている[5]。

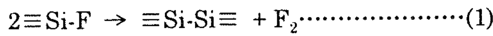

$$2\equiv\text{Si-F} \rightarrow \equiv\text{Si-Si}\equiv + F_2 \cdots\cdots\cdots\cdots\cdots\cdots (1)$$

一方、我々は、フッ素無添加の試料中には酸素空孔が含まれていること、また、酸素空孔が破壊電界を大幅に減少させている可能性を報告してきた[6]。もし仮に、膜を堆積させるプラズマ中にフッ素を導入させれば式（1）の逆反応が生じ、試料内の酸素空孔が減少すれば、絶縁破壊電界が上昇することが期待される。酸素空孔はエネルギー7.6eV の光子により励起したとき 4.4eV 近傍に発光帯を持つことが報告されている[6,7]。そこで、7.6eV 光で励起したときの発光スペクトルと、そのスペクトルを波形分離して得た 4.21eV、4.26eV、4.37eV にピークを持つ 3 つのガウス型ピークの発光強度とフッ素含有率の関係を図 8 に示す。このことより、フッ素含有率の多い試料ほど、発光強度は増加しており、酸素空孔が多量に含まれていることがわかる。プラズマ中にフッ素を導入したことにより、≡Si-F が増え、（1）式の反応が促進されたのであろうが、本試料の破壊電界の上昇の原因として、酸素空孔数が減少していたことは考えられない。

次に(iv)、(v)の機構について考える。我々は以前、TEOS よりプラズマ CVD で堆積させた SiO_2 薄膜にフッ素を添加した場合、無添加試料に比べ、微視的な構造の乱れが少なくなり均一で安定な膜が得られることを報告した[1]。図 9 は、真空紫外域での吸収スペクトルより算出した光学的禁制帯幅のフッ素含有率依存性を示している。フッ素含有率が増加するにつれて、構造の乱れに起因するバンド端部の局在準位が減少するからであろうが、禁制帯幅が単調に増加している。禁制帯幅が上昇すると、電子が衝突電離を引き起こすのに、より大きなエネルギーが必要になる。衝突電離に必要なエネルギーが光学的禁制帯幅の 1.5 倍である[8]と仮定した場合、図 9 より、フッ素含有率 2.3%の膜(F3)においては、フッ素を含有していない膜(F0)に比べて、衝突電離に必要なエネルギーは、0.53eV 大きいことになる。また、真空放出法を用い、SiO_2 中の電子の平均エネルギーの電界依存性を測定した結果によれば、7.5MV/cm 以上の高電界下の SiO_2 中における、電子の平均エネルギーは、陽極電界との間に、0.72eV·cm/MV なる近似関係を有していると報告されている。[9]この関係を用い、電子の平均エネルギーを、フッ素無添加膜(F0)と 2.3%含有膜(F3)との間の衝突電離エネルギー差である 0.53eV 引き上げるのに必要な電界は 0.73MV/cm と見積もることができる。この値は、両膜の

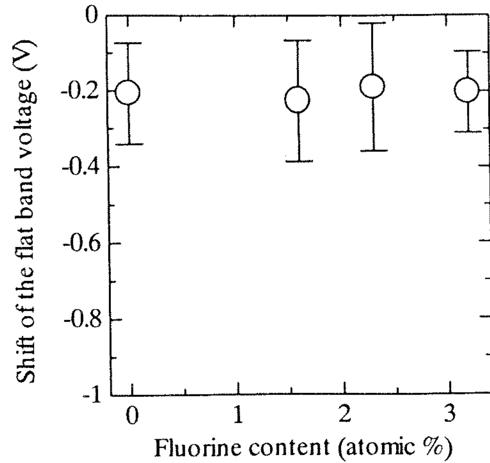

図 6 フラットバンドシフト電圧のフッ素含有率依存性

Fig.6. Relation between the shift of the flat band voltage and fluorine content.

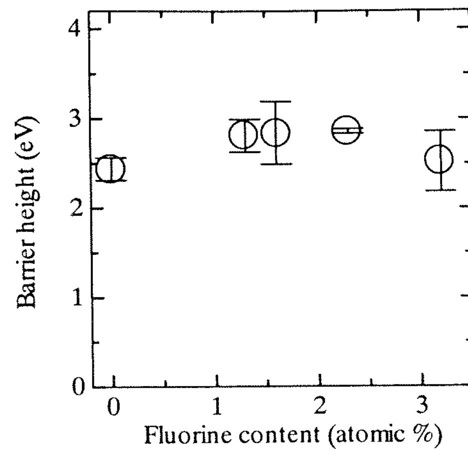

図 7 バリヤハイトのフッ素含有率依存性

Fig.7. Relation between the barrier height and fluorine content.

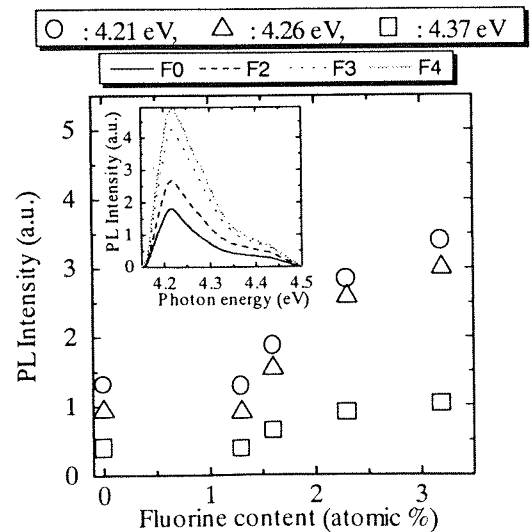

図 8 PL スペクトルと、それを波形分離して得たガウス型ピークの発光強度

Fig.8. Photoluminescence spectra of the specimens, and the intensities of component peaks at 4.21, 4.26, and 4.37 eV as a function of fluorine content.

間で実測された破壊電界の差である 1.7MV/cm のおよそ約 4 割に相当する。以上のことから、破壊電界の上昇の原因の 1 つとして、上記機構(iv)が挙げられる。

最後に機構(v)であるが、フッ素は非常に電気陰性度の大きい原子であるため、電子を散乱し、電子の平均自由行程が減少するので、破壊電界が上昇するとするモデルである。図 10 にフッ素無添加膜(F0)と 2.3%含有膜(F3)における破壊電界の膜厚依存性を示している。一般に、電極からの注入電荷により単一なだれ破壊が引き起こるとき、(2)、(3)式が成り立つ[10]。

$$\alpha = c\exp\left(-\frac{E_i}{eF_b\lambda}\right) \quad \cdots\cdots(2)$$

$$N_c = N_o \exp(\alpha d) \quad \cdots\cdots(3)$$

ただし、α:電離係数、c:定数、E_i:衝突電離のしきい値エネルギー、e:電子の電荷量、F_b:破壊電界、λ:平均自由行程、N_c:破壊を引き起こすのに必要な電子数、N_0:初期電子数、d:膜厚。

(2)、(3)式を変形して、

$$F_b = \frac{1}{K_1 \log d + K_2} \quad \cdots\cdots(4)$$

を得る。ここで $K_1 = \dfrac{e\lambda}{E_i}$ $K_2 = K_1 \log\left(\dfrac{c}{A}\right)$

$$A = \log\left(\frac{N_c}{N_o}\right).$$

そこで、図 10 に示した破壊電界の膜厚依存性を(4)式で最小 2 乗近似し(実線および破線)、式中の K_1 を各薄膜について求め、さらに、E_i を光学的禁制帯幅の 1.5 倍であると仮定し λ を算出した。その結果、F0 では λ=6.6nm、F3 では λ=5.2nm となり、フッ素を添加することにより λ が減少することがわかった。これより、機構(v)はフッ素添加により絶縁破壊電界が増加した原因の 1 つと考えられる。

さらに、この機構(v)の検証のために電界発光を測定した。図 11 のように、二層絶縁膜から成る試料を作った。まず、下部電極としての n 形 Si ウェハと上部電極としての透過率 55%の半透明金蒸着膜の間に、希土類である Tb を 1.3atomic%添加した SiO_2 薄膜とフッ素無添加の SiO_2 薄膜の二層を堆積させた試料 A と、同じ Tb 添加試料と 1.6atomic%フッ素を添加した SiO_2 薄膜の二層を堆積させた試料 B を作製した。さらに、両電極間に Tb 添加 SiO_2 薄膜のみを堆積させた試料 C と電極のついていない Tb 添加薄膜のみ(試料 D)も用意した。一般に Tb^{3+} は $^5D_4$ 準位から ^7D_j 準位への電子遷移に起因する発光を示す[11]。試料 D に KrF エキシマレーザーよりの 5.0eV の光子を照射したときの発光スペクトルを図 12 の実線で示す。また、

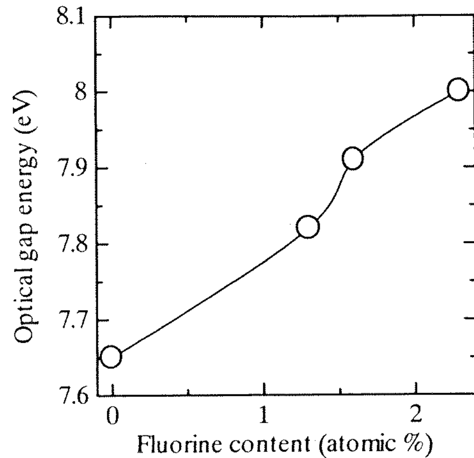

図 9 光学的禁制帯幅のフッ素含有率依存性
Fig.9. Relation between the optical gap energy and fluorine content.

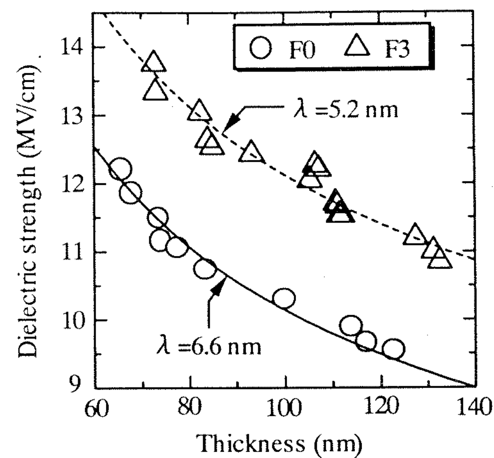

図 10 破壊電界の膜厚依存性
Fig.10. Thickness dependence of the dielectric strength.

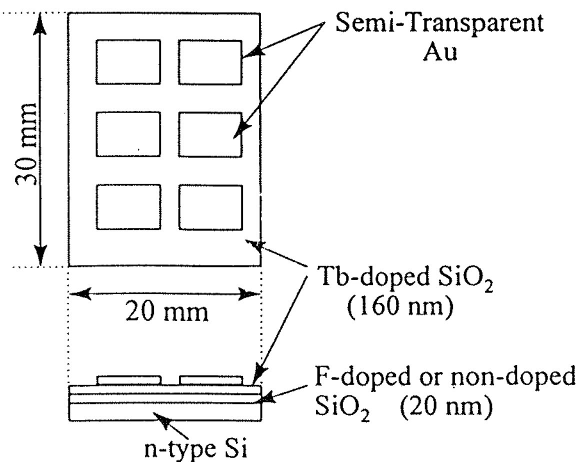

図 11 電界発光測定用の試料構造
Fig.11.Structure for the measurement of electroluminescence.(Specimen A and B)

試料 C において、Si 電極に-50V の直流電圧を印加して得た電界発光を同図中に破線で示す[11]。電界発光スペクトルはややブロードにはなっているが、発光が同一の原因に因ることは明らかである。試料 A,B においても、同じような電界発光スペクトルが得られた。これらの発光は、試料に電界を印加した際、Si 基板から、フッ素無添加、あるいはフッ素添加薄膜層を経て、Tb 添加薄膜層に注入された電子により発光している。図 12 において最も大きい発光強度を示した $^5D_4$ 準位から $^7F_5$ 準位への遷移による電界発光について、ほぼ同一強度の発光が観測された時点での印加電界を図 13 に示す。A では 2MV/cm 以下であるのに対し、B では 2MV/cm 以上であった。他の発光ピークについても同様な電界の差が見られた。すなわち

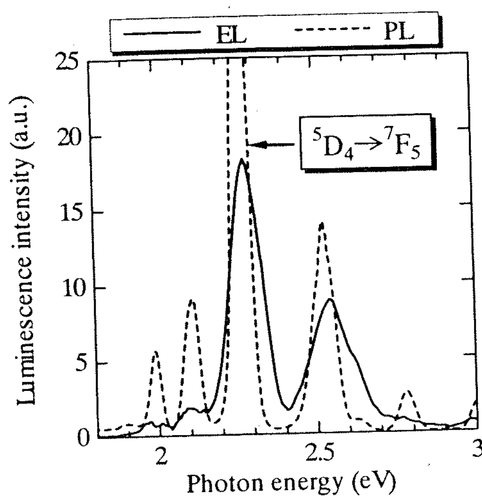

図 12 Tb-SiO_2の発光スペクトル (PL, EL)
Fig.12. Comparison of the electroluminescence and photoluminescence spectra from Tb-doped SiO_2.

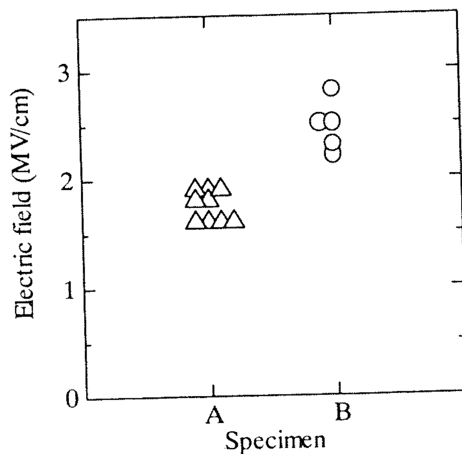

図 13 同一発光強度における印加電界
Fig.13. Comparison of the electric field strength electroluminescence was observed in specimens A and B.

試料 B においては電子はフッ素によって散乱され、同じエネルギーを得るのに高い電界を要したと考えられる。したがって、フッ素添加による絶縁破壊電界の上昇の原因の 1 つとして電子がフッ素に散乱され平均自由行程が減少したとする機構(v)は妥当であると考えられる。

4. 結論

SiO_2 薄膜にフッ素を添加することにより絶縁破壊電界が上昇した。この原因として、SiO_2 の光学的禁制帯幅が上昇したことと、フッ素により電子が散乱され、平均自由行程が減少したことが挙げられる。

5. 謝辞

本研究は、文部省より科研費(09450132) および、ハイテク・リサーチ・センター研究費の支援を受けた。また、シンクロトロン放射光を用いての測定は平成 8,9 年度 UVSOR 共同研究として行われた。

(平成 10 年 7 月 23 日受付，平成 10 年 12 月 15 日再受付)

文　献

(1)K. Ishii, A. Takami, and Y. Ohki, J. Appl. Phys. **81**, 1470 (1997).

(2)F. J. Grunthaner, P. J. Grunthaner, and J. Maserjian, IEEE Trans. Nucl. Sci. NS-**29**, 1462 (1982).

(3)F. J. Grunthaner, B. F. Lewis, N. Zamini, and J. Maserjian, IEEE Trans. Nucl. Sci. NS-**27**, 1640 (1980).

(4)K. Hirao, T. Kawano, K. Tanaka, and N. Soga, J. Ceram. Soc. Jpn. **99**, 600 (1991) (in Japanese).

(5)F. J. Feigl, W. B. Fowler, and K. L. Yip, Solid State Commun. **14**, 225 (1974).

(6)K. Ishii, D. Isshiki, Y.Ohki, H. Nishikawa, and M. Takiyama, Jpn. J. Appl. Phys. **34**, 205 (1995).

(7)K. Ishii, Y. Ohki, and H. Nishikawa, J. Appl. Phys. **76**, 5418 (1994).

(8)R. A. Logan and H. G. White, J. Appl. Phys. **36**, 3945 (1966).

(9)S. D. Brorson, D. J. DiMaria, M. V. Fischetti, F. L. Pesavento, P. M. Solomon, and D. W. Dong, J. Appl. Phys. **58**, 1302 (1985).

(10)K. Ishii and Y. Ohki, Trans. IEE Jap. **112-A**, No. 3, 188 (1992).

(11)G.Blasse and A. Bril, Philips. Res. Rept. **22**, 481 (1967).

加藤　宙光（学生員）1976年3月21日生。1998年4月早稲田大学大学院理工学研究科電気工学専攻修士課程入学、現在に至る。酸化膜の絶縁破壊特性評価の研究に従事。1998年猪瀬学術奨励金受領。

高見　明宏（非会員）1972年6月24日生。1998年3月早稲田大学大学院理工学研究科電気工学専攻修士課程修了。現在、（株）東芝。シリコン酸化膜の絶縁破壊特性評価の研究に従事。

酒井　真吾（非会員）1975年3月9日生。1997年4月早稲田大学大学院理工学研究科電気工学専攻修士課程入学、現在に至る。Tb添加シリコン酸化膜における電界発光の研究に従事。

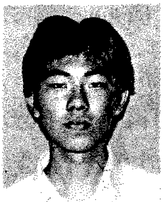

石井　啓介（正員）1965年8月12日生。1995年3月早稲田大学大学院博士課程修了、博士（工学）。1993年4月同大学理工学部助手、1995年4月同大学大学院理工学研究科訪問研究員、1997年1月防衛大学校電子工学科助手。電気絶縁薄膜の電気的・光学的特性および圧電セラミックスの研究に従事。

大木　義路（正員）1950年12月21日生。1978年3月早稲田大学大学院博士課程修了、工学博士。1976年4月同大学理工学部助手。現在、同教授。無機および有機誘電体材料（光透過材料、半導体用薄膜絶縁材料、電力用絶縁材料）の電気物性と光物性の研究に従事。1989年および1997年電気学会論文賞、1995年矢崎学術賞受賞。

Effects of ion implantation and thermal annealing on the photoluminescence in amorphous silicon nitride

Kwang Soo Seol,[a] Tsuyoshi Futami, Takashi Watanabe, and Yoshimichi Ohki[b]
Department of Electrical, Electronics, and Computer Engineering, Waseda University, 3-4-1 Ohkubo, Shinjuku-ku, Tokyo 169-8555, Japan

Makoto Takiyama
NSC Electron Corporation, 3434 Shimada, Hikari-shi, Yamaguchi 743-0063, Japan

(Received 16 November 1998; accepted for publication 27 January 1999)

When amorphous silicon nitride films are irradiated by a KrF excimer laser, they exhibit broad photoluminescence (PL) centered around 2.4 eV. The PL intensity gradually decreases and the PL peak energy shifts to a lower energy with an increase of the implanted dose of Ar^+ ions. This means that the PL consists of two components with peak energies at 2.66 and 2.15 eV and that implantation-induced defects such as vacancies are not the PL centers. The PL intensity is found to decrease if the film was thermally annealed, while the decreased PL intensity of the ion-implanted film recovers by the thermal annealing. Based on these results, it is concluded that the defects generated by hydrogen release or bond breaking act as nonradiative recombination centers that quench the PL. © *1999 American Institute of Physics.* [S0021-8979(99)03609-9]

I. INTRODUCTION

Amorphous silicon nitride (a-SiN_x) is one of the most important insulating materials in microelectronics, and is used as a gate insulator in field-effect or thin-film transistors, or as a charge storage layer in metal/nitride/oxide/silicon nonvolatile memories, or as a capacitor dielectric in dynamic random access memories. Generally, localized states in the band gap or at band tails due to defects or impurities govern the electrical properties of insulating films. The a-SiN_x film is not an exception to this. In order to examine the relation between the defects and electrical properties, much research has been carried out. Electrical and electron spin resonance studies have shown that intrinsic paramagnetic defects related to Si dangling bonds[1–3] and N dangling bonds[2–4] are the key charge trapping centers in a-SiN_x films. On the other hand, optical measurements such as photoluminescence (PL) and optical absorption have also been applied to characterization of the localized states in the nitride. For near-stoichiometric or nitrogen-rich a-SiN_x films, several PL bands have been reported in the range of 1.8–4.0 eV.[5–8] However, their origins are still in question.

The present article reports our investigation on the effects of ion implantation and thermal annealing upon the PL observed in a-SiN_x films prepared by the low-pressure chemical vapor deposition (LPCVD) method.

II. EXPERIMENT

The a-SiN_x film investigated in this study was deposited on a p-type (100) silicon substrate by LPCVD with a mixture of dichlorosilane (SiH_2Cl_2) and ammonia (NH_3) gases with a pressure of 65 Pa around 700 °C. The flow rate of NH_3/SiH_2Cl_2 was 15 for sample A and 10 for sample B. The thickness, measured by ellipsometry, is about 75 nm for sample A and 100 nm for sample B. The hydrogen content and the atomic ratio of N/Si, investigated by Rutherford backscattering, are, respectively, 6 mol % and 1.52 for sample A deposited at 650 °C, and 4 mol % and 1.44 for sample B. Some films were implanted by Ar^+ ions with an acceleration energy of 70 keV up to a dose of 1×10^{12}–5×10^{14} ions/cm^2. Both the as-deposited and the ion-implanted films were annealed in N_2 (1 atm) or in vacuum (4.0×10^{-2} Pa) by a rapid thermal annealing apparatus for 20 min.

Chemical change induced by thermal annealing was examined by Fourier-transform infrared absorption and thermal desorption spectroscopy (TDS). The PL spectra were measured at room temperature using a monochromator equipped with a multichannel detector under excitation by a KrF excimer laser [wavelength: 248 nm (5.0 eV); pulse width: ~20 ns; pulse energy: ~100 mJ/cm^2]. The PL excitation spectra

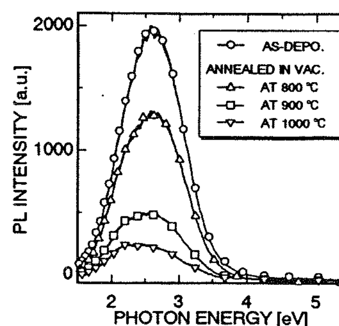

FIG. 1. Typical PL spectrum observed in a-SiN_x film (sample A) and its change caused by vacuum annealing.

[a]Present address: Applied Laser Chemistry Lab., The Institute of Physical and Chemical Research (RIKEN), 2-1 Hirosawa, Wako-shi, Saitama 351-0198, Japan.
[b]Electronic mail: yohki@mn.waseda.ac.jp

 © 1999 American Institute of Physics

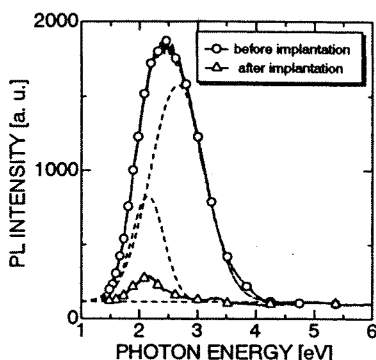

FIG. 2. Comparison of the PL spectrum of sample B before and after the implantation of Ar^+ ions with a dose of 5×10^{14} ions/cm^2. The broken curves are Gaussian components of the PL spectrum before the implantation.

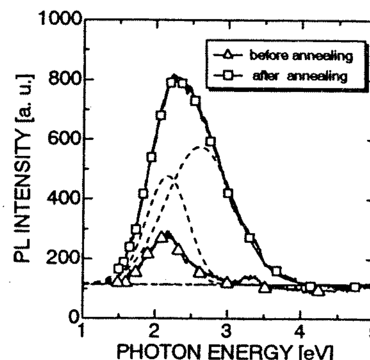

FIG. 4. Recovery of the PL intensity of sample B that had been quenched by ion implantation by thermal annealing at 900 °C for 20 min in N_2. The broken curves are Gaussian components of the recovered PL.

were obtained at 77 K using synchrotron radiation (SR) at the BL1B line of UVSOR facility (Institute for Molecular Science, Okazaki, Japan). The PL lifetime was measured with a single-photon counting technique using SR at 13 K.

III. RESULTS AND DISCUSSION

Figure 1 shows the typical PL spectrum observed in sample A, and its change by the thermal annealing done in vacuum. A broad PL band centered at about 2.4 eV is seen, and it decreases with the annealing. Figure 2 shows a comparison of the PL spectrum observed in sample B before and after the implantation of Ar^+ ions with a dose of 5×10^{14} ions/cm^2. A dramatic decrease in the intensity and redshift of the peak were observed after the implantation. The broken curves shown in Fig. 2 are the results of fitting the PL spectra with two Gaussian curves. This clearly indicates that the PL spectrum observed before ion implantation is composed of two PL bands centered at 2.66 and 2.15 eV, and that the 2.66 eV PL band completely disappears by the ion implantation. We have confirmed the reproducibility of the PL characteristics shown in Figs. 1 and 2 using 18 samples and have found that it is good regardless of the sample type being A or B. Furthermore, both the samples A and B show a similar PL intensity. Likewise, the characteristics described below are observed in both the samples A and B. From this viewpoint, the PL characteristics are common features of samples A and B.

Figure 3 shows the relation between the intensity of each PL band observed in sample B and the dose of implanted Ar^+ ions. The PL intensity decreases according to a power law with an increase in dose, and the exponent is larger for the 2.66 eV PL than the 2.15 eV PL. This is the reason that the PL shape shifts toward red.

In a-SiO_2 films, several PL bands such as the ones due to the oxygen vacancies and the nonbridging oxygen hole centers are induced by ion implantation.[9–11] The intensities of these PLs become larger with an increase in implantation dose.[9–11] In some a-SiO_2 films such as the one synthesized by plasma-enhanced chemical vapor deposition or the method called SIMOX (separation by implanted oxygen), these PLs are seen without ion implantation.[12,13] From these results, the PLs are considered to be associated with oxygen-deficient or oxygen-rich defects[14] and that the ion implantation has an action of manifesting weak sites such as strained bonds by converting them into PL-detectable defects.[9,10] However, the PL observed in the present study decreases its intensity with an increase of implanted dose of ions. This is the exact opposite of the result of a-SiO_2. Therefore, the PL in a-SiN_x is considered not to be due to implantation-induced defects such as vacancies or bond breaks.

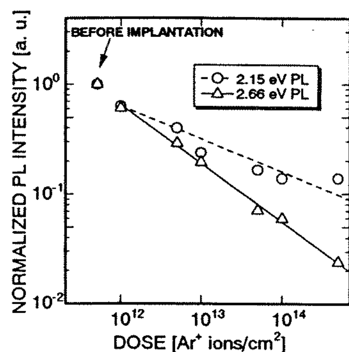

FIG. 3. Relation between the intensity of each PL band observed in sample B and the dose of implanted Ar^+ ions.

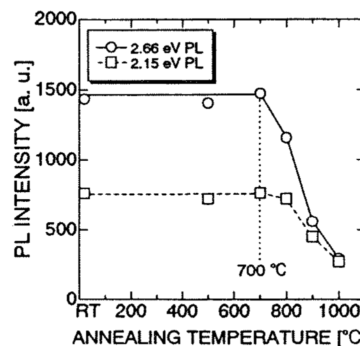

FIG. 5. Change in PL intensity at 2.66 and 2.15 eV by thermal annealing in vacuum for the nonimplanted sample A.

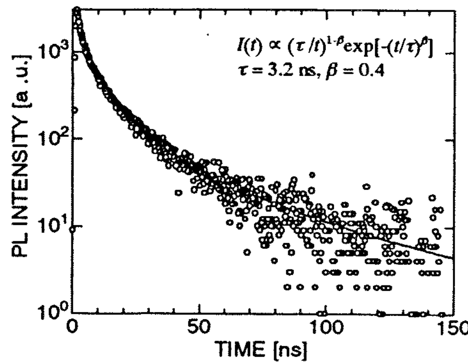

FIG. 6. PL decay excited by 5.0 eV photons from SR observed in the as-deposited sample A. I is the PL intensity, t the time, τ the effective lifetime, and β is a parameter which has a value between 0 and 1.

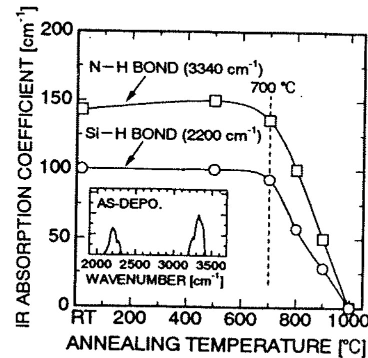

FIG. 8. Change in IR absorption due to Si–H bonds (2200 cm^{-1}) and N–H bonds (3340 cm^{-1}) by thermal annealing in vacuum, observed in sample A.

Figure 4 shows how the PL that had been quenched by ion implantation is recovered by thermal annealing done at 900 °C for 20 min in N_2. The broken curves are Gaussian components of the PL spectrum of the annealed sample. Although the recovered intensity is about one third of the intensity before ion implantation, the two PL bands of sample B are recovered by the thermal annealing. In a-SiO_2, the increased intensity by ion implantation decreases by similar thermal annealing.[15] This is also the opposite result of the present case of a-SiN_x.

Figure 5 shows the change in the respective PL intensities of the 2.66 and 2.15 eV bands by thermal annealing in vacuum, observed in nonimplanted sample A. The PL intensities decrease abruptly by the annealing at temperatures above 700 °C. Figure 6 shows the PL decay excited by 5.0 eV photons from SR, observed in the as-deposited sample A. It is clear that the decay is expressed by a stretched exponential function,

$$I(t) \propto (\tau/t)^{-\beta} \exp[-(t/\tau)^{\beta}],$$

where I is the PL intensity, t the time, τ the effective lifetime, and β is a parameter which has a value between 0 and 1.[16] When this sample is thermally annealed in vacuum, τ decreases as shown in Fig. 7, which β hardly changes.

Shown in Fig. 8 is the change in infrared (IR) absorption coefficients of sample A caused by the thermal annealing in vacuum. It is clear that the absorption at 3340 cm^{-1} due to N–H bonds and the one at 2200 cm^{-1} due to Si–H bonds abruptly decrease by thermal annealing at temperatures above 700 °C. This is very similar to the change of the PLs shown in Fig. 5. The above IR result indicates that hydrogen is released by the thermal annealing. In order to confirm this, TDS of hydrogen was measured for the as-deposited sample A. As shown in Fig. 9, it is confirmed that the desorption of hydrogen starts around 700 °C.

Figure 10 shows the relation between the PL intensity and the IR absorption coefficient. Both the 2.66 and 2.15 eV PL bands clearly show a linear relationship with the hydrogen-related bonds. The earlier-mentioned results suggest that the PL is related to the desorption of hydrogen. Therefore, the nonimplanted sample A was thermally annealed at 900 °C for 20 min in vacuum or in 100% hydrogen at 1 atm, and PL spectra were observed. As shown in Fig. 11, no change is seen for the H_2 annealing, while the PL intensity decreases significantly by the vacuum annealing. This clearly supports the above assumption that the PL in SiN_x is related to hydrogen desorption.

Shown in Fig. 12 are the PL excitation spectra of sample A monitored at 2.66 and 2.15 eV, measured at 77 K using SR. It is clear that the PL bands are excited by the photons with energies above 4.5 eV. The energy of 4.5 eV is close to the value of optical band gap for the near-stoichiometric SiN_x.[17] Therefore, the PL bands are considered to be related to recombination of electrons and holes, generated by interband photon absorption.

Previous studies[6–8] reported several PL bands between 1.8 and 4.0 eV in near-stoichiometric or silicon- or nitrogen-

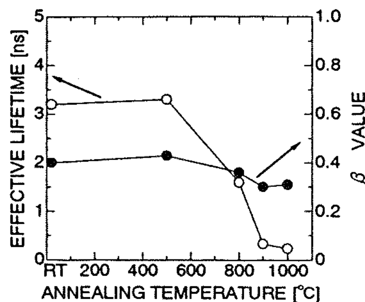

FIG. 7. Change in the effective lifetime (τ) and β parameter by thermal annealing in vacuum, observed in sample A.

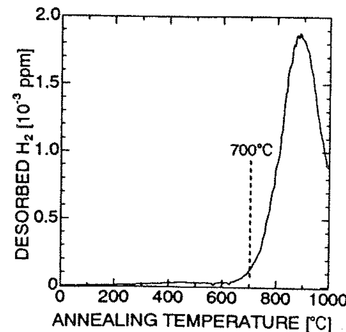

FIG. 9. TDS spectrum of hydrogen for the as-deposited sample A.

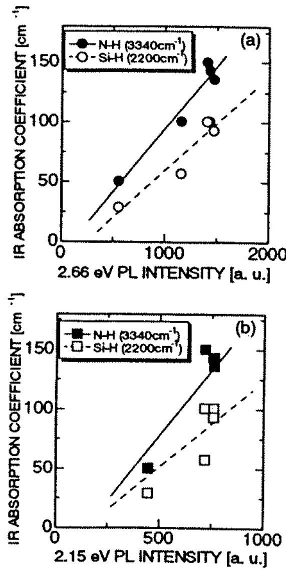

FIG. 10. Relationships between the PL intensity and the IR absorption coefficient of Si–H or that of N–H for (a) the 2.66 eV PL band and (b) the 2.15 eV PL band, observed in sample A.

rich amorphous SiN_x. Among those, a broad PL centered around 2.5 eV is commonly observed in near-stoichiometric or nitrogen-rich SiN_x. Based on the fact that the peak energy of the PL is similar to the calculated energy between the state of silicon dangling bond and valence or conduction band edge, the PL was previously attributed to the radiative recombination at the silicon dangling bond.[6] However, the present results suggest that the PL is not due to implantation-induced defects, and that the PL intensity decreases if hydrogen is released. Furthermore, the properties of the PL observed in the present study are very similar to those of the PL observed in hydrogenated amorphous silicon (a-Si:H).[18] In a-Si:H, the PL intensity also decreases if hydrogen is desorbed. The reason for this is considered to be that hydrogen in a-Si:H effectively eliminates the nonradiative sites relating to Si dangling bonds.[18] Furthermore, the PL in a-Si:H is quenched by ion implantation that could easily break Si–H bonds and Si–Si regular bonds.[18] These are quite close to the present results of SiN_x shown in Figs. 1–8. This similarity suggests that the ion-induced defects such as Si dangling

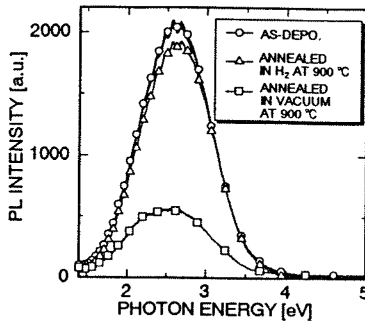

FIG. 11. Effect of thermal annealing in hydrogen or in vacuum on the PL spectrum observed in sample A.

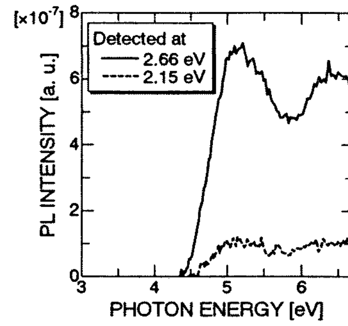

FIG. 12. PL excitation spectra for the 2.66 and 2.15 eV PL bands observed in sample A.

bonds are not the origin of PL in a-SiN_x but nonradiative recombination centers that quench the PL. Hydrogen is thought to eliminate the recombination centers.

IV. CONCLUSION

The effects of ion implantation and thermal annealing upon the PL have been investigated in a-SiN_x prepared by LPCVD. A broad PL band centered at 2.4 eV, consisting of two component PL bands at 2.66 and 2.15 eV, is observed in the as-deposited sample. When the a-SiN_x is implanted by ions or annealed at high temperatures, both PL bands are quenched. However, similar thermal annealing done to the ion-implanted sample recovers the PL intensity that had decreased by the ion implantation. The PL intensity is found to decrease if hydrogen is released from the sample. From these results, it is concluded that the defects formed by hydrogen release or bond breaking act as PL-quenching nonradiative recombination centers in a-SiN_x.

ACKNOWLEDGMENTS

This work was partly supported by the 1997 Joint Studies Program of UVSOR Facility, Institute for Molecular Science, Okazaki, Japan, by a Grant-in-Aid (No. 09450132) from the Ministry of Education, Science, Sports, and Culture of Japan, and by Kawasaki Steel 21st Century Foundation.

[1] P. M. Lenahan, D. T. Krick, and J. Kanicki, Appl. Surf. Sci. **39**, 392 (1989).
[2] W. L. Warren, J. Kanicki, F. C. Rong, and E. H. Poindexter, J. Electrochem. Soc. **139**, 880 (1992).
[3] W. L. Warren, F. C. Rong, E. H. Poindexter, G. J. Gerardi, and J. Kanicki, J. Appl. Phys. **70**, 346 (1991).
[4] W. L. Warren, P. M. Lenahan, and J. Kanicki, J. Appl. Phys. **70**, 2220 (1991).
[5] S. V. Deshpande, E. Gulari, S. W. Brown, and S. C. Rand, J. Appl. Phys. **77**, 6534 (1995).
[6] D. Chen, J. M. Viner, P. C. Taylor, and J. Kanicki, J. Non-Cryst. Solids **182**, 103 (1995).
[7] V. V. Vasilev, I. P. Mikhailovskii, and K. K. Svitashev, Phys. Status Solidi A **95**, K37 (1986).
[8] V. V. Vasilev and I. P. Mikhailovskii, Phys. Status Solidi A **90**, 355 (1985).
[9] H. Nishikawa, E. Watanabe, D. Ito, M. Takiyama, A. Ieki, and Y. Ohki, J. Appl. Phys. **78**, 842 (1995).
[10] K. S. Seol, A. Ieki, Y. Ohki, H. Nishikawa, and M. Takiyama, Proceed-

ings of the 1995 International Symposium on Electrical Insulating Materials, Tokyo, Japan, p. 85.
[11] K. S. Seol, Y. Ohki, H. Nishikawa, M. Takiyama, and Y. Hama, J. Appl. Phys. **80**, 6444 (1996).
[12] K. Ishii, Y. Ohki, and H. Nishikawa, J. Appl. Phys. **76**, 5418 (1994).
[13] K. S. Seol, A. Ieki, Y. Ohki, H. Nishikawa, and M. Tachimori, J. Appl. Phys. **79**, 412 (1996).
[14] Y. Ohki, K. Ishii, K. S. Seol, and H. Nishikawa, Trans. Inst. Electr. Eng. Jpn., Part A **116**, 387 (1996).
[15] K. S. Seol, T. Karasawa, Y. Ohki, H. Nishikawa, and M. Takiyama, Microelectron. Eng. **36**, 193 (1997).
[16] C. Tsang and R. A. Street, Phys. Rev. B **19**, 3027 (1979).
[17] J. Robertson, Philos. Mag. B **63**, 47 (1991).
[18] R. A. Street, Adv. Phys. **30**, 593 (1981).

Volume 11, Issue 12, 29 March 1999

J. Phys.: Condens. Matter **11** (1999) 2589–2594. Printed in the UK PII: S0953-8984(99)97617-8

Paramagnetic centres induced in Ge-doped SiO_2 glass with UV irradiation

Makoto Fujimaki†, Tetsuya Katoh, Toshiaki Kasahara, Nahoko Miyazaki and Yoshimichi Ohki

Department of Electrical, Electronics and Computer Engineering, Waseda University, 3-4-1 Okubo, Shinjuku-ku, Tokyo 169-8555, Japan

Received 16 September 1998, in final form 18 January 1999

Abstract. Changes in concentrations of the photo-induced paramagnetic centres, Ge E′ centre, Ge electron centre (GEC) and positively charged Ge lone-pair centre ($(GLPC)^+$) in four Ge-doped SiO_2 glasses with Ge contents of 1.0, 1.4, 6.9 and 9.2 mol% were investigated, using a KrCl excimer lamp (5.6 eV, 7.0 mW cm^{-2}) and a KrF excimer laser (5.0 eV, 4 MW cm^{-2}) as photon sources. When the glasses were irradiated with photons from the lamp, the Ge E′ centre and the GEC were induced in all the glasses. However, the $(GLPC)^+$ was observed only in the sample with Ge content of 1.4 mol% where the concentration of the induced Ge E′ centre was smaller than that of the induced GEC. The irradiation of photons from the laser induced the GEC and $(GLPC)^+$ in all the glasses. When the photon irradiation from the laser was continued onto the glasses, the Ge E′ centres were induced and the concentration of the $(GLPC)^+$ was found to decrease with an increase in the concentration of the Ge E′ centres. From these phenomena, it was concluded that the generation of the Ge E′ centres diminishes the concentration of the $(GLPC)^+$.

1. Introduction

Refractive-index changes accompanied by structural changes are induced in Ge-doped SiO_2 glass by the irradiation of ultraviolet (UV) photons. Because of the photo-sensitivity of Ge-doped SiO_2 glass, the glass is used as optical elements, such as an optical-filter which reflects a specific wavelength by Bragg gratings [1] fabricated in Ge-doped SiO_2 optical fibre by UV photons. It has been reported that the Ge oxygen-deficient centres (GODCs) existing in the oxygen-deficient type glass are considered to be responsible for the structural change which causes the refractive-index change [2–7]. Two kinds of GODC, the neutral oxygen monovacancy (NOMV) and the Ge lone-pair centre (GLPC), have been reported [2]. The structures of these defects are shown in figure 1. It has been reported that the NOMV and the GLPC have absorption bands at 5.06 and 5.16 eV, respectively [2]. As shown in figure 1, the NOMV becomes the Ge E′ centre by the irradiation of UV photons during which an electron is released [2].

Two electron spin resonance (ESR) signals, named Ge(1) and Ge(2) [8], are reported to appear in Ge-doped SiO_2 glass exposed to photons from a KrF excimer laser [9, 10]. The Ge(1) signal is known to be due to the Ge electron centre (GEC) [11–15]. In our previous paper, we reported that the Ge(2) signal is due to the positively charged GLPC ($(GLPC)^+$), which donated an electron to generate the GEC, by analysing the absorption change around 5.0 eV induced

† Research Fellow of the Japan Society for the Promotion of Science.

0953-8984/99/122589+06$19.50 © 1999 IOP Publishing Ltd

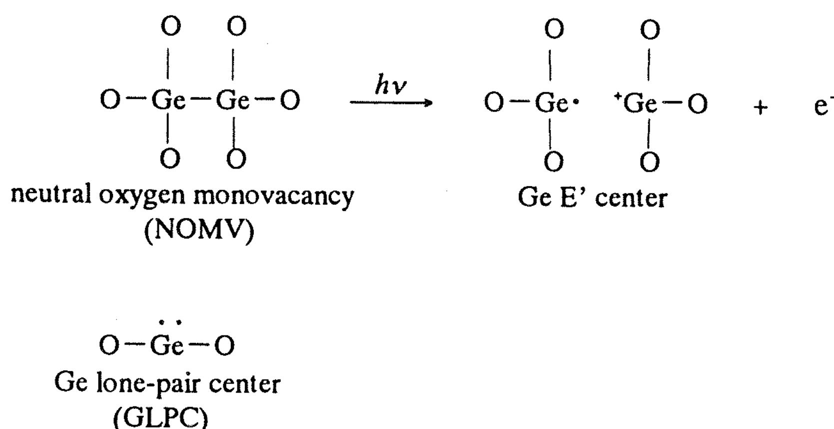

Figure 1. Structures of the defect centres in Ge-doped SiO_2 glass. The NOMV is known to become the Ge E′ centre by UV photon irradiation.

by photon irradiation from a KrF excimer laser and the thermally stimulated luminescence (TSL) which was observed at 3.1 eV in the sample pre-irradiated by the KrF excimer laser [9]. In the present research, further details of generation mechanisms of paramagnetic centres, GEC, $(GLPC)^+$ and Ge E′ centres, upon high-dose irradiation of UV photons are examined by observing the ESR signals induced in four different samples with different Ge contents.

2. Experiment

Four Ge-doped SiO_2 glasses, A, B, C and D with Ge contents of 1.0, 1.4, 6.9 and 9.2 mol%, respectively, were prepared by the vapour-phase axial deposition method. The samples were cut and polished into plates of 0.3 mm thick. A KrF excimer laser (Lambda Physik, LPX 105i, 5.0 eV) and a KrCl excimer lamp (Ushio, UEM 20-222, 5.6 eV) were used as the irradiation photon sources. The pulse duration of the excimer laser is about 20 ns, and its energy density is 80 mJ cm^{-2} per pulse, which corresponds to 4 MW cm^{-2}, while the energy density of the excimer lamp is 7.0 mW cm^{-2}. Because of this difference in energy density, the KrF excimer laser induces a two-photon process in addition to a one-photon process, while only a one-photon process is induced by the KrCl excimer lamp. The ESR spectra were obtained by a JEOL RE-2XG spectrometer at the X band frequency. The concentration of paramagnetic centres was evaluated by double numerical integration of first-derivative spectra, and comparison with the signal from diphenylpicrylhydrazyl (DPPH, $g = 2.0036$) of a known weight. The accuracy of the standard is believed to be ±20%. All the experiments were done at room temperature.

3. Results

Figure 2(a) shows the ESR spectrum of sample A irradiated by the KrCl excimer lamp for 15 hours. In this spectrum, the ESR signal of Ge(1) which is due to the GEC and that of Ge E′ centres overlap each other as clearly indicated in figure 2(a′). The Ge(2) signal is not seen in this spectrum, which means that the $(GLPC)^+$ does not exist in the sample after the irradiation. Similarly, the GEC and Ge E′ centre were observed in samples C and D after similar irradiation, and the $(GLPC)^+$ was not. Figures 2(b) and 2(b′) are the ESR spectra observed in sample B after irradiation by the lamp for 15 hours. The Ge(2) signal due to the $(GLPC)^+$ is seen besides the signals due to the GEC and Ge E′ centre. Table 1 shows the concentrations of

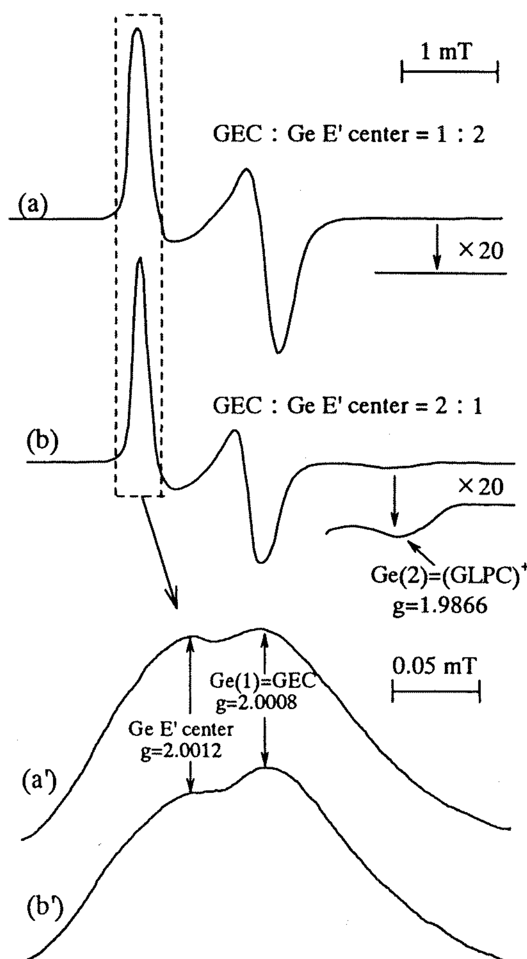

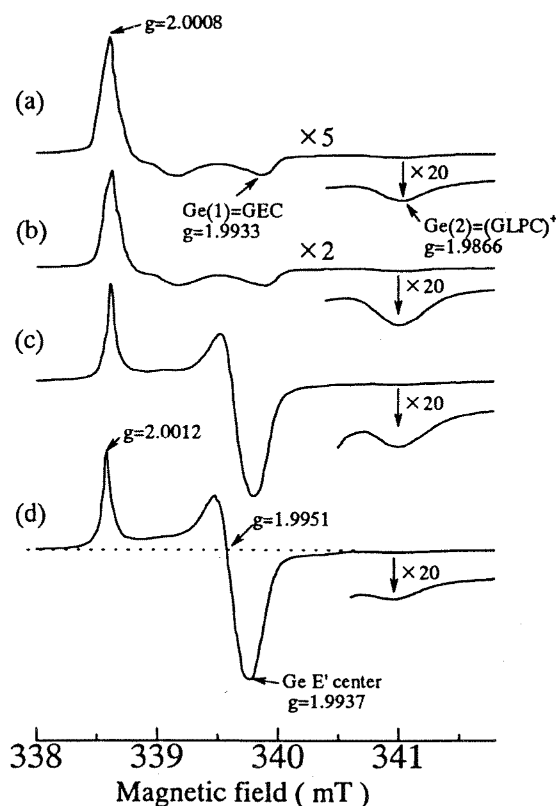

Figure 2. ESR spectra in sample A (a) and sample B (b) observed after the photon irradiation of KrCl excimer lamp for 15 hours. Spectra (a′) and (b′) represent the expansion of spectra (a) and (b) in the region surrounded by the dotted box, respectively.

Figure 3. ESR spectra in sample C observed after the photon irradiation of KrF excimer laser. (a) 10 shots, (b) 1×10^2 shots, (c) 1.3×10^6 shots, (d) 2.3×10^6 shots.

Table 1. Concentrations of the paramagnetic centres, Ge E′ centre, GEC and $(GLPC)^+$ induced in the samples with photon irradiation from the KrCl excimer lamp. The ambiguity comes from errors in calibration of the total concentration and separation of the peaks.

Sample	Ge content (mol%)	Ge E′ centre (cm^{-3})	GEC (cm^{-3})	$(GLPC)^+$ (cm^{-3})
A	1.0	$(7 \pm 2) \times 10^{15}$	$(4 \pm 2) \times 10^{15}$	—
B	1.4	$(2 \pm 0.5) \times 10^{15}$	$(3 \pm 1) \times 10^{15}$	$(2 \pm 0.5) \times 10^{15}$
C	6.9	$(2.4 \pm 0.2) \times 10^{16}$	$(3.5 \pm 2) \times 10^{15}$	—
D	9.2	$(2.6 \pm 0.2) \times 10^{16}$	$(4 \pm 2) \times 10^{15}$	—

these paramagnetic centres induced in the samples. The concentration of the Ge E′ centre is higher than that of GEC in samples A, C and D, while it is smaller than that of GEC in sample B. The result shown in table 1 also implies that the efficiency of the generation of the Ge E′ centre might be higher in glasses with higher Ge contents.

The ESR spectrum of sample C was found to change as shown in figure 3 when irradiated with the KrF excimer laser. The GEC and $(GLPC)^+$ are observed in the sample which was

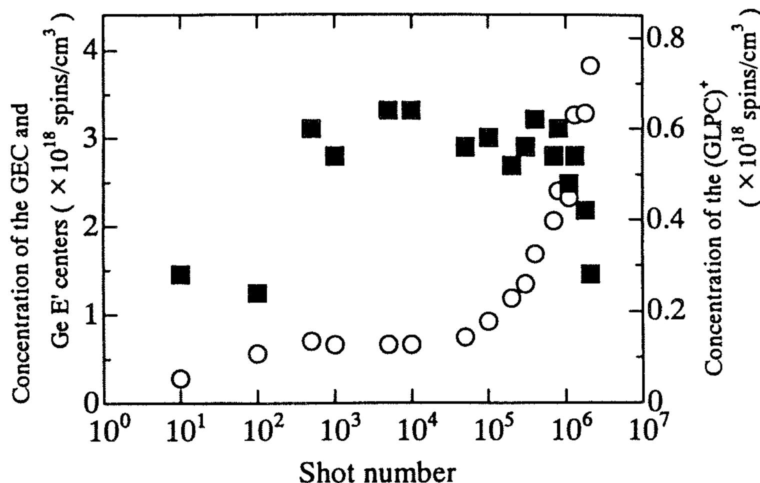

Figure 4. Change in the concentration of paramagnetic centres in sample C induced by the photon irradiation of a KrF excimer laser. The sum of the concentration of the GEC and Ge E′ centre (open circle) and the concentration of the $(GLPC)^+$ (solid square). The concentration of the $(GLPC)^+$ is estimated from the concavity at 341 mT.

irradiated with ten laser pulses. With the further irradiation, the Ge E′ centre was induced in addition to the GEC and $(GLPC)^+$. Figure 4 shows the change in the concentrations of the paramagnetic centres as a function of the number of laser shots. Since the accurate separation of the signals due to the GEC and Ge E′ centres was impossible, the sum of the two centres is shown by the open circle, while the solid square denotes the concentration of the $(GLPC)^+$. Here, the concentration of the $(GLPC)^+$ is estimated as follows. In [9], by investigating the decrease of the GLPC and the induction of the GEC by the photon irradiation from the same excimer laser that is used in the present research, we have confirmed that the concentration of the $(GLPC)^+$ is equal to that of the GEC when the glass is irradiated with a few tens of pulses by the present KrF excimer laser. Therefore, the concentration of the $(GLPC)^+$ is estimated to be a half of the total concentration of the induced paramagnetic centres, GEC and $(GLPC)^+$, in the sample irradiated with ten laser pulses. When further irradiation is applied to the glass, the concentration of the $(GLPC)^+$ can be estimated by the depth of the concavity of ESR spectrum around 341 mT ($g = 1.9866$), since no other signals overlap at this magnetic field and the concentration of the $(GLPC)^+$ is considered to be proportional to the depth. The concentration of the $(GLPC)^+$ showed saturation by the laser shots of about 5×10^2, and decreased with further irradiation. From our previous study, it is considered that the concentration of the GEC was saturated by the irradiation of 5×10^2 pulses and was virtually unchanged with further irradiation [7]. Therefore, the increment of the total paramagnetic centres with irradiation of more than about 10^5 shots is considered to be due to the increment of the Ge E′ centres.

4. Discussion

The $(GLPC)^+$ which are observed as the Ge(2) signal in the ESR spectrum were induced by the irradiation with the KrCl excimer lamp in sample B, while they were not in samples A, C and D. The result shown in table 1 indicates that the $(GLPC)^+$ is observed in the sample where the concentration of the induced Ge E′ centre is smaller than that of the induced GEC. From this result, it is expected that the generation of the Ge E′ centre diminishes the $(GLPC)^+$. As seen in figure 4, the concentration of the $(GLPC)^+$ begins to decrease when the concentration

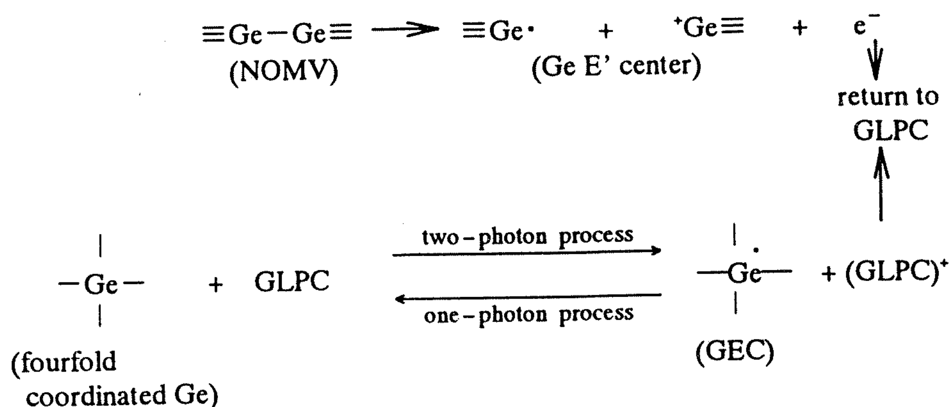

Figure 5. Proposed model for the structural changes induced by the photon irradiation of KrF excimer laser.

of the Ge E′ centres shows an increase after about 10^5 shots of the KrF excimer laser. This phenomenon validates the above-mentioned expectation. As shown in figure 1, electrons are known to be released upon the formation of the Ge E′ centres from the NOMVs [2]. The $(GLPC)^+$ traps the released electron and becomes the GLPC. Figure 5 shows the proposed series of structural changes. Since the Ge E′ centres are scarcely induced up to 5×10^2 shots of the KrF excimer laser [7, 10], the concentration of $(GLPC)^+$ or the Ge(2) signal intensity increases. If the number of $(GLPC)^+$ which become GLPCs by trapping the electrons released from the GECs [7] or the ones released from the NOMVs upon the formation of the Ge E′ centres is equal to that of the $(GLPC)^+$ which are induced from the GLPC's, the Ge(2) signal intensity should be unchanged. This is exactly what was observed during the irradiation of 5×10^2 to 10^6 shots of KrF excimer laser photons. With further irradiation, as the number of electrons released from the NOMVs increases, the decrease of $(GLPC)^+$ with trapping the electrons becomes larger than the increase of the $(GLPC)^+$, and thus the Ge(2) signal intensity decreases.

In [9] we assumed that the concentration of the GEC is equal to that of the $(GLPC)^+$, while in [3] and [12] the concentration of Ge(1) (=GEC) was reported to be larger than that of Ge(2) (=$(GLPC)^+$) when the glass was irradiated by UV photons or γ-rays. The model shown in figure 5 gives a clear solution to this discrepancy. The concentration of the GEC (=Ge(1)) and that of $(GLPC)^+$ (=Ge(2)) are considered to be equal, when the Ge E′ centre is not induced, which corresponds to the case reported in [9]. On the other hand, the concentration of the $(GLPC)^+$ becomes smaller than that of the GEC as reported in [3] and [12], when the Ge E′ centre is observed in addition to the GEC and $(GLPC)^+$. In [14], it has been reported that when Ce^{3+} is doped as an electron donor in Ge-doped SiO_2 glass, the GEC (=Ge(1)) is induced but the $(GLPC)^+$ (=Ge(2)) is not. In the present research, the NOMV plays the role of Ce^{3+} to be an electron donor and diminishes the $(GLPC)^+$ when high-dose UV photons are irradiated.

The above-mentioned conclusion is deduced based on the model that the Ge(2) signal is due to the $(GLPC)^+$ [9]. It might be unreasonable to assign the Ge(2) signal, whose g value is smaller than 2.0023, to a hole centre. However, it has been reported that the defect which shows the Ge(2) signal acts like a hole centre [14]. Furthermore, a trapped hole on Sn^{2+} shows the ESR signal with g values smaller than 2.0023, $g_{\parallel} = 1.972$ and $g_{\perp} = 2.000$, where Sn^{2+} indicates the Sn lone-pair centre in tin oxide [16]. Since Sn is a congener of Ge, this fact supports the assumption that the Ge(2) signal is due to the $(GLPC)^+$, even though the g value is smaller than 2.0023.

5. Conclusion

Through the analysis of ESR spectra induced by photon irradiation, the following conclusions were obtained. The Ge(1) signal is due to the GEC, while the Ge(2) signal is due to the $(GLPC)^+$ which donated an electron for the formation of the GEC. When both the Ge E′ centres and the GECs exist in the glass, the $(GLPC)^+$ trap electrons which were released from the NOMVs during the formation of the Ge E′ centres and become the GLPCs.

Acknowledgments

The authors express their thanks to Dr K Muta and Ms M Kato of Showa Electric Wire and Cable for providing the samples. This work was partly supported by Grants-in-Aid for JSPS Fellows and for Scientific Research (09450132) and a High-Tech Research Center Project, all from the Ministry of Education, Science, Sports and Culture of Japan.

References

[1] Hill K O, Fujii Y, Johnson D C and Kawasaki B S 1978 *Appl. Phys. Lett.* **32** 647
[2] Hosono H, Abe Y, Kinser D L, Weeks R A, Muta K and Kawazoe H 1992 *Phys. Rev.* B **46** 11 445
[3] Neustruev V B, Dianov E M, Kim V M, Mashinsky V M, Romanov M V, Guryanov A N, Khopin V F and Tikhomirov V A 1989 *Fiber Integr. Opt.* **8** 143
[4] Atkins R M and Mizrahi V 1992 *Electron. Lett.* **28** 1743
[5] Meltz G, Morey W W and Glenn W H 1989 *Opt. Lett.* **14** 823
[6] Dong L, Archambault J L, Reekie L, Russell P St J and Payne D N 1995 *Appl. Opt.* **34** 3436
[7] Fujimaki M, Yagi K, Ohki Y, Nishikawa H and Awazu K 1996 *Phys. Rev.* B **53** 9859
[8] Friebele E J, Griscom D L and Siegel G H Jr 1974 *J. Appl. Phys.* **45** 3424
[9] Fujimaki M, Watanabe T, Katoh T, Kasahara T, Miyazaki N, Ohki Y and Nishikawa H 1998 *Phys. Rev.* B **57** 3920
[10] Nishii J, Fukumi K, Yamanaka H, Kawamura K, Hosono H and Kawazoe H 1995 *Phys. Rev.* B **52** 1661
[11] Watanabe Y, Kawazoe H, Shibuya K and Muta K 1986 *Japan. J. Appl. Phys.* **25** 425
[12] Friebele E J and Griscom D L 1986 *Mater. Res. Soc. Symp. Proc.* vol 61 (Pittsburgh, PA: Materials Research Society) p 319
[13] Tsai T-E, Griscom D L and Friebele E J 1987 *Diffus. Defect Data* **53/54** 469
[14] Anoikin E V, Guryanov A N, Gusovskii D D, Mashinskii V M, Miroshnichenko S I, Neustruev V B, Tikhomirov V A and Zverev Yu B 1991 *Sov. Lightwave Commun.* **1** 123
[15] Neustruev V B 1994 *J. Phys.: Condens. Matter* **6** 6901
[16] Kawazoe H, Nishii J, Hosono H, Kanazawa T and Imagawa H 1982 *J. Physique Coll.* **43** C9 155

PHYSICAL REVIEW B VOLUME 59, NUMBER 3 15 JANUARY 1999-I

Temperature dependence of the lifetime of 4.3-eV photoluminescence in oxygen-deficient amorphous SiO_2

Kwang Soo Seol, Makoto Fujimaki, and Yoshimichi Ohki
Department of Electrical, Electronics, and Computer Engineering, Waseda University, Shinjuku-ku, Tokyo 169-8555, Japan

Hiroyuki Nishikawa
Department of Electrical Engineering, Tokyo Metropolitan University, 1-1 Minami Osawa, Hachioji, Tokyo 192-0397, Japan
(Received 14 July 1998; revised manuscript received 14 September 1998)

The temperature dependence of the lifetime of 4.3-eV photoluminescence (PL) excited by three PL excitation bands in oxygen-deficient amorphous silica has been investigated in the range of 13–280 K. When the PL is excited at the 5.0- or 6.7-eV band, it decays single exponentially with a constant lifetime of about 4 ns irrespective of temperature. On the other hand, PL excited at 7.3 eV decays nonexponentially, and its effective lifetime monotonically decreases with an increase in temperature. Such a temperature dependence of the PL lifetime is explained by assuming an energy diagram involving two configurations of the oxygen-deficient defect. [S0163-1829(99)06604-7]

I. INTRODUCTION

Photoluminescence (PL) at 4.3–4.4-eV together with its companion PL at 2.7 eV excited by ultraviolet and vacuum ultraviolet photons is best known among many PL's observed in amorphous silica (a-SiO_2).[1–11] The PL band has long been a subject of intensive studies, since it directly relates to the oxygen deficiency of a-SiO_2.[4–13] Up to the present, the two PL bands at 4.3 and 2.7 eV are considered to be due to transitions to the ground singlet state (S_0) from the lowest excited singlet state (S_1) and from the lowest excited triplet state (T_1) at the oxygen-deficient defect, respectively. However, electrons must have been raised up to a state which has the same energy as the PL excitation (PLE) band. For the 4.3-eV PL, three PLE bands are known to exist. Especially when the 4.3-eV PL is excited by 7.6-eV photons, the path through which electrons go down to the excited state (i.e., S_1 or T_1) from the state to which the electrons were first raised up is still a matter of question. Recently, we have attempted to cast light on this question by observing the decay characteristics of PL.[6–9] In the present study, the decay profile of 4.3-eV PL as a function of temperature was measured in more detail with a single-photon-counting technique using synchrotron radiation (SR) for all the three PLE bands.

II. EXPERIMENT

The samples used in the present study were carefully selected two types of oxygen-deficient amorphous silica with quite different manufacturing methods and shapes. One is bulk-shaped high-purity silica ([Cl]≅0 ppm, [OH]<1 ppm) manufactured by the soot remelting method. The other is of a thin film made by the method known as SIMOX (separation by implantation of oxygen) (Ref. 14) by implanting oxygen to a dose of $3.7\times 10^{17}\,cm^{-2}$ with an energy of 180 keV into a p-type (100) Si substrate and subsequent annealing at 1350 °C in Ar mixed with O_2 for a total of about 10 h. The Si overlayer of the SIMOX sample was removed by soaking in KOH solution for PL measurements. The oxide thickness is about 130 nm for the SIMOX sample and 0.7 mm for the bulk sample.

The PL spectrum was measured using a polychromator (Jobin-Yvon HR320) equipped with a multichannel detector (Princenton RY-1024) under excitation by a KrF excimer laser [wavelength, 248 nm (5.0 eV); pulse energy, 10–20 mJ/cm^2; Lambda Physik LPX105i]. The PLE spectrum and the PL decay were measured using SR operated at an electron energy of 750 MeV (BL1B line of UVSOR, Institute for Molecular Science, Okazaki, Japan). The PLE spectrum was observed under multibunch operation, while the decay kinetics was obtained by a time-correlated single-photon-counting technique under single-bunch operation (the time interval of the SR pulses, 177.6 ns; the apparent SR pulse width, 550 ps). The emitted photons dispersed by a bandpass filter were detected by a photomultiplier (Hamamatsu R955) for PLE or by a microchannel-plate photomultiplier (Hamamatsu R2287U-06) for decay kinetics. The obtained experimental results were normalized to the source intensity and corrected for the system response. The measurements were carried out over a temperature range from 13 to 280 K.

III. RESULTS AND DISCUSSION

Figure 1 shows the PL spectrum in the range of 3.5–4.7 eV, which was excited by 5.0-eV photons at room temperature, and the PLE spectrum of 4.3-eV PL for the (a) bulk and (b) SIMOX samples measured at 13 K. The PLE spectra have two distinct bands at 5.0 and 7.3 eV. Fitting the PLE spectra with Gaussian curves reveals that another PLE band exists around 6.7 eV.[6–9] For the three PLE bands, the peak energy and full width at half maximum (FWHM) are listed in Table I.

In the range of particular interest, 6–8 eV, the PLE spectra shown in Fig. 1 are consistent with the previous reports on a neutron-irradiated silica,[1] an ion-implanted a-SiO_2 sample,[15] or SIMOX.[16,17] However, it is different from the spectra previously measured on the pure silica glasses,[6–9]

 ©1999 The American Physical Society

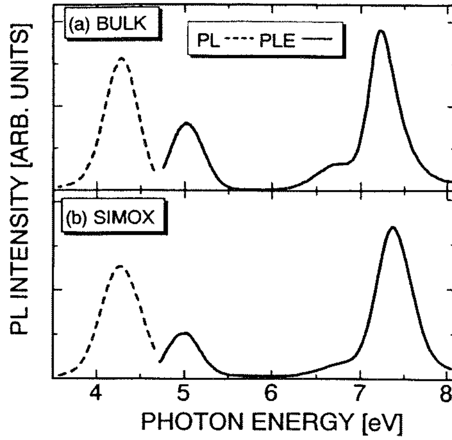

FIG. 1. PL spectrum excited at 5.0 eV and PLE spectrum measured at 13 K for (a) the bulk sample and (b) the SIMOX sample.

which show an intense PLE band at 6.8 eV. Such a difference is considered to be due to the sample-to-sample difference of the absorption strength at different wavelengths even if the sample is of the same type. In PL experiments, the PL or PLE spectral shape has a relatively weak importance than the PL lifetime. Although the lifetime of the present 4.3-eV PL, which is the subject of this paper, depends on the measuring temperature and excitation energy, it is between 0.5 and 4.2 ns. This difference is negligibly small if we consider the lifetime for the purpose of identifying the origin of the PL band or its transition path, since the lifetime varies over many digits from less than 1 ps to more than 1 h if the PL origin is different. However, the difference is important for the purpose of discussing the surrounding structure of the PL origin. Therefore, despite the difference in the PLE spectra, it is clear that the two present samples are oxygen deficient[4,6,7] and that the 5.0-eV PLE band corresponds to the $B_2\alpha$ band,[4] which is considered to be due to the S_0-S_1 transition of the oxygen-deficient defect.[6–10] The 7.3-eV PLE band corresponds to the E band at 7.6 eV,[1] which is distorted in shape due to its very strong absorption.[6] The 6.7-eV PLE band is attributed to the S_0-S_2 (S_2 is the second excited singlet state) transition of the defect.[6–9]

Decay profiles of 4.3-eV PL were measured for the bulk sample at eight different temperatures. Shown in Figs. 2, 3, and 4 are typical examples of the decay profiles of PL excited by 5.0-, 6.7-, and 7.3-eV photons, respectively. When the PL was excited at 5.0 and 6.7 eV, it decays single exponentially with a lifetime (τ) of ~4.2 ns regardless of the temperature. On the other hand, the PL decays nonexponentially for the excitation of 7.3-eV photons, and the decay deviates more from a single-exponential function at higher temperature. Such nonexponential decays can be fitted with the time derivative of a stretched-exponential function,

$$I(t)\propto(\beta/\tau')(\tau'/t)^{1-\beta}\exp[-(t/\tau')^{\beta}]. \quad (1)$$

Here τ' and β are the effective lifetime and a parameter which takes a value of $0<\beta<1$, respectively. For the SIMOX sample, although similar measurements were difficult due to the weak PL intensity, the decay was successfully observed at 13 and 180 K. Figure 5 shows all the observed results of the lifetime and β. The open rectangles and open circles are the lifetime data obtained for the bulk and SIMOX samples, respectively, while the open triangles and double circles are the β values obtained for the bulk and SIMOX

TABLE I. Peak energy and FWHM of the PLE bands.

Sample	Peak energy [eV]	FWHM [eV]
	5.02	0.41
Bulk	6.65	0.32
	7.25	0.43
	4.99	0.41
SIMOX	6.69	0.32
	7.38	0.50

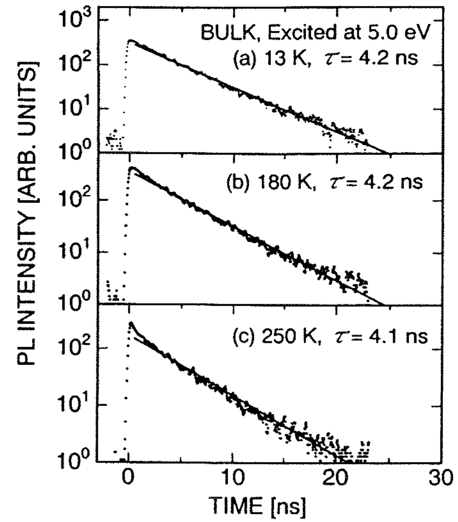

FIG. 2. Decay profiles of 4.3-eV PL excited by 5.0-eV photons measured for the bulk sample at (a) 13 K, (b) 180 K, and (c) 250 K. Solid lines are fitted with single-exponential functions.

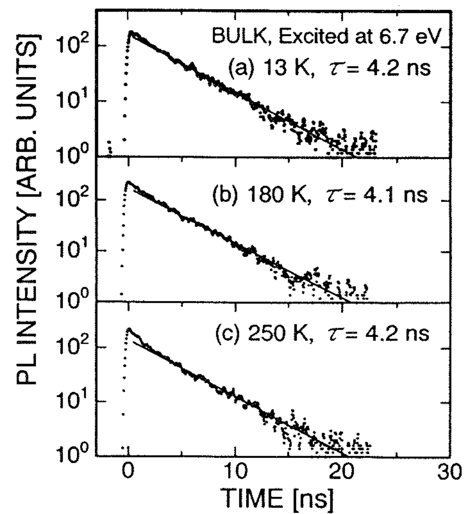

FIG. 3. Decay profiles of 4.3-eV PL excited by 6.7-eV photons measured for the bulk sample at (a) 13 K, (b) 180 K, and (c) 250 K. Solid lines are fitted with single-exponential functions.

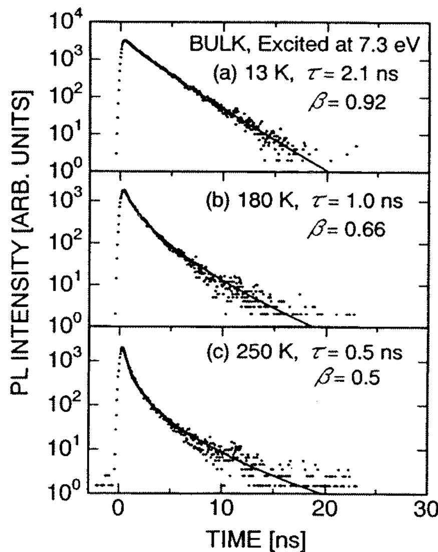

FIG. 4. Decay profiles of 4.3-eV PL excited by 7.3-eV photons measured for the bulk sample at (a) 13 K, (b) 180 K, and (c) 250 K. Solid lines are fitted with the stretched-exponential functions [Eq. (1)].

samples, respectively. The solid circles and solid triangles are previously reported lifetime data in Refs. 6 and 8, respectively.

Recently, we proposed an energy diagram involving two configurations of the oxygen-deficient defect, based on the fact that the lifetime of 4.3-eV PL measured at 45 K was 4.2 ns when excited at 5.0 or 6.9 eV and 2.1 ns when excited at 7.6 eV.[6] Figure 6 shows the proposed diagram.[6] The defect is assumed to have two configurations, depending on the ambient atmosphere. The 5.0- and 6.9-eV bands are, respectively, attributed to S_1 and S_2 states of the configuration C_1, while

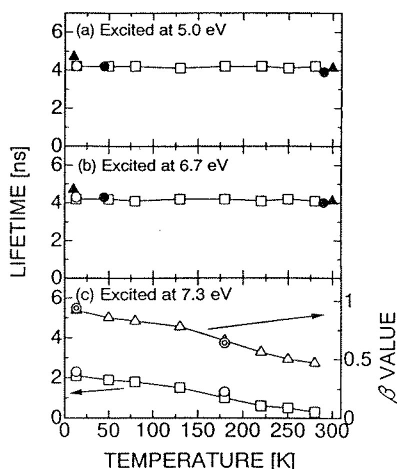

FIG. 5. Lifetime of 4.3-eV PL as a function of temperature for the excitation at (a) 5.0 eV, (b) 6.7 eV, and (c) 7.3 eV. Open rectangles and open circles are the lifetime obtained for the bulk and SIMOX samples, respectively, while solid circles and solid triangles are the data reproduced after Refs. 6 and 8, respectively. Open triangles and double circles are the β values obtained for the bulk and SIMOX samples, respectively.

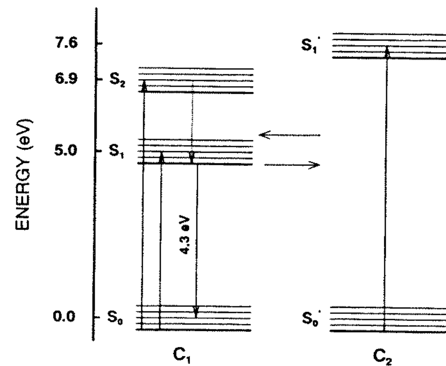

FIG. 6. Schematic energy diagram for the two-configuration model after Ref. 6. The 4.3-eV PL ($S_1 \rightarrow S_0$) is excited at 5.0 eV ($S_0 \rightarrow S_1$) and 6.9 eV ($S_0 \rightarrow S_2$) in the configuration C_1 and at 7.6 eV ($S_0' \rightarrow S_1'$) in the configuration C_2.

the 7.6-eV band is attributed to the lowest excited singlet state S_1' of the configuration C_2. Conversion between the two configurations can be caused when electrons are at the excited states. Therefore, electrons excited from the S_0' state by 7.6-eV photons can transfer to S_1. These electrons can move not only to S_0, but also to S_0', since the defect to which electrons belong had originally the configuration C_2. However, when the excitation is caused by 5.0- or 6.9-eV photons, the configuration C_2 plays no role.

Boscaino *et al.* threw doubt on the model based on their observed temperature dependence of the decay of 4.3-eV PL excited around 7.6 eV.[8,9] According to their results,[8,9] the 4.3-eV PL had virtually no temperature dependence. This is clearly contradictory to Figs. 4 and 5(c). As shown in Fig. 1, three distinct PLE bands are seen around 5.0, 6.7, and 7.3 eV in the present research. Compared to this, their PLE spectra showed two maxima centered around 5.0 and 6.8 eV. That is to say, their 6.8-eV PLE band existed at a higher energy than ours, and it became broader and shifted toward even higher energy at 10 K than at 300 K. They further reported that their PL lifetime measured at 300 K is the same for the 6.8- and 7.6-eV excitation.[8] From these situations, we cannot deny the possibility that their samples had a very weak PL intensity when excited at 7.6 eV and that they might have excited the tail of the 6.7-eV PLE band by 7.6-eV photons. If this is correct, their result cannot be the basis for throwing any doubt on our model.

Next, we would like to discuss the present data in the light of a model alternative to our proposed model, Fig. 6. Such a comparison better outlines the physics addressed by the present work. Recently, Pacchioni and Ierano[18] have proposed a model based on an *ab initio* calculation. They assumed that the 4.3-eV PL is directly related to the 7.5- (7.6-) eV excitation and that there is a slow nonradiative decay path between the state at 5.3 (5.0) eV and the state responsible for the 4.3-eV PL. This decay path explains well the longer lifetime for the 5.0-eV excitation. However, as shown in Fig. 4, the lifetime of PL when excited at 7.3 eV becomes shorter when the temperature increases. According to Pacchioni-Ierano model, the transition which causes the 4.3-eV PL is the same in both cases of 7.5- and 5.3-eV

excitations. This requires that the lifetime of the PL excited by 5.0- (5.3-) eV photons should become shorter by the temperature increase similarly to the one excited by 7.6- (7.3-) eV photons. Figure 2 (or 3) does not show such a phenomenon, nor did our previous experiment.[6,7]

Recently, there have been several other papers on theoretical calculations[19–21] in this matter, assuming neutral oxygen vacancy or twofold-coordinated silicon. In these papers, 4.3-eV PL is ascribed to the deexcitation process of the 5.0-eV excitation, which is in line with our assumptions. However, there is no description of the 7.6-eV excitation.

Another important finding in the present study is that the decay of PL excited at 7.3 eV shows a lower β value at a higher temperature. This means that the PL deviates more from a single-exponential decay at higher temperatures. Gee and Kastner assumed that the activation energy for the nonradiative decay from the upper electronic state should be distributed, originating from the structural disorder of glass.[1,2] Accepting this, one can easily consider that the number of activated paths with different decay constants increases at higher temperatures. This should be the reason for the low β value.

IV. CONCLUSION

A detailed study of the temperature dependence of the decay of 4.3-eV PL in a-SiO_2 shows that the decay of PL excited at 7.3 eV has a strong temperature dependence, differently from PL's excited at 5.0 or 6.7 eV. Such a temperature dependence is consistent with the model assuming an energy diagram involving two configurations of the oxygen-deficient defect.

ACKNOWLEDGMENTS

The authors express their thanks to M. Tachimori and M. Takiyama of Nippon Steel Corporation for providing samples and to H. Koike and T. Futami for their help in doing experiments. This work was partly supported by the Joint Studies Program (1996 and 1997) of UVSOR Facility, Institute for Molecular Science, Okazaki, Japan, a Grant-in-Aid for Scientific Research (No. 09450132) from the Ministry of Education, Science, Sports, and Culture of Japan, and by Kawasaki Steel 21st Century Foundation. One of authors (M.F.) would like to thank the Japan Society for the promotion of science for financial support.

[1] C. M. Gee and M. A. Kastner, Phys. Rev. Lett. **42**, 1765 (1979).
[2] C. M. Gee and M. A. Kastner, J. Non-Cryst. Solids **40**, 577 (1980).
[3] J. H. Stathis and M. A. Kastner, Phys. Rev. B **35**, 2972 (1987).
[4] R. Tohmon, H. Mizuno, Y. Ohki, K. Sasagane, K. Nagasawa, and Y. Hama, Phys. Rev. B **39**, 1337 (1989).
[5] H. Nishikawa, T. Shiroyama, R. Nakamura, Y. Ohki, K. Nagasawa, and Y. Hama, Phys. Rev. B **45**, 586 (1992).
[6] H. Nishikawa, E. Watanabe, D. Ito, and Y. Ohki, Phys. Rev. Lett. **72**, 2101 (1994).
[7] H. Nishikawa, Y. Miyake, E. Watanabe, D. Ito, K. S. Seol, Y. Ohki, K. Ishii, Y. Sakurai, and K. Nagasawa, J. Non-Cryst. Solids **222**, 221 (1997).
[8] R. Boscaino, M. Cannas, F. M. Gelardi, and M. Leone, J. Phys.: Condens. Matter **8**, L545 (1996).
[9] R. Boscaino, M. Cannas, F. M. Gelardi, and M. Leone, Phys. Rev. B **54**, 6194 (1996).
[10] L. N. Skuja, J. Non-Cryst. Solids **149**, 77 (1992).
[11] A. N. Trukhin, L. N. Skuja, A. G. Boganov, and V. S. Rudenko, J. Non-Cryst. Solids **149**, 96 (1992).
[12] H. Imai, K. Arai, H. Imagawa, H. Hosono, and Y. Abe, Phys. Rev. B **38**, 12 772 (1988).
[13] E. P. O'Reilly and J. Robertson, Phys. Rev. B **27**, 3780 (1983).
[14] K. Izumi, M. Doken, and H. Ariyoshi, Electron. Lett. **14**, 593 (1978).
[15] H. Nishikawa, E. Watanabe, D. Ito, M. Takiyama, A. Ieki, and Y. Ohki, J. Appl. Phys. **78**, 842 (1995).
[16] K. S. Seol, A. Ieki, Y. Ohki, H. Nishikawa, and M. Tachimori, J. Appl. Phys. **79**, 412 (1996).
[17] K. S. Seol, T. Karasawa, H. Koike, Y. Ohki, and M. Tachimori, in *Amorphous and Crystalline Insulating Thin Films—1996*, edited by W. L. Warren, J. Kanichi, R. A. B. Devine, M. Watsumura, S. Cristoloveanu, and Y. Hamma, MRS Symposia Proceedings No. 446 (Materials Research Society, Pittsburgh, 1997), p. 219.
[18] G. Pacchioni and G. Ierano, Phys. Rev. Lett. **79**, 753 (1997).
[19] B. L. Zhang and K. Raghavachari, Phys. Rev. B **55**, R15 993 (1997).
[20] V. B. Sulimov, V. O. Sokolov, and B. Poumellec, Phys. Status Solidi B **196**, 175 (1996).
[21] V. B. Sulimov and V. O. Sukolov, J. Non-Cryst. Solids **191**, 260 (1995).

論　文

プラズマ CVD 法による希土類添加シリカ薄膜
―― 成膜法の開発と発光の物性研究への応用 ――

非会員　四元茂之（早稲田大学）
非会員　酒井真吾（早稲田大学）
正　員　大木義路（早稲田大学）

Rare-earth-doped SiO_2 Films Prepared by Plasma-enhanced Chemical Vapor Deposition
―― Development of Deposition Method and Application of Its Luminescence to Research in Physics ――

Shigeyuki SHIMOTO, Non-member, Shingo SAKAI, Non-member,
Yoshimichi OHKI, Member (Waseda University)

Rare-earth-doped thin SiO_2 films were made by plasma-enhanced chemical vapor deposition using a complex containing chelating ligands and tetraethoxysilane. By this means of deposition, the film was successfully doped with terbium or erbium and the luminescence from the film was detected. Furthermore, by making a two-layered sample consisting of the terbium-doped SiO_2 film and non-doped SiO_2 film or fluorine-doped SiO_2 film and by examining the electroluminescence intensity, it was found that the acceleration of electrons by electric field is difficult in the fluorine-doped SiO_2 film.

キーワード：希土類添加シリカ、プラズマ CVD、低温堆積法、電子エネルギー、電界発光

1. はじめに

希土類元素は、レーザ、蛍光体、光メモリ、光ファイバ増幅器など様々なところで注目されている[(1)~(5)]。また、これまでは光学材料としての関心が強かったが、最近では磁性材料としての期待も高い[(6)]。これら希土類を添加した素子の開発に伴い、現在、回路の集積化に向けて、光学素子を平板型に構成する技術が注目されている[(7)~(9)]。これまで、平板型の導波路等のデバイスを作成する手段としては、電子ビーム蒸着、RF スパッタ法、火炎堆積法(FHD 法)などが報告されている。しかしながら、このうち、現在の主流である火炎堆積法はそのプロセスの中に、1000℃以上の高温下での反応過程を含む方法であるため[(10)]、今後は回路設計の面から低温化を実現することが重要になっていくと考えられる。

一方、シリカ(SiO_2)は、光ファイバや半導体の絶縁膜など極めて多方面に使用されている重要な材料である。したがって、希土類元素が添加される母体材料としてシリカを用いることができれば、エレクトロニクスおよび光エレクトロニクス分野の他のデバイスやプロセス技術との整合性が高まり、極めて有益である。

我々は、希土類のキレートとテトラエトキシシラン(TEOS)を原料として、プラズマ化学的気相堆積法(CVD 法)により希土類添加シリカ薄膜の低温堆積に成功した。本稿において、その方法を紹介する。さらに、この薄膜とシリカ薄膜またはフッ素添加シリカ薄膜の二層構造の試料における電界発光強度を比較することにより、シリカ薄膜中の電子のエネルギーに与えるフッ素の影響を検討した結果について述べる。

2. 実験方法

<2. 1>　成膜方法　　希土類添加シリカ薄膜は、図 1 に示す装置を用いてプラズマ CVD 法により堆積させた。キャリア気体兼酸化気体としての酸素を 0.5 μm のフィルターを経由して、ガラス製ベルジャーの上部より流入させ、容量性結合を介して投入した 13.56 MHz 高周波電力によりプラズマ化させた。この酸素プラズマの空間的アフターグロー（すなわちテールフレーム）に気化後 70℃に保ちながら輸送した TEOS を注入した。TEOS の流量は超高温微差圧用流量調整器（日立金属　SFC-670）により調整した。添加する希土類はテルビウム(Tb)またはエルビウム(Er)とし、tris(2, 2, 6, 6-tetramethyl-3, 5-heptanedionato) Tb (III)（または Er (III)）を用いた。この化合物は常温では固体であるため、加熱して昇華させ、キャリアーガスのアルゴン気流中に載せて TEOS ガスと共に O_2 プラズマのテールフレーム中に導入し、温度可変真空ヒータ上の n 型 Si ウェハに希土類添加シリカ薄膜を堆積した。気体流量、圧力、RF 電力などの堆積条件を表 1 に示す。

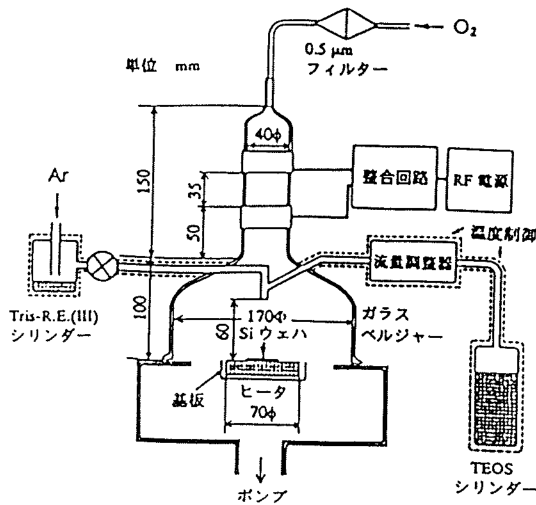

図1 プラズマ CVD 装置

Fig. 1 The apparatus for plasma-enhanced chemical vapor deposition.

表1 堆積条件

Table 1 The deposition conditions.

O_2流量	10 sccm
TEOS流量	1 sccm
圧力	50 Pa
RF電力	20 W
TEOS温度	70 ℃
Tris-R.E.(III) 温度	150 ℃
基板温度	室温 ～ 500 ℃
膜厚	150 ～ 500 nm

膜厚は He-Ne レーザ光（波長 632.8 nm）によるエリプソメータ（ULVAC ESM-1）により測定した。膜質の評価のために、AlK$_\alpha$線（エネルギー1486.7 eV）による X 線光電子分光（XPS, 日本電子 JPS-90MX）、誘導結合プラズマ原子発光分光（ICP-AES, 日本ジャーレルアッシュ IRIS-AP）、X 線蛍光分光（XRF, セイコー電子 SEA-2001L）、赤外分光（IR, PERKIN-ELMER 1600 Series FT-IR）の各スペクトルを測定した。さらに希土類元素含有率を電子プローブ微小部分析（EPMA, 日本電子 JAX-8600）により測定した。

<2. 2> 発光測定　Si ウェハ上に堆積した希土類添加シリカ薄膜に KrF エキシマレーザ光（Lambda Physik 105i, 光子エネルギー 5.0 eV = 248 nm）を照射したときの発光をモノクロメータ（Jobin-Yvon HR320）で分光したのち、マルチチャンネル検出器（Princeton Instruments SMA）または光電子増倍管（浜松ホトニクス R955）により計測した。さらに電界発光測定のために、図 2 に示すように、下部電極を n 型 Si ウェハ、上部電極を透過率 55%の半透明金蒸着膜とした 3 種類の試料 A, B および C を作製した。

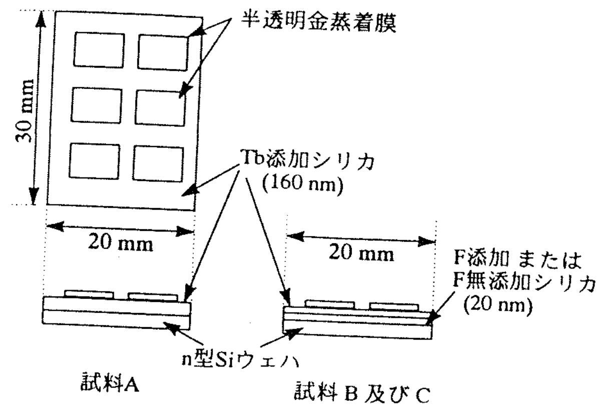

図 2 電界発光測定用試料の構造

Fig. 2 The structure for the measurement of electroluminescence.

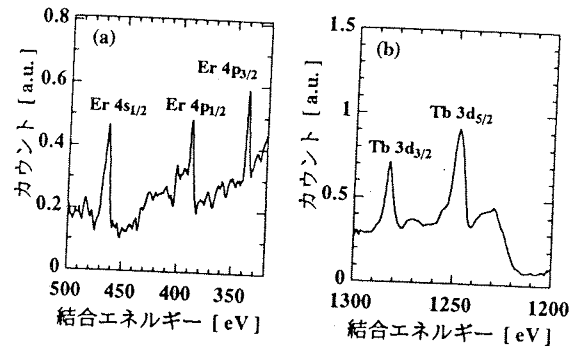

図 3 300℃で堆積した(a)Er^{3+}添加(b)Tb^{3+}添加シリカ薄膜の XPS スペクトル

Fig. 3 XPS spectra of (a) Er^{3+}-doped and (b) Tb^{3+}-doped SiO_2 films deposited at 300 ℃.

試料 A は、下部電極と上部電極の間に、希土類である Tb を 1.3 atomic%添加したシリカ薄膜を堆積させた試料である。試料 B は、フッ素無添加のシリカ薄膜と Tb を 1.3 atomic%添加したシリカ薄膜の二層を堆積させた試料である。試料 C は、フッ素を 1.6 atomic%添加したシリカ薄膜と Tb を 1.3 atomic%添加したシリカ薄膜の二層を堆積させた試料である。なお、ここでフッ素添加は、CF_4を O_2と混合させることにより行われた[11]。

また、本方法によりシリカ薄膜中に添加したフッ素は、そのほとんどが≡Si-F（“≡”は、3 つの異なる酸素との結合）の形で存在していることや、フッ素添加により、Si-O-Si の結合のゆがみが緩和されることが確かめられている[12]。

3. 実験結果および考察

<3. 1> 成膜について　シリカ薄膜中に希土類が添加されていることは機器分析により確認された。図 3 は、希土類として Er（正しくはエルビウム 3 価正イオン、Er^{3+}）および Tb^{3+}を添加し、基板温度 300℃で堆積させた膜の XPS スペクトルである。Er^{3+}あるいは Tb^{3+}に起因するいくつか

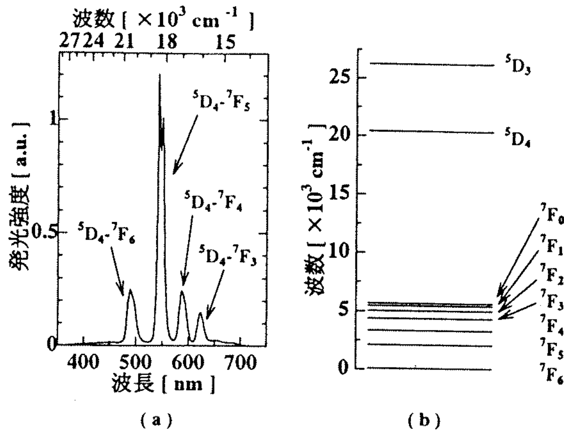

図 4 (a)Tb^{3+}添加シリカ薄膜のレーザ光誘起発光スペクトル (b)$LaCl_3$ 中の Tb^{3+}イオンのエネルギー準位図

Fig. 4 (a) The photoluminescence spectrum obtained from Tb^{3+}-doped film excited by KrF excimer laser and (b) the electronic energy levels of Tb^{3+} ion in $LaCl_3$.

のピークが見られている。同様のスペクトルは基板温度を室温から 500℃まで変化させて成膜した全ての試料について得られた。

さらに、Tb^{3+}添加膜について、膜中の Tb の存在を ICP-AES、XRF によっても確認した。つぎに、標準試料(13)と EPMA の測定結果を比較することにより、Tb 含有率 0.2～7.6 atomic%の膜を得られることがわかった。すなわち、開発したプラズマ CVD 法により、希土類をシリカ薄膜中に添加させることが可能であることがわかった。

希土類添加シリカ薄膜の堆積速度は、基板温度によって異なる。同一基板温度の場合でも多少のばらつきはあるが、例えば Tb^{3+}添加膜の場合で、基板温度 300℃のとき 11 nm/min、500℃のとき 18 nm/min であった。試料の膜質を赤外分光法で評価したところ、Si-O-Si の伸縮振動にもとづく 1070 cm^{-1} の吸収等の結果より、500℃で堆積した Tb^{3+}添加シリカ薄膜に比べて、300℃あるいは 400℃で堆積した膜の方が、より緻密で安定な構造であることがわかった。このため、本論文においては、300, 400℃成膜の試料の結果を用いて記述した。

膜厚の均一性については、膜厚約 500 nm の試料において、同一試料上で±10%程度の膜厚の差が生じたが、電界発光測定用の膜厚約 160 nm の試料では、その膜厚変化の割合はさらに小さかった。したがって、膜厚の不均一性は、実験結果の信頼性に大きな影響は与えていないと考えられる。

<3. 2> 発光特性 図 4(a)に基板温度 300℃で堆積した膜厚約 500 nm の Tb^{3+}添加シリカ薄膜に KrF エキシマレーザ光を照射したときに観測された発光スペクトルを示す。470～630 nm にわたる黄緑色の強い発光が生じている。図

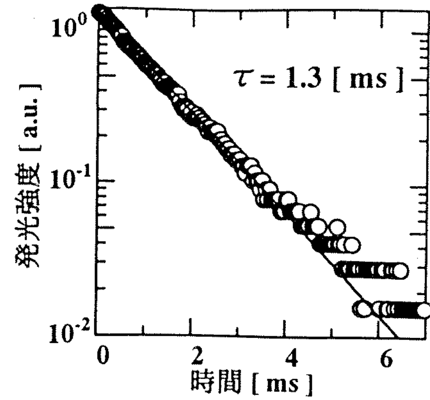

図 5 300℃で堆積した Tb^{3+}添加シリカ薄膜の 550 nm 発光の時間減衰曲線

Fig. 5 The decay profile of the 550 nm luminescence for Tb^{3+}-doped SiO_2 film deposited at 300 ℃.

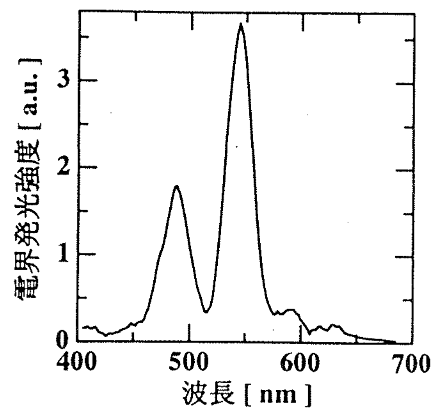

図 6 400℃で堆積した Tb^{3+}添加シリカ薄膜（試料 A）の電界発光スペクトル

Fig. 6 The electroluminescence spectrum obtained for Tb^{3+}-doped SiO_2 film (sample A). The sample was deposited at 400 ℃.

4(b)には $LaCl_3$ 中の Tb^{3+}イオンにおける $4f^8$ 配位の電子エネルギーレベルが示されている(14)。同図を参照することにより、発光は $^5D_4$ 準位から ^7F 準位への脱励起反応によっていることがわかる。^7F 準位はスピン軌道相互作用により 7 つの準位に分かれるが、図 4(a)のスペクトルでは、それぞれの準位の幅が広い。非晶質固体に特徴的な性質である構造の非一様性を反映して、シュタルク効果によりピークが広がる程度が様々となったことが原因と考えられる。

図 5 は、$^5D_4$ 準位から $^7F_5$ 準位への遷移に基づく発光の時間的減衰を示している。なお、励起は、図 4(a)と同様に KrF エキシマレーザ光により行われたが、レーザ光のパルス幅は 20 ns であり、図 5 のスケールでは無視しうるほど短い。図 5 より、この発光の減衰時定数は 1.3 ms と求められる。この値は文献(15)に報告されている値とほぼ一致している。一般に、発光の時定数は、“蛍光”と呼ばれる許容遷移に

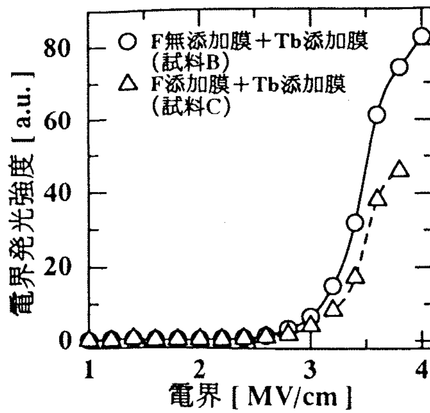

図 7　550 nm 発光強度の電界依存性

Fig. 7　Relation between the EL intensity and the strength of electric field applied.

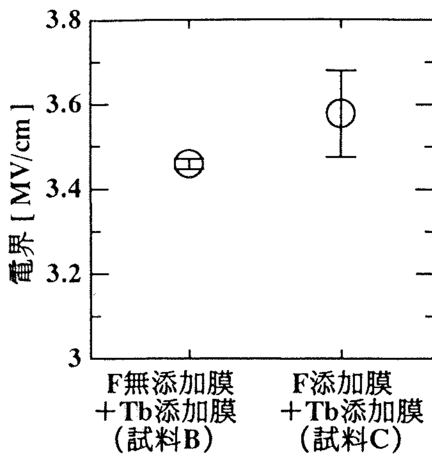

図 8　同一発光強度における印加電界

Fig. 8　Comparison of the electric field strength at which a certain intensity of electroluminescence was observed in specimens B and C.

よるものでピコ秒オーダの極めて速いものから、“燐光”と呼ばれる禁制遷移に基づく分〜時間オーダの極めて遅いものまで、優に 10 数桁変わりうるので、時定数が一致したことにより、この発光が本当に Tb^{3+}によるものであることが確実となった。

次に、基板温度約 400℃で堆積させた膜厚約 150 nm の電界発光測定用試料 A の下部電極（n 型 Si ウェハ）に－50 V の直流電圧を印加して得た電界発光スペクトルを図 6 に示す。電界発光の強度が弱いため分光器のスリットを大きく開けたために、図 4(a)に示すレーザ光誘起発光のスペクトルよりも幅広くなっているものの、本質的には図 4(a)と同一のスペクトルが得られた。フッ素無添加あるいはフッ素添加のシリカ薄膜と Tb 添加シリカ薄膜との二層試料である試料 B, C においても、同じような電界発光スペクトルが得られた。これらの発光は、試料に電界を印加した際、Si 基板から、フッ素無添加、あるいはフッ素添加シリカ薄膜層を経て、Tb 添加シリカ薄膜層に注入された電子により発光している。

図 4(a), 6 において最も大きい発光強度を示した $^5D_4$ 準位から $^7F_5$ 準位への遷移による電界発光について、発光強度の印加電界依存性を試料 B と C で比較し図 7 に示す。フッ素の入っていないシリカ薄膜層から Tb 添加シリカ薄膜層へ電子が入る試料 B に比べて、フッ素の添加されたシリカ薄膜層から Tb 添加層へ電子が入る試料 C の方が発光強度が弱いことがわかる。さらに、この発光について、ほぼ同一強度の発光が観測された時点での印加電界を図 8 に示すが、試料 B より試料 C の電界が高くなっている。他の発光ピークについても同様な電界の差が見られた。これらの結果は、フッ素添加シリカ薄膜中においては、無添加シリカ薄膜中に比べて電子が電界によって加速されにくくなっていることを示しており、フッ素が電子を散乱する(11)ことが原因であろうと思われる。

4.　結論

希土類のキレートとテトラエトキシシランを原料とするプラズマ CVD 法により希土類添加シリカ薄膜が堆積できることを示した。また、堆積膜よりレーザ光誘起発光と電界発光のスペクトルを得ることに成功した。電界発光強度を比較することにより、フッ素が添加されているシリカ中においては、添加されていないシリカ中に比べて、電子が電界によって加速されにくくなっていることを示した。

なお本研究は、一部文部省よりハイテク・リサーチ・センター研究費の支援を受けた。また、研究に協力いただいた吉原眞紀、関屋昭志、森田哲生、石井啓介、宇佐美哲男の諸氏に感謝致します。

（平成 10 年 5 月 20 日受付，平成 10 年 9 月 10 日再受付）

文　献

(1)　R. J. Mears, L. Reekie, I. M. Jauncey and D. N. Payne : "Low-noise erbium-doped fibre amplifier operating at 1.54 μm", Electron. Lett., **23**, 1026-1028 (1987)

(2)　D. M. Krol , R. P. van Stapele, J. H. Haanstra, T. J. A. Popma, G. E. Thomas and A. T. Vink : "Luminescence and Absorption of Tb^{3+} in $MO \cdot Al_2O_3 \cdot B_2O_3 \cdot Tb_2O_3$ glasses", J. Lumin., **37**, 293-302 (1987)

(3)　T. Hoshina : "Radiative Transition Probabilities in Tb^{3+} and Fluorescence Colors Producible by Tb^{3+}-Activated Phosphors", Japan. J. Appl. Phys., **6**, 1203-1211 (1967)

(4)　R. J. Mears, L. Reekie, S. B. Poole and D. N. Payne : "Neodymium-doped silica single-mode fibre lasers", Electron. Lett., **21**, 738-740 (1985)

(5)　A. Winnacker, R. M. Shelby and R. M. Macfarlane : "Photon-gated hole burning: a new mechanism using two-step photoionization", Opt. Lett., **10**, 350-352 (1985)

(6)　M. Shiga and H. Wada : "Magnetic and thermal properties

of $TbMn_2$ and $Tb(Mn_{1-x}Al_x)_2$ compounds", J. Magn. Magn. Mater., **151**, 225-230 (1995)

(7) R. Tumminelli, F. Hakimi and J. Haavisto : "Integrated-optic Nd:glass laser fabricated by flame hydrolysis deposition using chelates", Opt. Lett., **16,** 1098-1100 (1991)

(8) K. Shuto, K. Hattori, T. Kitagawa, Y. Ohmori and M. Horiguchi : "Erbium-doped phosphosilicate glass waveguide amplifier fabricated by PECVD", Electron. Lett., **29,** 139-141 (1993)

(9) K. Hattori, T. Kitagawa, M. Oguma, M. Wada, J. Temmyo and M. Horiguchi : "Erbium-doped silica-based planar waveguide amplifier pumped by 0.98 μm laser diodes", Electron. Lett., **29,** 357-359 (1993)

(10) M. Kawachi : "Silica waveguides on silicon and their application to integrated-optic components", Opt. Quant. Electron., **22,** 391-416 (1990)

(11) 高見明宏, 加藤宙光, 酒井真吾, 大木義路, 石井啓介 : 「プラズマ CVD 堆積 SiO_2 薄膜の絶縁破壊電界におよぼすフッ素添加の効果」, 電気学会誘電・絶縁材料研究会資料, **DEI-98-2,** 7-12 (1998)

(12) K. Ishii, A. Takami and Y. Ohki : "Effects of fluorine addition on the structure and optical properties of SiO_2 films formed by plasma-enhanced chemical vapor deposition", J. Appl. Phys., **81,** 1470-1474 (1997)

(13) P&H Developments社 : REEG ; Rare Earth Elements Glass Standard for EPMA

(14) W. T. Carnall, P. R. Fields and K. Rajnak : "Electronic Energy Levels of the Trivalent Lanthanide Aquo Ions. III. Tb^{3+}", J. Chem. Phys., **49,** 4447-4449 (1968)

(15) G. Amaranath and S. Buddhudu : "Optical properties of rare-earth-doped HMF glasses", J. Non-Cryst. Solids, **143,** 252-256 (1992)

四元　茂之

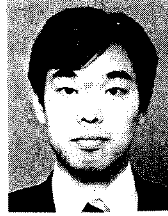

(非会員)　1974 年 5 月 14 日生。1997 年早稲田大学理工学部電気電子情報工学科卒業。同年 4 月同大学大学院理工学研究科電気工学専攻修士課程入学、現在に至る。希土類添加シリカおよびゲルマニウム添加シリカの光学的特性の研究に従事。

酒井　真吾

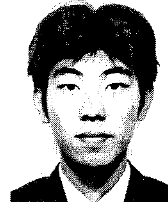

(非会員)　1975 年 3 月 9 日生。1997 年早稲田大学理工学部電気電子情報工学科卒業。同年 4 月同大学大学院理工学研究科電気工学専攻修士課程入学、現在に至る。希土類添加シリカおよびフッ素添加シリカの光学的、電気的特性の研究に従事。

大木　義路

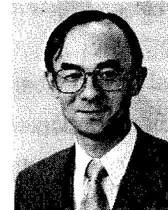

(正員)　1950 年 12 月 21 日生。1978 年 3 月早稲田大学大学院博士課程修了。1976 年 4 月同大学理工学部助手。現在、同教授。工学博士。無機および有機誘電体材料の電気物性と光物性の研究に従事。1989 年および 1997 年電気学会論文賞，1995 年矢崎学術賞受賞。

論 文

内部酸化がSIMOX埋め込み酸化膜の酸素欠乏性と絶縁破壊電界に及ぼす影響

学生員 薛 光 洙 (早稲田大学)

非会員 小 池 英 巳 (早稲田大学)

非会員 二 見 毅 (早稲田大学)

正 員 大 木 義 路 (早稲田大学)

Effects of internal oxidation on the oxygen deficiency and dielectric strength of buried oxide formed by the separation-by-implanted-oxygen (SIMOX) process

Kwang Soo Seol, Student member, Hidemi Koike, Non-member,
Tsuyoshi Futami, Non-member, Yoshimichi Ohki, Member (Waseda University)

Effects of internal oxidation on the buried silicon dioxide have been studied. The dioxide examined was the buried insulator in a silicon-on-insulator (SOI) structure fabricated by implantation of oxygen ions into Si, or the SIMOX process. The internal oxidation is an oxidation process given to the SOI structure after its fabrication. It was observed that the photoluminescence intensity due to neutral oxygen vacancies ($O_3\equiv Si\text{-}Si\equiv O_3$, "≡" denotes bonds with three separate oxygens) increased after the internal oxidation. The oxide thickness and the number of E'_γ centers ($O_3\equiv Si\cdot$, "·" denotes an unpaired electron) were also found to increase similarly. The measurements repeatedly done by changing the oxide thickness revealed that the increased part of oxide by the internal oxidation contains the vacancies with a similar density to the original part. It is concluded that the internal oxidation scarcely affects the oxygen deficiency of the oxide. It was also observed that the number of breakdowns at low electric fields remarkably decreased after the internal oxidation, indicating that electrically weak spots such as silicon pipes were effectively reduced.

キーワード：埋め込みシリコン酸化膜，シリカ薄膜，酸素欠乏性欠陥，SIMOX，絶縁破壊

1. まえがき

次世代の低消費電力の大規模集積回路 (VLSI) の製造に向けて，シリコン基板は従来のバルクシリコン基板から SOI (Silicon-On-Insulator) 構造を持つ基板 (SOI 基板) へシフトしつつある。SOI 基板は，内部に絶縁膜と表面にシリコンの極薄層を持ち，半導体素子を作った場合に素子の動作速度は落とさずに消費電力を従来のものより抑えることができる特徴を持つ。

現在，この SOI 基板を作る最も有望な技術として SIMOX (separation by implanted oxygen) が挙げられる。SIMOX 基板は，通常，加速電圧 180keV でドーズ量 4×10^{17}～$2\times10^{18}cm^{-2}$ で O^+ をシリコン基板に注入し，その後，数時間の熱アニール (1300～1350℃) の条件で形成する。特に，比較的ドーズ量の少ない，例えばドーズ量が約 $4\times10^{17}cm^{-2}$ で形成した SIMOX 基板が注目されている。これは，高ドーズ注入で作成したものと比べて，低コストで作成できるということと，貫通転位密度の低い表面シリコン層が得られるためである[1]。しかしながら，この低ドーズ SIMOX 基板の埋め込み酸化膜には高密度のシリコン柱，すなわち Si 原子の連結などのショーティング・ディフェクトが存在することが知られている。これに対して，SIMOX 埋め込み酸化膜の形成後に高温 (1100～1350℃) で酸化することで，埋め込み酸化膜の膜厚が増加するのに伴い[2]，埋め込み酸化膜中のショーティング・ディフェクトの密度が低下することが報告されている[3,4]。これは，SIMOX 基板を高温酸化する時，上部のシリコン膜を通った酸素によって，埋め込み酸化膜とシリコン膜の界面近傍からシリコン膜の酸化 (これを内部酸化と呼ぶ) がおこり，その結果として埋め込み酸化膜が上方へ成長すると同時に，埋め込み酸化膜中のシリコン柱なども酸化することによるとされている。このため，内部酸化プロセスは近年の低ドーズ SIMOX 基板製作に欠かせないものになりつつあ

る。

しかし，この内部酸化がSIMOX埋め込み酸化膜の膜質に与える影響や内部酸化によって成長した部分の膜質などについては未だにわからない部分が多い。今回の研究では，フォトルミネッセンス法や電子スピン共鳴法を用いて，内部酸化が埋め込み酸化膜の酸素欠乏性に与える影響を調べると共に，破壊電界測定を通して絶縁特性における内部酸化の影響を調べた。

2. 実験装置および方法

SIMOX基板は，p-type(100)Cz-Si基板に，O^+イオンを加速電圧 180keV，ドーズ量 $3.7\times10^{17}cm^{-2}$ で注入し，$Ar+O_2$ 雰囲気で 1350℃の熱処理を 6 時間行い作製した。断面透過電顕で観察したところ，厚さ約 350～360nm の表面シリコン層と厚さ約 85～90nm の埋め込み酸化膜が形成されていた。次に，このSIMOX基板を少量のArを混合した1気圧のO_2雰囲気中1350℃で高温内部酸化し，表面に厚さ約 650nm の酸化膜，その下に，厚さ約 60～70nm のシリコン層および約 125～130nm の埋め込み酸化膜を有する試料を得た。すなわち，内部酸化による埋め込み酸化膜厚の増大に伴い，元々あった埋め込み酸化膜に新たに約 40nm の酸化膜が追加された。実験遂行上，埋め込み酸化膜を露出させる必要があるため，HF 溶液を用いて上方の熱酸化膜を，ついで KOH 溶液を用いてシリコンを取り除いた。

測定手段として，フォトルミネッセンス測定には，KrF エキシマレーザ（発振波長：248nm［フォトンエネルギー ＝ 5.0eV］，パルス幅：～20ns），シンクロトロン放射光（岡崎国立共同研究機構内の分子科学研究所 UVSOR 施設の BL1B ライン）を励起光源として，試料からの発光を分光し，室温あるいは約 10K の温度で測定した。

SiO_2 へのプラズマ照射は，ESR（電子スピン共鳴）で検出できない反磁性点欠陥を検出可能な常磁性点欠陥に変えるということが知られている[5,6]。そこで，露出された埋め込み酸化膜に，13.56MHz（出力 ：60W）の高周波電源で励起された Ar プラズマ（ガス圧力 ：40Pa）を室温で照射し，誘起された常磁性欠陥を，ESR スペクトロメータ（JEOL RE-2XG）を用いて室温で分析した。観測された吸収スペクトルは，2 回積分し，DPPH(1,1-diphenyl-2-picrylhydrazyl) の標準サンプルと比較し，欠陥密度を見積もった。

破壊電界測定には，Au/SiO_2(埋め込み酸化膜)/p-Si の MOS 構造を作製し，Au 側に負のパルス幅 1 μs の方形パルス電圧を印加し，自己修復性破壊法を用いて破壊電界を測定した。この破壊電界測定に関する詳細は，既報を参照して頂きたい[7]。

3. 実験結果と考察

<3･1> 内部酸化が埋め込み酸化膜中の酸素欠乏性に与える影響　図1(a)は，KrF エキシマレーザからの 5.0eV 光励起による，内部酸化前の埋め込み酸化膜からの発光スペクトルである。4.3eV と 2.7eV に中心を持つ二つの発光帯が観測できる。図1(b)は 4.3eV 発光帯の発光励起スペクトルを示す。5.0eV と約 7.5eV に発光励起帯が観測される。このような発光帯とその励起帯は酸素空孔によるもので[8]，これらの発光は，試料が酸素欠乏であることを表している。また，異なるドーズ量（$2\times10^{16}cm^{-2}$）で作成した SIMOX 埋め込み酸化膜でも同じ発光が観測された[9]ことは，酸素欠乏性が埋め込み酸化膜に共通の特性であることを示している。

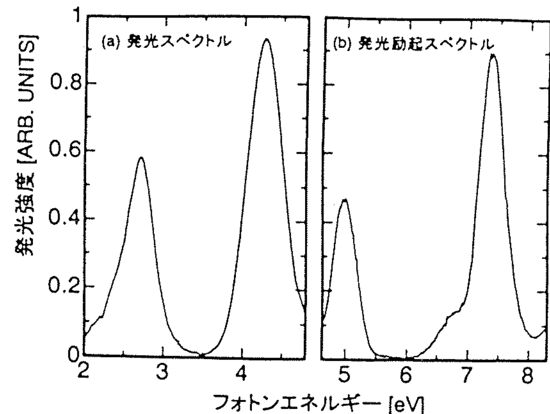

図1　内部酸化無しの埋め込み酸化膜からの5.0eV光励起による発光スペクトル(a)と4.3eV発光の発光励起スペクトル(b)

Fig.1. PL spectrum induced by 5.0 eV photons (a) and PL excitation spectrum for the 4.3 eV PL (b) from the buried oxide before the internal oxidation.

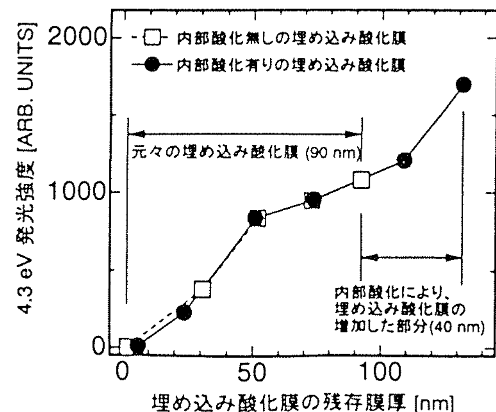

図 2　内部酸化を施した場合と施さなかった場合の埋め込み酸化膜に対し、エッチングを施したときの残存酸化膜厚と 4.3eV 発光強度の関係

Fig.2. Intensity of the 4.3 eV PL as a function of the remaining oxide thickness for oxides with and without the internal oxidation.

発光強度の空間的な依存性を調べるために，埋め込み酸化膜を HF 溶液でエッチングし，その厚さを変化させた。図 2

は，残存埋め込み酸化膜厚に対する 4.3eV 発光強度を示す。破線と白抜き四角，実線と黒丸は，それぞれ内部酸化を行う前後での埋め込み酸化膜に対する結果を示している。埋め込み酸化膜からの発光強度は内部酸化により 1.6 倍になっている。同時に，埋め込み酸化膜厚は，1.5 倍になっている。また，図 2 を見ると，内部酸化の有無に関わらず，エッチングによる埋め込み酸化膜厚の減少と発光強度の減少は完全に一致している。この事実から，内部酸化による発光強度の増加は，膜厚の増加によるものであり，増加した埋め込み酸化膜部分は，元々あった埋め込み酸化膜と同程度の酸素空孔を含んでいることがわかる。また、この結果より、内部酸化には、元々あった埋め込み酸化膜の酸素欠乏欠陥の数を減らす働きはないことがわかる。これは内部酸化がシリコン柱を効果的に無くすプロセスであるという報告[3,4]とは対照的である。次節で詳しく述べるが、本研究においても内部酸化により著しい低電界での絶縁破壊は生じなくなる。この理由は、おそらくシリコン柱の減少によると思われる。結局、内部酸化は極端に酸素が欠乏しているシリコン柱を酸化し絶縁性にする働きは有しているようであるが、酸素欠乏性を完全に解消させる働きは有していないと思われる。

図 3 は，内部酸化を行い，Ar プラズマを 30 分間照射した埋め込み酸化膜の ESR スペクトルを示す。このスペクトルは，E'_γ 中心($O_3 \equiv Si\cdot\ {}^{+}Si \equiv O_3$，・は不対電子，≡は 3 個の O との結合を表す)に相当する。ESR 信号はプラズマ照射をしないときには検出されないため，プラズマ照射は，次のような反応を起こして，酸素空孔を E'_γ 中心に変えると考えられる。

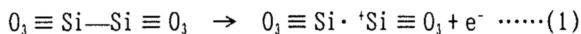

$$O_3 \equiv Si\text{—}Si \equiv O_3 \ \rightarrow\ O_3 \equiv Si\cdot\ {}^{+}Si \equiv O_3 + e^- \quad \cdots\cdots(1)$$

図 4 は，内部酸化を施した場合と施さなかった場合の埋め込み酸化膜における，E'_γ 中心の面積密度とプラズマ照射時間の関係を示す。比較のために，内部酸化により増大した酸化膜部分をエッチング除去した試料および内部酸化の形成時にできた表面の熱酸化膜における同様の関係も記している。さらに，両試料に対してプラズマを照射したのち，エッチングにより膜厚を減じながら求めた E'_γ 中心の面積密度を図 5 に示す。E'_γ 中心の面積密度と残存膜厚の間には良好な比例関係が見られている。さらに図 5 には内部酸化により増大した酸化膜部分を除去してからプラズマを当てたときの E'_γ 中心の密度も示しているが，同一膜厚における他の 2 試料の測定値とほぼ一致している。これらの特性は，プラズマによる常磁性化の効果が少なくとも深さ 130nm までは均一に生じていることを示している。熱酸化膜については，誘起される E'_γ 中心の絶対数が少ないため，図 5 のような検討ができなかったため，プラズマの効果が熱酸化膜全体に及んでいるかは確認できなかった。しかし，前述したように 130nm まではほぼ均一な効果を有していることから，650nm においても相応の効果は有しているものと判断される。このように考えて算出した E'_γ 中心の飽和体積密度を面積密度や酸化膜の厚さとともに表 1 に示す。

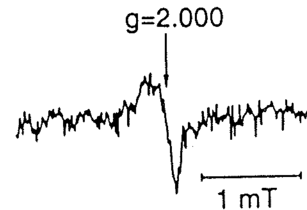

図 3 内部酸化後の埋め込み酸化膜に Ar プラズマを照射した時の ESR スペクトル

Fig.3. ESR spectrum induced by the Ar plasma exposure for the buried oxide with the internal oxidation.

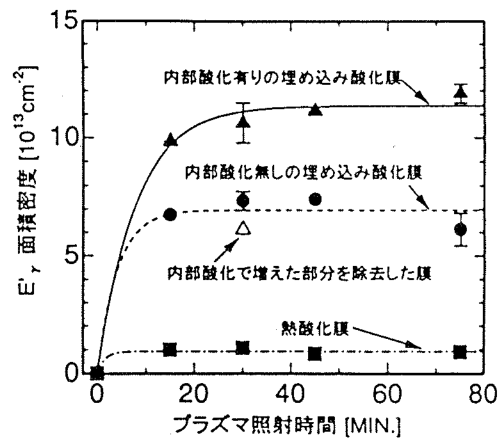

図 4 内部酸化を施した場合と施さなかった場合の埋め込み酸化膜および熱酸化膜におけるプラズマ照射時間に対する E'_γ 中心の密度の変化

Fig.4. Growth curves of E'_γ centers as a function of the plasma exposure time for buried oxides with and without the internal oxidation and thermal oxide.

表 1 様々な酸化層の厚さと E'_γ 中心の飽和値

Table 1. Saturation level of E'_γ centers for various SiO_2 films.

試料	厚さ [nm]	面積密度 [$10^{13}cm^{-2}$]	体積密度 [$10^{17}cm^{-3}$]
内部酸化前の埋め込み酸化膜	90	～7	～78
内部酸化後の埋め込み酸化膜	130	～11	～85
内部酸化で増えた部分を除去した埋め込み酸化膜	90	～6	～67
熱酸化膜	650	～1	～1.5

内部酸化をした埋め込み酸化膜の飽和面積密度 約 1.1×10^{14}cm^{-2} は，内部酸化前に埋め込み酸化膜で観測された飽和値 7×10^{13}cm^{-2} の約 1.6 倍の値となっている。この 1.6 倍という比は，膜厚の増加分の比と近い。さらに，内部酸化で埋め込み酸化膜の増加した部分を除去した時，飽和値は 6×10^{13}cm^{-2} になり，内部酸化前に観測された密度と非常に近い値となっている。さらに，図 5 に示したように，内部酸化の有無は面積密度の残存膜厚依存性に殆ど影響を与えていない。これらの結果は，内部酸化による E'_γ 中心の数の増加は，図 2 の発光測定の結果と同様に，埋め込み酸化膜の厚さが増加したことで単純に説明できることを示している。なお，上記 E'_γ 中心の飽和値は必ずしも存在していた酸素空孔の全体量であるとは限らず，酸素空孔のある一定割合がプラズマ照射により E'_γ 中心に変換されていれば同じ議論が成り立つ。ただし，プラズマ照射は，X 線や γ 線の照射といった他の手法と比べて，効果的に酸素空孔を E'_γ 中心に変えると知られている[5,10]ので，表 1 に示した体積密度は，前駆体である酸素空孔密度にある程度近い値と考えてもよいと思われる。図 4 で他に重要なことは，埋め込み酸化膜と熱酸化膜の間での E'_γ 中心の密度の大きな相違である。これは，SIMOX 埋め込み酸化膜が熱酸化膜より酸素空孔をはるかに多く含んでいるという，以前の我々の報告と一致している[9]。

〈3·2〉 内部酸化が埋め込み酸化膜の絶縁破壊電界に及ぼす影響　埋め込み酸化膜の破壊電界測定の結果を図 6 に示す。図 6 は，内部酸化を行わなかった埋め込み酸化膜（膜厚：～85nm）と内部酸化を行った埋め込み酸化膜（膜厚：～125nm）における自己修復性破壊の回数と破壊電界の関係を示している。破壊回数が増えるにつれて，破壊電界が上昇し，飽和しているのがわかる。内部酸化を行った埋め込み酸化膜では初期の低電界(～8.9MV/cm 以下)で破壊が生じる回数が著しく減少している。これは，実用的，工業的見地からは極めて重要なことであり，内部酸化により埋め込み酸化膜膜内のシリコン柱に代表されるショーティング・ディフェクトの数が確かに著しく減少することを示している[4]。

一方，物理学的な限界としての真性破壊電界値の目安を与えるであろう最大破壊電界値は，内部酸化による埋め込み酸化膜の膜厚の増加に伴って減少するのが観測された。すなわち，内部酸化により破壊電圧は上昇しているが，膜厚がそれ以上に 50%近くも増えているために破壊電界値は減少している。我々は，酸素空孔は SiO_2 の絶縁破壊を引き起こす欠陥の 1 つであることを指摘した[7]。しかしながら，〈3・1〉で述べたように埋め込み酸化膜中の酸素空孔の密度は変わっていないことから，この減少は酸素空孔の増加によるものではない。むしろ，次に述べるように，このような膜厚増加に伴う破壊電界の減少は，本試料のような薄膜絶縁体については当然のことである。

まず，この最大破壊電界値の低下の原因を探るために，最大破壊電界の膜厚依存性を調べた。その結果を図 7 に示す。図 7 より，エッチングによる埋め込み酸化膜の膜厚の減少に伴って，最大破壊電界値が増加していることがわかる。

ここで，電子なだれ機構による破壊モデル[11]を仮定してみる。熱破壊が無視でき，電極よりの注入電荷による単一なだれが破壊を引き起こすとき，次の (2)，(3) 式が成り立つ[12]。すなわち，Shockley の式[13]によれば，電離係数 α は次式で与えられる。

$$\alpha = c\exp(-\varepsilon_i / eF_b\lambda) \quad \cdots\cdots(2)$$

ここで，c：定数，ε_i：衝突電離のしきい値エネルギー，F_b：破壊電界，λ：平均自由行程。

破壊を生じるのに必要な電子数を N_c とすれば，次式で与えられる。

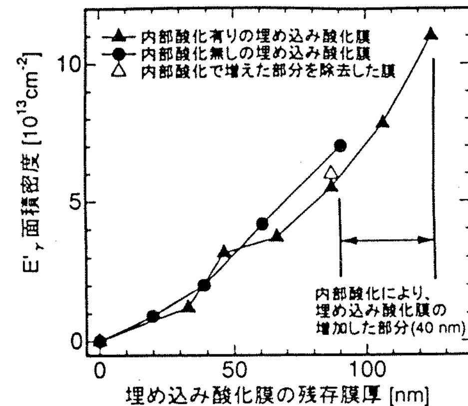

図 5　内部酸化を施した場合と施さなかった場合の埋め込み酸化膜に対し、エッチングを施したときの残存酸化膜厚とプラズマ誘起 E'_γ 中心の密度の関係

Fig.5.　Density of the plasma induced E'_γ centers as a function of the remaining oxide thickness for oxides with and without the internal oxidation.

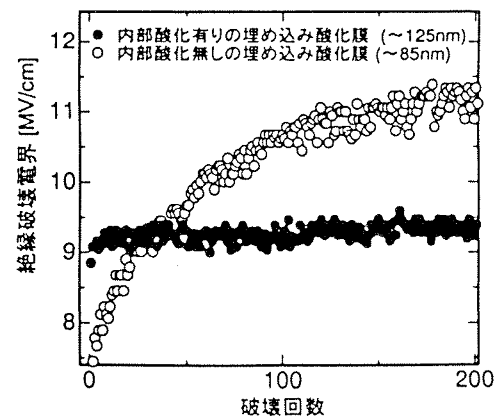

図 6　内部酸化を施した場合と施さなかった場合の埋め込み酸化膜における自己修復性破壊の回数に対する絶縁破壊電界の変化

Fig.6.　Change in dielectric strength during repeated measurements of self-healing breakdowns for buried oxides with and without the internal oxidation.

$$N_c = N_0 \exp(\alpha d) \quad \cdots\cdots(3)$$

ここで，N_0：初期電子数，d：膜厚。

(2)，(3) 式を変形すると，破壊電界の式は，

$$F_b = \frac{1}{K_1 \log d + K_2} \quad \cdots\cdots(4)$$

となる。ここで，

$$K_1 = \frac{e\lambda}{\varepsilon_i},\ K_2 = K_1 \log(\frac{c}{A}),\ A = \log(\frac{N_c}{N_0}) \quad \cdots\cdots(5)$$

である。図7に示した測定値を(4)式に最小2乗近似することにより，図7の曲線が得られた。このとき，

$K_1 = 5.42 \times 10^{-10}$

$K_2 = 9.72 \times 10^{-9}$

であった。さらに，ε_iは一般に光学ギャップエネルギーの1.5 倍程度が適当であるとされている[14,15]ので，SiO_2 の光学ギャップエネルギー 8[eV]より，ε_i = 12[eV]を(5)式の第一式に代入すると，平均自由行程λは約 6.5nm と算出される。この値は，プラズマ CVD 法により作成した TEOS-SiO_2 における電子の平均自由行程 5～6nm[16]や熱酸化膜における平均自由行程 3.2nm[17,18]に近い値である。すなわち，この結果は埋め込み酸化膜の最大破壊電界値の変化は電子なだれによる破壊モデル[11]で説明できることを意味する。つまり，内部酸化による膜厚の増加によって，電極より注入された電子がなだれ増倍する回数が増え，より低い電界でも破壊に必要な数にまで増倍されることを意味する。したがって，最大破壊電界が低下したことは，電子なだれによって破壊が生じていることから必ずもたらされる物理学的必然性であって，内部酸化により膜質が劣化したとか，欠陥密度が増大したとか言ったことが原因ではない。また，内部酸化有りの埋め込み酸化膜をエッチングし低減させた膜厚に対して得られた破壊値と，同一膜厚における内部酸化無しの埋め込み酸化膜の破壊値が一致していることは，図 2 で内部酸化による膜厚増加分を取り去ったときに発光強度が元々の埋め込み酸化膜と一致していることと符合しており，内部酸化が最大破壊電界値を決める物理量には影響を与えていないことを示している。

4. むすび

SIMOX 基板の埋め込み酸化膜に関する内部酸化効果を調べた。得られた結果は，次の通りである。

(1) 内部酸化によって，埋め込み酸化膜の膜厚は増加する。発光と ESR 測定から，埋め込み酸化膜の増加した部分の酸素欠乏性は，元々あった埋め込み酸化膜とほぼ同じであり，熱酸化膜と比べればはるかに欠乏性が大きいことがわかった。

(2) 自己修復性破壊法による絶縁破壊測定によれば，初期の低電界での破壊を生じる回数は内部酸化により著しく減少する。これは，内部酸化によりシリコン柱などの弱点部が著しく減少することを示唆しており，実用的見地からは内部酸化法は有効であることがわかった。また，内部酸化によって，最大破壊電界値の低下が観測されたが，これは内部酸化により埋め込み酸化膜の膜厚が増加することによる必然的なものであり，膜質の劣化によるものではない。破壊値の膜厚依存性から見積もった電子の平均自由行程は約 6.5nm であった。

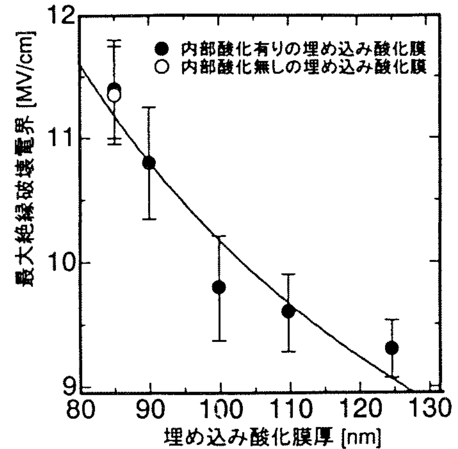

図 7 内部酸化を施した場合と施さなかった場合の埋め込み酸化膜における最大絶縁破壊電界の酸化膜厚依存性。実線は、単一電子なだれ破壊を仮定したときの計算値を示す。

Fig.7. The maximum dielectric strength as a function of the oxide thickness for buried oxides with and without the internal oxidation. The solid curve shows calculated values based on the single avalanche theory.

5. 謝辞

ESR 測定等について日頃ご指導賜わる本学理工総研浜義昌教授に感謝致します。本研究は，文部省より科研費 (09450132) ならびに 1997 年度ハイテクリサーチセンター研究費の助成を受け，さらに，川鉄 21 世紀財団の支援を受けた。また，シンクロトロン放射光を用いての測定は平成 8，9 年度 UVSOR 共同研究として行われた。

（平成９年１２月８日受付、平成１０年３月１２日再受付）

文　献

[1] S. Nakashima and K. Izumi, J. Mater. Res. 8, 523 (1993).

[2] Y. Takahashi, T. Ishiyama, and M. Tabe, Appl. Phys. Lett. 65, 2987 (1994).

[3] B.J. Mrstik, P.J. McMarr, H.L. Hughes, M.J. Anc, and W.A. Krull, Appl. Phys. Lett. 67, 3283 (1995).

[4] K. Kawamura, J. Nakashima, I. Hamaguchi, T. Yano, Y. Nagake, and M. Tachimori, in Proceedings of the 1995 IEEE

International Conference on SOI, p. 156.
[5] R.A.B. Devine, J-L. Leray, J. Margail, Appl. Phys. Lett. 59, 2275 (1991).
[6] K. Vanheusden and A. Stesmans, J. Appl. Phys. 74, 275 (1993).
[7] K. Ishii, D. Isshiki, Y. Ohki, H. Nishikawa, and M. Takiyama, Jpn. J. Appl. Phys., 34, 205 (1995).
[8] R. Tohmon, H. Mizuno, Y. Ohki, K. Sasagane, K. Nagasawa, and Y. Hama, Phys. Rev. B 39,1337 (1989).
[9] K.S. Seol, A. Ieki, Y. Ohki, H. Nishikawa, and M. Tachimori, J. Appl. Phys. 79, 412 (1996).
[10] R.A.B. Devine, D. Mathiot, W.L. Warren, D.M. Fleetwood, and B. Aspar, Appl. Phys. Lett. 63, 2926 (1993).
[11] 石井・大木： 電学論 A, 112, 188 (1992-3).
[12] 有井・木谷・犬石： 電学論 A, 93, 313 (1973-8).
[13] W. Shockley, Solid-State Electronics 2, 35 (1961).
[14] R. A. Logan, H. G. White, J. Appl. Phys. 36, 3945 (1966).
[15] 白藤・犬石： 応用物理 39, 508 (1971-10).
[16] 高見・石井・大木： 第 44 回春季応物 29a-A-6
[17] S. Tam, P-K. Ko, C. Hu, IEEE Trans. Electron Devices, ED-31, 1116 (1984).
[18] D. R. Young, J. Appl. Phys. 47, 2098 (1976).

薛　光洙　（学生員） 1970 年 1 月 5 日生。1994 年 2 月韓国高麗大学大学院理工学研究科材料工学専攻修士課程修了。1995 年 4 月早稲田大学大学院理工学研究科電気工学専攻博士後期課程入学，1997 年 4 月同大学理工学部助手，現在に至る。シリコン酸化膜および窒化膜中の欠陥の光学的評価の研究に従事。1996 年電気学会論文発表賞受賞。博士(工学)。

小池　英巳　（非会員） 1973 年 7 月 6 日生。1996 年 4 月早稲田大学大学院理工学研究科電気工学専攻修士課程入学。シリコン酸化膜中の欠陥の物性評価の研究に従事。

二見　毅　（非会員） 1973 年 8 月 5 日生。1997 年 4 月早稲田大学大学院理工学研究科電気工学専攻修士課程入学，現在に至る。シリコン酸化膜および窒化膜中の欠陥の物性評価の研究に従事。

大木　義路　（正員） 1950 年 12 月 21 日生。1978 年 3 月早稲田大学大学院博士課程修了。1976 年 4 月同大学理工学部助手。現在，同教授。工学博士。無機および有機誘電体材料の電気物性と光物性の研究に従事。1989 年および 1997 年電気学会論文賞，1995 年矢崎学術賞受賞。

Structures and generation mechanisms of paramagnetic centers and absorption bands responsible for Ge-doped SiO_2 optical-fiber gratings

Makoto Fujimaki, Tomofumi Watanabe, Tetsuya Katoh, Toshiaki Kasahara, Nahoko Miyazaki, and Yoshimichi Ohki
Department of Electrical, Electronics, and Computer Engineering, Waseda University, 3-4-1 Okubo, Shinjuku-ku, Tokyo 169, Japan

Hiroyuki Nishikawa
Department of Electrical Engineering, Tokyo Metropolitan University, 1-1 Minami Osawa, Hachioji, Tokyo 192-03, Japan

(Received 10 April 1997; revised manuscript received 22 October 1997)

Paramagnetic centers and absorption bands induced by ultraviolet photons in Ge-doped SiO_2 glass are investigated. Four kinds of samples with different Ge contents were exposed to ultraviolet photons from a KrF excimer laser (5.0 eV), a XeCl excimer lamp (4.0 eV), and a KrCl excimer lamp (5.6 eV). Irradiation with the KrF excimer laser induces two paramagnetic centers, named Ge(1) and Ge(2), in proportion with a decrease in the absorption at 5.1 eV and with an increase in absorption at 4.5 and 5.8 eV. The total density of the induced paramagnetic centers is linearly proportional to each induced change of the three absorption components and their proportionality constants are independent of the Ge content of the samples. The 4.0-eV photons from the XeCl excimer lamp induce only a Ge E' center, while the 5.6-eV photons from the KrCl excimer lamp induce a Ge(1) besides a Ge E' center. From these results, Ge(1) and Ge(2) are, respectively, assigned to the Ge electron center (GEC) and the positively charged Ge oxygen-deficient center $(GODC)^+$, which donated an electron to the GEC. The oscillator strength of the GODC for the absorption at 5.1 eV was found to be 0.1. From this, it is considered that the GODC that acts as the electron donor is the Ge lone pair center (GLPC). Thermally stimulated luminescence (TSL) is also examined in Ge-doped SiO_2 glass that was exposed to photons from the KrF excimer laser. The TSL spectrum is very similar to the photoluminescence spectrum that is known to be due to the GLPC's. It was found that the absorption, which was induced by the KrF excimer laser photons, decreases during the TSL measurement and that this decrement of the absorption is proportional to the TSL intensity. As mentioned above, the electrons that are to be trapped to generate the GEC's are released from the GLPC's during the photon irradiation. Then, in its reverse reaction, these electrons are thermally detrapped from the GEC's to regenerate the GLPC's, and the TSL is caused by an electronic de-excitation in such formed GLPC's. To conclude, the TSL phenomenon further validates the assumption that the GLPC is the electron donor to generate the GEC's. [S0163-1829(98)05407-1]

I. INTRODUCTION

Ultraviolet (uv) photosensitivity of Ge-doped SiO_2 glass is attracting much attention especially for Bragg gratings,[1] where the photorefractive index change caused by the uv-induced absorption[2–8] is utilized.[9,10] Two structural changes responsible for the absorption change have been reported. One is the generation of Ge E' center ($\equiv$Ge$^\bullet$, where symbols "$\equiv$" and "$\bullet$" denote bonds with three separate oxygens and an unpaired electron, respectively) accompanied by the decrease of absorption near 5.1 eV due to Ge oxygen-deficient center (GODC) and the emergence of absorption near 6.4 eV. Although there are two kinds of GODC's, it has been reported that the GODC responsible for this structural change is the neutral oxygen vacancy (NOV; $\equiv$Ge—$T\equiv$, where T is either Ge or Si).[2] The other change is the generation of the Ge electron center (GEC), where an electron is trapped at a fourfold coordinated Ge.[4,5,11,12] The generation of Ge E' center is fairly well understood, but the generation of the GEC is not fully understood. Although it has been known that GEC's are induced by strong uv photons from a KrF or a XeCl excimer laser through a two-photon process,[4,5] the structure of the electron donor to generate the GEC is still debated among two types of GODC's (Refs. 5 and 12) and the bridging oxygen.[4] If this puzzle can be solved, the mechanism of the generation of the GEC should be clarified. As a result, it will become possible to increase the photosensitivity of Ge-doped SiO_2 glass, thus enabling fabrication of Bragg gratings with a much higher efficiency.

Besides the NOV, the Ge lone-pair center (GLPC; $-\ddot{\mathrm{Ge}}-$ where "$\bullet\bullet$" denotes a lone electron pair), which also has a large absorption at 5.1 eV,[2,13,14] has been reported as the other type of the GODC's. Absorbing around 5.1-eV photons, the GLPC shows two photoluminescence (PL) bands at 4.3 and 3.1 eV. These two PL bands are due to the electronic transition to the ground state (S_0) from the lowest excited singlet state (S_1) and that from the lowest excited triplet state (T_1) at the GLPC, respectively.[14] It has been reported that the intensity of the 3.1-eV PL decreases with the occurrence of the uv-induced structural change.[7,15] Therefore, it is important to investigate the 3.1-eV PL in order to understand the mechanism of the structural change induced by uv-photon irradiation.

In the present research, we have measured the induced paramagnetic species and optical-absorption change in four different Ge-doped SiO_2 glasses upon irradiation of uv photons from three different photon sources. Furthermore, we report that thermally stimulated luminescence (TSL), which

0163-1829/98/57(7)/3920(7)/$15.00 © 1998 The American Physical Society

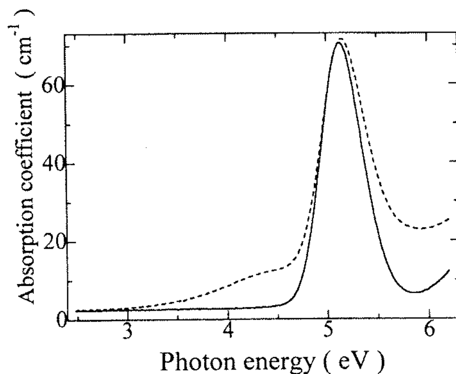

FIG. 1. Absorption spectra of sample A before (solid line) and after (dotted line) the irradiation of 20 shots of 5.0-eV photons from the KrF excimer laser.

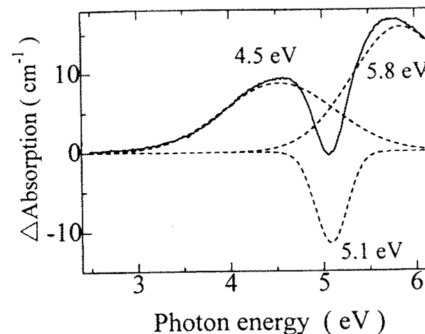

FIG. 2. Absorption spectrum induced by the irradiation of 20 shots of 5.0-eV photons from the KrF excimer laser in sample A (solid line). Dotted lines are three spectral components with Gaussian line shapes whose peak positions and FWHM's are shown in Table I.

is believed to be due to the same origin of the 3.1-eV PL, appears in the oxygen-deficient Ge-doped SiO_2 glass irradiated by strong 5.0-eV photons, and we examine the correlation between the TSL and the uv-induced paramagnetic centers. Based on these experimental results, we propose a model of the photochemical reaction occurring in the generation of the GEC's.

II. EXPERIMENT

Four Ge-doped SiO_2 glasses, A, B, C, and D with Ge contents of 1.0, 1.4, 6.9, and 9.2 mol %, respectively, were prepared by the vapor-phase axial deposition method. They were cut and polished into plates 0.3 mm thick. A KrF excimer laser (248 nm=5.0 eV, 80 mJ/cm^2 pulse, pulse duration of 20 ns), a XeCl excimer lamp [308 nm=4.0 eV, 10 mW/cm^2, full width at half maximum (FWHM) of 0.03 eV], and a KrCl excimer lamp (222 nm=5.6 eV, 7 mW/cm^2, FWHM of 0.05 eV) are used as irradiation photon sources. The absorption spectra from the visible to uv region were measured by a Shimadzu UV 160 spectrophotometer. The induced paramagnetic centers were detected by electron spin resonance (ESR) with a JEOL RE-2XE spectrometer at the X-band frequency, and their concentration was evaluated by comparing the double-integrated intensity of the first-derivative spectrum with that of the signal from a standard diphenylpicrylhydrazyl sample of a known weight (the accuracy of the standard is believed to be $\pm 20\%$).

For the PL and TSL measurements, the KrF excimer laser was used as the photon source. To measure the PL or TSL spectrum at a defined temperature, the PL or TSL dispersed by a monochromator (Jobin Yvon, HR320) was observed by a multichannel detector (Princeton, RY1024). To measure the change in the TSL intensity with temperature, the dispersed TSL was detected by a photomultiplier while heating the sample at a rate of 3–8 °C/min. The laser photon irradiation, the absorption measurement, and the ESR measurement were done at room temperature.

III. RESULTS

A. Photoinduced absorption and paramagnetic centers

The solid line in Fig. 1 shows the original absorption spectrum of sample A. The absorption at 5.1 eV, which really consists of two different absorption components due to the two types of GODC's, NOV, and GLPC,[2,13,14] is observed in the spectrum. This absorption is observed in all the samples. This means that all the samples are of the oxygen-deficient type. The dotted line in Fig. 1 is the absorption spectrum of sample A after a 20-shot irradiation of photons from the KrF excimer laser. The photoinduced absorption spectrum obtained by subtracting the solid line from the dotted line is shown in Fig. 2. The induced spectrum is divided into one negative and two positive Gaussian components with peak positions and FWHM's shown in Table I. Laser irradiation of the other samples also induced similar absorption changes.

The ESR spectrum induced in sample A by the 20-shot irradiation of photons from the KrF excimer laser is shown in Fig. 3. Two signals named Ge(1) and Ge(2) (Refs. 8, 11, and 12) are observed, although there still remain debatable points on the assignment of their structures. In Ref. 11, Ge(1) and Ge(2) are assigned to two kinds of GEC's. Namely, Ge(1) is assigned to the GEC of which all the next-nearest four neighbors are silicons (referred to as the NNS in the present paper), while Ge(2) is assigned to the GEC which has one Ge atom at the next-nearest neighbors (NNG). On the other hand, in Ref. 12, they are, respectively, assigned to the GEC and the hole center of the GODC, which donated an electron to GEC. The total density of the induced paramagnetic centers shown in Fig. 3, i.e., the sum of Ge(1) and Ge(2), is 7.1×10^{17} cm^{-3}. Similar ESR spectra were observed in all the other samples after similar irradiation by laser photons.

Figure 4 shows the correlation between the intensity of each Gaussian absorption component and the total induced density of the paramagnetic centers for the four samples upon the irradiation of photons up to 20 shots from the KrF excimer laser. A good proportionality with a sample-independent slope is seen between the intensity of each component and the density of the induced paramagnetic centers.

Figure 5 shows the ESR spectra induced in sample A after 50-h irradiation of photons from the two excimer lamps. The spectrum (a) is for 4.0-eV photons from the XeCl excimer lamp and (b) is for 5.6-eV photons from the KrCl excimer lamp. Spectra (a′) and (b′) represent the expansion of spec-

TABLE I. Peak positions and values of FWHM of the three absorption components.

Peak position (eV)	FWHM (eV)
4.5	1.3
5.1	0.4
5.8	1.2

tra (a) and (b) in the region surrounded by the dotted box, respectively. Spectrum (a) is recognized as the signal of Ge E' centers with a density of 5.7×10^{15} cm^{-3}, while spectrum (b) is divided into the signal of Ge E' centers ($\sim7.1\times10^{15}$ cm^{-3}) and that of Ge(1) ($\sim3.5\times10^{15}$ cm^{-3}). The signal of Ge(2) is not seen in the two spectra, even if the measurements were done under increased sensitivity. For all the other samples, a similar ESR spectrum was observed if the irradiation condition was similar. Contrary to the fact that ESR signals were thus induced, no change was observed in the absorption spectrum by the irradiation of photons from either of the two lamps in any of the four samples. This is because the number of paramagnetic centers induced by the irradiation, which is two orders of magnitude smaller than that induced by 20-shot irradiation of KrF excimer laser photons, is too small.

B. PL and TSL

Sample B was used for the PL and TSL measurements. To measure the TSL spectrum, the sample, which had been irradiated by the KrF excimer laser photons at room temperature and kept at room temperature for a few minutes, was put on a hot plate whose temperature was set to be 300 °C. The absorption similar to that shown in Fig. 2 and paramagnetic centers, Ge(1) and Ge(2), were observed after the irradiation. The solid line in Fig. 6 shows the TSL spectrum obtained. No TSL was observed without the laser photon irradiation. The dotted line in Fig. 6 shows the PL spectrum, which occurs with the irradiation of the KrF excimer laser photons.

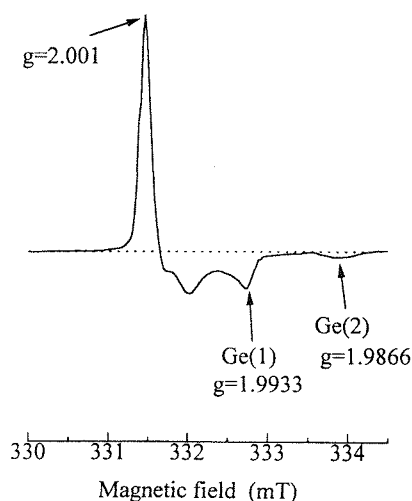

FIG. 3. ESR spectrum induced by the irradiation of 20 shots of 5.0-eV photons from the KrF excimer laser in sample A. Two ESR signals, named Ge(1) and Ge(2), are observed.

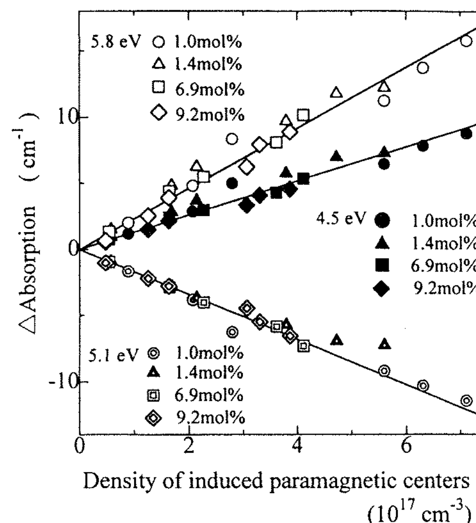

FIG. 4. Correlations between the intensities of the three absorption bands at 4.5, 5.1, and 5.8 eV and the total density of the paramagnetic centers in the four samples induced by the irradiation of photons of 5.0 eV up to 20 shots of the KrF excimer laser.

This 3.1-eV PL is due to the electronic transition from T_1 state to S_0 state at GLPC.[14] The TSL spectrum is very similar to the 3.1-eV PL spectrum. Figure 7 shows the change in the TSL intensity monitored at 3.1 eV while heating the sample after the irradiation of six laser pulses at room temperature. The TSL intensity reaches maximum around 220 °C and becomes almost zero around 300 °C. There is no difference among the TSL spectra at different temperatures

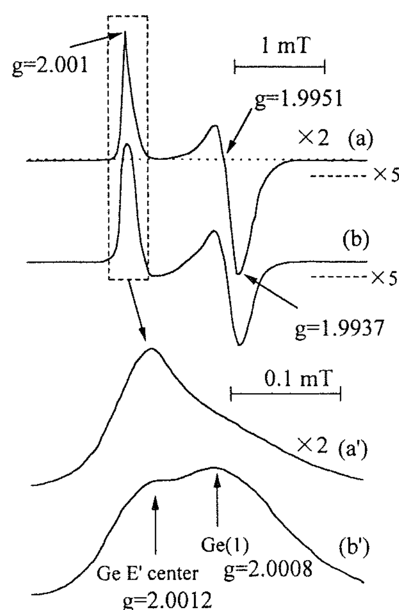

FIG. 5. ESR spectra induced in sample A by 4.0-eV photons from the XeCl excimer lamp (a) and by 5.6-eV photons from the KrCl excimer lamp (b). Broken lines are the signals observed under increased sensitivity of five magnifications. Spectra (a′) and (b′) represent the expansion of spectra (a) and (b) in the region surrounded by the dotted box, respectively.

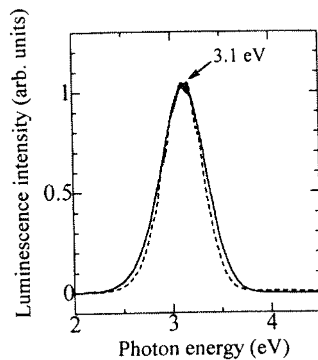

FIG. 6. TSL spectrum observed at 300 °C (solid line) and PL spectrum due to the GLPC (dotted line).

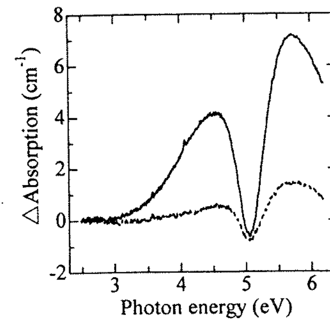

FIG. 8. Differential absorption spectra obtained by subtracting the absorption spectrum before the laser photon irradiation from those before (solid line) and after (dotted line) the TSL measurement shown in Fig. 7.

as shown in the inset, where normalized spectra at 100 °C (a), 200 °C (b), and 300 °C (c) are shown. The solid and the dotted lines in Fig. 8 show the spectra obtained by subtracting the absorption spectrum observed before the laser-photon irradiation from those observed before and after the TSL measurement shown in Fig. 7, respectively. From this figure, it is obvious that the photoinduced absorption seen before the TSL measurement almost disappears after the TSL measurement. Samples with different intensities of the photoinduced absorption were prepared by changing the number of irradiated pulses. With these samples, measurements similar to those shown in Figs. 7 and 8 were done, and correlation between the thermally decreased intensity of the absorption during the TSL measurement and the total TSL intensity calculated by integrating the observed TSL curve with the measurement time is investigated. Figure 9 shows the result, where the decreased absorption is divided into the three Gaussian components shown in Table I. A good linear proportionality is observed between the total TSL intensity and the decrement or the increment of each absorption component. Since the increment of the 5.1-eV absorption means the recovery of this absorption that had been decreased by the laser irradiation, the TSL and the regeneration of the defect responsible for the 5.1-eV absorption are induced by a thermal process that bleaches the photoinduced defects responsible for the absorptions at 4.5 and 5.8 eV.

A sample was loaded with H_2 at a pressure of 170 atm for two weeks at room temperature and then irradiated with six laser pulses. The ESR spectrum observed in this sample is shown in Fig. 10. Only Ge(1) (2.1×10^{17} cm^{-3}) is observed, and Ge(2) is not. Even though the laser irradiation condition is the same as that for the non-H_2-loaded sample, showing the TSL, the TSL was hardly observed in the H_2-loaded sample; about three orders of magnitude smaller than the non-H_2-loaded sample.

IV. DISCUSSION

A. Generation mechanism of GEC

First, the absorption bands, the ESR signals, and the structures that are being discussed are tabulated in Table II for convenience. By the irradiation of photons from the KrF excimer laser, the absorption change shown in Fig. 2 is induced, and the paramagnetic centers named Ge(1) and Ge(2) are generated. As there is a good proportionality between the intensity of the decreased absorption at 5.1 eV and the total density of the induced paramagnetic centers, it is natural to consider that some defect that has absorption at 5.1 eV strongly contributes to the generation of the paramagnetic centers. Since there is no absorption around 5 eV in oxygen-rich Ge-doped SiO_2 glass,[13,16,17] the defect should be either of the two types of GODC's. As mentioned above, there are two assumptions concerning the correspondence of the de-

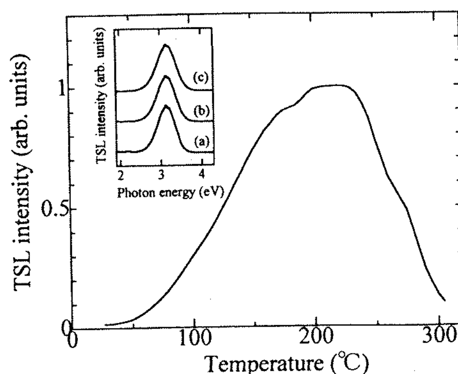

FIG. 7. Change in the TSL intensity, monitored at 3.1 eV, while heating the sample. The inset shows normalized TSL spectra observed at 100 °C (a), 200 °C (b), and 300 °C (c).

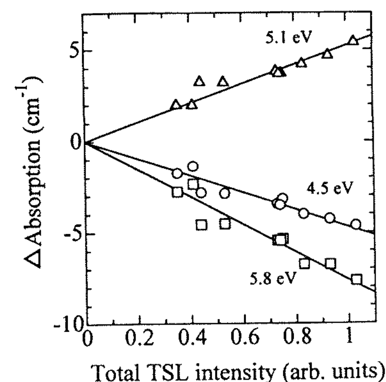

FIG. 9. Correlation between the total TSL intensity and the thermally breached intensity of the laser photon-induced absorption during the TSL measurement. The increment of the 5.1-eV absorption means the recovery of this absorption, which was decreased by the photon irradiation.

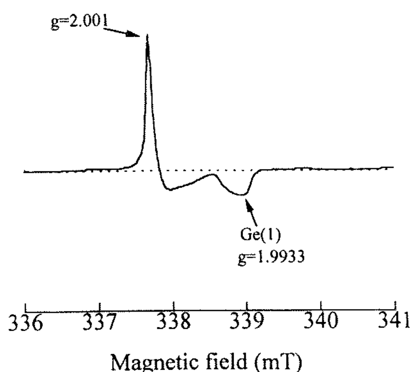

FIG. 10. ESR spectrum of the paramagnetic centers induced in the H_2-loaded sample by the laser irradiation.

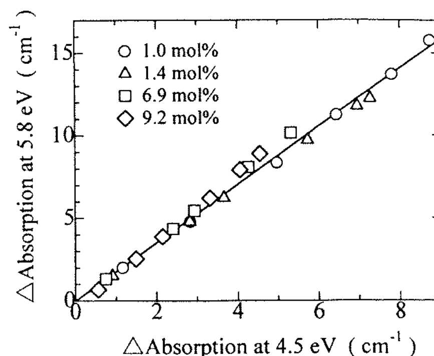

FIG. 11. Correlation between the 4.5- and the 5.8-eV absorption bands in the four samples.

fect structure of the GEC to the ESR signals Ge(1) and Ge(2).[11,12] Whichever assumption we may stand on, the GEC is an electron trapped center at a fourfold coordinated Ge. This indicates that the GODC should be the electron donor. Therefore, the following photochemical reaction is proposed:

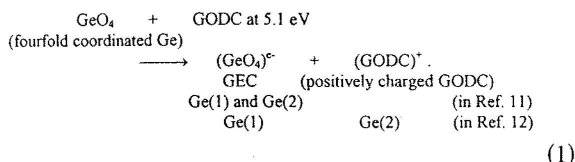

(1)

The bottom two lines of the right term show the ESR signals that should be assigned. Of course, there may exist electrons that are released from the GODC but are not trapped at any fourfold coordinated Ge. Therefore, the following relation between the number of GEC's and that of electrons (e^-) are established:

$$\mathrm{GEC}:e^- = y:1-y, \quad 0<y\leq 1. \tag{2}$$

The ratio y should be higher in the sample with a higher content of Ge, since fourfold coordinated Ge should exist more and the probability that the electrons are trapped should be higher in such a sample. The only one exception occurs when $y=1$. Namely, if all the electrons released from the GODC's are trapped, y is unity and becomes independent of the sample. In Fig. 4, it is clearly shown that the linear relationship between the decreased intensity of the 5.1-eV absorption and the total density of the induced paramagnetic centers, Ge(1) and Ge(2), does not depend on the sample. This means that the value of y is unity. Therefore, it is concluded that the number of induced GEC's is equal to the number of induced $(GODC)^+$'s in the present samples.

TABLE II. Absorptions, ESR signals, and structures being discussed. Note that the side-to-side correspondence is not indicated.

Absorption	ESR signal	Structure	
4.5 eV	Ge(1)	GEC	(1) NNS
			(2) NNG
5.8 eV	Ge(2)	$(GODC)^+$	(1) $(GLPC)^+$
			(2) $(NOV)^+$
5.1 eV		GODC	(1) GLPC
			(2) NOV

The induced absorption bands at 4.5 and 5.8 eV are also proportional to the induced paramagnetic centers as shown in Fig. 4. Here, according to Ref. 11, let us first assume that Ge(1) and Ge(2) are the two kinds of GEC's, i.e., NNS and NNG, respectively. In this case, the abscissa in Fig. 4 represents the total density of GEC's. From the good proportionality shown in Fig. 4, these absorption bands and GEC's should correlate with each other. Figure 11 shows that the ratio between the induced absorption intensities at 4.5 and at 5.8 eV is constant throughout all four samples examined. Since the probability of the existence of Ge atoms at the next-nearest neighbors should be higher in the sample with a higher content of Ge, NNG should be induced more in such a sample. Therefore, if the two absorptions at 4.5 and 5.8 eV are, respectively, assigned to NNS and NNG as was assumed in Ref. 18, the intensity ratio of the induced absorption at 5.8 eV to that at 4.5 eV should be higher in the sample with a higher content of Ge. This contradicts the result shown in Fig. 11. Therefore, the above assignment that the two absorptions at 4.5 and 5.8 eV are, respectively, due to NNS and NNG is unlikely to be correct. The reverse assignment that NNS to the 5.8-eV absorption and NNG to the 4.5-eV absorption is also unlikely for the same reason. Next, since the difference in g value between the two ESR signals Ge(1) and Ge(2) means that their excited states are different, NNS and NNG should have different absorptions.[19] Therefore, it is difficult to consider that both NNS and NNG have either of the two absorption bands at 4.5 and 5.8 eV or both. To conclude, the only one remaining possibility is that either the NNS or NNG has both absorptions, provided that the two GEC's, NNS and NNG, have different ESR signals.

As discussed in relation to Eq. (1), it is highly probable that two paramagnetic centers, the GEC and $(GODC)^+$, are induced when the sample is exposed to the KrF excimer laser photons. Therefore, if the GEC is distinguishable by the number of neighboring Ge atoms, there must exist at least three kinds of ESR signals in the irradiated sample. Provided that Ge(1) and Ge(2) were, respectively, assigned to NNS and NNG, there would be no ESR signal to be assigned to the $(GODC)^+$. The model that the paramagnetic centers Ge(1) and Ge(2) should be, respectively, assigned to the GEC and $(GODC)^+$ (Ref. 12) seems to be more probable. In this model, the two GEC's (NNS and NNG) would have to be indistinguishable by ESR. Then, the above-mentioned assignment of the absorptions at 4.5 and 5.8 eV has to be modified. Since, as mentioned above, the induced density of

the GEC is considered to be equal to that of the $(\mathrm{GODC})^+$, the linear proportionality between the induced absorption intensities at 4.5 and 5.8 eV shown in Fig. 11 is explainable by assuming that one of the two absorptions is due to the GEC whose ESR signal is Ge(1) and the other is due to the $(\mathrm{GODC})^+$ whose ESR signal is Ge(2). Therefore, the two absorptions are considered to be, respectively, due to the GEC and $(\mathrm{GODC})^+$, even though which absorption is due to which defect cannot be determined. However, there still remains the possibility that both absorptions at 4.5 and 5.8 eV are due to either the GEC or the $(\mathrm{GODC})^+$. More analyses about the assignment of the absorptions at 4.5 and 5.8 eV will continue in a future paper.

So far it has been concluded that the induced paramagnetic centers consist of the GEC and $(\mathrm{GODC})^+$. Because the number of the induced GEC is considered to be equal to the number of the induced $(\mathrm{GODC})^+$, and also because the accurate separation of the two signals is very difficult, the density of $(\mathrm{GODC})^+$ is estimated to be half of the total density of the two signals. This $(\mathrm{GODC})^+$ density induced by the irradiation should be equal to the decreased density of the GODC. From the intensity and the FWHM of the decreased 5.1-eV absorption band due to the GODC and the decreased density of GODC, the oscillator strength (f) of the GODC for the 5.1-eV absorption is calculated by the following Smakula's formula:[20]

$$Nf = 0.87\times 10^{17} n\alpha\omega/(n^2+2)^2, \quad (3)$$

where n is the refractive index of glass, α (cm^{-1}) the absorption coefficient at the peak of the absorption band, ω (eV) the FWHM, and N (cm^{-3}) the defect concentration. From Eq. (3), we obtained f of ~ 0.1. From the above contention, it is concluded that the electron donor to generate GEC is the GODC, which has absorption at 5.1 eV with the oscillator strength of 0.1. For the absorption at 5.1 eV, two types of GODC's, NOV and GLPC, have been assigned.[2] Although it is known that NOV is converted to the Ge E' center by the irradiation of uv photons and that electrons are released during this reaction,[2,21] the released electrons do not generate a GEC.[2] Furthermore, the oscillator strength of a NOV for the 5.1-eV (in Ref. 2, 5.06 eV) absorption has been reported to be 0.4,[2] which is far larger than the calculated value in the present study. On the contrary, the oscillator strength of the GLPC for the 5.1 eV (in Ref. 2, 5.16 eV) absorption is reported to be 0.1,[2] which agrees quite well with the present result. These two important facts that it is Ge E' center and not GEC which is induced from NOV and that the oscillator strength of NOV is 0.4 were also confirmed for all the present samples by similar experiments to those reported in Ref. 2 using a Hg/Xe lamp. Furthermore, it has been reported Ge E' centers are induced from NOV through a one-photon process of 5-eV photons, and that GEC's are induced through a two-photon process of 5-eV photons.[4,5] From these reports and our results, it is concluded that the electron donor to generate GEC is not a NOV but a GLPC. This in turn advances the aforementioned assignment of Ge(2) to the conclusion that Ge(2) should be assigned to $(\mathrm{GLPC})^+$.

As shown in Fig. 5, the irradiation of 4.0-eV photons from the XeCl excimer lamp induces only Ge E' centers, and the generation of GEC's is not observed. On the other hand, 5.6-eV photons from the KrCl excimer lamp induce the ESR signal of Ge(1), which should be assigned to a GEC as mentioned above, besides Ge E' centers. It has been also reported that the irradiation of photons from a Hg/Xe lamp induces only Ge E' centers[2] and that the irradiation of strong 4.0-eV photons from a XeCl excimer laser induces GEC's as well as Ge E' centers.[4] From these results, we can estimate the threshold photon energy to induce the GEC. A two-photon process easily occurs in the case of the XeCl excimer laser, while it never occurs in the case of the Hg/Xe or the two excimer lamps. Therefore, the above results, together with the above-mentioned fact that the generation of GEC is not observed in the case of a one-photon process of 5-eV photons, indicate that the threshold photon energy of the ionization of, or the electron release from, the GLPC to generate the GEC is higher than 5.0 eV and lower than 5.6 eV. The authors have revealed that the absorption beginning from a position slightly below 6 eV seen in Fig. 1 is caused by the electronic transition from the ground state of the GLPC to the conduction band.[17] It is reasonable to assume that the ionization of the GLPC is caused by exciting electrons into the edge of the conduction band and that the transfer of electrons to generate the GEC is done through the conduction band, at least for the case of the KrCl excimer lamp. To the authors' knowledge, the lowest reported photon energy to induce the GEC was 8.0 eV through a two-photon process of the photons from a XeCl excimer laser.[4] By the present study, the threshold energy is found to be much lower.

From Fig. 5, another important fact is deduced. While Ge(1) and Ge E' center were induced by the KrCl excimer lamp, Ge(2) was not. This might contradict the conclusion that Ge(1) (=GEC) and Ge(2) $[=(\mathrm{GLPC})^+]$ are induced in the same number. The Ge E' centers are mainly generated from NOV's by releasing electrons.[2,21] The released electrons would neutralize the $(\mathrm{GLPC})^+$'s, which otherwise should have been observed in the same number as GEC's. Furthermore, these facts strongly support the model that Ge(2) is not the NNG but the $(\mathrm{GLPC})^+$. If Ge(1) and Ge(2) should, respectively, correspond to the NNS and NNG, the above-mentioned results would never be observed.

B. TSL

It is obvious that the TSL is due to a photoinduced structural change, since it is not observed without the laser irradiation. Furthermore, since the two spectral shapes shown in Fig. 6 are almost the same and since no other PL bands have been reported around 3.1 eV, it can be concluded that the TSL is due to the electronic transition from T_1 state to S_0 state at the GLPC as in the case of the 3.1-eV PL. Then, we can assume that electrons first trapped at a certain defect are thermally detrapped and move to T_1 state of the GLPC. Therefore, the total TSL intensity should be proportional to the number of electrons thermally supplied to the GLPC's. Since, as shown in Fig. 9, the total TSL intensity is proportional to the thermally bleached intensity of each photoinduced absorption component shown in Fig. 2, it is considered that the TSL is induced by the thermally bleaching process of the GEC's, namely, the reverse reaction of Eq. (1).

The present results on TSL give strong validation to the model that the electron donor to generate the GEC's is the GLPC. As mentioned above, the reverse reaction of Eq. (1) causes the TSL. That is to say, the electrons thermally detrapped from the GEC's are supplied to positively charged electron donors and that the subsequent electronic transition in the neutral electron donors shows the TSL. On the other hand, the TSL should be due to the electronic transition at the GLPC as mentioned above. Therefore, if we suppose that the electron donor is the bridging oxygen,[4] the TSL phenomenon cannot be explained. The only possibility that can explain TSL is that the electron donor must be the GLPC. The electrons thermally detrapped from the GEC's are captured by the $(GLPC)^+$'s, and the neutralized GLPC's are then deexcited by moving down the electrons to S_0 state via T_1 state, through which the TSL occurs. The fact that the 5.1-eV absorption that is considered to be due to the GLPC (Ref. 2) increases proportionally with the total TSL intensity strongly indicates that the regeneration of the GLPC causes the TSL.

As shown in Fig. 10, Ge(2) is not induced in the H_2-loaded sample by the laser irradiation. Since both Ge(1) and Ge(2) are observed in the non-H_2-loaded sample, Ge(2) should be due to a defect whose generation is suppressed by hydrogen or a defect that is generated but soon becomes a different structure by reacting with hydrogen. This result also supports that Ge(1) and Ge(2) are assigned to the GEC and $(GLPC)^+$, respectively. The disappearance of Ge(2) in the H_2-loaded sample indicates that the $(GLPC)^+$ is terminated by hydrogen. Therefore, the TSL should not be observed in this sample. This is really the case in the present research.

V. CONCLUSIONS

The generation mechanism of the GEC in Ge-doped SiO_2 glass has been investigated through absorption and ESR measurements with three different photon sources. It was found that clear proportionalities, which do not depend on the Ge content in the sample, exist between the generation of paramagnetic centers [Ge(1) and Ge(2)], the decrease in the 5.1-eV absorption, the increase in the 4.5-eV absorption, and the increase in the 5.8-eV absorption. It was also found that the 5.6-eV photons from the KrCl excimer lamp induce the GEC. Furthermore, TSL with quite a similar spectrum as that of the PL due to the GLPC's appears in the sample that was irradiated by the KrF excimer laser. From these experimental results, the following facts are clarified. (1) By the laser irradiation, electrons are released from the GLPC's and the GEC's are generated. The reverse reaction can be induced thermally, where electrons are detrapped from the GEC's and are supplied to the $(GLPC)^+$'s. The electrons are further deactivated to S_0 state of the GLPC via T_1 state, and this process causes the TSL. (2) The ESR signals Ge(1) and Ge(2) are assigned to the GEC and a hole trapped at the GLPC, respectively. (3) The threshold photon energy to generate the GEC is between 5.0 and 5.6 eV.

ACKNOWLEDGMENTS

The authors express their thanks to Dr. K. Muta and M. Kato of Showa Electric Wire and Cable, for providing the samples. Their appreciation is also extended to Dr. K. Awazu of Electrotechnical Laboratory for his valuable comments. This work was partly supported by a Grant-in-Aid for Scientific Research from the Ministry of Education, Science and Culture of Japan (06452222).

[1] K. O. Hill, Y. Fujii, D. C. Johnson, and B. S. Kawasaki, Appl. Phys. Lett. **32**, 647 (1978).
[2] H. Hosono, Y. Abe, D. L. Kinser, R. A. Weeks, K. Muta, and H. Kawazoe, Phys. Rev. B **46**, 11 445 (1992).
[3] H. Hosono, M. Mizuguchi, H. Kawazoe, and J. Nishii, Jpn. J. Appl. Phys., Part 2 **35**, L234 (1996).
[4] J. Nishii, K. Fukumi, H. Yamanaka, K. Kawamura, H. Hosono, and H. Kawazoe, Phys. Rev. B **52**, 1661 (1995).
[5] M. Fujimaki, K. Yagi, Y. Ohki, H. Nishikawa, and K. Awazu, Phys. Rev. B **53**, 9859 (1996).
[6] D. L. Williams, S. T. Davey, R. Kashyap, J. R. Armitage, and B. J. Ainslie, Electron. Lett. **28**, 369 (1992).
[7] M. Gallagher and U. Osterberg, J. Appl. Phys. **74**, 2771 (1993).
[8] V. B. Neustruev, J. Phys.: Condens. Matter **6**, 6901 (1994).
[9] R. M. Atkins and V. Mizrahi, Electron. Lett. **28**, 1743 (1992).
[10] L. Dong, J. L. Archambault, L. Reekie, P. St. J. Russell, and D. N. Payne, Appl. Opt. **34**, 3436 (1995).
[11] T. E. Tsai, D. L. Griscom, and E. J. Friebele, Diffus. Defect Data, Part B **53–54**, 469 (1987).
[12] E. V. Anoikin, A. N. Guryanov, D. D. Gusovskii, V. M. Mashinskii, S. I. Miroshnichenko, V. B. Neustruev, V. A. Tikhomirov, and Yu. B. Zverev, Sov. Lightwave Commun. 1, 123 (1991).
[13] M. Kohketsu, K. Awazu, H. Kawazoe, and M. Yamane, Jpn. J. Appl. Phys., Part 1 **28**, 622 (1989).
[14] L. Skuja, J. Non-Cryst. Solids **149**, 77 (1992).
[15] E. M. Dianov, D. S. Starodubov, and A. A. Frolov, Electron. Lett. **32**, 246 (1996).
[16] K. Awazu, H. Kawazoe, and M. Yamane, J. Appl. Phys. **68**, 2713 (1990).
[17] M. Fujimaki, Y. Ohki, and H. Nishikawa, J. Appl. Phys. **81**, 1042 (1997).
[18] E. J. Friebele and D. L. Griscom, in *Defects in Glasses*, edited by F. L. Galeener, D. L. Griscom, and M. J. Weber, MRS Symposia Proceedings No. 61 (Materials Research Society, Pittsburgh, 1986), p. 319.
[19] T. E. Tsai and D. L. Griscom, Proc. SPIE **1516**, 14 (1991).
[20] A. Smakula, Z. Phys. **59**, 603 (1930).
[21] R. Kashyap, G. D. Maxwell, and D. L. Williams, Appl. Phys. Lett. **62**, 214 (1993).

COMMUNICATIONS

Concentration of neutral oxygen vacancies in buried oxide formed by implantation of oxygen

Kwang Soo Seol, Tsuyoshi Futami, and Yoshimichi Ohki[a)]
Department of Electrical, Electronics, and Computer Engineering, Waseda University, 3-4-1 Ohkubo, Shinjuku-ku, Tokyo 169, Japan

(Received 15 September 1997; accepted for publication 4 November 1997)

Using synchrotron radiation as a photon source, photoluminescence spectra were obtained for buried oxide formed by implantation of oxygen. From the spectra, the oxide was known to have relaxed and unrelaxed neutral oxygen vacancies with respective concentrations of 1.4×10^{20} and 1.0×10^{17} cm^{-3}. © *1998 American Institute of Physics.* [S0021-8979(98)01204-3]

Buried oxide (BOX) layers in the silicon-on-insulator structure separated by implanted oxygens (SIMOXs) have become widely used for a high speed metal–oxide–semiconductor (MOS), a radiation-hardened complementary MOS (CMOS), and other smart devices.[1–4] Many studies have been done recently on the nature of BOX,[5–7] since it plays an important role in determining the device properties. It has been known that the BOX is far more oxygen-deficient than the conventional thermal oxide,[5,6] and that this deficiency is believed as one reason for unusual behavior of BOX, such as enhanced electrical conductivity, charge buildup, and sensitivity to defect generation.[5]

Our previous photoluminescence (PL) studies[6,7] have shown that BOX contains neutral oxygen vacancies (≡Si–Si≡, "≡" denotes bonds with three separate oxygens) which are typical in oxygen-deficient amorphous SiO_2.[8] In the present article, the vacancy concentration in BOX is estimated by measuring the PL intensity.

In any material, the concentration (N) of photoabsorbing defects can be easily estimated from the following equation by measuring the optical absorbance (A) if their absorption cross section (σ) and the sample thickness (L) are known:

$$A=L\alpha=L\sigma N, \quad (1)$$

where α is the optical absorption coefficient. However, in the case of the present BOX sample, it is impossible to measure A because of the opaqueness of the Si substrate. One possible method to estimate the concentration of oxygen vacancies is to measure the PL emitted from the vacancies. It is known that the 4.3–4.4 eV PL is the luminescence from the vacancies[9] and that its two excitation bands at 5.0 and 7.6 eV are due to absorptions by "unrelaxed" and "relaxed" oxygen vacancies, respectively.[8] Here, the unrelaxed vacancy has a larger bond length between the two silicons and the relaxed vacancy has a shorter one.[8] The PL intensity (I_{PL}) normalized by the excitation photon intensity (I_{EXC}) is given by,[9]

$$I_{PL}/I_{EXC}=\eta\times[1-\exp(-\alpha L)]. \quad (2)$$

Here, η is the quantum efficiency of the PL. It is reasonable to assume that the true quantum efficiency for a specific PL by a specific PL excitation band, namely the PL photon numbers induced by a certain number of incident photons, is independent of the sample whether it is a thick silica glass or a thin BOX layer. Of course, such a true efficiency cannot be measured in actual experiments. First, since I_{EXC} was measured with a photomultiplier coated with sodium salicylate whose fluorescent quantum yield is constant between 4 and 20 eV,[10] I_{EXC} in the present research represents only a relative number of the incident photons. Second, although all the experimental conditions such as the configuration of photodetecting systems were exactly the same for the two samples, the two samples differ in the point that the BOX layer has a Si substrate at its back. Some of the incident photons, which should pass through the silica glass, could be reflected by the Si substrate. Reflectance at the interface between crystalline Si and vacuum is reported to be 60%–70% at 4.3, 5.0, and 7.6 eV.[11] The reflectance at the present SiO_2/Si interface should be somewhat smaller, while the reflectance at SiO_2/vacuum interface could be assumed zero. The reflectance at SiO_2/Si increases not only the effective incident photons but also the effective PL intensity. Therefore, if we assume the reflectance at the SiO_2/Si interface to be 60%, the effective value of η for the BOX sample becomes $(1.6)^2$ times as high as that for the silica glass.

We first measured PL intensities from an oxygen-deficient silica glass, the α value of which had been calculated by measuring the absorbance. Then, under the same condition, PL intensities were measured on the BOX layer. The PL measurement was carried out at 13 K using synchrotron radiation at the Institute for Molecular Science, Okazaki, Japan, with the measurement details described in Refs. 6 and 7. The investigated silica glass was manufactured by

a)Electronic mail: yohki@mn.waseda.ac.jp

 © 1998 American Institute of Physics

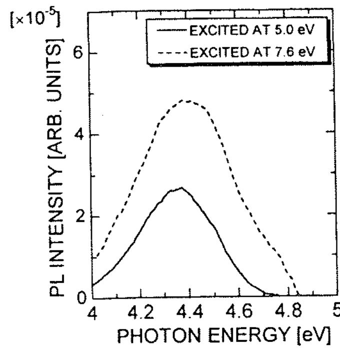

FIG. 1. PL spectra excited by 5.0 and 7.6 eV photons measured for the BOX layer at 13 K. The PL intensity is calibrated by the intensity of excitation photons.

TABLE I. Summary of the obtained values.

	Silica glass	BOX layer
L	0.7 mm	130 nm
α at 5.0 eV (cm^{-1})	7.0×10^{-3} (By transmission)	2.0 (By calculation)
α at 7.6 eV (cm^{-1})	2.4×10^{1} (By transmission)	1.1×10^{4} (By calculation)
I_{PL}/I_{EXC} at 5.0 eV	2.0×10^{-4}	2.6×10^{-5}
I_{PL}/I_{EXC} at 7.6 eV	1.1×10^{-4}	4.8×10^{-5}
η at 5.0 eV	4.0×10^{-1}	1.0
η at 7.6 eV	1.4×10^{-4}	3.6×10^{-4}
N of unrelaxed vacancies (cm^{-3})	3.5×10^{14}	1.0×10^{17}
N of relaxed vacancies (cm^{-3})	3.0×10^{17}	1.4×10^{20}

(Note). L:thickness; α: absorption coefficient; I_{PL}: PL intensity; I_{EXC}: intensity of PL excitation photons; η: apparent quantum efficiency of PL; and N: vacancy concentration.

the soot remelting method and its thickness is 0.7 mm. The SIMOX sample was fabricated by implanting O^+ ions up to a dose of 3.7×10^{17} cm^{-2} with an energy of 180 keV into a Si substrate, and subsequent annealing in an Ar atmosphere followed by oxidation at 1350 °C for several hours.[7] The thickness of the BOX layer is about 130 nm. For the PL measurement, the thermal oxide and the Si layer over the BOX were, respectively, removed by soaking the sample in a HF solution and subsequently in a KOH solution.

Figure 1 shows the PL spectra from the BOX layer excited by 5.0 and 7.6 eV photons. The PL band with a peak at 4.3–4.4 eV appears regardless of the excitation photon energy. The PL intensity shown in Fig. 1 was calibrated by taking the intensity variation of the excitation photons into consideration. Quite similar PL spectra were obtained for the glass sample. The measured apparent values of I_{PL}/I_{EXC} excited at the 5.0 eV excitation band and at the 7.6 eV band are, respectively, 2.0×10^{-4} and 1.1×10^{-4} for the glass sample, while they are, respectively, 2.6×10^{-5} and 4.8×10^{-5} for the BOX layer. The values of the absorption coefficient α of the glass sample are calculated to be 7.0×10^{-3} and 24 cm^{-1} at 5.0 and 7.6 eV, respectively, by measuring the absorbance A at each photon energy. Then, by substituting the values of I_{PL}/I_{EXC}, α, and L into Eq. (2), the value of η for the silica glass measured with the present system is calculated to be 4.0×10^{-1} and 1.4×10^{-4} for the 5.0 eV photons and the 7.6 eV photons, respectively. As mentioned above, the effective values of η for the BOX layer are considered to be $(1.6)^2$ times as high as these values. If so, using the values of I_{PL}/I_{EXC} and L for the BOX layer, α can be obtained as 2.0 for the 5.0 eV absorption band and 1.1×10^{4} for the 7.6 eV band. Since σ is known to be 2×10^{-17} and 8×10^{-17} cm^2 for the 5.0 and 7.6 eV bands, respectively,[8] the concentration N of the photoabsorbing defects in the present BOX layer is calculated to be 1.0×10^{17} cm^{-3} for the unrelaxed neutral oxygen vacancies and 1.4×10^{20} cm^{-3} for the relaxed ones. The concentrations in the glass sample are similarly calculated to be 3.5×10^{14} and 3.0×10^{17} cm^{-3} for the unrelaxed and the relaxed vacancies, respectively. The values obtained above are tabulated in Table I for readability. It can be concluded that the vacancy concentrations in the BOX layer are about 300–400 times as high as those in the glass sample.

In our previous article,[7] we measured concentrations of E'_γ centers (≡Si·, "·" denotes an unpaired electron) of BOX layers with electron spin resonance after exposing the samples to a plasma. The E'_γ concentration in the BOX layer formed under the same condition as that of the present sample was about 1.0×10^{19} cm^{-3}. The fact that the sum of the concentrations of the two types of oxygen vacancies estimated in the present research is larger than the concentration of E'_γ centers, but not so significantly with a ratio of about 14 times, is understandable since both of the neutral oxygen vacancies are believed to be converted into E'_γ centers,[8] and since plasma exposure is known to induce E'_γ centers very efficiently compared with other activation sources such as x- and γ-rays.[12] Furthermore, the concentration ratio between the relaxed vacancies and the unrelaxed vacancies, 0.8×10^{3} for the glass or 1.4×10^{3} for the BOX, is also reasonable since the two values are not so different and since the relaxed state is more stable than the unrelaxed state.[8]

The authors express their thanks to M. Tachimori of Nippon Steel Corporation for valuable discussions and for his help in supplying the samples. This work was partly supported by the Joint Studies Program, 1997 of UVSOR Facility, Institute for Molecular Science, Okazaki, Japan, a Grant-in-Aid for Scientific Research (No. 09450132) from the Ministry of Education, Science, Sports, and Culture of Japan, and by Kawasaki Steel 21st Century Foundation.

[1] Y. Omura and K. Izumi, in *Proceedings of the Fourth International Symposium on Silicon-on-Insulator Technology and Devices*, edited by D. N. Schmidt, PV 90-6 (Electrochemical Society, Pennington, NJ, 1990), p. 509.

[2] T. Ohno, M. Shimaya, K. Izumi, and N. Shiono, IEEE Trans. Circuits Devices **CD-3**, 21 (1986).

[3] T. Ohno, S. Matsumoto, and K. Izumi, Electron. Lett. **25**, 1071 (1989).

[4] T. W. Houston, H. Lu, P. Mei, T. G. W. Blake, L. R. Hite, R. Sundaresan, M. Matloubian, W. E. Baily, J. Lui, A. Peterson, and G. Pollack, in *IEEE SOS/SOI Technology Conference Proceedings* (IEEE, New York, 1989), p. 137.

[5] For example, A. G. Revesz and H. L. Hughes, Microelectron. Eng. **36**,

343 (1997); K. Vanheusden and A. Stesmans, Appl. Phys. Lett. **62**, 2405 (1993).
[6]K. S. Seol, A. Ieki, Y. Ohki, H. Nishikawa, and M. Tachimori, J. Appl. Phys. **79**, 412 (1996).
[7]K. S. Seol, T. Karasawa, H. Koike, Y. Ohki, and M. Tachimori, in *Amorphous and Crystalline Insulating Thin Films—1996*, edited by W. L. Warren, J. Kanichi, R. A. B. Devine, M. Matsumura, S. Cristoloveanu, and Y. Homma, MRS Symposia Proceedings, Vol. 446 (Materials Research Society, Pittsburgh, PA, 1997), p. 219.
[8]H. Imai, K. Arai, H. Imagawa, H. Hosono, and Y. Abe, Phys. Rev. B **38**, 12 772 (1988).
[9]H. Nishikawa, E. Watanabe, D. Ito, and Y. Ohki, Phys. Rev. Lett. **72**, 2101 (1994).
[10]R. Allison, J. Burns, and A. J. Tuzzolino, J. Opt. Soc. Am. **54**, 747 (1964).
[11]H. R. Philipp, J. Phys. Chem. Solids **32**, 1935 (1971).
[12]R. A. B. Devine, D. Mathiot, W. L. Warren, D. M. Fleetwood, and B. Aspar, Appl. Phys. Lett. **63**, 2926 (1993).

ELSEVIER

Journal of Non-Crystalline Solids 222 (1997) 221-227

JOURNAL OF
NON-CRYSTALLINE SOLIDS

Photoluminescence of oxygen-deficient-type defects in a-SiO_2

N. Nishikawa[a,*], Y. Miyake[a], E. Watanabe[a], D. Ito[a], K.S. Seol[b], Y. Ohki[b], K. Ishii[c], Y. Sakurai[d], K. Nagasawa[d]

[a] *Department of Electrical Engineering, Tokyo Metropolitan University, 1-1 Minami-Osawa, Hachioji-shi, Tokyo 192-03, Japan*

[b] *Department of Electrical, Electronics, and Computer Engineering, Waseda University, 3-4-1 Ohkubo, Shinjuku-ku, Tokyo 169, Japan*

[c] *Department of Electronics, The National Defense Academy, 1-10-20 Hashirimizu, Yokosuka, Kanagawa 239, Japan*

[d] *Department of Electrical Engineering, Shonan Institute of Technology, 1-1-25 Tsujido-Nishikaigan, Fujisawa, Kanagawa 251, Japan*

Abstract

Oxygen-deficient-type defects in a-SiO_2 were studied by means of photoluminescence (PL) measurements. Various properties of the 4.4-eV PL such as the decay lifetime and the temperature dependence in oxygen-deficient-type a-SiO_2 can be explained in terms of an energy diagram involving two configurations of the oxygen-deficient-type defect. The 4.4-eV PL observed from the ion-implanted thermal oxides and the oxides prepared by the plasma-enhanced CVD method, has a stretched-exponential decay, suggesting a large structural distribution in the local network structures. A PL band at ~1.8 eV associated with highly oxygen-deficit states is also observed in oxygen-deficient-type a-SiO_2 after high-dose γ-irradiation (dose: 10 MGy). © 1997 Elsevier Science B.V.

1. Introduction

Recent research on the properties of Si crystals in a-SiO_2 [1,2] gives renewed interest in oxygen-deficit states in a-SiO_2. One of the well-studied defects in a-SiO_2 associated with the oxygen-deficit states is the E'_1 center [3,4]. A model has been developed by Fowler et al. [5,6]:

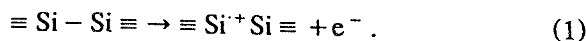

$$\equiv Si - Si \equiv \rightarrow \equiv Si^{\cdot +} Si \equiv + e^- . \quad (1)$$

While the E'_1 center in a-SiO_2 has been thoroughly investigated by means of electron-

* Corresponding author. Tel.: +81-426 772 738; fax: +81-426 772 737; e-mail: nishi@eei.metro-u.ac.jp

0020-9093/97/$17.00 © 1997 Published by Elsevier Science B.V. All rights reserved
PII S0022-3093(97)00398-0

spin-resonance [3,4], our knowledge of the neutral oxygen vacancy (≡ Si–Si ≡) in the left hand side of Eq. (1), has been limited mostly to the UV and VUV optical absorption [7–11]. Also, photoluminescence (PL) data had been limited to those obtained by conventional measurement techniques [8,12,13]. However, our understanding has recently been advanced by the study of the PL decay kinetics using synchrotron radiation (SR) [14–17]. Based on these studies, we proposed an energy diagram shown in Fig. 1 for the 4.4-eV PL in oxygen-deficient-type a-SiO_2 [14].

In the present paper, we report our study on the PL associated with oxygen-deficient-type defects in various forms of a-SiO_2 including thin films, such as buried oxides as well as bulk silica, on the basis of the temperature dependencies of the PL and PLE spectra, and the decay lifetimes. We also report our recent observation of a visible PL band induced by high-dose γ-irradiation, which is similar to the Si crystals in a-SiO_2 [1,2].

2. Experimental procedures

Samples used in the present study are oxygen-deficient-type bulk silica and thin films with a thickness of ~ 100–1000 nm. We define in the present paper the term 'oxygen-deficient-type a-SiO_2' as a sample which has either optical absorption bands at 5.0 eV and 7.6 eV or PL bands at 2.7 eV and 4.4 eV, whose intensities can be varied as a function of oxygen supply during the synthesis [18]. Bulk silica samples were prepared by either the chemical-vapor-deposition (CVD) soot-remelting method [19] or the Ar-plasma method [18]. Thin-film samples include thermal oxides on Si, plasma-enhanced CVD (PE-CVD) oxides prepared at a substrate temperature of 600°C [15], and buried oxides prepared using the separation by the implantation of oxygen (SIMOX) technique [17]. In order to introduce oxygen-deficient-type defects, phosphorus ions were implanted into the thermal oxides [16]. In an attempt to create further oxygen-deficit states, we carried out a high-dose $^{60}Co\gamma$ irradiation (dose: 10 MGy) on oxygen-deficient-type bulk a-SiO_2 [20].

Optical absorption and PL measurements were carried out in the ultraviolet (UV) and vacuum UV (VUV) regions using a synchrotron radiation (SR) facility at UVSOR (Institute for Molecular Science, Okazaki, Japan) or using a KrF excimer laser. During the PL measurements, the sample temperature was varied from 10 to 300 K. The PL decay kinetics were measured by means of a time-correlated single photon counting technique using the SR under a single bunch operation [14].

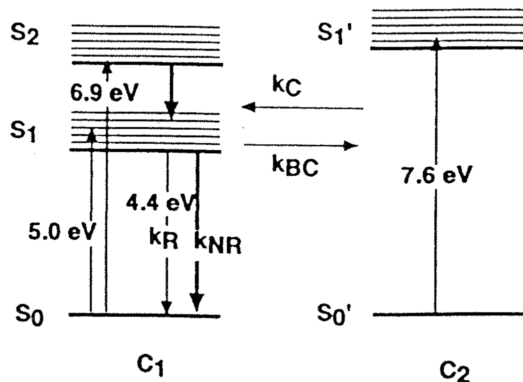

Fig. 1. Proposed energy diagram for the 4.4-eV PL band in oxygen-deficient-type a-SiO_2 [11]. Two configurations, C_1 and C_2 of the oxygen-deficient-type defect are illustrated. The C_1 configuration is responsible for the luminescence at 4.4 eV ($S_1 \rightarrow S_0$) for the 5.0 eV ($S_0 \rightarrow S_1$) and 6.9 eV ($S_0 \rightarrow S_2$) excitations, and C_2 for the 7.6 eV excitation ($S'_0 \rightarrow S'_1$). The symbols, k_R and k_{NR} represent radiative and non-radiative decay rate constants, respectively. Also illustrated is the conversion from C_2 to C_1 upon the 7.6 eV excitation with a rate constant, k_C, followed by reconversion back to the C_2 configuration with k_{BC}.

3. Results

3.1. Bulk a-SiO_2

Shown in Fig. 2 are (a) PL and optical absorption spectra and (b) PL excitation (PLE) spectrum obtained for an oxygen-deficient-type a-SiO_2 sample measured at 10 K. The absorption spectrum has peaks at 5.0 eV and 7.6 eV. The PL band at 4.4 eV was observed under excitation at 5.0 eV and at 6 to 8 eV, as shown in the PLE spectrum of Fig. 2b. It should be noted that the 2.7-eV band [21], which is usually observable together with the 4.4-eV band was not observed here due to the spectral response of the system.

In order to see the difference between the PL

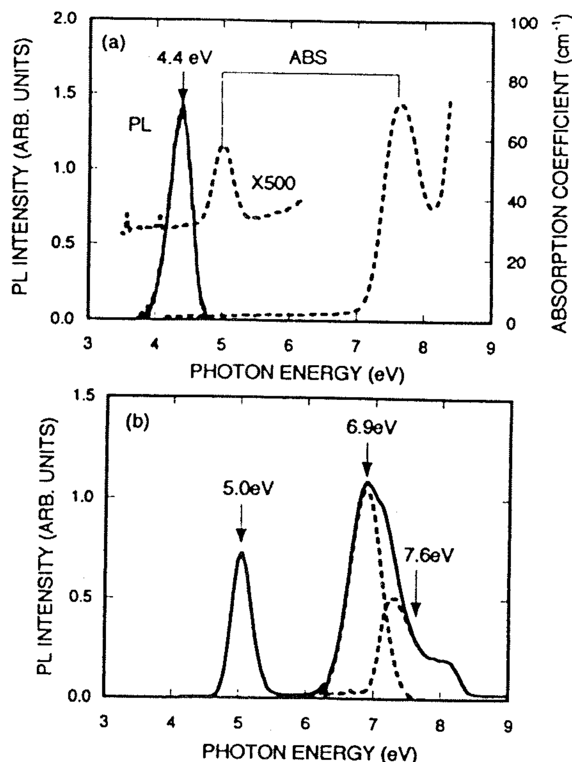

Fig. 2. (a) Photoluminescence and optical absorption spectra and (b) PLE spectrum obtained at 10 K for the 4.4-eV PL band in oxygen-deficient-type a-SiO_2.

observed under different excitation energies, we measured the energy dependence of the PL decay lifetime. Fitting was performed on the decay curves obtained under different excitation energies using a function

$$I(t) = \sum_i I(0)_i \exp(-t/\tau_i), \tag{2}$$

where the values of 4.2 ns, 4.3 ns and 2.1 ns were employed for τ_1, τ_2, and τ_3, respectively, based on previous data [14]. Following this procedure, we obtained a distribution of the PL decay lifetimes as a function of excitation energy, as shown in Fig. 3. For comparison, the PLE spectrum is also indicated. The sum of the three components (closed circles in Fig. 3) is in good accord with the PLE curve.

Shown in Fig. 4 are temperature dependencies of (a) the decay lifetime and (b) the intensity of

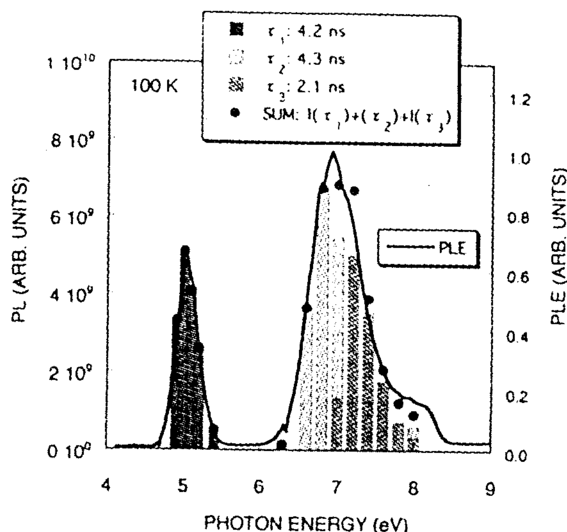

Fig. 3. Distribution of the decay lifetime as a function of excitation energy obtained for the 4.4-eV PL measured at 100 K.

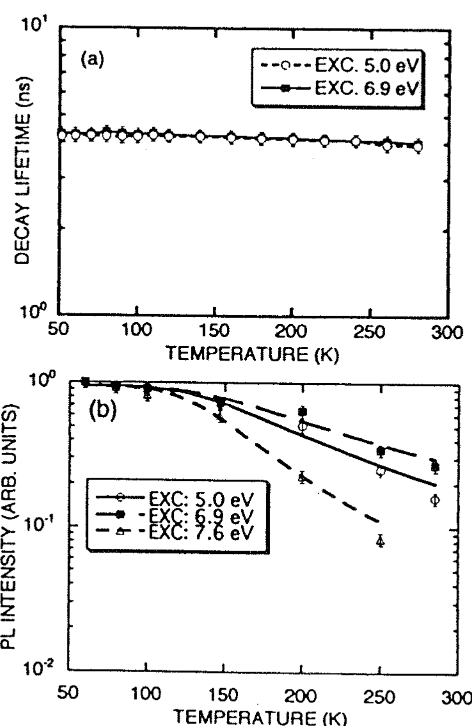

Fig. 4. Temperature dependencies of (a) the decay lifetime and (b) the PL intensity for the 4.4-eV PL band obtained for the oxygen-deficient-type bulk a-SiO_2 sample.

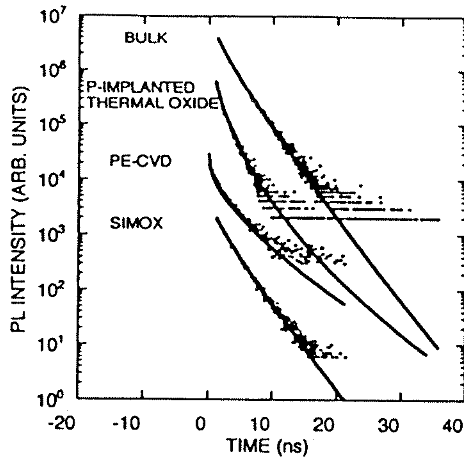

Fig. 5. Comparison of the PL decay profiles obtained under excitation at 7.6 eV for the bulk oxygen-deficient-type a-SiO_2, the P-implanted thermal oxide, PE-CVD oxides, and the SIMOX buried oxides.

the 4.4-eV PL band measured at temperatures ranging from 50 to 300 K. Here, the decay lifetime was not obtained for the 7.6-eV excitation, since the signal-to-noise ratio was too small at temperatures above 100 K. While the decay lifetimes are almost invariant at temperatures from 50 to 280 K, the PL intensities produced by excitation at 5.0, 6.9 and 7.6 eV begin to decrease at temperatures more than 100 K. The discrepancy between the PL decay lifetime and the intensity will be discussed later.

3.2. Thin-film a-SiO_2

As in the case of the oxygen-deficient-type bulk a-SiO_2, almost the same PL spectra were observed for the P-implanted thermal oxide samples, the PE-CVD oxide samples, and the SIMOX oxide samples (data not shown). Shown in Fig. 5 are PL decay curves obtained under excitation at 7.6 eV for these samples. For comparison, the PL decay for bulk a-SiO_2 sample is also shown in Fig. 5. To analyze these PL decay curves, fitting was performed using a stretched exponential function [15]:

$$I(t) \propto (\beta/\tau)(\tau/t)^{1-\beta}\exp\{-(t/\tau)^{\beta}\}. \qquad (3)$$

Here, τ and β $(0<\beta<1)$ are an effective decay

Table 1
Fitting parameters for the decay of PL at 4.3 eV in Fig. 5 to the stretched exponential function of Eq. (3)

Sample	τ (ns)	β
Bulk	1.9	0.88
P-implanted thermal oxide	0.5	0.57
PE-CVD	2.8	0.78
SIMOX	2.2	0.91

constant and a parameter, respectively. The least-squares fitting to the data yields the solid curves shown in Fig. 5. The values of τ and β are listed in Table 1.

3.3. Effects of high-dose γ-irradiation

From the dense excitation induced by large-dose γ-irradiation [20], it is expected that a high concentration of the oxygen-deficient-type defects can be created as a result of the non-radiative decay of self-trapped excitons. Shown in Fig. 6 are PL spectra obtained under excitation at 2.5 eV and at room temperature for high-dose ($\sim$ 10 MGy) γ-irradiated bulk a-SiO_2 prepared under various oxygen partial pressures (PO_2) during the Ar plasma process [18]. A visible PL band can be

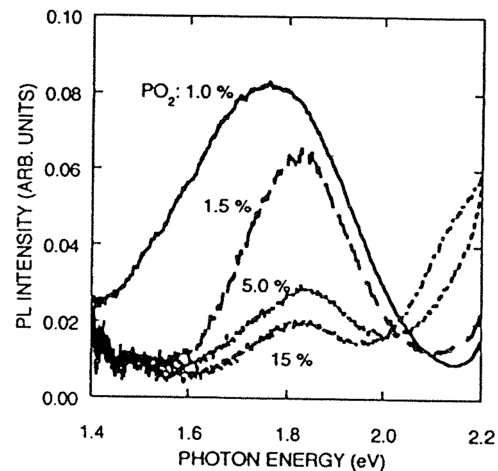

Fig. 6. PL bands observed at room temperature under excitation at 2.5 eV after high-dose γ irradiation (dose: 10 MGy) in oxygen-deficient-type a-SiO_2 prepared under different oxygen partial pressures (PO_2) from 1.0 to 15%.

seen at ~ 1.8 eV. The PL intensity increases with decreasing PO_2. Furthermore, the peak energy slightly red-shifts with decreasing PO_2.

4. Discussion

4.1. Temperature dependence of the 4.4-eV PL

Firstly, we will discuss the temperature dependence of the 4.4-eV PL. Taking into account the energy diagram in Fig. 1, the PL decay lifetime, τ, and the intensity, I_{PL}, can be, respectively, described as

$$\tau = (k_R + k_{NR})^{-1}, \quad (4)$$

and

$$I_{PL} \propto k_R/(k_R + k_{NR}) = k_R \tau, \quad (5)$$

where the k_R and k_{NR} are, respectively, defined as the radiative and the non-radiative decay rate constants shown in Fig. 1. From Eq. (5), the I_{PL} will be proportional to τ. Contrary to this, however, there is a discrepancy between the decay lifetime and the PL intensity, as shown in Fig. 4.

Table 2
Activation energy E of the reaction leading to a metastable state for various excitation energies (see Fig. 7). These values were obtained by fitting the data in Fig. 4b to Eqs. (5) and (6)

PL excitation energy (eV)	E (eV)
5.0	0.067 ± 0.007
6.9	0.064 ± 0.006
7.6	0.084 ± 0.008

We assume that some non-radiative decay channel plays a role in the PL quenching at temperatures above 100 K. A possibility is the existence of a reaction path leading to a metastable state, as illustrated in Fig. 7. Eq. (5) should be replaced with the following equation:

$$I'_{PL} = k_{PL}/(k_{PL} + k_{Meta}) \cdot k_R/(k_R + k_{NR}). \quad (6)$$

We assumed an Arrhenius-type temperature dependence for the rate constant, k_{Meta}:

$$k_{Meta} = A\exp(-E/k_B T), \quad (7)$$

where the A, E, k_B, and T are a pre-exponential factor, the activation energy, Boltzmann constant,

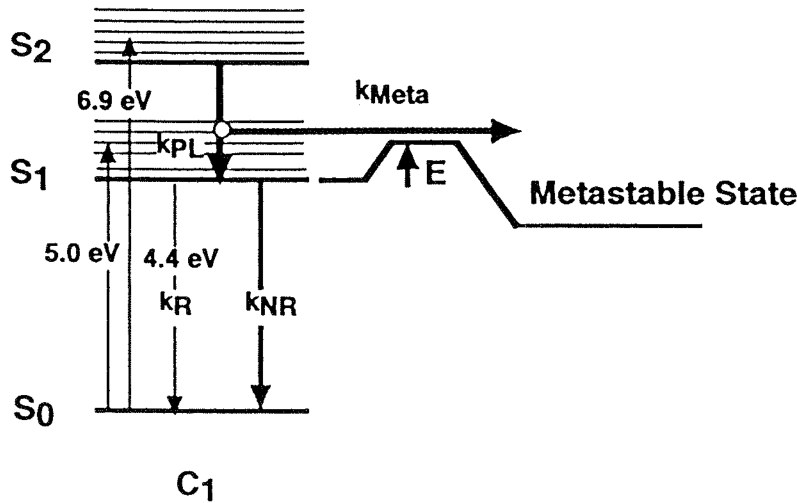

Fig. 7. Schematic illustration of the PL quenching mechanism of the 4.4-eV PL band for the C_1 configuration shown in Fig. 1, which is associated with the 5.0 and 6.9 eV excitations. The model involves a non-radiative reaction path leading to a metastable state. The symbols k_{PL} and k_{Meta} determine the branching ratios into the initial state of PL and the metastable states, respectively.

and the temperature, respectively. By fitting the data of Fig. 4b using both Eqs. (6) and (7), we obtained the activation energy, E, as listed in Table 2. We assume that the PL quenching occurs through the thermally-activated process with the activation energy of ~ 65 meV for the 5.0 eV and 6.9 eV excitations. The existence of such a metastable state is supported by previous reports [9,22,23] that the absorption band associated with oxygen deficiency at 5.0 eV can be bleached by a KrF excimer laser ($h\nu$: 5.0 eV). On the other hand, a somewhat larger activation energy of ~ 80 meV obtained for the 7.6 eV excitation suggests that the PL quenching mechanism somewhat differs from those of the 5.0 eV and 6.9 eV excitations.

4.2. Local structures of the oxygen-deficient-type defect

As shown in Fig. 5, the PL decay curves vary depending on the preparation methods of the a-SiO_2. It can be seen from Table 1 that the PL decay for the bulk and the SIMOX samples has $\beta \sim 0.9$, while that for the PE-CVD sample is β less than 0.8. The largest deviation, $\beta \sim 0.57$, from 1 is obtained for the P-implanted thermal oxide that experienced the ion implantation process. Since larger deviation from a single exponential function means a larger distribution in the surrounding network, the structure of the SIMOX sample [17] is almost similar to the bulk a-SiO_2 prepared by the CVD soot-remelting method [14], and more uniform than those of the ion-implanted thermal a-SiO_2 [16] and the as-grown PE-CVD a-SiO_2 [15]. Although the SIMOX sample was ion implanted during manufacture, the structural distribution is assumed to be annealed by a subsequent heat treatment at 1300°C [17]. We also note that the average decay lifetime, τ, is the smallest in the P-implanted thermal oxides. This difference is ascribed to quenching of the PL by E′ centers ($\sim 10^{19}$ cm^{-3}) in the P-implanted sample [24]. Since the PL decays are affected by the sample preparation conditions and the thermal history as we have shown here, PL decay can be a useful probe to investigate the local network structures of a-SiO_2.

4.3. Oxygen-deficit states induced by high-dose γ-irradiation

As shown in Fig. 6, the PL intensity around 1.8 eV increases with reduction of PO_2 from 15 to 1%. Thus, the 1.8-eV PL is correlated with the oxygen-deficit states in a-SiO_2 as in the case of the 4.4-eV band [20]. Taking into account our previous report that the concentration of the E'_δ centers (i.e. Si clusters comprised of five Si having an unpaired spin [25]) increases with decreasing PO_2 in the same series of samples [18], we assume that a precursor for the structure responsible for the 1.8-eV PL band is a Si cluster introduced during the manufacturing process. It was reported [1,2] that Si-implanted a-SiO_2 annealed at 1100°C exhibits PL at 1.7 eV due to Si crystals. Interestingly, the present PL band in the high-dose γ-irradiated silica (PO_2: 1.0%) is similar to that reported for the Si-implanted a-SiO_2 [1,2] with respect to the Gaussian spectral shape with a peak energy of 1.73 eV and an FWHM of 0.35 eV and the excitation energy of 2.5 eV. A possible explanation is that the Si clusters as detected by the presence of the E'_δ centers introduced during the manufacture grow into another oxygen-deficit state, for example, Si crystals. If this is the case, a driving force in the formation of such highly oxygen-deficit states is considered to be the displacement of oxygen by the non-radiative decay of a self-trapped exciton [26]. Although a further investigation is necessary to clarify the oxygen-deficit states induced by the high-dose γ-irradiation, it is considered that high-dose γ-irradiation can be a useful technique to induce structural modifications in a-SiO_2.

5. Conclusions

(1) Oxygen-deficient-type defects exhibit a photoluminescence band at 4.4 eV, which has three PLE bands at 5.0, 6.9, and 7.6 eV. Based on the detailed analyses of the PL decay lifetime and the temperature dependencies, the PL mechanisms involve two configurations of the oxygen-deficient-type defect. Especially, the one involved in the excitation transitions at 5.0 eV and 6.9 eV

includes a non-radiative decay channel leading to a metastable state.

(2) The 4.4-eV PL decay is sensitive to the local network structures. The PL decay curves can deviate from a single exponential function, and follow a stretched exponential function, depending on the structural distribution of the surrounding SiO_2 network.

(3) A PL band at ~1.8 eV is observed in high-dose γ-irradiated oxygen-deficient-type a-SiO_2, in which highly oxygen-deficit states can be created by the irradiation.

Acknowledgements

This work is partly supported by Grants-in-Aid from the Tokyo Metropolitan University, the Japanese Ministry of Education, Science, and Culture (No. 07805033), Murata Science Promotion Foundation, Saneyoshi Scholarship Foundation, and by the Joint Studies Program (1995-1996) of the Institute for Molecular Science, UVSOR.

References

[1] T. Shimizu-Iwayama, M. Ohshima, T. Niimi, S. Nakao, K. Saitoh, T. Fujita, N. Itoh, J. Phys.: Condens. Matter 5 (1993) L375.
[2] T. Shimizu-Iwayama, K. Fujita, S. Nakao, K. Saitoh, T. Fujita, N. Itoh, J. Appl. Phys. 75 (1994) 7779.
[3] D.L Griscom, in: F.L. Galeener, D.L. Griscom, M.J. Weber (Eds.). Defects in Glasses, Materials Research Society, Pittsburgh, PA, 1986, p. 213.
[4] R.A. Weeks, J. Non-Cryst. Solids 179 (1994) 1.
[5] F.J. Feigl, W.B. Fowler, K.L. Yip, Solid State Commun. 14 (1974) 225.
[6] K.L. Yip, W.B. Fowler, Phys. Rev. B 11 (1975) 2327.
[7] D.L. Griscom, J. Ceram. Soc. Jpn. 99 (1991) 923.
[8] L.N. Skuja, J. Non-Cryst. Solids 149 (1992) 77.
[9] H. Imai, K. Arai, H. Imagawa, H. Hosono, Y. Abe, Phys. Rev. B 38 (1988) 12772.
[10] R. Tohmon, H. Mizuno, Y. Ohki, K. Sasagane, K. Nagasawa, Y. Hama, Phys. Rev. B 39 (1989) 1337.
[11] H. Hosono, Y. Abe, H. Imagawa, H. Imai, K. Arai, Phys. Rev. B 44 (1991) 12043.
[12] C.M. Gee, M.A. Kastner, Phys. Rev. Lett. 42 (1979) 1765.
[13] J.H. Stathis, M.A. Kastner, Phys. Rev. B 35 (1987) 2972.
[14] H. Nishikawa, E. Watanabe, D. Ito, Y. Ohki, Phys. Rev. Lett. 72 (1994) 2101.
[15] K. Ishii, Y. Ohki, H. Nishikawa, J. Appl. Phys. 76 (1994) 5418.
[16] H. Nishikawa, E. Watanabe, D. Ito, M. Takiyama, A. Ieki, Y. Ohki, J. Appl. Phys. 78 (1995) 842.
[17] K.S. Seol, A. Ieki, Y. Ohki, H. Nishikawa, M. Tachimiori, J. Appl. Phys. 79 (1996) 412.
[18] H. Nishikawa, E. Watanabe, D. Ito, Y. Sakurai, K. Nagasawa, Y. Ohki, J. Appl. Phys. 80 (1996) 3513.
[19] T. Izawa, S. Sudo, Optical Fibers, KTK Scientific, Tokyo, 1987, p. 82.
[20] Y. Sakurai, K. Nagasawa, H. Nishikawa, Y. Ohki., J. Appl. Phys. 75 (1994) 1372.
[21] R. Tohmon, Y. Shimogaichi, H. Mizuno, Y. Ohki, K. Nagasawa, Y. Hama, Phys. Rev. Lett. 62 (1989) 1388.
[22] K. Arai, H. Imai, H. Hosono, Y. Abe, H. Imagawa., Appl. Phys. Lett. 53 (1988) 1891.
[23] K. Nagasawa, H. Mizuno, Y. Yamasaka, R. Tohmon, Y. Ohki, Y. Hama, in: J. Arndt, R.A.B. Devine, A. Revesz (Eds.). The Physics and Technology of Amorphous SiO_2, Plenum, New York, 1988, p. 193.
[24] H. Nishikawa, H. Fukui, E. Watanabe, D. Ito, K.S. Seol, K. Ishii, Y. Ohki, M. Takiyama, M. Tachimori, in: H.Z. Massoud, E.H. Poindexter, C.R. Helms (Eds.), Proceedings of The Physics and Chemistry of SiO_2 and the Si-SiO_2 Interface-3, vol. 96-1, Electrochemical Society, New Jersey, 1996, p. 418.
[25] K. Vanheusden, A. Stesmans, J. Appl. Phys. 74 (1993) 275.
[26] C. Itoh, T. Suzuki, N. Itoh, Phys. Rev. B 41 (1990) 3794.

J. Phys. D: Appl. Phys. **30** (1997) 1908–1912. Printed in the UK

PII: S0022-3727(97)79527-5

Rare-earth-doped SiO_2 films prepared by plasma-enhanced chemical vapour deposition

M Yoshihara, A Sekiya, T Morita, K Ishii, S Shimoto, S Sakai and Y Ohki

Department of Electrical, Electronics and Computer Engineering, Waseda University, 3-4-1 Ohkubo, Shinjuku-ku, Tokyo 169, Japan

Received 13 November 1996, in final form 10 March 1997

Abstract. Rare-earth-doped thin SiO_2 films were made by plasma-enhanced chemical vapour deposition using a complex containing chelating ligands and tetraethoxysilane. By this means of deposition, the film was successfully doped with terbium or erbium and the luminescence properties were investigated. In the case of Tb^{3+}-doped films, strong luminescence peaks from the $^5D_4$ level were observed during excitation by a KrF excimer laser. Upon thermal treatment at 800 or 900 °C, luminescence peaks from the $^5D_3$ level appear. Under DC voltages, electroluminescence from the $^5D_4$ level was also observed.

1. Introduction

Since silica glass is an important material for its versatility in various optical and electronic/electrical applications, it is more suitable for a host material into which active guest materials are to be incorporated than are fluoride and borate glasses. Silica glass with doped rare-earth ions is especially important for practical applications such as in lasers, fibre amplifiers and electroluminescence devices. Among the various rare-earth ions, Er^{3+} and Tb^{3+} are important for an optical fibre amplifier which radiates photons at 1.55 μm and for a bright electroluminescence device which emits intense green photons, respectively [1–3]. For high-speed mass telecommunications systems, demand for the development of a planar waveguide amplifier and other optical devices is rapidly growing [4–6]. So far, such optical devices have generally been formed by flame-hydrolysis deposition [7]. However, from an application viewpoint, this method has the disadvantage of very high deposition temperature of about 1000 °C. Therefore, it is important to realize deposition at lower temperatures.

The present paper discusses the possibility of synthesizing rare-earth-doped thin SiO_2 films at a relatively low deposition temperature using plasma-enhanced chemical vapour deposition with a complex containing chelating ligands and tetraethoxysilane (TEOS). Some preliminary photoluminescence and electroluminescence results obtained for the deposited films are also reported.

2. Experimental methods

The rare-earth-doped thin SiO_2 films were prepared by plasma-enhanced chemical vapour deposition using the apparatus shown in figure 1. Oxygen, used as a carrier and oxidation gas, was introduced from the top of a glass bell jar through a line filter and excited with a RF power of 13.56 MHz through capacitive coupling. The TEOS gas was vaporized and transported at 70 °C into the 'tail flame' of the oxygen plasma. The TEOS flow rate was controlled with a mass-flow controller (Hitachi Metal, SFC-670) for use at a high temperature with a low-vapour-pressure gas. A chelato-complex, *tris* (2,2,6,6-tetramethyl-3,5-heptanedionato) RE (III) (RE = Er or Tb) [8], was introduced through vapour phase transport with argon as a carrier gas. Since this material is solid at room temperature, the cylinder and all the pipelines were heated to 150 °C. The flow rate of argon was controlled to keep the pressure inside the glass bell jar at 50 Pa. The deposition parameters are listed in table 1.

Table 1. The deposition conditions.

O_2 flow rate	10 sccm
TEOS flow rate	1 sccm
Pressure	50 Pa
RF power	20 W
TEOS temperature	70 °C
Tris-RE (III) temperature	150 °C
Substrate temperature	Room temperature to 500 °C
Thickness	150–500 nm

The films were deposited onto an n-type silicon monocrystal wafer set on a stage whose temperature was changed from room temperature to 500 °C. The film thickness was measured by ellipsometry with the 632.8 nm line of a He–Ne laser. Please note that such a measured

0022-3727/97/131908+05$19.50 © 1997 IOP Publishing Ltd

(July 7, '97)

Figure 1. The apparatus for plasma-enhanced chemical vapour deposition.

thickness is a kind of estimation because of the nature of single-wavelength ellipsometry with a material of unknown complex refractive index. The x-ray photoelectron spectra (XPS) were obtained by using a dual x-ray-source spectrometer (JEOL, JPS- 90MX) with Al $K\alpha$ x-rays ($h\nu$ = 1486.7 eV). Analyses by atomic emission spectroscopy from an inductively coupled plasma (ICP-AES) and x-ray fluorescence spectroscopy (XRF) were carried out by using a Nippon Jarrel-Ash IRIS-AP and a Seiko Instruments SEA-2001L, respectively. Furthermore, the terbium content was estimated by electron-probe micro-analysis (EPMA, JAX-8600) by comparing the signal intensity with that of a standard sample [9]. Photoluminescence measurements were performed at room temperature, using the KrF excimer laser photons (248 nm = 5.0 eV) from a Lambda Physik LPX105i laser. The fluorescence through a MgF_2 window, focused with two silica lenses and dispersed by a monochromator (Jobin-Yvon, HR320), was measured by using a multi-channel detector (Princeton Instruments, SMA) or a photomultiplier (Hamamatsu Photonics, R955). By applying a DC electric field of 2.5×10^8 V m^{-1}, electroluminescence was observed at room temperature. The n-type silicon substrate was used as the lower electrode and semi-transparent gold deposited by vacuum evaporation with a transmittance of 40–60% was used as the upper electrode.

3. Results and discussion

The presence of rare-earth elements in the deposited films was confirmed by instrumental analyses. Figures 2(*a*) and (*b*) show XPS spectra of the Er^{3+}- and the Tb^{3+}-doped samples deposited at 300 °C, respectively. Several peaks due to Er^{3+} or Tb^{3+} are clearly observed. Similar spectra were obtained for the samples deposited at all other substrate temperatures tested (from room temperature to 500 °C). Furthermore, the existence of Tb was re-confirmed by ICP-AES and XRF, and its content was found to be variable in the range 0.2–7.6 at% from EPMA. Therefore, it can be said that the deposited films can be doped successfully with Er^{3+} or Tb^{3+} using the present plasma-enhanced chemical vapour deposition method, irrespective of the deposition temperature.

The photoluminescence and electroluminescence of the deposited Tb^{3+}-doped films were studied. Figure 3(*a*) shows the photoluminescence spectrum obtained from the Tb^{3+}-doped film deposited at 300 °C (thickness about 500 nm). When it was excited by the KrF excimer laser, strong yellowish-green luminescence was seen in the range 470–630 nm. In figure 3(*b*) for comparison the electronic energy levels of the $4f^8$ configuration of Tb^{3+} ions in $LaCl_3$ are shown [10]. By consulting this, the observed luminescence is considered to be due to de-excitation from the $^5D_4$ level.

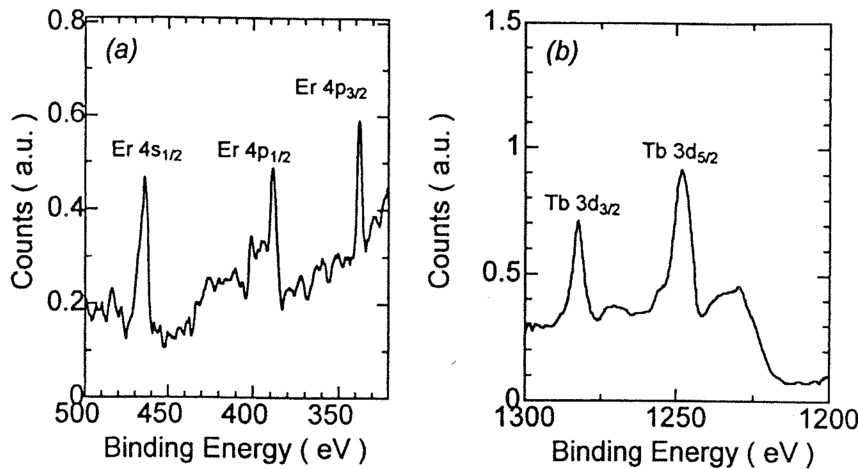

Figure 2. XPS spectra of (*a*) Er^{3+}-doped and (*b*) Tb^{3+}-doped SiO_2 films deposited at 300 °C.

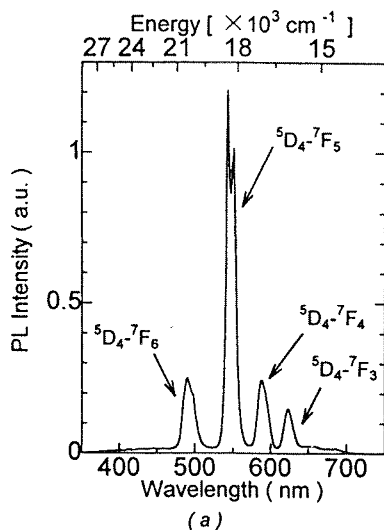

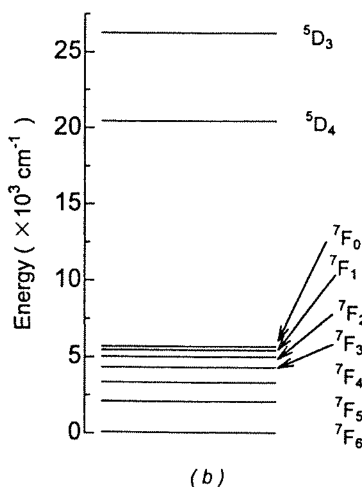

Figure 3. (*a*) The photoluminescence spectrum obtained from Tb^{3+}-doped film excited by KrF excimer laser and (*b*) the electronic energy levels of Tb^{3+} ion in $LaCl_3$.

The ^7F state which is split into seven levels by spin–orbit coupling is further split by the Stark effect. The fact that the observed peaks are broad indicates that the structure surrounding the Tb^{3+} ions is not uniform, reflecting the structural heterogeneity of a glass.

A spectrum similar to figure 3(*a*) was obtained for the samples deposited at temperatures other than 300 °C, except for the fact that a very broad luminescence band in the range 350–600 nm, which is likely to be due to impurities, appeared for the films deposited at room temperature and 200 °C. Figure 4 shows the change in luminescence intensity of the 550 nm peak of the film deposited at 300 °C as a function of the time elapsed after the excitation. The measurement was performed at room temperature. The lifetime was calculated to be about 1.3 ms, which is similar to the reported value for the corresponding peak of a Tb^{3+}-doped heavy-metal-fluoride glass [11]. Quite similar lifetimes were obtained when the lifetime was measured at liquid-nitrogen temperature and when the samples had been deposited at temperatures other than 300 °C. The fact that the measured lifetime agrees with the reported value [11] proves that the observed luminescence is surely due to Tb^{3+}. A similar spectrum was also induced by excitation with photons from an ArF excimer laser ($h\nu = 6.4$ eV) and an F_2 excimer laser ($h\nu = 7.9$ eV). This indicates that electrons which had first been excited to the 5d states or to the conduction band fell into the $^5D_4$ level.

Luminescence from the $^5D_3$ level was not observed in figure 3(*a*). This can be explained by assuming that cross relaxation occurs between $^5D_3$–$^5D_4$ and $^7F_6$–$^7F_0$ [12]. Figure 5 shows photoluminescence spectra as a function of the temperature at which the sample had been annealed thermally in dry nitrogen for 0.5 h. The luminescence intensity increased monotonically with increasing annealing temperature. At 800 °C, a profound change occurred. Luminescence peaks from the $^5D_3$ level began to appear at 800 °C and they became clear at 900 °C. In accordance with this appearance of luminescence from the $^5D_3$ level, a photoluminescence-excitation band for the luminescence at 436 nm clearly appeared, as shown in figure 6. Since the luminescence from the $^5D_3$ level diminished due to the cross relaxation between Tb^{3+} ions, it must become stronger if the average distance between the ions is enlarged, as is known to occur in many glasses [13, 14].

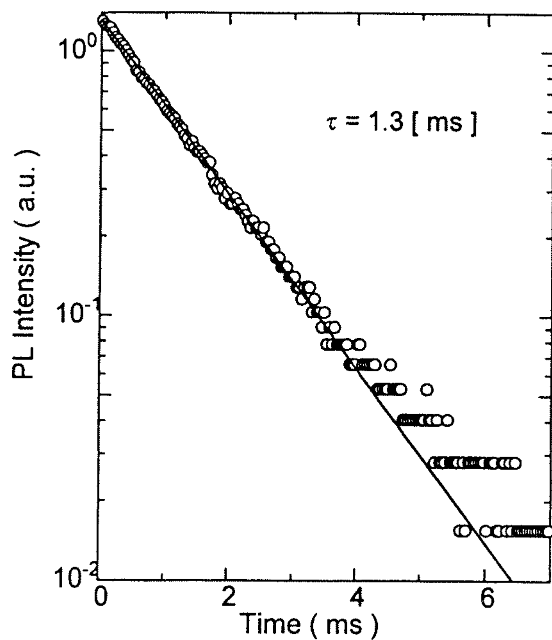

Figure 4. The decay profile of the 550 nm luminescence for Tb^{3+}-doped SiO_2 film deposited at 300 °C. The full line is drawn as a guide to the eye.

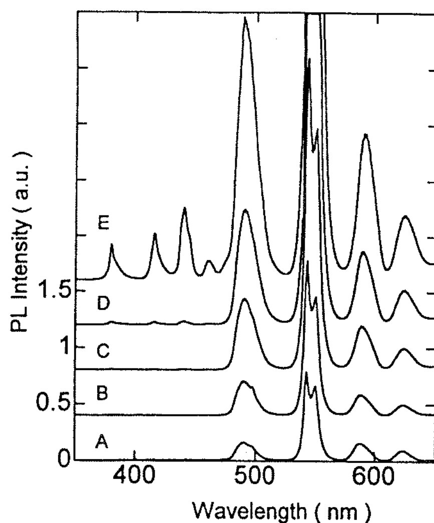

Figure 5. The effect of the annealing temperature on the luminescence spectrum of Tb^{3+}-doped SiO_2 film deposited at 300 °C: Curve A, as-deposited; curve B, annealed at 500 °C; curve C, annealed at 700 °C; curve D, annealed at 800 °C; and curve E, annealed at 900 °C.

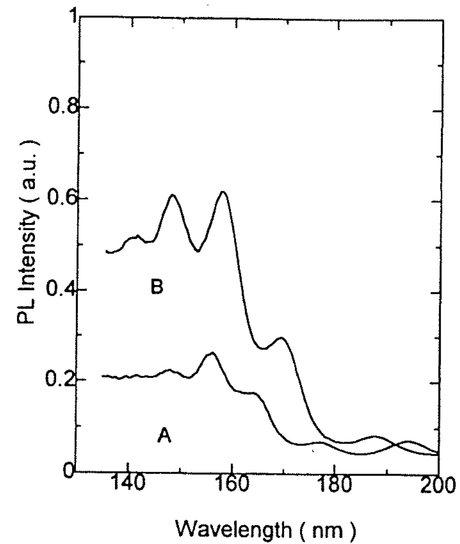

Figure 6. The effect of thermal annealing on the excitation spectrum of the 436 nm luminescence of Tb^{3+}-doped SiO_2 film deposited at 300 °C: curve A, as-deposited; and curve B, annealed at 900 °C.

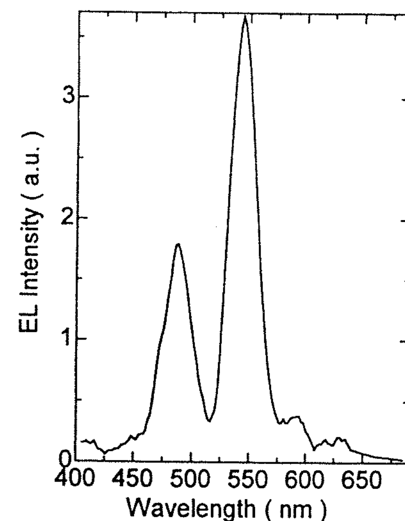

Figure 7. The electroluminescence spectrum obtained for Tb^{3+}-doped SiO_2 film. The sample was deposited at 400 °C and post-annealed in oxygen at a pressure of 5×10^4 Pa for 1 h at 500 °C.

Therefore, under the condition that the Tb^{3+} ions are inhomogeneously distributed in as-deposited films, it can be assumed that the anealing at high temperatures helps the ions distribute themselves uniformly and enlarge their average mutual separation. However, the possibility that some unknown structural change caused by the thermal annealing resulted in the change in the luminescence property cannot be denied.

Figure 7 shows the electroluminescence spectrum observed for the sample of thickness about 150 nm deposited at 400 °C. Since the luminescence intensity from the as-deposited sample was too weak, the sample was post-annealed in oxygen at a pressure of 5×10^4 Pa for 1 h at 500 °C. Although a simple comparison of the peak shapes between the photoluminescence and the electroluminescence is impossible because the slit width of the monochromator was much larger in the case of the electroluminescence, it is clear that the electroluminescence spectrum is essentially the same as the photoluminescence spectrum seen in figure 3(*a*).

4. Conclusion

By plasma-enhanced chemical vapour deposition using chelato-complexes and tetraethoxysilane, Tb^{3+}- and Er^{3+}-doped SiO_2 films were successfully synthesized at a relatively low temperature. In the case of Tb^{3+}-doped films,

photoluminescence peaks from the $^5D_4$ level were observed. Upon thermal treatment at 800 or 900 °C, luminescence peaks from the $^5D_3$ level also appeared.

Acknowledgment

This work was partly supported by grants for scientific research from the Ministry of Education of Japan (grants 06452222 and 08750377).

References

[1] Mears R J, Leekie L, Jauncey I M and Payne D N 1987 *Electron. Lett.* **23** 1026
[2] Corol D M, Van Stapele R P, Haanstra J H, Popma T J A, Thomas G E and Vink A T 1987 *J. Lumin.* **37** 293
[3] Hoshina T 1967 *Japan. J. Appl. Phys.* **6** 1023
[4] Tumminelli R, Hakimi F and Haavisto J 1991 *Opt. Lett.* **16** 1098
[5] Shuto K, Hattori K, Kitagawa T, Ohmori Y and Horiguchi M 1993 *Electron. Lett.* **29** 139
[6] Hattori K, Kitagawa T, Ogawa M, Wada M, Temmyo J and Horiguchi M 1993 *Electron. Lett.* **29** 357
[7] Kawachi M 1990 *Opt. Quant. Electron.* **22** 391
[8] Purchased from Johnson Matthey Company
[9] Purchased from P&H Developments
[10] Carnall W T, Fields P R and Rajnak K 1968 *J. Chem. Phys.* **49** 4447
[11] Amaranath G and Buddhudu S 1992 *J. Non-Cryst. Solids* **143** 252
[12] Blasse B and Bril A 1967 *Philips Res. Rep.* **22** 481
[13] Robbins D J, Cockayne B, Lent B and Glasper J L 1976 *Solid State Commun.* **20** 673
[14] Bondenschatz N, Wannemachar R and Heber J 1991 *J. Lumin.* **47** 159